# Prediction of Fatigue Crack Growth behaviour of tubular joints used in offshore structures

Delft University of Technology

Petros Dratsas

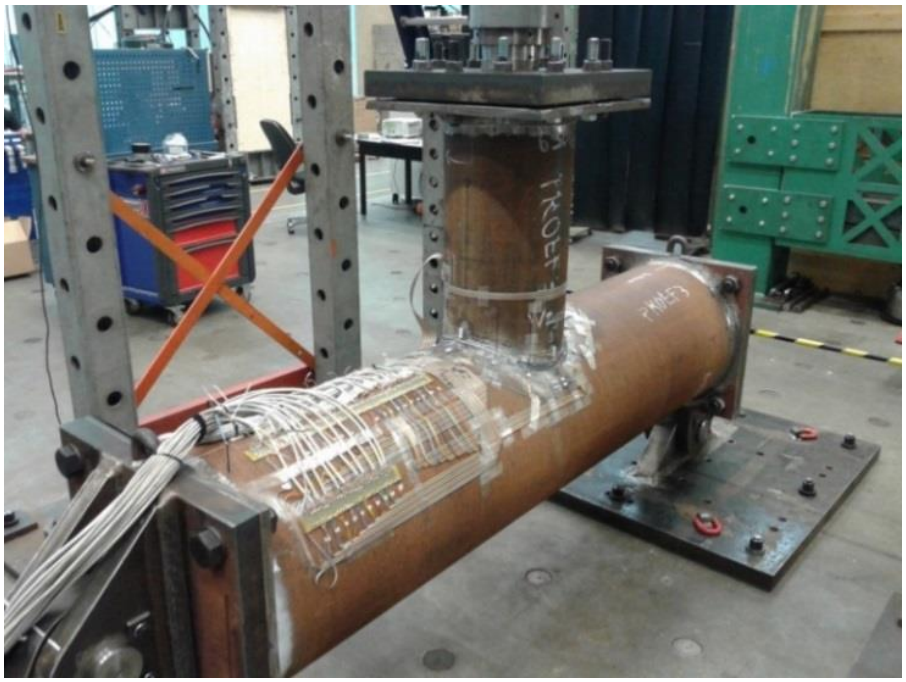

Delft, March 2016

TU Delft

TNO innovation for life

TU Delft

Master of Science Thesis
Department of Civil Engineering and Geosciences
Delft University of Technology

# Prediction of Fatigue Crack Growth behaviour of tubular joints used in offshore structures

by

Petros Dratsas

**Master of Science**

in Civil Engineering, – Structural Engineering Track

Thesis Committee:

| | |
|---|---|
| Prof.ir. F.S.K. Bijlaard | Delft University of Technology |
| Dr.ir. R. Abspoel | Delft University of Technology |
| Dr.ir. M. Janssen | Delft University of Technology |
| Prof.dr.ir. J. Wardenier | Delft University of Technology |
| Dr.Ir. R.J.M. Pijpers | TNO |

## ACKNOWLEDGEMENTS

I would like to express my gratitude to my daily supervisor Dr.Ir. R.J.M. Pijpers for his invaluable assistance and aspiring guidance. His advices turned problems into challenges and motivated me to continue working hard and overcome any difficulties. I would like also to thank Prof.ir. F.S.K. Bijlaard, Prof.dr.ir. J. Wardenier, Dr.ir. R. Abspoel and Dr.ir. M. Janssen for their supervision, their useful comments and the fruitful discussions we have during the thesis meetings.

Special thanks go to the technicians from the Structural Dynamics Lab of TNO for their technical assistance during the experiments.

Furthermore I owe special gratitude to all my “Delftian” friends whose psychological boost and encouragement were very important for me.

Lastly, I am indebted to my family for supporting and encouraging me all these years of my master studies.

Petros Dratsas

5/3/2016

# Table of Contents

## List of symbols

| | |
|---|---|
| a | Crack size |
| B | Specimen thickness |
| C | Crack propagation constant |
| c | Half crack length |
| da/dN | Crack growth rate |
| $d_{brace}$ | Brace external diameter |
| E | Modulous of elasticity |
| f | Crack opening function |
| k | Thickness exponent |
| $K_C$ | Critical Stress Intensity factor |
| $K_{max}$ | Maximum stress intensity factor |
| $K_{min}$ | Minimum stress intensity factor |
| $K_{OP}$ | Opening Stress intensity factor |
| L | Weld width |
| $l_{in}$ | Inner span |
| logC | Intercept of logN-axis by S-N curve |
| $l_{out}$ | Outer span |
| m | Negative inverse slope of S-N curve |
| M | Stress intensity correction factor |
| m | Crack propagation exponent |
| $M_{b,a}$ | Bending part of stress intensity correction factor in crack depth direction |
| $M_{b,c}$ | Bending part of stress intensity correction factor in crack length direction |
| $M_k$ | Stress intensity concentration factor |
| $M_{k,b}$ | Bending part of stress intensity concentration factor |
| $M_{k,m}$ | Membrane part of stress intensity concentration factor |
| $M_{m,a}$ | Membrane part of stress intensity correction factor in crack depth direction |
| $M_{m,c}$ | Membrane part of stress intensity correction factor in crack length direction |
| N | Loading cycles |
| $N_d$ | Delay cycles |
| R | Stress ratio |
| $S_{dtv}$ | Standard deviation |
| t | Thickness |
| T | T-plated joint plate thickness |
| $t_0$ | Chord thickness |
| $t_{ref}$ | Reference thickness |
| U | Plasticity induced crack closure |
| V | Voltage measurement |
| *v* | Poisson ratio |
| W | Specimen width |
| Y | Geometric factor |
| α | Crack depth |
| β | Width ratio between braces and chord |
| γ | Half diameter-to-thickness ratio of the chord |

| | |
|---|---|
| $\Delta$ | Probe tip spacing |
| $\Delta K_{baseline}$ | Stress intensity factor baseline |
| $\Delta K_{eq}$ | Equivalent Stress Intensity factor range |
| $\Delta\alpha$ | Crack increment |
| $\Delta\varepsilon$ | Strain range |
| $\Delta K$ | Stress Intensity Factor range |
| $\Delta K_{eff}$ | Effective Stress Intensity Factor range |
| $\Delta K_{th}$ | Stress intensity factor range threshold |
| $\Delta\sigma$ | Stress range |
| $\Delta\sigma_b$ | Bending stress range |
| $\Delta\sigma_{geom}$ | Geometric stress range |
| $\Delta\sigma_m$ | Membrane stress range |
| $\Delta\sigma_{nom}$ | Nominal stress range |
| $\Delta\sigma_{tot}$ | Total Stress range |
| $\varepsilon_{max}$ | Maximum strain |
| $\varepsilon_{min}$ | Minimum strain |
| $\theta$ | Weld toe angle |
| $\theta$ | Brace angle |
| $\sigma_b$ | Bending stress |
| $\sigma_m$ | Membrane stress |
| $\sigma_{max}$ | Maximum stress |
| $\sigma_{min}$ | Minimum stress |
| $\sigma_p$ | Peak stress |
| $\sigma_r$ | Residual stress |
| $\tau$ | Brace-to-chord wall thickness |
| $\phi$ | Distribution function of the Gaussian distribution probability of exceedence 95% |
| $\Phi(\alpha,c)$ | Elliptical integral |

## Abbreviations

| | |
|---|---|
| 4PB | 4-Point bending test |
| ACPD | Alternate Current Potential Drop |
| BM | Base material specimen |
| BP | Bead weld on plate specimen |
| CAL | Constant Amplitude Loading |
| CHS | Circular Hollow section |
| CP | Cathodic protection |
| FM | Fracture mechanics |
| IPB | In plane bending |
| NDT | Non destructive test |
| OL | Overload |
| OL/UL | Tensile overload followed by a compressive underload |
| OLR | Overload ratio |
| OPB | Out-of-plane bending |
| OWT | Offshore wind turbines |
| SCF | Stress concentration factor |
| SIF | Stress Intensity Factor |
| SW | Seawater |
| UL | Underload |
| UL/OL | Compressive underload applied just before a tensile overload |
| VAL | Variable Amplitude Loading |

## SUMMARY

The high levels of wind and wave loads on offshore structures make fatigue analysis a significant parameter that has to be taken into consideration throughout an offshore structure design. Steel tubular members are widely used in offshore (wind) industry due to their efficient structural behaviour. The welded connections between the different tubular members are denoted tubular joints and they are the most susceptible locations of the structure to fatigue damage. This study is concentrated on the fatigue crack growth behaviour of tubular joints.

The main objective of the thesis is the application of a procedure that predicts the fatigue crack growth behaviour in case of a tubular T-joint under axial load. This procedure relies on the basic formula of fracture mechanics approach during crack propagation (Paris law) and uses simplified geometries to simulate stress field at the vicinity of the crack and fatigue crack growth results from small-scale steel welded specimens to introduce material constants. The validity of the applied procedure is checked by fatigue crack growth tests on a realistic geometry tubular T-joints.

Furthermore, the differences in fatigue crack growth behaviour between welded and base material specimens are examined as well as the effect of a single stress tensile peak on welded, base material small-scale specimens and tubular joints. The effects of stress range, stress ration, mean stress and load sequence are also included in this study.

# 1. INTRODUCTION – OBJECTIVES OF THE THESIS

The offshore (wind) industry development has given a boost in the structural use of steel tubular members. A large part of steel structures which consist of tubular members assembled by welded joints are used in offshore engineering applications (Figure 1. 1) because of their good structural and mechanical properties.

Figure 1. 1: Tubular steel members on offshore structures

Due to the high level of fatigue loads as well as a large number of load cycles caused by wind and wave loads together (Figure 1. 2), fatigue performance of welded connections is a design driving criterion for offshore steel tubular structures. The welded connections between the different tubular members are denoted tubular joints and they are the most susceptible locations of the structure to fatigue damage. The wide use of tubular steel members in offshore structures enhances the need of examining further the fatigue crack growth behaviour of tubular joints under fatigue loading and various load sequence effects by developing new, less conservative crack growth models which incorporate adequately the interactions between various load sequence effects.

Figure 1. 2: Wave loading on tubulars members of support offshore structures

In this study, the fatigue crack growth behaviour of a particular loading case is examined: an axial load on the tubular T-joint (Figure 1. 3) under constant amplitude loading and tensile overloads. The hot-spot stress method and a numerical integration procedure on the basis of the fracture mechanics approach (which incorporates results from small-scale specimens) are applied for the aforementioned case and their results are compared with the experimental results from the laboratory.

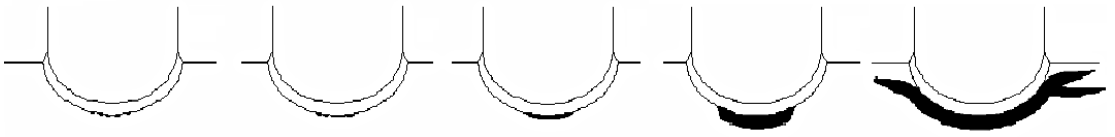

Figure 1. 3: Crack propagation on a tubular T-joint

The main objectives of this study are:

- The prediction of fatigue crack growth behaviour of tubular T-joint under constant amplitude loading and discrete overloads is based on the fracture mechanics approach and uses as an input experimentally derived data. This calculation procedure is applied through a MathCAD routine, called FAFRAM (FAtigue FRActure Mechanics), and relies on the Paris-Erdogan law:

$$\frac{da}{dN} = C\Delta K^m$$

  Where da/dN is the crack growth rate, ΔK called stress intensity factor range and incorporates the stress condition and the geometry of the structure and are calculated according to a simplified T-plated joint geometric model in FAFRAM.

  C, m are constants dependent on environment and material and derived from small-scale specimen tests

Secondary objectives of this study that can be observed during the investigation of the aforementioned ones are the following:

- The investigation of steel structures susceptibility to fatigue loading in relation with the material (welded/base material) and stress ratio R by deriving the crack propagation constants C.

- The comparison of experimentally derived crack propagation constants with those that are provided from the guidelines the BS7910.

- The comparison of overload effects on welded and base materials and necessary argumentation to explain the differences and the identification of the dominant mechanism that causes overload effect.

- The experimental verification of literature research regarding load sequence effects on fatigue crack growth in welded steel specimens.

- The verification and evaluation of ACPD (Alternating Current Potential Drop method) method for measuring crack depth growth at the weld toe of a tubular joint.

- The experimental investigation of surface crack development in tubular joints under fatigue loading.

- The experimental investigation of geometric stress range with the use of linear extrapolation

- The application and evaluation of the S-N curve method in the examined structural and loading case.

- The investigation of the main assumptions that are applied in FAFRAM for the correct modelling of the examined case

- The evaluation and comparison of the effect of a single tensile stress peak (overload) applied in a constant amplitude fatigue loading on fatigue crack growth behaviour of tubular joint and small-scale specimen.

- The comparison of crack propagation constants derived from steel small-scale specimens and tubular joint.

**Chapter 2** provides the theoretical background and the main concepts that are related with the experiments. **Chapter 3** describes the experimental procedure of fatigue crack growth tests on small scale welded steel specimens and the interpretation process of the results. In this chapter constant cyclic loading and load sequence effects on fatigue crack propagation of base material and welded steel plate specimens are examined. **Chapter 4** shows the experimental procedure of an axially loaded tubular T-joint and the results. Constant amplitude loading and discrete tensile overload are applied on this specimen and their effects are depicted. In **Chapter 5**, the S-N curve method is applied for the particular tested case of the previous chapter. **Chapter 6** presents the main assumptions and the application of FAFRAM routine *[1]* (by using as an input the crack propagation constant derived from Chapter 3) in order to predict the fatigue crack growth behaviour of the examined loading case and compare crack growth results with the experimental ones from Chapter 4. All the conclusions from the study are summarized in the last chapter.

## References

**[1]** O.D. Dijkstra, H.H. Snijder, H.J.M. van Rongen - Assessment of the remaining fatigue life of defective welded joints (1990) - IABSE reports

# 2. LITERATURE RESEARCH

## 2.1. Introduction

This chapter presents the basic theoretical tools (S-N curves, fracture mechanics approach) that can be applied and the conditions that have been taken into consideration in order to predict the fatigue crack growth behavior of a tubular joint.

The examined case in this study is the constant amplitude loading (CAL) and load sequence effects on fatigue crack growth behaviour of an axially brace loaded tubular T-joint (Figure 2. 1). The parameters that affect the response of the aforementioned specimen are presented in this chapter as well as the expected effect they have according to the literature.

The basic objective of this chapter is to provide the theoretical background related to the experiments and numerical integrations in the following chapters in order to be compared, verified and explained by the (experimental and numerical) results.

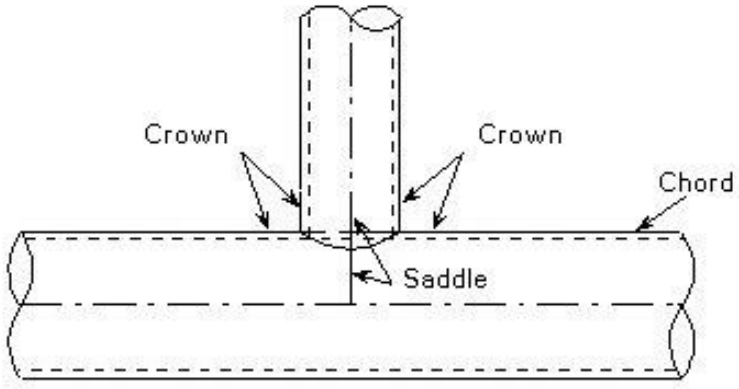


Figure 2. 1: Tubular T-joint

## 2.2. S-N method combined with hot-spot stress method

### 2.2.1. S-N curves

The nominal stress theory with S-N curves, or Wöhler lines, is the most commonly used method by engineers in order to determine the fatigue behavior of a structure. The various S-N curves are based on fatigue tests, resulting in fatigue strength curves with a defined stress range $\Delta\sigma$ on the vertical axis and the fatigue life or the number of cycles N to a specific failure criterion on the horizontal axis. Each data pair ($\Delta\sigma_i$, $N_i$) represents the life or number of cycles of a constant stress range that causes fatigue failure for such a structural detail.

The majority of the S-N data are derived by fatigue tests on small specimens in laboratories representative of typical weld details. For simple test specimens the testing is performed until the specimens fail (fracture). The criterion for failure is generally through thickness

crack size, a specified crack length or rupture. The relation between the number of cycles to failure N and the stress range Δσ is given by the following formula *[1]*:

$$N = C \cdot \Delta\sigma^{-m} \qquad \textit{(eq. 2.1a)}$$

or:

$$\log N = \log C - m \cdot \log \Delta\sigma \qquad \textit{(eq. 2.1b)}$$

*(on a log-log scale this gives a straight line with a slope of –m)*

N = predicted number of cycles to failure for stress range Δσ
Δσ = stress range
m = negative inverse slope of S-N curve
logC = intercept of log N-axis by S-N curve

### 2.2.2. Thickness effect

The fatigue strength of welded joints depends to some extent on the member thickness. This thickness effect is mostly due to the sensitivity of the fatigue strength to the stress gradient and the local geometry of the weld toe in relation to thickness of the adjoining components. The thickness effect is accounted for by the modification on stress such that the stress ranges are changed in the following way:

$$\Delta\sigma_{mod} = \Delta\sigma \left( t / t_{ref} \right)^{k} \qquad \textit{(eq. 2.2.)}$$

The reference thickness and the thickness exponent are values that vary according to the code used *[2].*

### 2.2.3. Damage Accumulation

A cumulative fatigue assessment is applied in case of variable loading which is generally known as the Palmgren-*Miner rule* which operates under the assumption of a linear damage accumulation. This linear damage accumulation scheme assumes that, for a loading with different stress ranges, each stress range $\Delta\sigma_i$, occurring $n_i$ times, results in a partial damage which can be represented by the ratio $n_i/N_i$ (the histogram being distributed among $n_{tot}$ stress range classes). Here, $N_i$ represents the number of cycles to failure (fatigue life of the structural detail under study) under the stress range $\Delta\sigma_i$. In case the stress range distribution function is known, the summation of the partial damages due to each stress range level can be replaced by an integral function. The failure is defined with respect to the summation of the partial damages and occurs when the theoretical value *Dtot* = 1.0 is reached, see equation 2.3. This is represented in a graphical way in Figure 2. 2 where $\Delta\sigma_R$ is the applied stress range and $N_R$ the number of loading cycles to fatigue failure at a certain stress range.

$$\boldsymbol{D_{tot} = \frac{n_1}{N_1} + \frac{n_2}{N_2} + \frac{n_3}{N_3} + \cdots = \sum_{i=1}^{n_{tot}} \frac{n_i}{N_i} = \int \frac{dn}{N} \leq 1.0} \qquad \textit{(eq. 2.3.)}$$

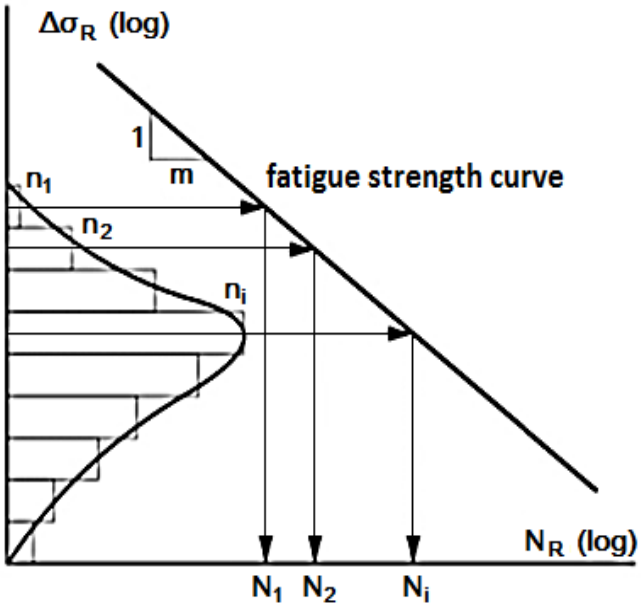


Figure 2. 2: Damage accumulation scheme

It should be noted that in this simple damage accumulation rule, the effect of the order of occurrence of the stress ranges in the history, in other words the load sequence effect is completely ignored. The Palmgren-Minor rule is thus a simplification.

In case where the highest stress range is lower than the constant amplitude fatigue limit (or endurance limit), a detailed fatigue analysis can be omitted as it is assumed that there will be no crack initiation and propagation for these low stress ranges. However, in case of a variable loading when some (but all) stress ranges are higher than the constant amplitude fatigue limit, the damage accumulation for these stress ranges can be computed using Equation (2.3). The stress ranges that are lower than the fatigue limit, do not contribute to the propagation of the crack until the crack reaches a certain size. This is the reason why the part of the histogram below the fatigue limit cannot be completely ignored; it contributes to the accumulation of damage when the crack becomes large. For stress ranges $\Delta\sigma_i$ lower than the fatigue limit a resistance curve is used with a slope *k* different from Wöhler's slope *m [3].*

The majority of fatigue test results are derived in the medium to high cycle domain (typically $10^4 < N \leq 5 \cdot 10^6$ cycles); for the giga high cycle domain, very limited test data are available ($N >> 5 \cdot 10^6$ cycles).

### 2.2.4. Selection of the appropriate code

There is a wide variety of codes and recommendations that provide standards and provisions for the fatigue assessment of steel structures. There are different standards for various structural details, types of structural members, fields of application and environmental conditions. The primary step of fatigue assessment is the selection of the appropriate guidelines that suit best with the examined case.

In this study the standards and recommendations from five widely used guidelines which provide sufficient data for fatigue assessment of tubular members are examined: DNV-RP-

C203, IIW Recommendations, ISO14347:2008 and API-RP 2A-WSD 2007 *[2]*. In the following paragraphs a short description of each code is presented.

DNV-RP-C203 code *[4]* is a limit state document dealing with design of steel offshore structures. This document provides necessary information for fatigue strength analysis which deals with the classification of structural details, stress concentration factors for tubular joints and cutouts. Separate sets of curves are given for joints in air, in seawater with cathodic protection (SW+CP) and in seawater with free corrosion (SW). No endurance limits are specified in these curves (SW+CP and SW), but conditions are given of situations where detailed fatigue analysis can be omitted. Modifications to the design S-N curves must be made to allow for thickness effects. Fatigue life enhancements are also allowable to introduce the influences of weld improvement techniques.

IIW Recommendations document *[5]* is not a code of practice or a standard but sets out recommendations for the fatigue design of welded joints and components. The fatigue resistance data given in the document refer to non-corrosive environments. No specific recommendations are given in the document for corrosion fatigue assessment. IIW (2008) for fatigue design of welded joints and components has made some changes *[1]* that are incorporated in Table 2. 1.

The ISO14347:2008 code is a limit state code dealing the design procedure for welded hollow section joints. The S-N curves provided in the case of tubular joints do not incorporate the effect of corrosion. The endurance limits are specified and modifications to the basic S-N curves should be made to incorporate thickness effects and influences of weld improvement techniques.

API-RP 2A-WSD code *[6]* deals with designing and constructing fixed offshore platforms. The S-N curves provided in the document relate to tubular joints in steel structures and modifications are to be applied to these to account for operating environment, thickness effects and so forth. There is no endurance limit.

In Table 2. 1 the basic features of the S-N curves are illustrated according to the aforementioned codes and in Figure 2.3 the S-N curves presented.

Figure 2.3 presents graphically the S-N curves according to the aforementioned codes.

Table 2. 1: Comparison of S-N curves for tubular joints in different environmental conditions

| Environmental conditions | Basic data | DNV | IIW | ISO | API |
|---|---|---|---|---|---|
| Air | $t_{ref}$ (mm) | 32 | 25 | 16 | 16 |
| | k | 0,25 – 0,30 | 0,10 – 0,30 | 0,3 | 0,2 |
| | Slope change N | $10^7$ | $10^7$ | $5\times10^6$ | $10^7$ |
| | m | 3 & 5 | 3 & 5 | 3 & 5 | 3 & 5 |
| | Fatigue limit (MPa)* | 52.63 | 89.1 | 84 | 67.1 |
| | Endurance limit | N/A | $10^8$ | $10^8$ | N/A |
| Seawater with cathodic protection | $t_{ref}$ (mm) | 32 | - | - | 16 |
| | k | 0,25 – 0,30 | - | - | 0,25 |
| | Slope change N | $10^6$ | - | - | $1,78\times10^6$ |
| | m | 3 & 5 | - | - | 3 & 5 |
| | Fatigue limit (MPa)* | 52.63 | - | - | 94.52 |
| | Endurance limit | N/A | - | - | N/A |
| Seawater with free corrosion | $t_{ref}$ (mm) | 32 | - | - | 16 |
| | k | 0,25 – 0,30 | - | - | 0,25 |
| | Slope change N | N/A | - | - | N/A |
| | m | 3 | - | - | 3 |
| | Endurance limit | N/A | - | - | N/A |

*Stress range corresponds to slope change for $t_{ref}$

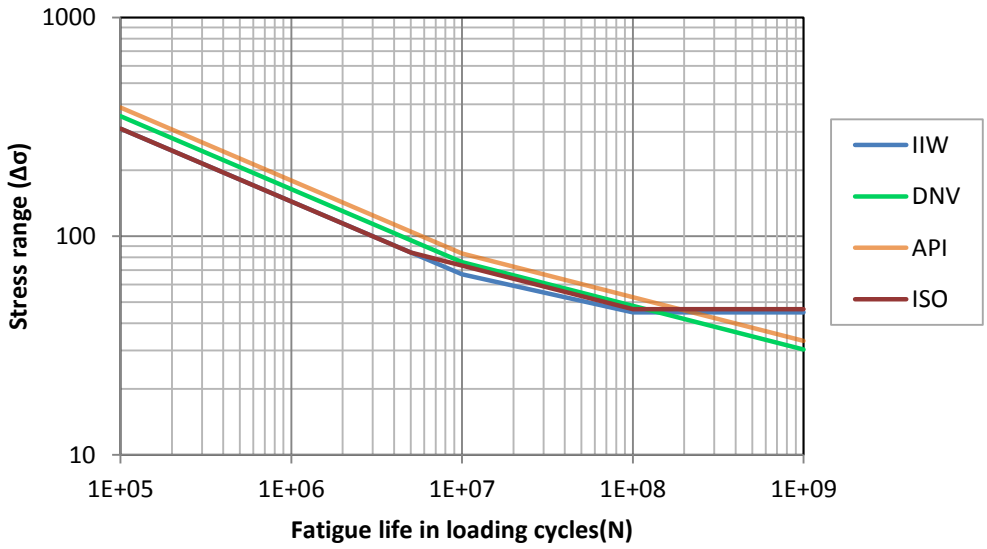


Figure 2.3: S-N lines in air conditions according to different codes

As can be depicted clearly in the table IIW recommendations and ISO code do not take into account the effect of environmental conditions. DNV and API are the only codes among the examined ones that are concentrated on offshore structures.

Although the designs for the majority of the wind offshore structures are derived from the equivalent structures for offshore oil platforms, there are significant differences regarding the applied fatigue loads. In case of wind offshore steel support structures the fatigue load does not come only from wave actions, but also from the wind turbine. In addition, there is a strong interaction between the foundation compliance and the reaction of the support structure to wind forces *[7]*. To conclude, for this study the use of DNV-RP-C203 guidelines is taken as the most appropriate code for the evaluation of the fatigue strength offshore wind support structures. In Figure 2. 4 a graphical presentation of design S-N curves is shown for different environmental conditions.

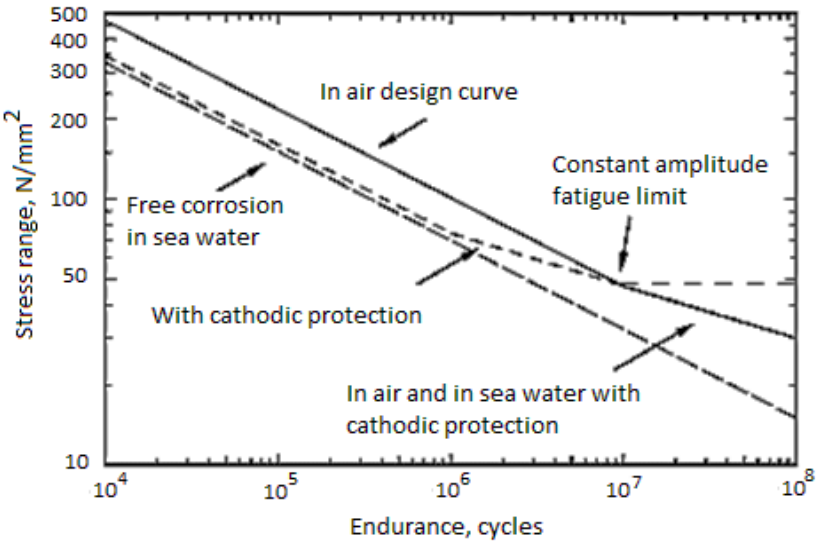


Figure 2. 4: DNV code design S-N curves according to environmental conditions

The design curves that are used in the DNV code are based on the mean-minus-two-standard-deviations for relevant experimental data. Thus the design S-N curves are associated with 97.7% probability of survival. In contrast to the simple test specimens, tests of tubular joints are normally of a larger scale. As a result a crack can grow through thickness and also along a part of the joint before fracture occurs during the test *[4]*.

Because of a large variety of structural details in tubular joints and the complexity of loading conditions (in Figure 2. 5 the most common configurations of tubular joints are shown and in Figure 2. 6 the loading conditions that are combined in a tubular joint), the concept of S-N curves based on nominal stress method is inefficient because of the fact that the stress concentration due to geometry is not taken adequately into account. Therefore the application of hot-spot stress analysis is developed for tubular joints.

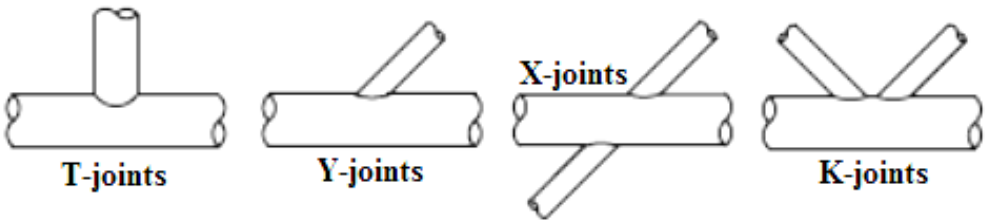


Figure 2. 5: Types of uniplanar joints

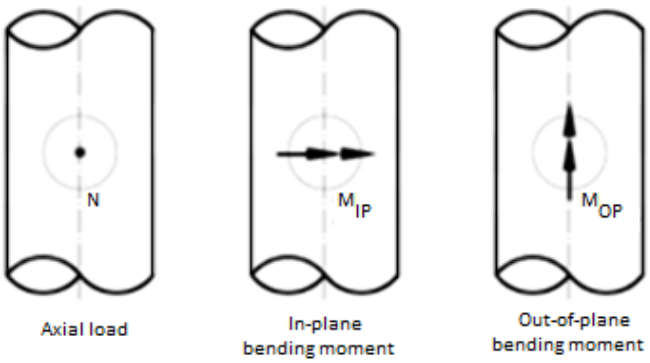


Figure 2. 6: The basic loading conditions in the brace

### 2.2.5. Hot-spot stress method

The hot spot stress method used in a tubular joint of an offshore wind turbine steel substructure is an approach that incorporates the global analysis of the structure and the local stress analysis of the joint. A global analysis determines the sectional forces and the nominal stresses in the various members of the structure. These nominal stresses establish the boundary conditions for local stress analyses of a tubular joint of the structure. A local stress analysis of a tubular joint indicates that the peak stresses near the welded intersections are several times higher than the nominal stresses which is the result of the differences in relative stiffness of the brace to chord connection along the perimeter. The locations of the highest stresses are called hot spots and are always found in the joints.

The hot spot stress range contains the geometrical influences but excludes the effects related to fabrication such as the configuration of the weld (flat, convex, concave) and the local condition of the weld toe (radius of weld toe, undercut, etc.).

By examination of the stresses close to the welds of tubular joints, a rather smooth increase can be observed in areas that are not too close to the weld. This increase is due to the geometric influence of the joint. Very close to the weld a rapid increase in stresses due to the weld geometry appears (Figure 2. 7).

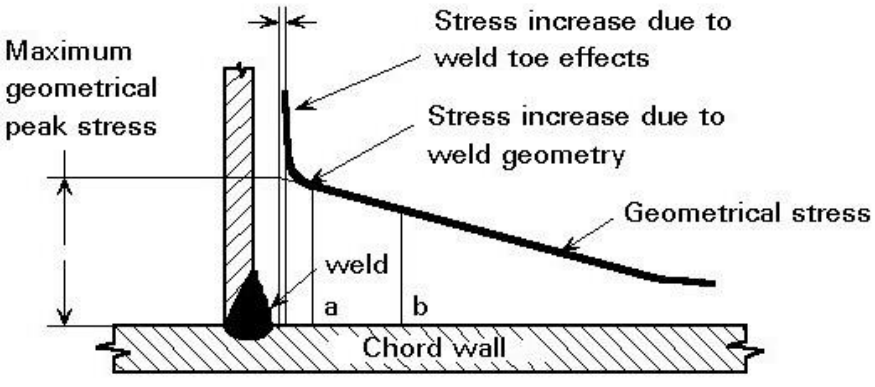


Figure 2. 7: Stress extrapolation in tubular joints (not to scale) *[8]*

The hot spot stress, also called geometric stress, is defined as the linearly extrapolated stress at a specified location to the weld toe. The extrapolation must be carried out both on the

brace and the chord from the region outside the influence of the discontinuities and weld geometry effects to the weld toe, but close enough to fall inside the zone of the stress gradient caused by the global geometrical effects of the joint (Figure 2. 7). Generally the geometric stress (or the hot spot stress) is the linearly extrapolated stress to the weld toe and can be determined by considering the stress normal to the weld toe since the orientation of the maximum principal stress is normal or almost normal to the weld toe *[1].*

The S-N curves are based on experiments in which measured strains have been extrapolated to the weld toe, so they incorporate hot-spot stress method. The type of extrapolation depends on the geometry and the mesh.

### 2.2.6. The Stress Concentration Factor

In order to determine the hot spot stress from the nominal stress in tubular joints, a stress concentration factor is applied on the nominal stress. The stress concentration factor (SCF) of the joint subjected to a particular loading condition has been obtained in experiments of numerical calculations by taking the ratio between the geometric peak stress excluding local effects, at a particular location in a joint (either in the chord or in the brace) and the nominal stress in the brace (as long as the load is applied on the brace). For the determination of the fatigue life the geometrical (peak) stress range has to be calculated for the various locations:

$$\Delta\sigma_{geom(i,j,k)} = \Sigma(\Delta\sigma_{nom(brace,j,k)} \cdot SCF_{i,j,k}) \qquad \textit{(eq. 2.4.)}$$

where:

| | |
|---|---|
| i | chord or brace |
| j | location, e.g. crown, saddle or in between for circular hollow section joints |
| k | type of loading |
| $\Delta\sigma_{geom}$ | geometrical stress range |
| $\Delta\sigma_{nom}$ | nominal stress range |

Existing parametric equations from standards are mainly based on Finite element (FE) analysis. The stress ranges determined by this approach are then used together with S-N curves that are based on welded specimens. The local weld effect is included in this S-N curve.

The SCF varies along the perimeter of a tubular joint intersection (from the saddle to the crown, see **Error! Reference source not found.**). SCF value and its variation depends on:

- the examined structural component (brace/chord),
- the location along the joint intersection (crown, saddle or somewhere between)
- joint configuration (T, Y, X, K-joint etc.),
- joint geometry (ß = diameter or width ratio between braces and chord, τ = brace- to-chord wall thickness ratio, γ = half diameter-to-thickness ratio of the chord)
- loading condition (axial, IPB, OPB, combination).

Thus, for all the potential critical locations along the perimeter of the joint, SCFs need to be determined.

In this study for the axially loaded T-joint examined, the highest SCF, according to the parametric equations, is located at the saddle point of the chord. This is clearly shown in

many literature references *([9], [10], [11], [12], [13] and [14])* that have used finite element analysis to calculate the stress distribution at the intersection of a tubular T-joint.

The SCF variation for an axially loaded T-joint according to the joint dimensions is shown graphically in Figure 2. 9(*[1],[8],[15]*). The following conclusions can be made for the saddle locations of the chord and brace:

- Generally the highest SCF occurs at the saddle position
- Highest SCFs at the saddle are obtained for medium β ratios
- SCF decrease with decreasing τ value
- SCF decrease with decreasing 2γ value

It should be noted that in the case of β ≥ 0.95, use SCFs for β =0.95 *[15].*

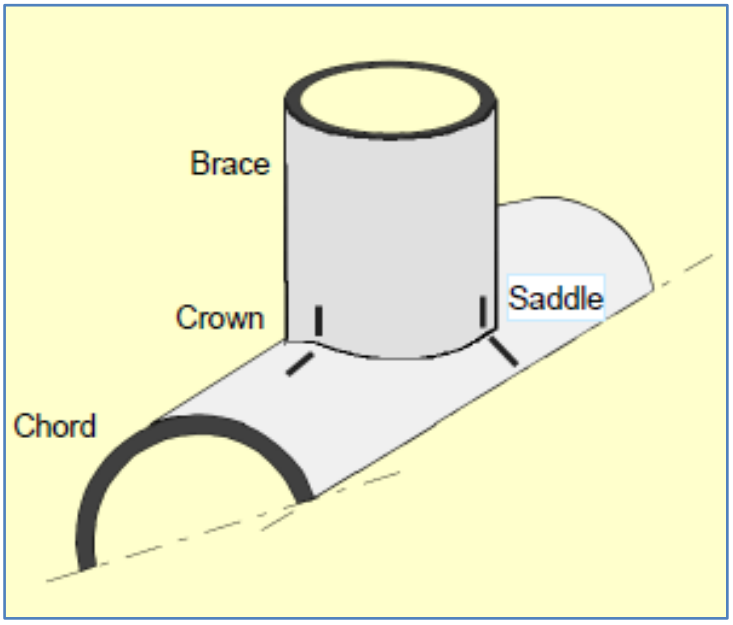


**Figure 2. 8: Locations of saddle and crpwn positions in a T-joint**

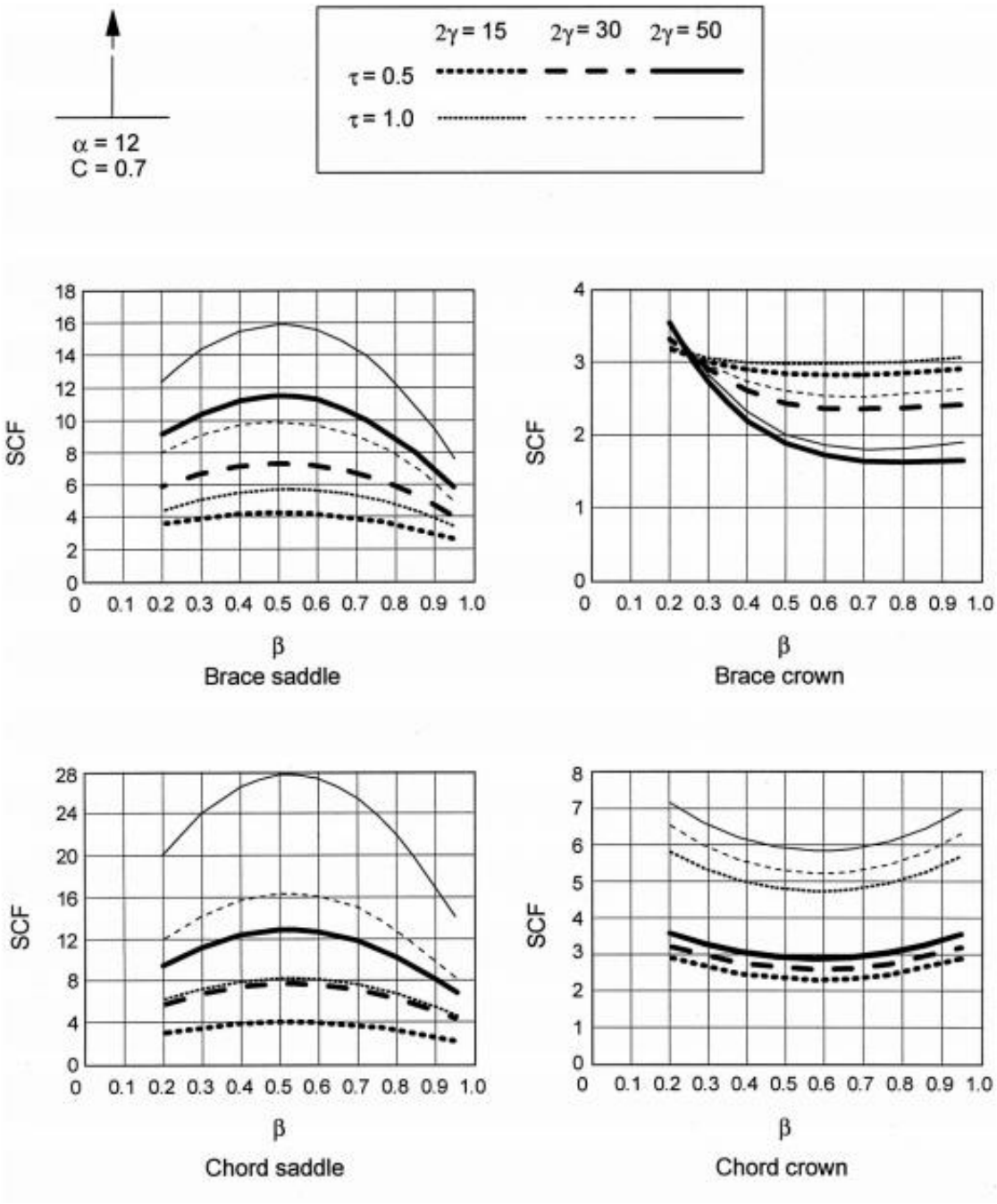


Figure 2. 9: SCF's for axially loaded T-joints *[1], [8], [15]*

## 2.3. Fracture Mechanics approach

### 2.3.1. Background of Fracture Mechanics approach

The main disadvantages of the S-N method are that it cannot be easily adapted to consider new conditions and cannot assess adequately the structural integrity of a cracked component in service. Under these circumstances it is more practical to use the fracture mechanics (FM) method which can be used for both fatigue life prediction and crack growth rates. By using FM the fatigue crack growth in an arbitrary structural detail can be calculated as well as the remaining fatigue life of a cracked structure. At present, this method is a very useful technological tool available to handle fatigue crack problems even the fact that it is more complicated than the S-N method and requires a variety of additional factors to be taken into consideration. Besides geometric aspects, material and environmental parameters as well as the load sequence effects can be taken into account by using FM.

### 2.3.2. Fatigue Crack growth under Constant Amplitude Loading

In most simple fatigue problems, the loading scenario used for fatigue analysis is simplified constant amplitude loading (CAL), where loading is represented as a sinusoidal stress-time pattern of constant amplitude and fixed frequency, applied for a specified number of cycles (Figure 2. 10).

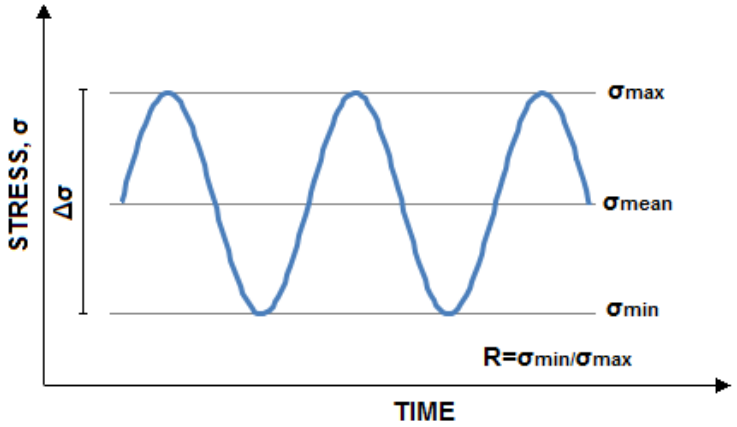


Figure 2. 10: Constant amplitude loading graphical representation

#### 2.3.2.1. Paris law

The FM approach for fatigue is based on crack growth models which give a relation between the fatigue crack growth rate (da/dN) and the stress intensity range (ΔK). A sigmoidal shape relationship is usually obtained when the logarithm of da/dN is plotted against the logarithm of ΔK (Figure 2. 11), with a linear central region where crack growth rates are best described by Paris Law:

$$\frac{da}{dN} = C(\Delta K)^m \qquad \textit{(eq. 2.5.)}$$

Where *C* and *m* are crack propagation constants

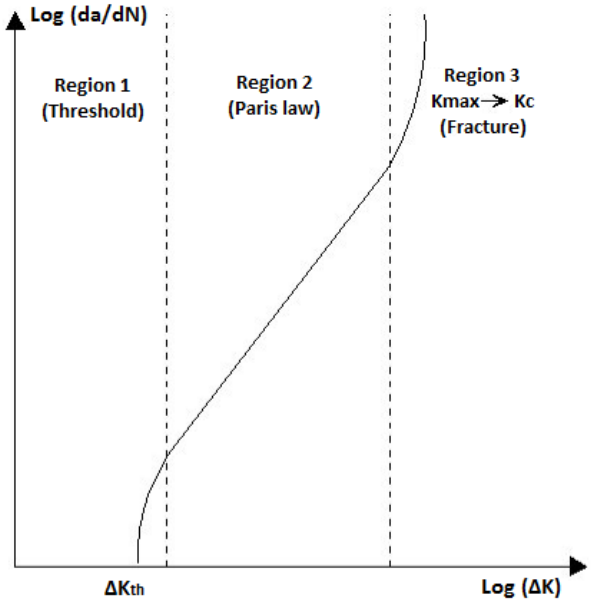


Figure 2. 11: Typical fracture mechanics fatigue crack propagation behavior

The Paris law is only strictly valid in the central region (region 2).

In region 1, there is a threshold stress intensity range, $\Delta K_{th}$, below which cracks either propagate at an extremely low rate or do not propagate at all. Knowledge of $\Delta K_{th}$ permits the calculation of permissible crack lengths and/or applied stresses in order to avoid fatigue crack growth. Above the threshold value the crack growth rate increases relatively rapidly with increasing ΔK. The $\Delta K_{th}$ may be determined in a certain value of crack growth rate. In the near threshold range (region 1) the influence of the threshold value of ΔK ($\Delta K_{th}$) can be incorporated in the relation:

$$\frac{da}{dN} = \boldsymbol{C} \cdot [(\boldsymbol{\Delta K} - \boldsymbol{\Delta K_{th}})/(\boldsymbol{1} - \boldsymbol{R})]^{\boldsymbol{m}} \qquad \textit{(eq. 2.6.)}$$

where R is the stress ratio:

$$\boldsymbol{R} = \boldsymbol{\sigma_{min}}/\boldsymbol{\sigma_{max}} \qquad \textit{(eq.2.7.)}$$

C, m and $\Delta K_{th}$ are material, environment and stress ratio R dependent parameters and independent of the geometry of the detail *[1].* $\Delta K_{th}$ is a value that indicates the situation where the crack initiates. The stress intensity factor is very crucial for a FM approach and is described in the next section.

#### 2.3.2.2. The Stress Intensity Factor

The stress intensity factor (SIF, K) is a measure for the magnitude of the stresses near the crack tip. The SIF can be separated in 3 different modes in accordance with the relationship between the directions of applied load, crack plane and growth direction. Mode I applied load perpendicular to the crack plane and growth direction. Mode II applied load parallel to the crack plane and the crack growth direction. Mode III applied load parallel to the crack plane and perpendicular to the growth direction.

The most simple geometry is an infinite plate with a central crack of length, *2a*, subjected to a uniform stress field σ, the general form of the mode I SIF is given by equation one below:

$$\boldsymbol{K = \sigma\sqrt{\pi a}} \qquad \textit{(eq. 2.8.)}$$

Where: σ = remotely applied stress
α = half crack length

For more complicated geometries with finite dimensions the cracks are exposed to a more complex stress field and the SIF depends not only on crack dimension (α) and stress (σ) but also on a geometry depending parameter (Y). SIF solutions in these cases must include various correction functions to account for boundary effects due to the mode of loading and the geometries of both the specimen and the crack. This leads to a stress intensity factor solution, which can be expressed as:

$$\boldsymbol{K = Y\sigma\sqrt{\pi a}} \qquad \textit{(eq. 2.9.)}$$

Where Y is called the stress intensity factor correction function, which will normally include the effect of factors such as; free front surface, finite plate width, crack geometry, non-uniform stress field, presence of geometrical discontinuity and changes in the structural restraint. Depending on the geometry and loading condition Y has to be split up in several factors (see chapter 3 of the current study).

The stress intensity range (ΔK) is the difference between the maximum SIF and the minimum SIF during a load cycle.

$$\boldsymbol{\Delta K = K_{max} - K_{min} = Y \cdot \Delta\sigma\sqrt{\pi a}} \qquad \textit{(eq. 2.10.)}$$

The stress variations for fatigue crack growth calculations have to be determined from the estimated loading during the (remaining part of the) service life.

There are some joints that make the derivation of SIF difficult due to their geometric complexity. In those analyses, well known stress intensity factor solutions for simple geometries that have quite similar stress field in the vicinity of the crack can be used with suitable correction factors. FA.FRA.M. routine *[1],* which is described further in Chapter 6*,* is based on this concept to evaluate the fatigue crack growth behavior for tubular joints.

The stresses in a welded detail can be separated in:

- Membrane stress ($\sigma_m$), being the average nominal stress across the section thickness.
- Bending stress ($\sigma_b$), being the bending part of the nominal stress across the section thickness.
- Residual stress ($\sigma_r$) across the section thickness. These stresses are self-equilibrating, $\sigma_r$ is often due to the welding or fabrication process of the detail.
- Peak stress ($\sigma_p$) including geometrical effect and local discontinuities (weld toes etc.)

The governing fatigue stresses for an as-welded structure are the nominal elastic stress ranges of the membrane stress ($\sigma_m$) and the bending stress ($\sigma_b$) at the crack location for the

uncracked geometry. The effect of the global geometry should be incorporated in the stress analysis, while the effect of the local geometry (weld shape etc.) will be incorporated in the determination of the stress intensity factor by the stress intensity concentration factor ($M_k$). The component of SIF *[ref. [1]*, $M_k$, is a function of the relative weld width, the weld dimensions and the weld type. $M_k$ is defined under the assumption of no interaction between the influence of relative weld width, the weld angle and the relative weld toe radius.

#### 2.3.2.3. British Standards 7910:2013 da/dN-ΔK curves for steel structures

BS7910:2013 guidelines *[17]* recommend fatigue crack law for steel components in air environment. More precisely it provides bilinear relationships between the mean and mean plus two standard deviations of log(da/dN) and log(ΔK) for R<0.5 (Figure 2. 12) and R≥0.5 (Figure 2. 13). These relationships are based on typical values of crack propagation constants in steel structures. In cases of welded components assessment, for conservatism reasons it is highly advised to use the upper bound (mean+2SD) values for R≥0.5 in order to allow the effect of the residual stresses.

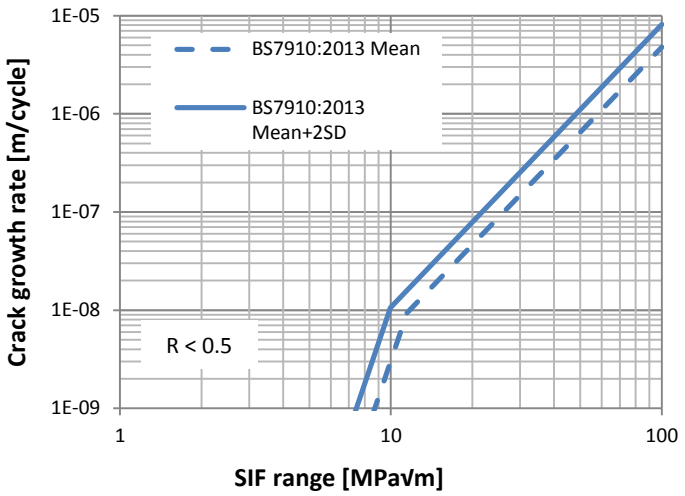


Figure 2. 12: Recommended fatigue crack growth laws according to BS7910:2013 for R<0.5

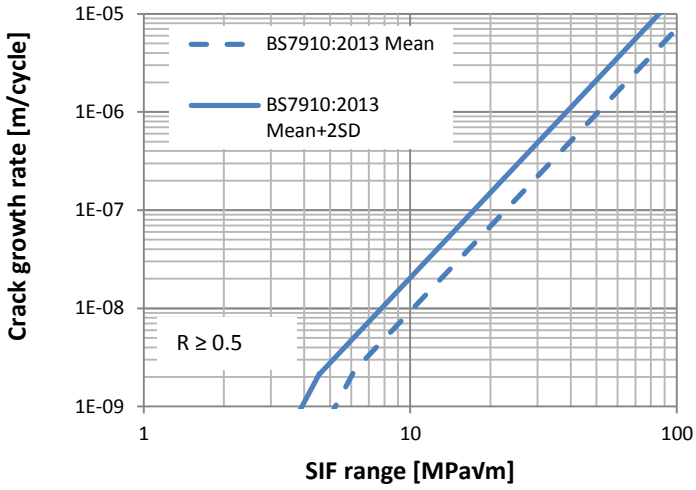


Figure 2. 13: Recommended fatigue crack growth laws according to BS7910:2013 for R≥0.5

#### 2.3.2.4. Stress ratio effect

The Paris equation states that the crack growth rate is solely determined by the SIF range. The effect of the stress ratio, R, was assumed to have a secondary effect, but there are plenty of experiments in steel specimens showing that the applied stress ratio can have an important influence on the fatigue crack growth behavior. In other words, besides the stress intensity range, ΔK, there is an influence of the relative values of $K_{max}$ and $K_{min}$, since R = $\sigma_{min}/\sigma_{max}$ = $K_{min}/K_{max}$. In accordance with numerous fatigue tests of a wide variety of steel specimens the crack growth rates at the same ΔK value are generally higher when R is more positive *[18], [19]* and *[20]*. The last mentioned statement can be verified by Figure 2. 14 and Figure 2. 15.

Figure 2. 14 comes from a study concentrated on AISI 4340 steel *[18]* and shows the fatigue crack growth of this steel material in ambient air. The data were collected from Newman, Vizzini, and Yamada (2010) and are represented in terms of Δ*K* for different *R*-ratios .

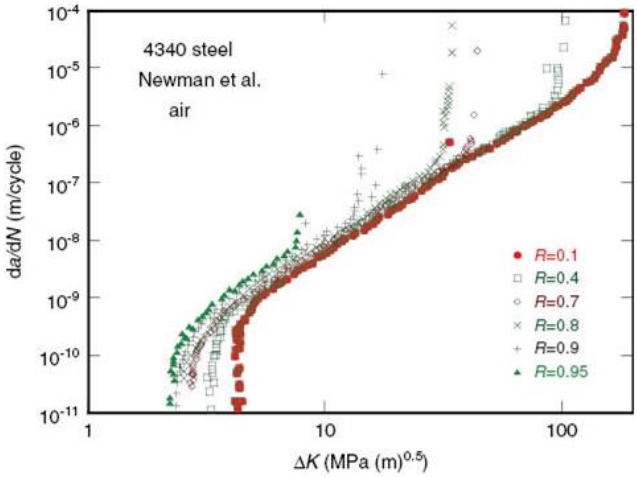


Figure 2. 14: Stress ratio effect on da/dN-SIF range curve for AISI 4340 steel *[18]*

Figure 2. 15 comes from a study regarding fatigue crack growth under variable loading *[20]* and depicts the stress ratio effect on a 350WT steel specimen.

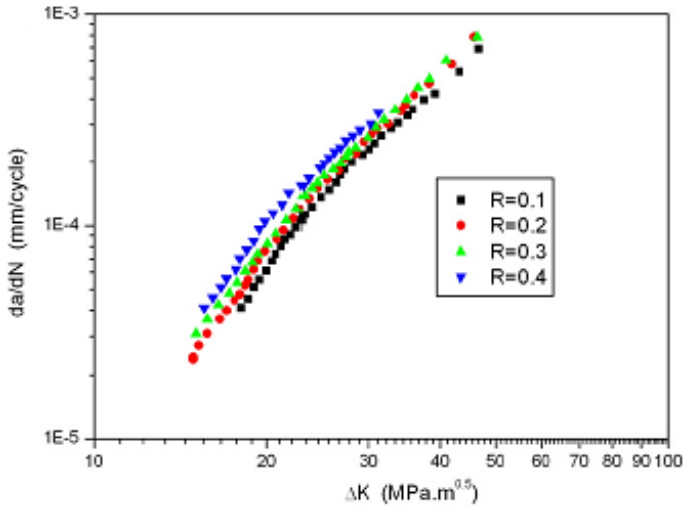


**Figure 2. 15: Stress ratio effect on da/dN-SIF range curve for 350WT steel *[20]***

It can be seen from the figures that the stress ratio effect is not so profound in steel material but surely it cannot be neglected. It is worth mentioning that in materials like aluminum R affects much more the crack growth rates.

In the past, traditionally the compressive load part of fatigue in the case of negative stress ratios was not taken into account on fatigue crack growth analysis. However, nowadays it is an accepted fact in fatigue community that compressive loads have an effect on fatigue crack growth. This effect depends on the type of specimen, the material properties and the crack length *[21], [22].* For negative stress ratios in CAL, the crack growth rate decreases as the stress ratio R becomes more negative. *(Silva 2005 [23])*

#### 2.3.2.5. Forman-Mettu approach

Unlike Paris law, the Forman-Mettu equation *[24]* describes the complete sigmoidal shape of the crack growth vs. SIF range relationship and includes the effects of stress ratios, mean stress level and other important parameters. This method follows a similar cycle-by-cycle integration method as discussed above using the sigmoidal crack growth relationship:

$$\frac{da}{dN} = C\left[\left(\frac{1-f}{1-R}\right)\Delta K\right]^n \frac{\left(1-\frac{\Delta K_{th}}{\Delta K}\right)^p}{\left(1-\frac{K_{max}}{K_c}\right)^q} \qquad \textit{(eq. 2.11.)}$$

where $N$ is the number of applied fatigue cycles, $\alpha$ is the crack length, and $C$,$n$,$p$ and $q$ are empirically derived constants, $f$ is the crack opening function for plasticity-induced crack closure (see section 2.3.3.), $\Delta K_{th}$ the threshold stress intensity range and $K_C$ the critical stress intensity factor. This approach is applied mainly on base material structures.

### 2.3.3. Constant Amplitude Loading with Overloads and Underloads

#### 2.3.3.1. Physical concepts behind the OL retardation effect

It is well known that the sequence of the load cycles may have a significant effect on the fatigue crack growth behaviour. One of the simplest and most important load sequence effects is generated by an incidental large stress peak – called overload (OL) - in a further constant amplitude loaded specimen. This large stress peak induces significant plasticity which has as a result the retardation of forthcoming crack growth rates compared with the ones during the pre-overload CAL stage *[25].* This retardation effect lasts only during a certain crack extension and can be explained by several different mechanisms. The most commonly used are listed below:

**a.** Residual stresses ahead of the crack tip
**b.** Plasticity-induced closure
**c.** Crack tip blunting
**d.** Crack branching and crack deflection
**e.** Roughness-induced closure

Some or all of these mechanisms may be introduced simultaneously in any particular instance *[26].*

In the first physical concept, an extended plastic zone ahead of the crack tip is considered to be introduced by the OL (Figure 2. 16). Residual compressive stresses are developed in this zone created by the OL and make the stress intensity ranges of the first stress cycles after the OL less effective. As a result, the corresponding crack growth rates are decreased until the sum of the subsequent crack extension and the secondary plastic zone (caused by CAL at the crack tip) has passed the extent of the primary plastic zone and the original crack growth rate has been resumed. On the basis of this mechanism an immediate reduction in crack growth rates occurs just after the OL application followed by a gradual increase *[25]*.

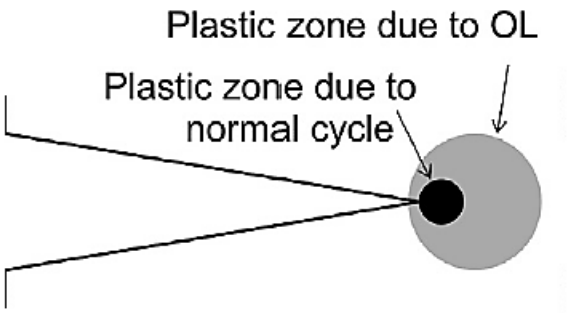


Figure 2. 16: Plastic zone at the crack tip *[25]*

In the second physical concept, a plastic wake zone is considered at the crack flanks (Figure 2. 17) that can contribute to closure. Crack growth retardation is a consequence of residual plastic elongation induced crack closure. Crack closure called the phenomenon where the crack is not fully open during the entire loading cycle which means that the minimum stress of the applied CAL is lower than the opening stress. The crack closure leads to an increase in the stress needed to re-open the crack in subsequent cycles after the OL compared to the

crack opening stress at an equivalent constant amplitude load before the OL application. The larger crack opening stress reduces the effective stress intensity range ($\Delta K_{eff}$) and thus decreases the crack growth rate. $\Delta K_{eff}$ value is expressed by the following formula:

$$\boldsymbol{\Delta K_{eff} = K_{max} - K_{op}} \qquad \textit{(eq. 2.11.)}$$

Where: $K_{max}$: the maximum value of stress intensity facton in CAL
$K_{op}$ : the stress intensity factor that corresponds to opening stress

The effect of the plastic wake created by the OL fades as the distance between the crack tip and that plastic wake increases until the crack opening stress at the constant amplitude load has been re-established *[25]*.

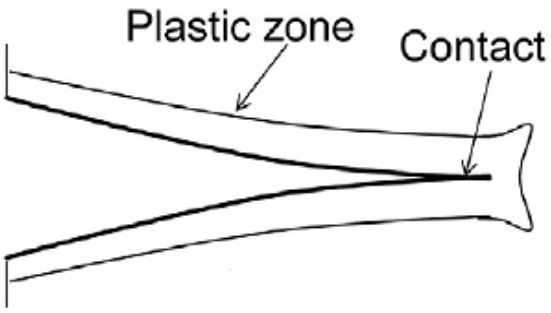


Figure 2. 17: Crack closure model *[25]*

To have a better evaluation of OL effect in terms of plasticity induced crack closure the U-value, which represents the plasticity induced crack closure, is calculated:

$$\mathbf{U} = \frac{\mathbf{\Delta K_{eff}}}{\mathbf{\Delta K}} \qquad \textit{(eq. 2.12.)}$$

The pre-overload and post-overload stress intensity ranges that correspond to the lowest measured crack growth rate after the OL application are defined as $\Delta K_{eff}$ and $\Delta K$ resepectivelly. The procedure of defining the aforementioned values to derive U is depicted in the example of a da/dN-ΔK curve for a steel specimen (Figure 2. 18).

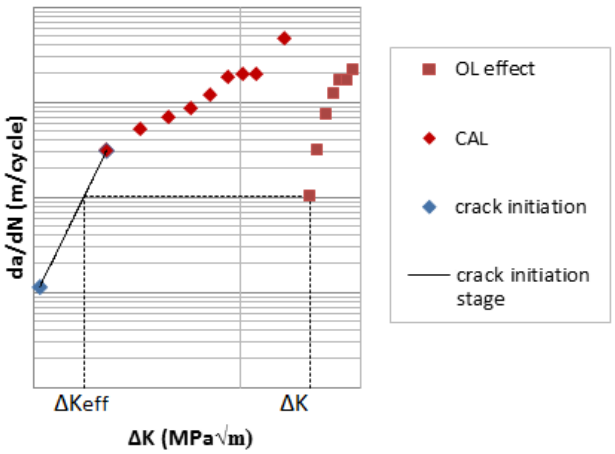


Figure 2. 18: ΔKeff projection in da/dN-ΔK curve of a bead weld on a plate specimen (BP351)

The projection of the lowest crack growth rate on the pre-overload $\Delta K_{eff}$ should take into account the crack initiation stage where the examined crack growth rate could be located (as in Figure 2. 18).

Crack tip blunting (Figure 2. 19) is a mechanism that pertains to the changes in the geometry of the crack tip and causes crack growth retardation. The crack tip re-sharpening is a necessary condition to overcome retardation effect. Retardation is supposed to be equal to the initiation period of the new crack in the less sharp rounded original crack tip. According to this concept, a crack arrest can be occurred lasting for a limited period until renewed initiation restarts *[25],[26].*

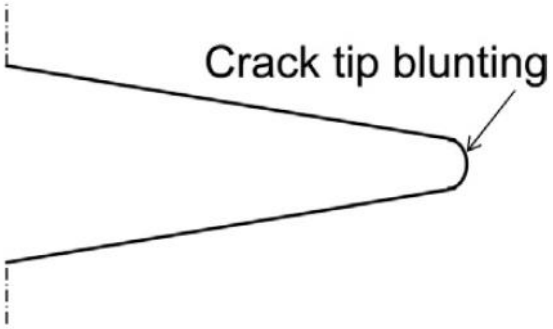


**Figure 2. 19: Crack tip blunting *[25]***

Crack tip branching (Figure 2. 20) and deflection are crucial mechanisms for materials with significant planarity of slip and can be enhanced by certain environmental conditions or microstructures. This mechanism has a strong influence on the crack tip driving force *[26]*.

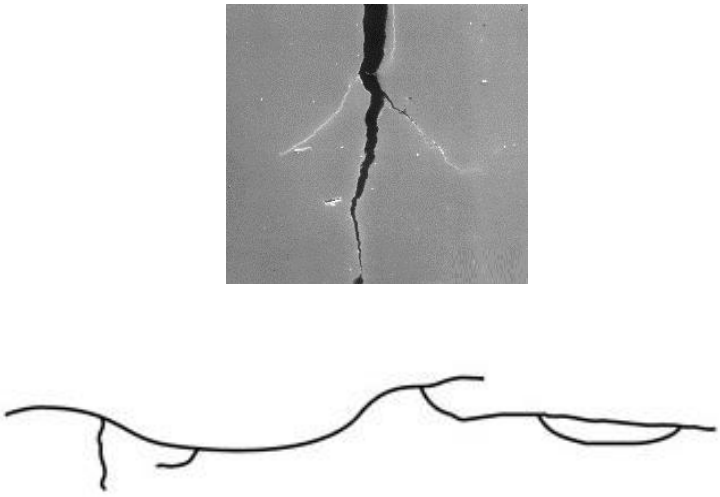

**Figure 2. 20: Crack branching cases**

Roughness induced closure is a mechanism related to fracture surface roughness and arises from crack path tortuosity and hence it is an important factor in planar slip materials. It can be claimed that materials with a significant faceted mode of crack growth near the threshold region or a tortuous crack path can present more profound retardation effect due to this mechanism *[22]*.

In cases of delayed retardation (where the lowest crack growth rate is not reached immediately after OL) either plasticity or roughness induced crack closure is the dominant mechanism, otherwise one of the remaining ones presented above should be selected as dominant *[26]*. The delayed retardation occurs because of factors behind the crack tip (roughness or plasticity induced crack closure is dominant mechanism). Since overload plasticity must occur ahead of the crack tip, plasticity induced closure does not manifest until the crack moves forward and the OL plastic zone is its wake *[26]*.

#### 2.3.3.2. Overloads and other load sequence effects

The repetitive application of overloads with a short recurrence period can result in almost regular crack growth curve with a much lower overall crack growth rate compared to the same load sequence without overloads. Retardations still occur, but they are superimposed on each other: this is, in fact, highly effective in slowing down the overall crack growth (see Figure 2. 21).

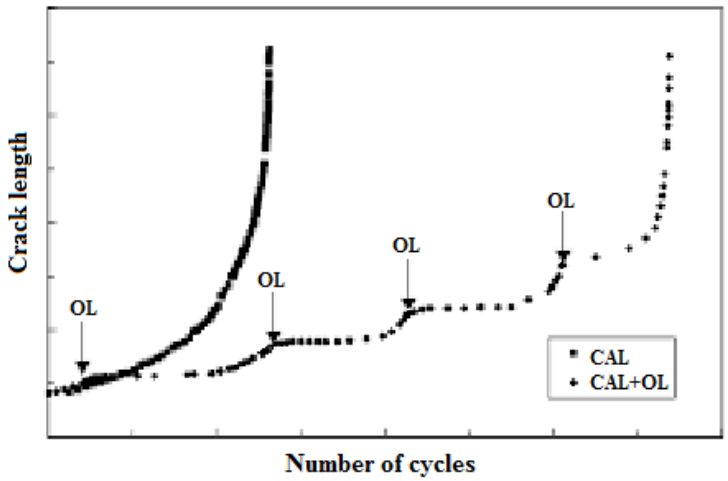


Figure 2. 21: OL's application with short re-occurrence

Theory for crack growth retardation originally comes from the aerospace industry, where particularly in the aluminum structures the effects of overloads are significant.

In contrast with an overload, when a deep stress valley – called underload (UL) – is interspersed in constant amplitude loading, the crack growth rate following the underload is shown to be higher than that of the constant amplitude load. The acceleration effect is smaller compared to the OL retardation effect but cannot be neglected.

Three load sequences, which have a significant effect on the fatigue crack growth rate, are a tensile overload (OL, exceedance yield), a compressive underload (UL) and a tensile OL

followed by a compressive UL (OL/UL), which are commonly referred to as crack retardation, crack acceleration and reduction in crack retardation, respectively *[27]*.

The interaction of the above-mentioned simple loading cases is strongly affected by the load sequence of these incidental loads. If an underload immediately follows an overload, the amount of retardation - compared to that of a single OL - is reduced but not omitted. On the other hand, a compressive underload applied prior to overloading (UL/OL) has a very slight crack retardation effect *[27].* According to Taheri et al. (2003) the majority of the fatigue models neglect crack acceleration because of the dominance of crack retardation.

These interactions, which are highly dependent upon the loading sequence, make variable amplitude loading much more complicated than constant amplitude loading. Another factor which makes the situation more complex is that the load sequence must be known so that the correct order may be applied during analysis. However, in reality, variable amplitude loading is difficult to predict.

### 2.3.4. Fatigue Crack Growth under Variable Amplitude Loading

Although CAL does occur in practice in civil engineering structures, the vast majority of loaded structures actually are subjected to variable amplitude loading (VAL). VAL sequences can be classified in the following categories: (i) repetitive cyclic stresses, (ii) semi-random or (iii) completely random loading sequences. The majority of structures' load sequence is not completely random in nature but rather semi-random. For instance the load sequence on an offshore wind turbine is semi-random because it depends upon waves and wind that are different from month to month and location to location. For this reason they are semi-random because high loads are clustered in certain periods (storms) rather than randomly scattered throughout the stress-time history *[27].*

From a structural point of view, crack growth in structures is a function of the stress range, stress ratio, frequency and the random nature of the load. The assessment of the behaviour of structure subject to variable amplitude loading (VAL), see Figure 2. 22, is more complex than when subjected to constant amplitude loading. As a result, numerous models for VAL have been developed and suggested over the past few decades, but no universal model exists yet *[20], [27].*

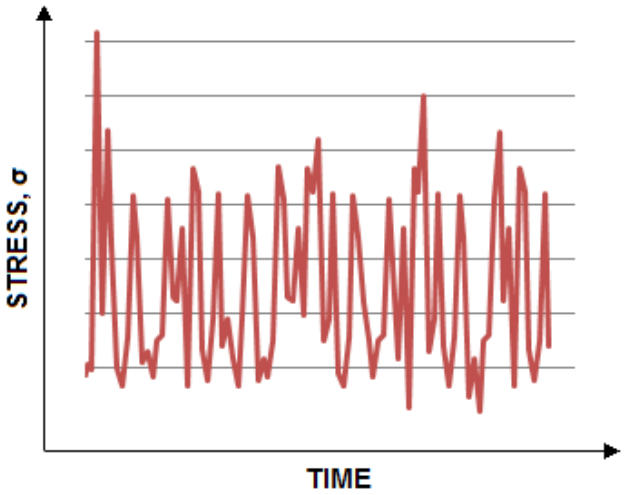


Figure 2. 22: Example of variable amplitude loading

During VAL, various load interactions occur which may significantly alter the growth behavior of a crack. In a VAL scenario, stresses of differing magnitude occur and affect the crack growth rate depending upon their sequences. A representative example of load sequence effect is presented in section 2.3.3 regarding the difference effect of an OL/UL compared to an UL/OL.

The simplest approach to fatigue crack growth for variable amplitude loading is to ignore all sequence effects and determine the crack growth on a cycle-by-cycle basis in conjunction with a constant amplitude fatigue crack growth law. The advantages of this approach are that it is relatively simple, inexpensive and not very time consuming. If it has been previously determined that the load sequencing effects may cancel each other or are entirely unpredictable, this may be the best method to use because nothing would be gained by conducting a more detailed analysis *[28].* However, in cases of variable loading with abrupt loading changes and irregularities this simplification is not recommended.

Another method that can be used to predict the crack growth behavior in VAL *[25]* is the calculation of the average crack growth rate for a VAL spectrum, $da/dN_{average}$, by subdividing each recorded crack increment by the number of stress cycles required to that increment. These average crack growth rates are functions of the correspondent equivalent stress intensity ranges, $\Delta K_{eq}$ which are equal to:

$$\boldsymbol{\Delta K_{eq} = Y \cdot \left(\frac{\sum_i N_i \Delta \sigma_i^m}{\sum_i N_i}\right)^{1/m} \cdot \sqrt{\pi \alpha}} \qquad \textbf{(eq. 2.12.)}$$

Where $\Delta\sigma_i$ and $N_i$ are the individual stress ranges and corresponding number of cycles in the spectrum and m comes from the lower part of the mean regression line of constant amplitude loading crack growth rate tests. The selected cycle counting method for the VAL spectrum is the rainflow method. Even the fact that the different stress ranges are taken into account in this method, the load sequence effects remain neglected. A variety of models have been proposed to incorporate the effect of load sequences in a cycle by cycles crack growth analysis. The Willenborg (generalized or modified version) and the Wheeler models are some of them that are based on the concept of plastic zone in front of the crack while state space model relies on the concept of crack closure due to plastic zone in the wake of the crack.

## References


**[1]** J. Wardenier, J.A. Packer, X.-L. Zhao, G.J. van der Vegte Hollow sections in structural applications (2010)

**[2]** Offshore Technology Report 2001/083, Comparison of fatigue provisions in codes and standards, Prepared by Bomel Limited for the Health and Safety Executive (2001)

**[3]** Nussbaumer, L. Borges, L. Davaine - Fatigue Design of Steel and composite structures (2012)

**[4]** Recommended Practice DNV-RP-C203 Fatigue Design of Offshore Steel Structures (2012) – Det Norkse Veritas

**[5]** X.-L.Zhao, J.A.Packer – Recommendations of IIW Subcommission XV-E – 52nd Annual Assembly (Lisbon, June 1999)

**[6]** Recommended Practice for Planning, Designing and Constructing Fixed Offshore Platforms – Working Steel Design (API RP 2A-WSD) 2007 edition

**[7]** J.A.Packer, A.Willibald – Survey of support structures for Offshore Wind Turbines (20060 – Tubular Structures XI)

**[8]** European Steel Design Education Programme WG12

**[9]** K. Hellier, M.P. Connolly, W.D. Dover – Prediction of the stress distribution in tubular Y- and T- joints (1990) – Int. Journal of Fatigue No1, pp 25-33

**[10]** E. Chang, W.D. Dover - Prediction of stress distributions along the intersection of tubular Y and T-joints (1999) - International Journal of Fatigue 21 (1999) 361–381

**[11]** M.F.Ghanameth, D.Thevenet, A.Zeghoul – Stress Concentration in Offshore Welded Tubular Joints Subjected to Combined Loading (2004) – J. Material Sci. Technol., Vol.20 Suppl.1

**[12]** M. Haghpanahi, H. Pirali - Hot Spot Stress Determination for a Tubular T-Joint under Combined Axial and Bending Loading (2006) - IUST International Journal of Engineering Science, Vol. 17, No.3-4, 2006, Page 21-28

**[13]** N'Diaye, S. Hariri, G. Pluvinage, Z. Azari - Stress concentration factor analysis for notched welded tubular T-joints (2007) - International Journal of Fatigue 29 (2007) 1554–1570

**[14]** N'Diaye, S. Hariri, G. Pluvinage, Z. Azari - Stress concentration factor analysis for welded, notched tubular T-joints under combined axial, bending and dynamic loading (2009) - International Journal of Fatigue 31 (2009) 367–374

**[15]** X.-L.Zhao, S.Herion, J.A.Packer, R.S.Puthli, G.Sedlacek, J.Wardenier, K.Weynand, A.M.van Wingerde, N.F.Yeomans – Design Guide for Circular and Rectangular Hollow Section Welded Joints under Fatigue Loading (2001) – Construction with Hollow Steel Sections CIDECT 8

**[16]** O.D. Dijkstra, H.H. Snijder, H.J.M. van Rongen - Assessment of the remaining fatigue life of defective welded joints (1990) - IABSE reports

**[17]** BS 7910:2013 - Guide to methods for assessing the acceptability of flaws in metallic structures - BSI Standards Publication

**[18]** K. Sadananda, A.K. Vasudevan - Crack growth behavior of 4340 steel under corrosion and corrosion fatigue conditions - Corrosion Reviews Volume 33, Issue 6 (November 2015)

**[19]** C.S. Kusko, J.N. Dupont, and A.R. Marder – Influence of Stress Ration on Fatigue Crack Propagation Behavior of Stainless Steel Welds – Welding Journal 59-S – 64-S (February 2004)

**[20]** H.Xiaoping, T.Moan, C.Weicheng - An engineering model of fatigue crack growth under variable amplitude loading - International Journal of Fatigue 30 (2008) 2–10

**[21]** F.S. Silva - Fatigue crack propagation after overloading and underloading at negative stress ratios - International Journal of Fatigue 29 (2007) 1757–1771

**[22]** X. Qian, S. Swaddiwudhipong, C. T. Nguyen, Y. Petchdemaneengam, P. Marshall, Z. Ou - Overload effect on the fatigue crack propagation in large-scale tubular joints (2012) - Fatigue Fract. Engng. Mater. Struct. 36, 427–438

**[23]** F.S. Silva - The importance of compressive stresses on fatigue crack propagation rate - International Journal of Fatigue (2005) 27:1441–52

**[24]** M. Koçak, S. Webster, J.J. Janosch, R. A. Answorth, R. Koers - FITNET Fitness-for-Service – Vol.1 Procedure (2010)

**[25]** J.Maljaars, R.Pijpers, H.Slot – Load sequence effects in fatigue crack growth of thick-walled welded C-Mn steel members – International Journal of Fatigue 79 (2015) 10-24

**[26]** K.Sadananda, A.K.Vasudevan, R.L.Holtz, E.U.Lee – Analysis of overload effects and related phenomena – International Journal of Fatigue 21 (1999) S233-S246

**[27]** F. Taheri, D. Trask, N. Pegg - Experimental and analytical investigation of fatigue characteristics of 350WT steel under constant and variable amplitude loadings - Marine Structures 16 (2003) 69–91

**[28]** M.Janssen, J.Zuidema, R.J.H.Wanhill – Fracture Mechanics – Second Edition 2002

# 3. 4-POINT BENDING TESTS

## 3.1. Introduction

This chapter describes the experimental procedure of 4-point (pure) bending (4PB) tests on small-scale steel strip specimens (Figure 3. 1) as well as the analysis and the interpretation (in accordance with fracture mechanics principles) of the results that have been generated from base material and welded steel specimens. From the interpretation procedure of these small-scale specimens the crack propagation constants C, m of Paris law $\left(\frac{da}{dN} = C\Delta K^m\right)$can be obtained.

Unlikely to S-N curves that give information only for the failure situation of a specimen, the fracture mechanics approach provides also data regarding crack growth during the whole propagation stage and it is applied in this study in order to provide a fatigue crack growth prediction. The crack propagation constants that are used for fatigue crack growth prediction on structures with complicated geometries, like tubular joints, are sometimes originated from the results of simple fatigue crack growth tests.

The main objectives of the fatigue crack growth tests are:

- the derivation of the crack growth parameters (which are material, environment and stress ratio dependent) in order to be used as an input in a numerical procedure that calculates crack growth for similar material, environment and stress ratios.

- the evaluation of load sequence effects (mainly tensile stress peaks) on the fatigue crack growth behavior of 4PB strip specimens.

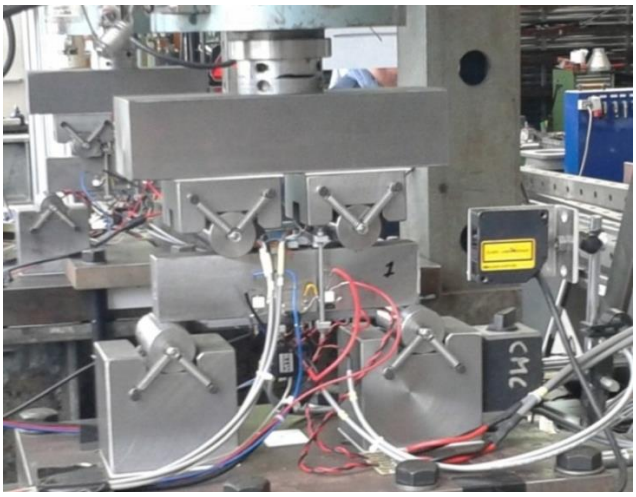

Figure 3. 1: 4PB tests in Structural Dynamics Lab of TNO

### 3.2. Test matrix

The fatigue crack growth tests were performed in a four point (pure) bending test set up (Figure 3. 1). The dimensions of the welded and the base material specimen and the positioning of rollers (that apply the force) for the 4PB test are depicted in Figure 3. 2.

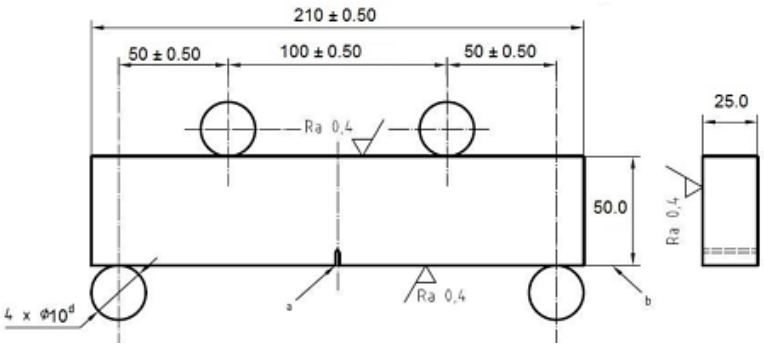


Figure 3. 2: Dimensions and support rollers positioning

Table 3. 1 provides an overview of the experimental programme where constant amplitude loading (CAL), overloads (OL), underloads (UL), and overload with a consecutive underload (OL/UL) are applied. In all CAL+OL and CAL+OL+UL+OL/UL cases, the minimum and maximum forces for a certain value of stress ratio R are equal to that of the constant amplitude apart from the loading cycles that cause discrete OL or UL where the maximum force increases or the minimum force decreases respectively. In the case of CAL, the nominal bending stress in the specimen (i.e. the stress in an uncracked specimen) is in the elastic range in all tests.

In all specimens an initial notch was milled by EDM (Electric Discharging Machining) at the middle point of the surface (for the base material specimen) and at the position of the weld toe in the heat affected zone (for welded specimens). This machined initial notch provides the onset for a straight and sharp fatigue crack and may differ at both sides of the same specimen due to machining inaccuracy.

Table 3. 1: Overview of the experimental programme

| Specimen number | Specimen type | initial notch $\alpha_i$ (mm) Side1 | Side2 | Load type | $N_{start}$ | Stress range Δσ (MPa) | Stress ratio R |
|---|---|---|---|---|---|---|---|
| **BP351** | As welded | 0.4 | - | CAL+OL | 0 | 216 | 0.1 |
| **BP352** | As welded | 0.55 | 0.55 | CAL+OL<br>CAL+OL+UL+OL/UL | 0<br>366868 | 216<br>96 | 0.1<br>0.5 |
| **BP353** | As welded | 0.70 | 0.95 | CAL<br>VAL | 0<br>366866 | 216<br>Figure 3. 34 | 0.1<br>Figure 3. 33 |
| **BM135** | Base mat. | 0.44 | 0.44 | CAL+OL<br>CAL+OL+UL+OL/UL | 0<br>210686 | 216<br>96 | 0.1<br>0.5 |
| **BM235** | Base mat. | 0.51 | 0.50 | CAL+OL | 0 | 216 | 0.1 |

In the following sections the main features of the 4PB experimental procedure are described. This procedure is executed according to the specifications of ISO 12108 (2012) *[1]*.

### 3.3. Specimens

The tested specimens are single edge notched 4 point bending (SEN 4PB) steel strip specimens derived from S355G10+M plates of nominal depth W=50mm and thickness B=25mm that are intended for use in offshore structures. S indicates the minimum yield strength in MPa which is equal to 355MPa, G followed by a maximum of two digits characterizing and indicating the steel grade within the groups 1, 2 or 3, as defined per table 4 of EN 10225 and M indicates normalizing rolling in terms of delivery condition. According to Table 5 of EN 10225, the tensile strength of the specimen varies from 470-630MPa. The chemical composition of the material of the 4PB specimens is presented on Table 3. 2.

**Table 3. 2: Chemical composition for the material of the 4PB specimen (according to Table 4 of EN10225:2009)**

| **C %** | Si % | Mn % | P % | S % | Al % | Cu % | Cr % |
|---|---|---|---|---|---|---|---|
| 0.12 | 0.15-0.55 | 1.65 | 0.015 | 0.005 | 0.015/0.055 | 0.30 | 0.20 |
| **Ni %** | **Mo %** | **V %** | **Ti %** | **Nb %** | **N %** | **B %** | **Ca %** |
| 0.70 | 0.08 | 0.060 | 0.025 | 0.030 | 0.010 | 0.0005 | 0.005 |

Base material specimens and welded specimens are tested. The base material test results are used as a reference to be compared with the corresponding results of the welded specimen in order to evaluate the contribution of the weld to the fatigue crack growth. These specimens have the same steel grade and dimensions as the welded ones and their only difference is that they have no welds (Figure 3. 3).

Bead weld on a plate specimens are tested (Figure 3. 4) which are most representative of a weld of a tubular brace to chord connection. As it can be seen in Figure 3. 4 the weld run is applied to one side of the parent material. In the Appendix A the welding procedure of this specimen is presented.

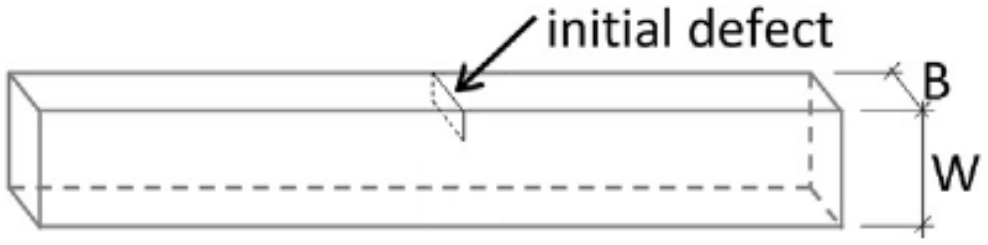


**Figure 3. 3: 4PB SEN base material specimen**

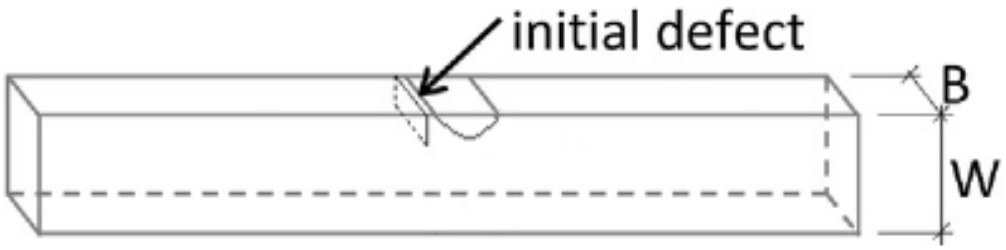


Figure 3. 4: 4PB SEN specimen with a bead weld on a plate

The initial notch is milled exactly over the fusion line of the bead weld.

### 3.4. Apparatus

Cycle to cycle variation of the peak force under CAL before crack propagation was held to ±2% of the desired peak force. The force range is also maintained within ±2% of the desired range.

Accuracy of the force measuring system is verified periodically in the testing machine. The force measuring system has been designed for tension and compression fatigue testing and possess great axial and lateral rigidity. The force transducer's capacity was sufficient to cover the range of force measured during a test.

The test fixture of the specimen has been designed to minimize frictional effects by allowing the support rollers to rotate and move apart slightly as force is applied to the specimen, hence permitting rolling contact. The support rollers are allowed to limited rotation and motion along plane surfaces parallel to the notched side of the specimen, but are initially positively positioned against stops that set the span length and are held in place by low tension springs (Figure 3. 5 and Figure 3. 6). Fixtures and rollers are made of high hardness material.

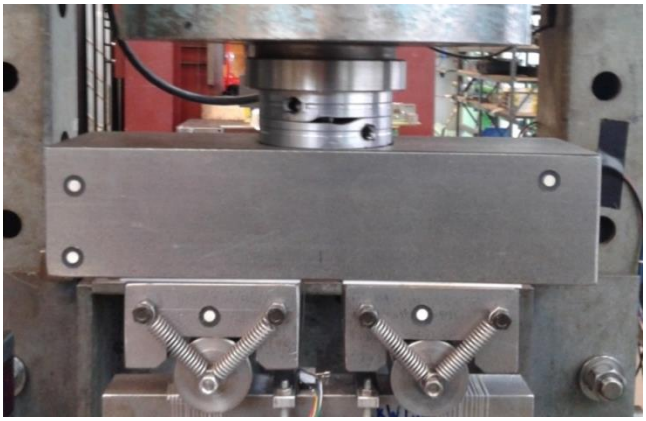

Figure 3. 5: Fixture and rollers of the upper side of the 4PB specimen

Figure 3. 6: Fixture and rollers of the lower side of the 4PB specimen

In addition, attention has been given to alignment of the testing machine and installation of the grips in the testing machine. Misalignment can cause non-symmetrical cracking, particularly for critical applications such as near-threshold testing, which in turn may lead to non-reliable data. Non-rotating joints are used to minimize off-axis motion.

For the crack growth testing, two 4PB test setups were built at the TNO Structural Dynamics Lab. Figure 3. 7 shows test rigs used for the execution of the fatigue crack growth. To obtain the correct boundary conditions in the specimen, special rolling supports and hinges were manufactured. The two test rigs have a loading capacity of 350kN.


Figure 3. 7: Test rig in the Structural Dynamics Lab

### 3.5. Data Acquisition system

A data acquisition system is used to count the applied loading cycles (Figure 3. 8). MTS MultiPurpose Testware (MPT) is used to record the force range applied by cylinders and generates the load sequence for the variable amplitude loading that is applied on the specimen. The load histories are looped and quasi-static loading is applied in between for accurate intermediate measurements (to avoid dynamic loading effects).

Figure 3. 8: System of data acquisition

### 3.6. Measuring method

For the determination of the crack depth a combination of visual and non-visual methods is applied. Crack length is monitored during the tests from initial notch size $a_i$ until final crack size $a_f$ with the corresponding number of cycles. The used non-visual method is based on crack gauge measurements. These gauges are designed to measure the progress of a crack and the rate of the crack growth in metallic specimens. The gauge is attached to the location of the initial notch.

The gauge consists of a pattern of resistor strands (grids) that are connected parallel (Figure 3. 9 -Figure 3. 10). When the gauge is bonded to a structure, progression of a surface crack through the gauge pattern causes successive open-circuiting of the strands (Figure 3. 11), resulting in an increase in total resistance. During the tests two types of crack gauges are used:

- Crack gauge that consists of 20 grid lines with spacing 0.25 mm (Figure 3. 9)

- Crack gauge that consists of 40 grid lines with spacing 0.50 mm (Figure 3. 10)

Figure 3. 9: Crack gauge consists of 20 grid lines with spacing 0.25 mm

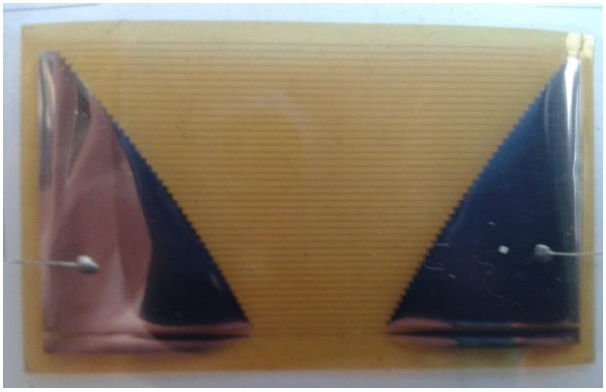

Figure 3. 10: Crack gauge consists of 40 grid lines with spacing 0.50 mm

Crack gauges are attached to both specimen sides with the grids located in a perpendicular direction in relation with the crack extension direction. An ohmmeter with milliohm sensitivity is connected and used as readout instrument in order to obtain a stepped curve of resistance against crack extension versus the applied loading cycles. Every stepped increment of crack resistance represents a grid breaking. The distance between two consecutive grid lines divided by the number of loading cycles applied for this crack extension provides the crack growth rate.

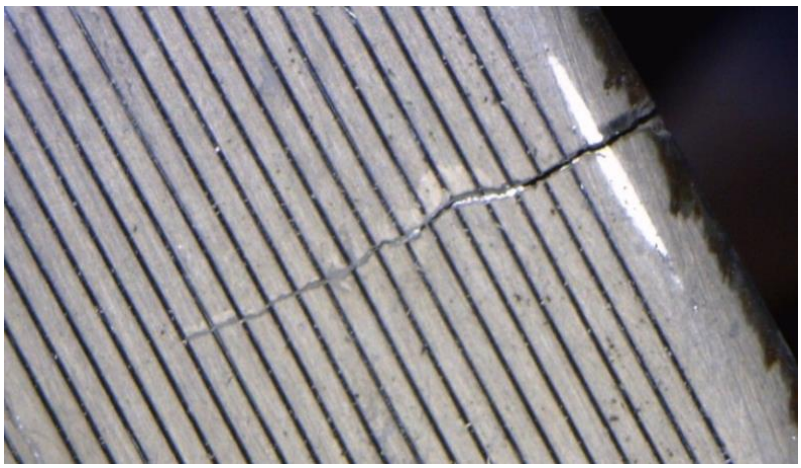

Figure 3. 11: Grid lines breaking as crack extends

The results of crack gauge measurements are validated by the use of a handheld microscopic Dino Lite type AM-413T, with magnification of 50-200x (Figure 3. 12).


Figure 3. 12: Dino camera

Allowable differences in crack depth between the two sides of the tested specimens (which can be partly justified by the differences in the initial notch size and sharpness) should not exceed the value of 0.25 of the specimen thickness otherwise the results are not considered valid *[1]*.

### 3.7. Crack growth rate vs. Stress intensity factor range Curve

The results of the experimental programme are evaluated in terms of crack depth, *a*, as a function of number of cycles, N, as well as the crack growth rate, da/dN, as a function of the stress intensity factor range, ΔK, or the effective stress intensity factor, $\Delta K_{eff}$ which has as a result the da/dN-ΔK curve. The crack growth rate and the corresponding ΔK are required for the design of da/dN-ΔK curve where a sample of this can be seen in Figure 2.10. This study is mainly focused on the crack growth data along the linear central region of da/dN-ΔK curve (Region 2).

The crack growth rate can be calculated by the procedure described in section 4.6. For the geometry considered, ΔK is calculated by the most widely used formula (Tada et al. *[2]*) for this case:

$$\Delta K = Y \cdot \Delta\sigma\sqrt{\pi a} \qquad \textit{(eq. 3.1.)}$$

$$Y = \frac{0.923+0.199(1-sin\theta)^4}{cos\theta}\sqrt{\frac{tan\theta}{\theta}} \qquad \textit{(eq. 3.2.)}$$

$$\theta = \frac{\pi a}{2W} \qquad \textit{(eq. 3.3.)}$$

$$\Delta\sigma = \frac{\frac{\Delta F}{2}\cdot(l_{in}-l_{out})/2}{B\cdot W^2/6} \qquad \textit{(eq. 3.4.)}$$

Where **α:** crack depth

**W:** specimen width (equals to 50mm)

**B:** specimen thickness (equals to 20mm)

$\mathbf{l_{out}}$ and $\mathbf{l_{in}}$**:** outer span and inner span (Figure 3. 13) differ by 100mm.

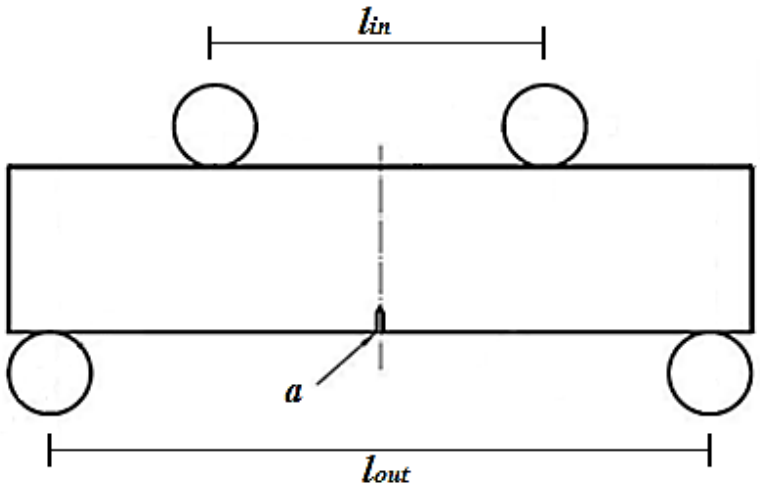


Figure 3. 13: Outer and inner length

ΔF is the force range applied through the cylinders. So the stress intensity factor for the standards specimen configuration SEN 4PB can also be calculated using the following relationship:

$$\Delta K = \frac{3 \cdot \Delta F}{B \cdot W^{1/2}} \cdot (2 \cdot tan\theta)^{1/2} \cdot \left[\frac{0.923 + 0{,}199(1 - sin\theta)^4}{cos\theta}\right] \qquad \textit{(eq. 3.5.)}$$

Equation 3.5 is valid for 0 ≤ a/W ≤ 1.

### 3.8. Loading Conditions

Specimens are tested in constant amplitude loading (CAL), with discrete overloads (OL) and underloads (UL) as well as in variable amplitude loading (VAL) generated by load sequence measurements taken from offshore wind turbine (OWT) substructures. The tests in CAL have been conducted in different stress ratios and the test frequency is 4-6 Hz. The effects of those loading conditions on fatigue crack growth behavior of the examined welded specimens are the main conclusions of this chapter.

### 3.9. Test results

The use of the test equipment that has been presented in the previous paragraphs of this chapter (digital device for elapsed loading cycles counting, crack gauges for measuring crack growth etc.) in association with the fracture mechanics equations (Tada formulas for the calculation of SIF) provides a number of data pairs that can be included in crack growth

curves (a-N) and da/dN-ΔK logarithmic scale diagram for a specific type of specimen and a certain stress ratio.

### 3.9.1. Results from CAL tests

The linear regression analysis in the data points of da/dN-ΔK diagram by setting the exponent m=3 results in the mean regression lines from where the crack growth parameter C is derived. The fixed value of m is derived from literature research *[3]* where other tests under comparable conditions (m=3 for steel and aluminium welded joints) are described. Every pair of data (da/dN, ΔK) measured in the tests is used as an input in the crack propagation equation in order to calculate the value logC which gives the crack growth parameter.

$$\boldsymbol{log\, C_i = log(da/dN)_i - m \cdot log\Delta K_i} \qquad \textit{(eq. 3.6.)}$$

The mean value of $logC_i$ has as a result the mean regression line. In eq.3.7 n is the number of data points (da/dN, ΔK) that have been gathered from the 4PB tests.

$$\boldsymbol{(logC)_m = \frac{\sum(logC_i)}{n}} \qquad \textit{(eq. 3.7.)}$$

In general terms, test results should be analyzed to produce the characteristic values (index k) that are used for design and provide a safety margin which applied to the mean values. These are values that represent 95% survival probability (i.e. 5% failure probability) calculated from the mean on the basis of two-sided tolerance limits at the 75% level.

$$\boldsymbol{(logC)_k = (logC)_m + k \cdot S_{dtv}} \qquad \textit{(eq. 3.8.)}$$

Where the standard deviation equals to:

$$\boldsymbol{S_{dtv} = \sqrt{\frac{\sum((logC)_m - (logC)_k)^2}{n-1}}} \qquad \textit{(eq. 3.9.)}$$

The factor **k** takes into consideration all the following effects *[3]*:

- variance of data
- probability distribution of the mean value by its confidence interval
- probability distribution of the variance by its confidence interval
- difference of the distribution of the whole set of data (population) and the distribution of the sample (Gaussian versus t-distribution)

Taking into account, in accordance with IIW Fatigue Recommendations *[3]*, that the probability distribution of the mean corresponds to a Student's law (t-distribution) and the probability distribution of the variance corresponds to a Chi-square's law the general formula for k is given by:

$$k = \frac{t_{(p,n-1)}}{\sqrt{n}} + \varphi_{(\alpha)}^{-1} \cdot \sqrt{\frac{(n-1)}{\chi^2_{(\frac{1+\beta}{2},\ n-1)}}} \qquad \textit{(eq. 3.10.)}$$

Where **t** = value of the two sided t-distribution (Student's law) for p=β=0.75, or of the sided t-distribution for a probability of p=(1+β)/2=0.875 at n-1 degrees of freedom.

**n** = number of test data points

**ϕ =** distribution function of the Gaussian distribution probability of exceedence of α=95% (subscript -1 indicates inverse function)

**$\chi^2$ =** Chi-square for a probability of (1+β)/2=0.875 at n-1 degrees of freedom

Because of the fact that the variance is assumed to be fixed from other tests or standard values, no confidence interval has to be considered and also the factor is given by *[3]*:

$$k = \frac{t_{(0.875,\ n-1)}}{\sqrt{n}} + \varphi_{(0.95)}^{-1} = \frac{t_{(0.875,\ n-1)}}{\sqrt{n}} + 1.645 \qquad \textit{(eq. 3.11.)}$$

The data points are gathered and projected on the graphs for a certain value of stress ratio R and a certain type of weld.

In the Figure 3. 14 and Figure 3. 15 the da/dN - ΔK curves for all the examined specimens are presented in the case of R=0.1 and R=0.5 respectively. In addition, the Figure 3. 16 - Figure 3. 19 display the da/dN – ΔK curves in the case of CAL for bead weld on a plate and base material specimens separately under fatigue loading for a stress ratio R=0.1 and R=0.5. The mean regression and characteristic lines generated by the experimental data points are also included. In the figures related to the welded specimens the fatigue crack growth laws for steel recommended by BS7910:2013 guidelines *[4]* are also illustrated. Following the recommendations of the guidelines, in case of welded specimens the values of crack propagation constants that correspond to characteristic line for R≥0.5 are used (even the fact that lower stress ratios are applied). So the blue lines in Figure 3. 14 - Figure 3. 17 depict the da/dN-ΔK curve in welded structures on the basis of BS7910:2013 guidelines.

From Figure 3. 16 and Figure 3. 17 it can be seen that the recommended BS7910 constants for welded specimens give quite reliable results in relation to the experimentally derived mean regression lines and they are a bit more conservative especially at the initial stage of crack propagation.

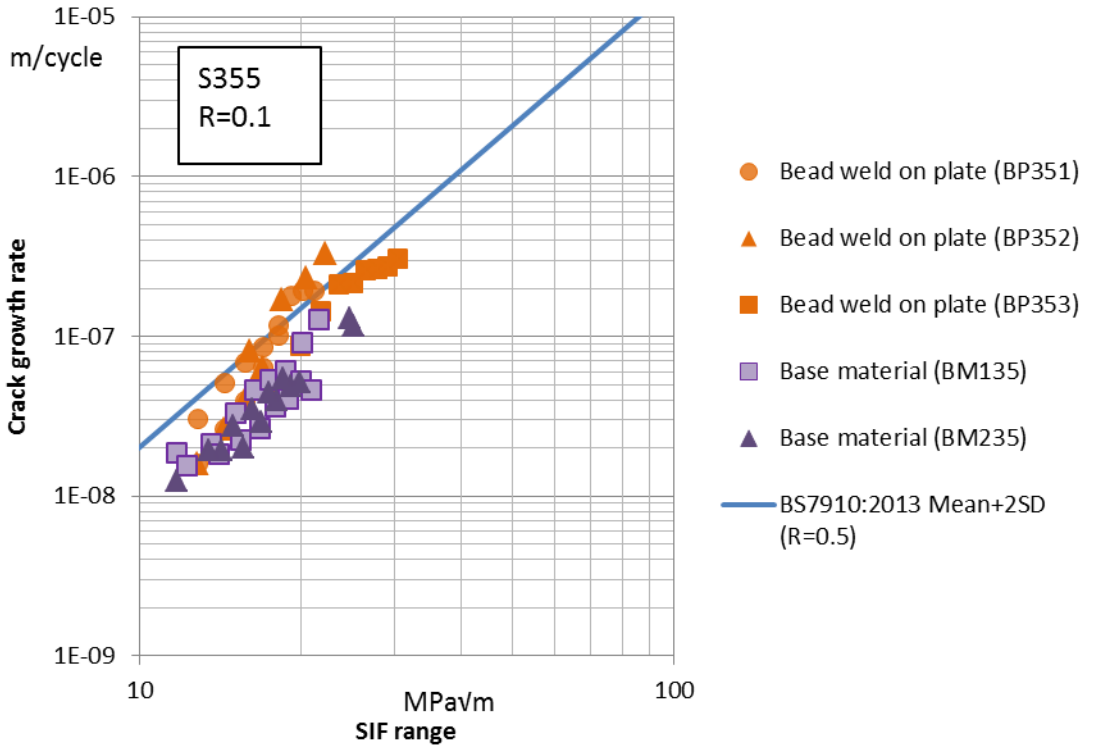


Figure 3. 14: da/dN-ΔK curve for all specimens with R=0.1

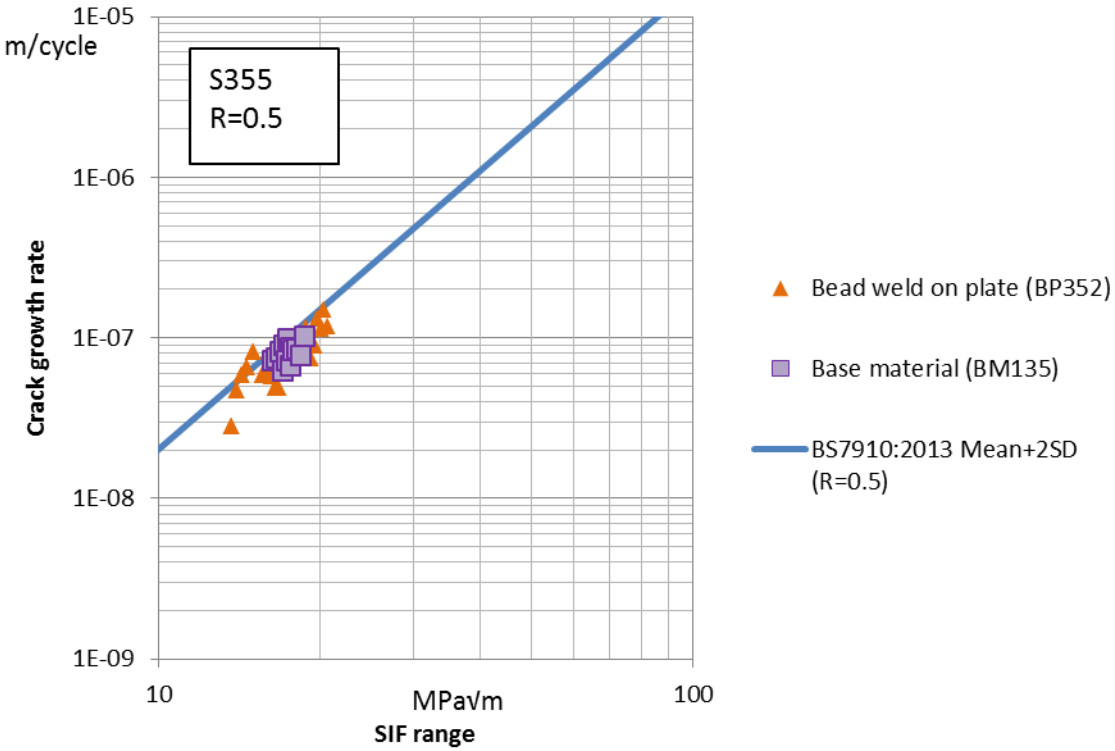


Figure 3. 15: da/dN-ΔK curve for all specimens with R=0.5

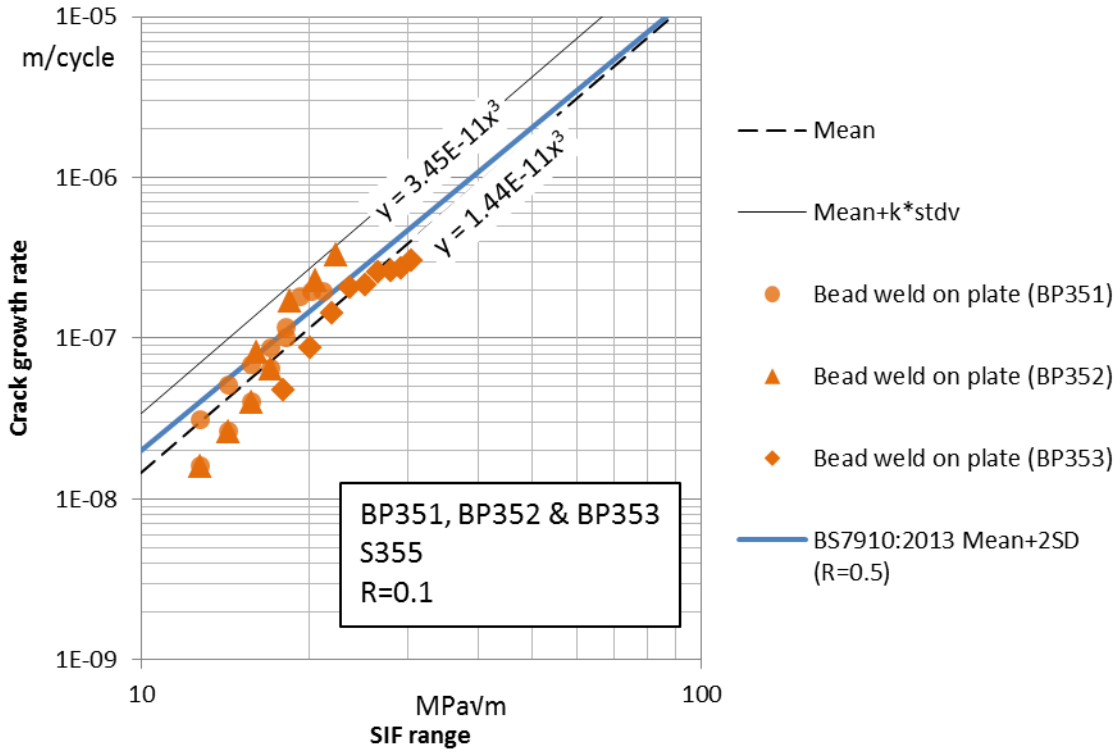


Figure 3. 16: da/dN-ΔK curve for bead weld on plate with R=0.1

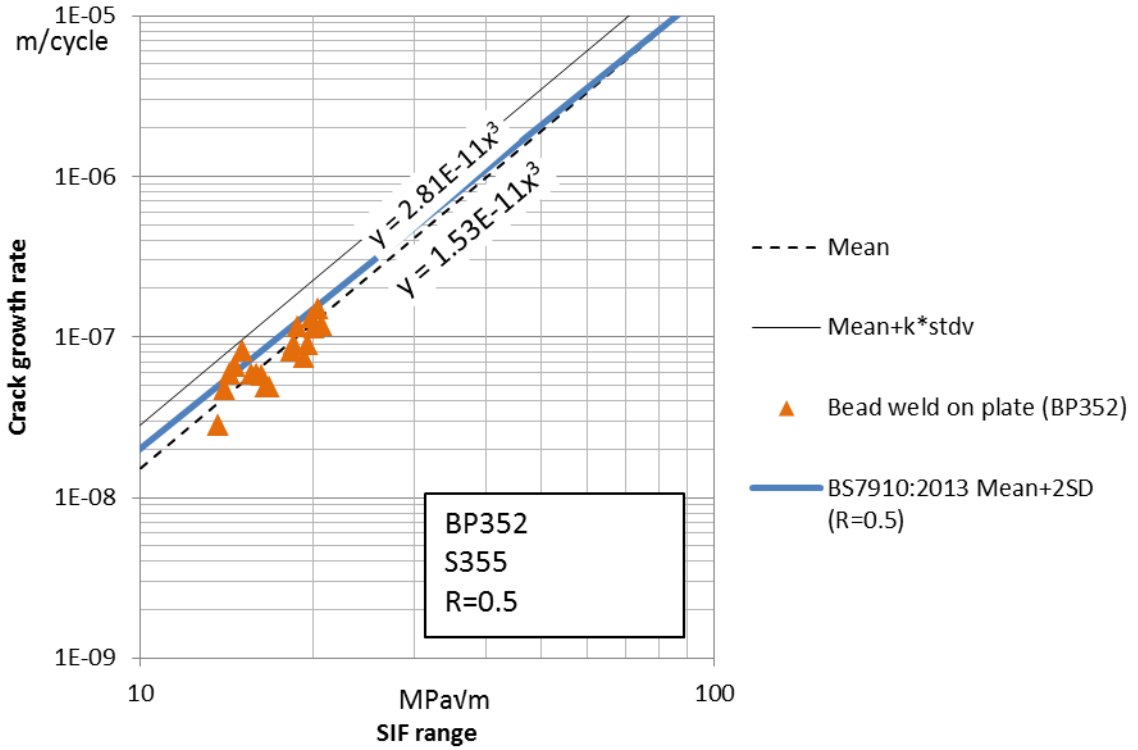


Figure 3. 17: da/dN-ΔK curve for bead weld on plate with R=0.5

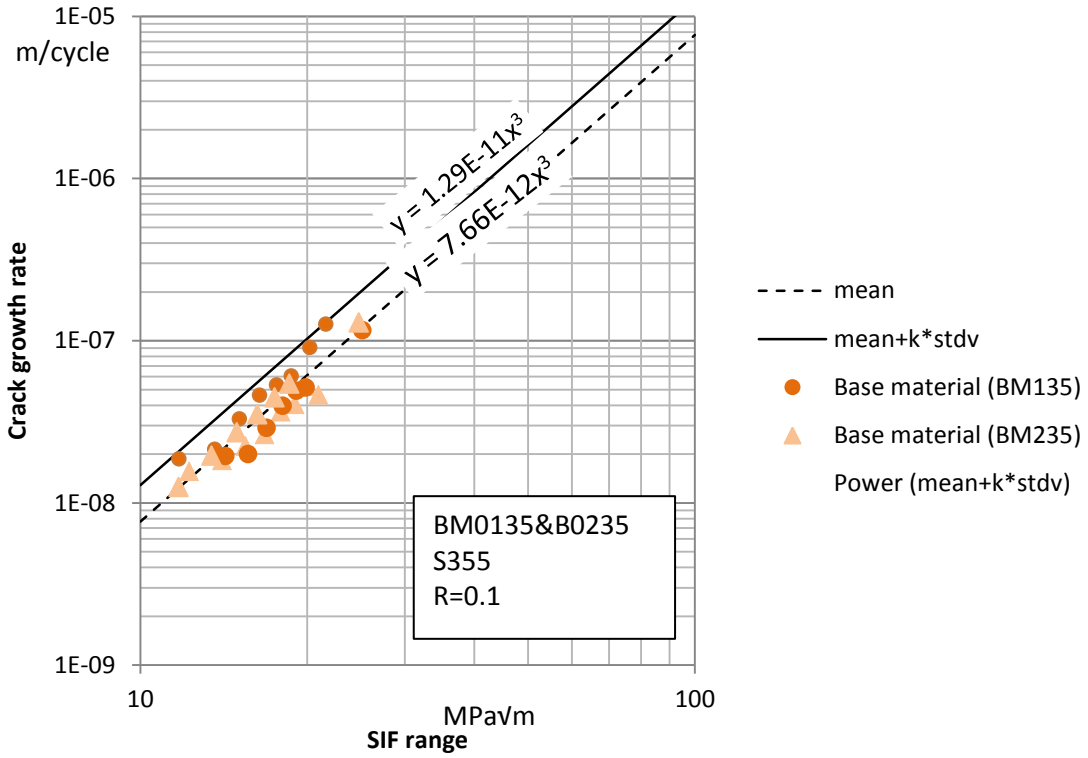


Figure 3. 18: da/dN-ΔK curve for base material with R=0.1

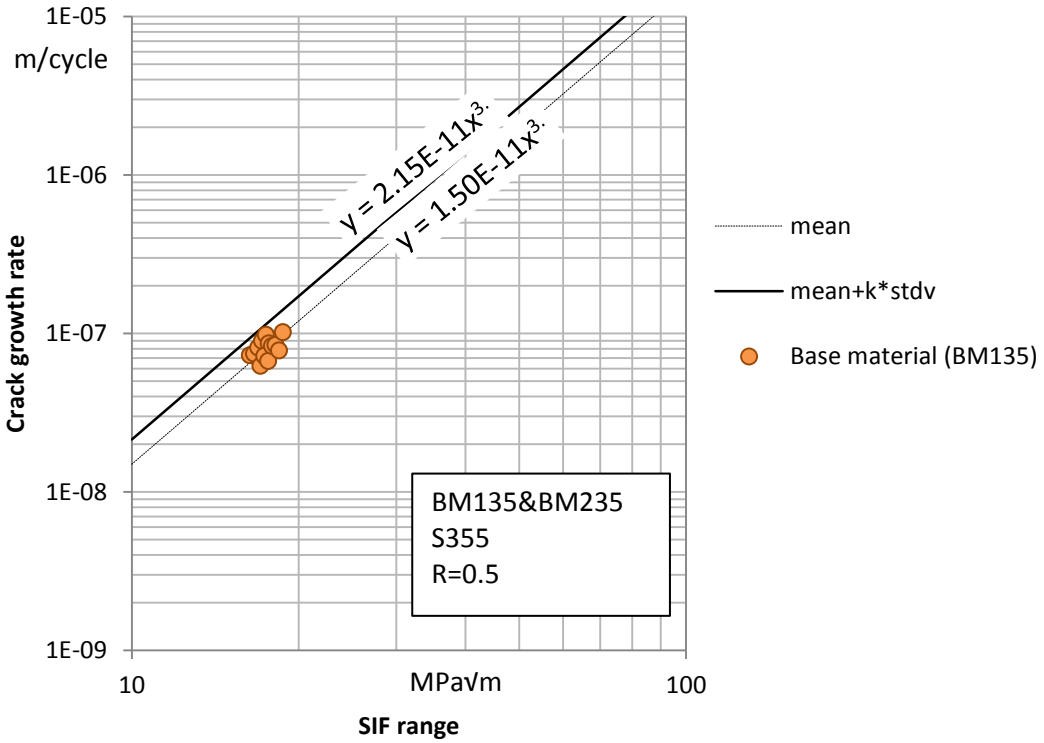


Figure 3. 19: da/dN-ΔK curve for base material with R=0.5

The crack propagations constants that have been derived from the aforementioned procedure for every examined case are depicted in Table 3. 3. The crack exponent is a fixed value equal to m=3 for the experimentally derived constants and m=2.88 according to British Standards 7910:2013 for welded and base material specimens.

The regression lines for free m values are depicted on the Appendix B. It can be seen that the use of fixed value m=3 does not lead to errors neither affects the quality of regression line. The fixed value m=3 is the recommended value for steel welded joints (IIW recommendations) and is introduced on FAFRAM model (Chapter 6).

**Table 3. 3: Crack propagation constants in certain types of specimens and stress ratios**

| Stress ratio R | Crack propagation constants | Bead weld on plate | Base material | BS7910:2013 welded specimens | BS7910:2013 base material |
|---|---|---|---|---|---|
| **0.10** | **Mean crack growth constant C [m per cycle/(MPa√m)]** | 1.44E-11 | 7.66E-12 | 2.70E-11 | 3.98E-13 |
| | **Crack growth exponent m** | 3.00 | 3.00 | 2.88 | 2.88 |
| **0.50** | **Mean crack growth constant C [m per cycle/(MPa√m)]** | 1.53E-11 | 1.50E-11 | 2.70E-11 | 5.86E-13 |
| | **Crack growth exponent m** | 3.00 | 3.00 | 2.88 | 2.88 |

The differences in crack propagation constants between welded and base material specimens are not so significant. This can be verified by the Figure 3. 20 and Figure 3. 21 where beside mean regression lines for each case their scatter band of the data is taken into account on the basis of a standard $s_{dtv}$=0.266 given by BS7910.

The limited number of data points does not allow more accurate results.

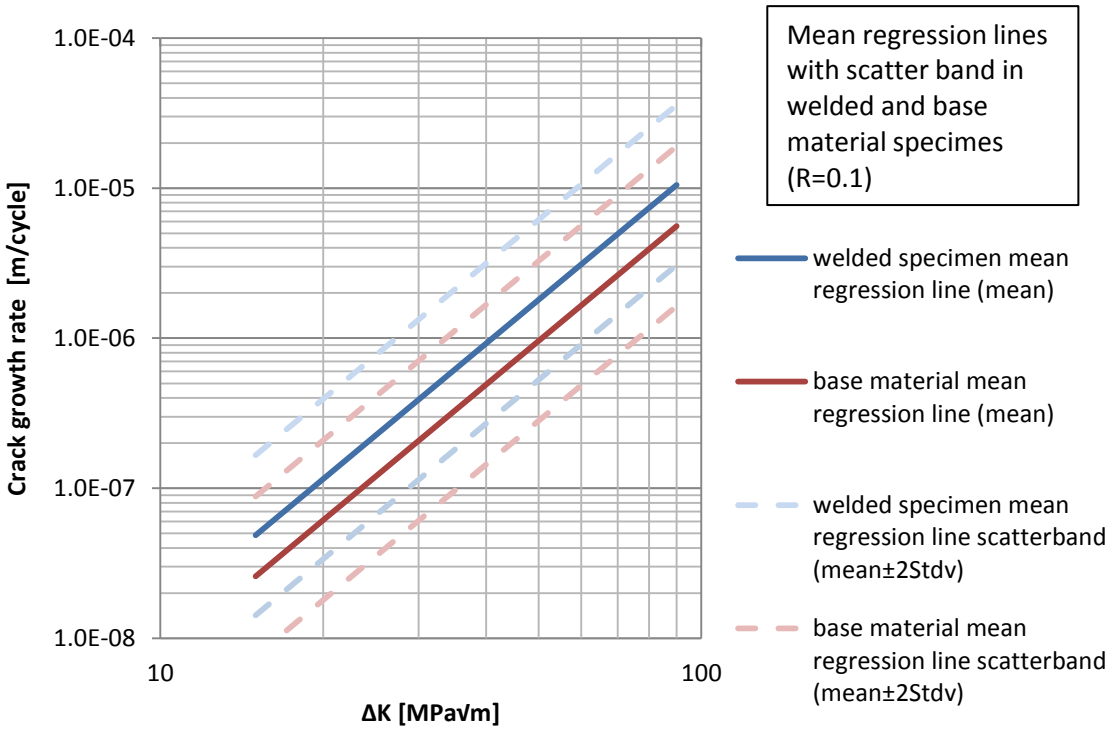


Figure 3. 20: Mean regression lines with scatter band in R=0.1

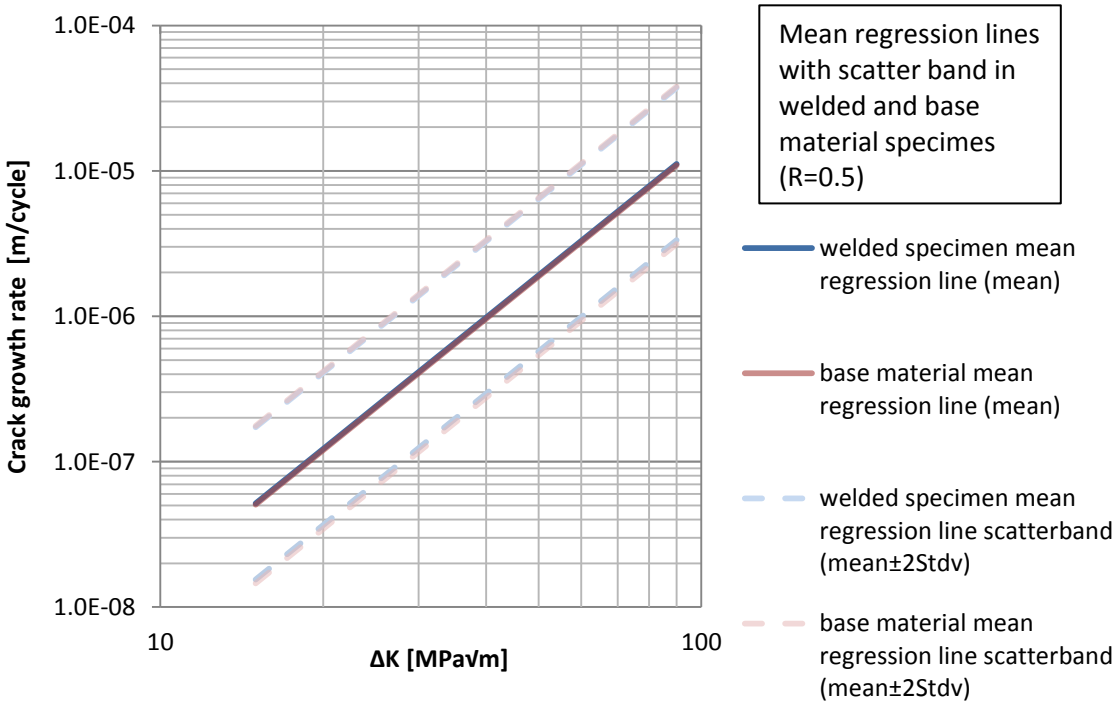


Figure 3. 21: Mean regression lines with scatter band in R=0.5

Despite the fact that experimental data points do not show significant differences in terms of crack propagation constants between welded and base material, the slight shift (depicted on Figure 3. 20) of welded specimen mean regression lines in relation with base material for R=0.1 can be explained by the differences in material microstructure (inhomogeneous welded material and heat treatment effect) and the tensile residual stresses that are developed at the heat affected zone of the bead weld *[5]*. Despite the fact that it is very complicated to quantify residual stresses in the examined case, it is considered that the residual stresses that are developed at the heat affected zone of the weld are tensile (see Appendix D *[5])*.

As it is stated in section 2.3.2.1 the crack propagation constants are mainly dependent on material, environment and applied stress ratio R. The tests results depicted on Table 3. 3 are referred on two different values of applied stress ratios (R=0.1 and R=0.5) and the same ambient air environmental conditions. At a given stress ratio the difference between the constants of welded and base material tested specimens is related to the material microstructure which in case of welded specimen permits higher crack growth rate compared to the base material. Besides material microstructure, the tensile residual stresses that are developed in welded steel (welds are not stress relieved) increase the applied tensile mean stress that in turn increases the crack growth rates compared to the base material specimens.

Another interesting remark that can be made from the crack propagation results is the effect of stress ratio R. The results in Table 3. 3 regarding base material show clearly the effect of stress ratio on crack growth rates. The increase of R leads to higher crack growth rates as mentioned before (see 2.3.2.4). On the other hand, the R-effect is not visible in case of welded specimens. A possible explanation of this could be the development of relatively high tensile residual stresses in the heat affected zone of the specimen. As illustrated in the following expressions the tensile residual stress can increase the R-value which leads to the reduction of its effect.

*In R=0.1* $R_{BM1} = \frac{\sigma_{min}}{\sigma_{max}} = 0.1$ $R_{BWP1} = \frac{\sigma_{min}+\sigma_{res}}{\sigma_{max}+\sigma_{res}} > 0.1$

*In R=0.5* $R_{BM2} = \frac{\sigma_{min}}{\sigma_{max}} = 0.5$ $R_{BWP2} = \frac{\sigma_{min}+\sigma_{res}}{\sigma_{max}+\sigma_{res}} > 0.5$

*R change* $\Rightarrow$ $R_{BM2} - R_{BM1} > R_{BWP2} - R_{BWP1}$ $\Rightarrow$

*R-effect* $\Rightarrow$ $\boldsymbol{Reffect_{BM} > Reffect_{BWP}}$

In welded specimens the real R-change is much lower than the corresponding change in base material (from R=0.1 to R=0.5) where the residual stresses do not exist. As a result, the specimen with the higher value of tensile residual stresses (namely: the bead weld on a plate specimen) will have the lower R-effect. In addition the higher yield strength of welded

specimen (compared to base material) is an additional reason for a less pronounced R-effect on welded specimens

However, in the examined case the R-effect on welded specimens seems to be almost negligible from the results of Figure 3. 21. This observation cannot be totally explained by the tensile residual stresses existence and the yield strength differences between welded and base materials. The data points of regression line of welded specimens in R=0.5 are derived in crack depths higher than the depth of welded area and this could be a possible explanation for the fact that the constants of bead weld on plate specimens are similar with those of base materials.

### 3.9.2. Results about load sequence effects

Besides the examination of CAL that leads to the derivation of crack propagation constants, some basic load sequence effects are also evaluated and verified on the basis of literature research. In this paragraph the OL effects (where the study is mainly focused) are evaluated and some additional load sequence effects are derived in order to be compared with the literature.

In the bead weld plate specimen BP351 and the base material specimen BM235 CAL with stress ratio 0.1 (24MPa-240MPa in both specimens) a single tensile overload is applied.

The overload ratio (in case of single overloads only) equals to 1.7 which means that a force peak of 170kN is provided while the minimum force remains the same with that of CAL in R=0.1 (Figure 3. 22). Overload ratio equals to the new stress peak (introduced by OL) divided by the minimum value of stress during the periodic loading.

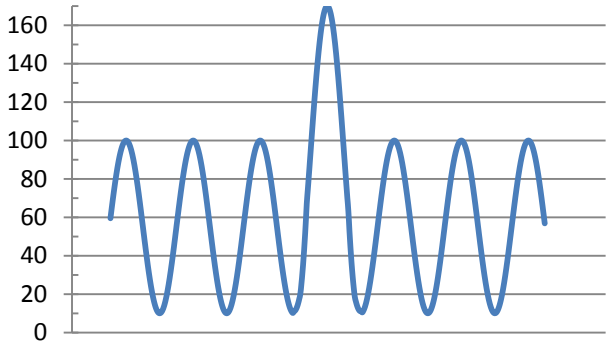


Figure 3. 22: Discrete OL application (units in kN)

In both specimens the OL is applied on the same levels of ΔK ($\Delta K_{baseline}$ equals to 21.15MPa√m for BP351 and 20.82 MPa√m for BM235). Figure 3. 23 and Figure 3. 24 present the crack growth curves for BP351 and BM235 where the OL retardation effect on crack growth can be seen clearly. In these curves the crack growth for CAL (R=0.1) before the OL, after the OL and the projected development of crack without the OL application are depicted. The retardation effect is measured in terms of delay cycles $N_d$ which is the total number of cycles involved during retardation (see Figure 3. 23 and Figure 3. 24).

The CAL crack growth curve without taking into account the OL effect is a useful tool for the evaluation of these load sequence effects in terms of delay cycles (fatigue life prolonging). The delay cycles $N_d$ caused by OL equals to the difference between the number of cycles needed to reach a certain post-overload crack growth rate and number of cycles needed to reach the same crack growth rate (after the point of OL application) without taking into consideration the OL retardation effect (Figure 3. 23 and Figure 3. 24).

Maximum crack growth rate deceleration is observed some loading cycles later than OL application point and this effect, called delayed retardation *[6]* as mentioned in the Literature Research (see section 2.3.3.1).

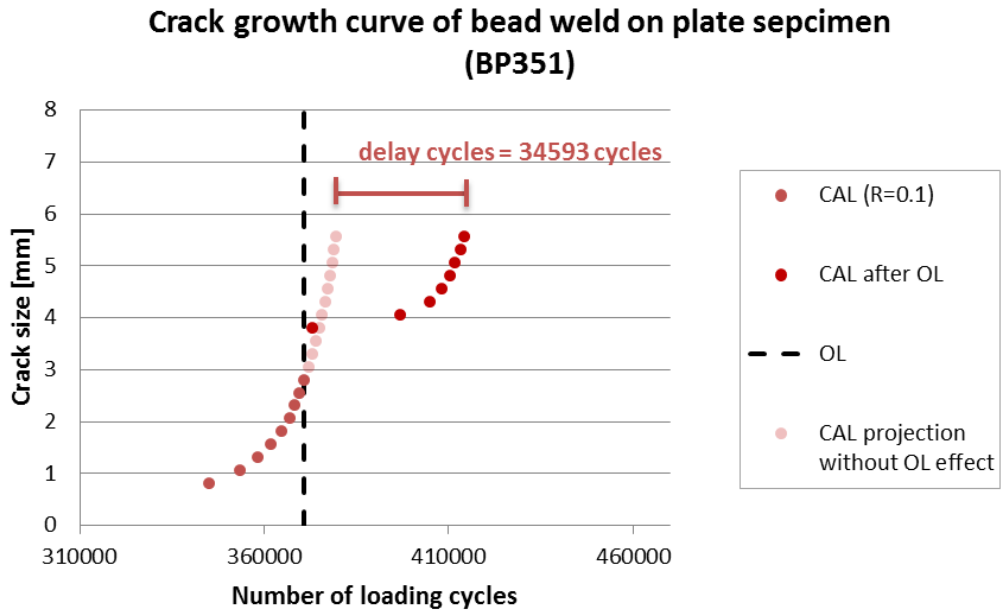


Figure 3. 23: Crack growth curve of welded specimen where the delay cycles depicted

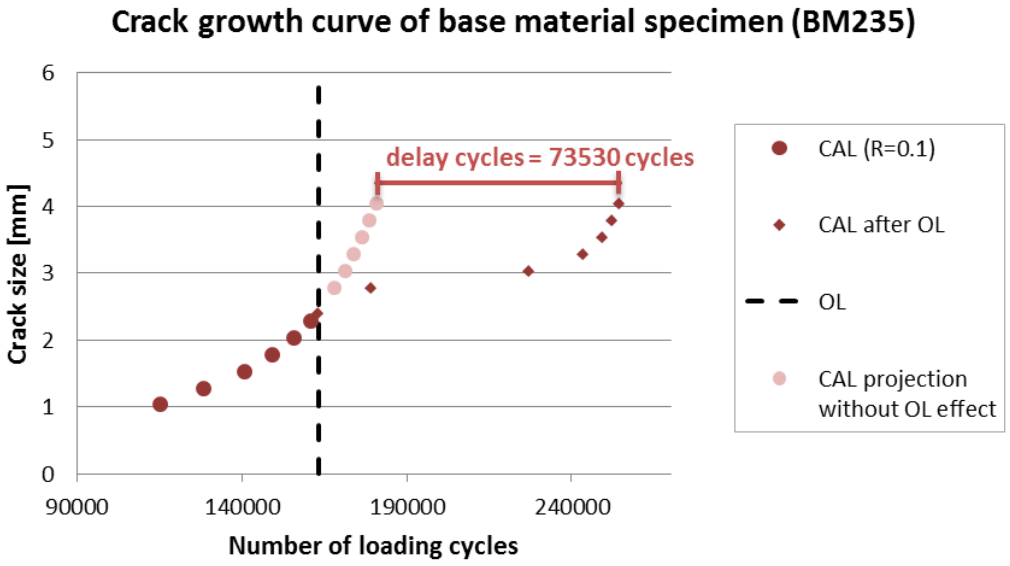


Figure 3. 24: Crack growth curve of base material specimen where the delay cycles depicted

Appendix E presents in a more detailed how the number of delay cycles $N_d$ is calculated by the use of crack growth curves. The CAL crack growth curve without taking into consideration the OL effect is projected on the basis of Paris law using the crack propagation constants derived from da/dN-ΔK mean curves.

The total number of loading cycles applied to cause the measured crack extension is dependent on the initial notch size and shape which differs in these two cases and mainly affect the crack initiation stage. However the initial notch has negligible effect on the crack propagation stage.

The multiplication factor of remaining life is the ratio of the specimen's remaining fatigue life after the OL ($N_{RET}$ -$N_{OL}$ as depicted in Figure 3. 25) to remaining fatigue life without taking into account the retardation effect ($N_{CAL}$ -$N_{OL}$ as depicted in Figure 3. 25).

$$multiplication\ factor = \frac{N_{RET} - N_{OL}}{N_{CAL} - N_{OL}} \qquad \textit{(eq. 3.11.)}$$

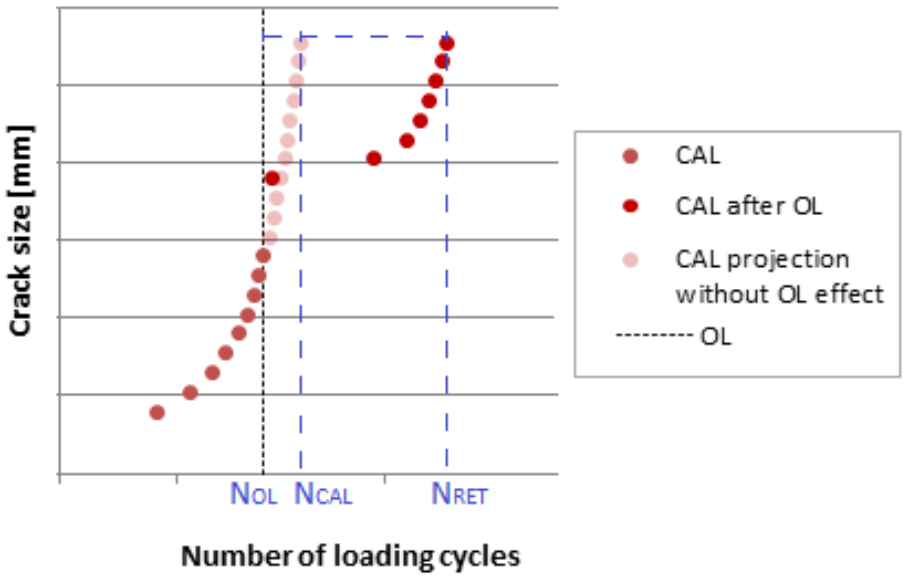


Figure 3. 25: Calculation of remaining life multiplication factor

Table 3. 4 presents various aspects of OL effect in both examined cases.

Table 3. 4: OL retardation effect evaluation

| Retardation effect | | |
|---|---|---|
| **Specimen** | **BP351** | **BM235** |
| **OLR** | 1.7 | 1.7 |
| **$\Delta K_{OL}$ [(m per cycle)/(MPa√m)]** | 21.15 | 20.82 |
| **Crack size [mm]** | 2.8 | 2.4 |
| **Delay cycles $N_d$** | 34593 | 73530 |
| **Multiplication factor of remaining fatigue life** | 5.0 | 5.2 |

The OL retardation effect on welded specimen BP351 is less pronounced than that in the base material specimen BM235 in almost similar conditions (in terms of specimen geometry, OLR, $\Delta K_{baseline}$). The basic reasons for this important difference in retardation effects are related to the mechanical properties, the residual stresses and the material microstructure of the specimens. Concerning the mechanical properties, it is known that welds contribute to the increase in yield strength of a steel specimen, even the fact that it is quite complicated to measure this increase accurately. The specimen that has the lower yield strength will present larger plasticity by a single tensile OL which means more pronounced retardation effect *[6]*. According to this statement it is very rational that the base material specimen presents a more profound OL retardation effect. Furthermore, tensile residual stresses in heat affected zone and weld microstructure enhance the crack growth rate so they reduce the period of recovery from OL retardation effect in the welded specimen.

In the bead weld of the plate specimen BP352 with CAL in different stress ratios (R=0.1 and 0.5) and a variety of load sequence effects is applied. The overview of the applied loading is presented in Table 3. 5.

Table 3. 5: Overview of BP352 test

| Starting loading cycle | Number of cycles | Loading condition |
|---|---|---|
| **1** | 311798 | CAL (R=0.1) |
| **311799** | 1 | Single tensile OL (OLR=1.7) |
| **311800** | 27692 | CAL (R=0.1) |
| **339492** | 1 | Single tensile OL (OLR=1.7) |
| **366868** | 85851 | CAL (R=0.5) |
| **425344** | 1 | Single Underload UL |
| **425345** | 8257 | CAL (R=0.5) |
| **433600** | 2 | OL/UL |
| **433602** | 28233 | CAL (R=0.5) |

The two single tensile overloads that are applied have the same OLR and absolute values of stresses with the applied OL at the specimens BP351 and BM235 (depicted in Figure 3. 22). On the other hand, the discrete underload make the minimum force equal to zero and the highest one has no change compared to the CAL in R=0.5 (Figure 3. 26).

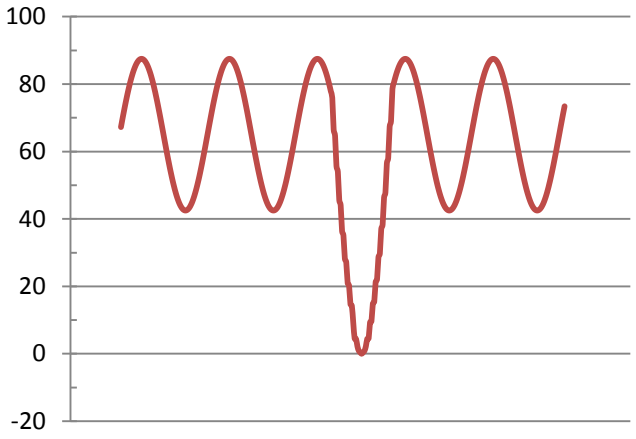


Figure 3. 26: Discrete UL application (units in kN)

The overload application accompanied with a consecutive underload is a different test case from the single overload application. In this case the OL ratio equals to 1.39 so a force peak of 125kN is reached while the successive UL leads to a force valley of zero (Figure 3. 27).

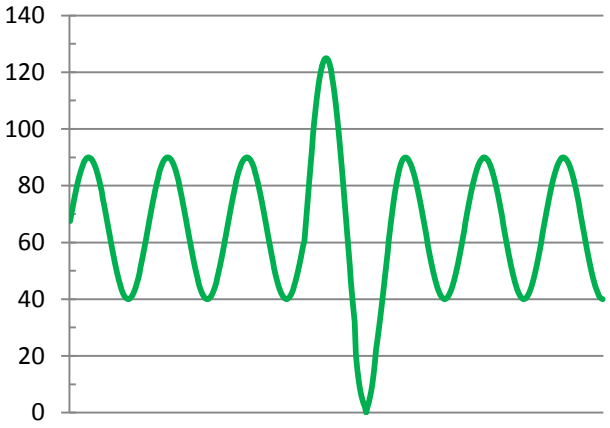


Figure 3. 27: OL/UL application (units in kN)

The crack growth curve at both sides is depicted on Figure 3. 28 as well as the da/dN-ΔK for both sides and stress ratios on Figure 3. 30 and Figure 3. 31.

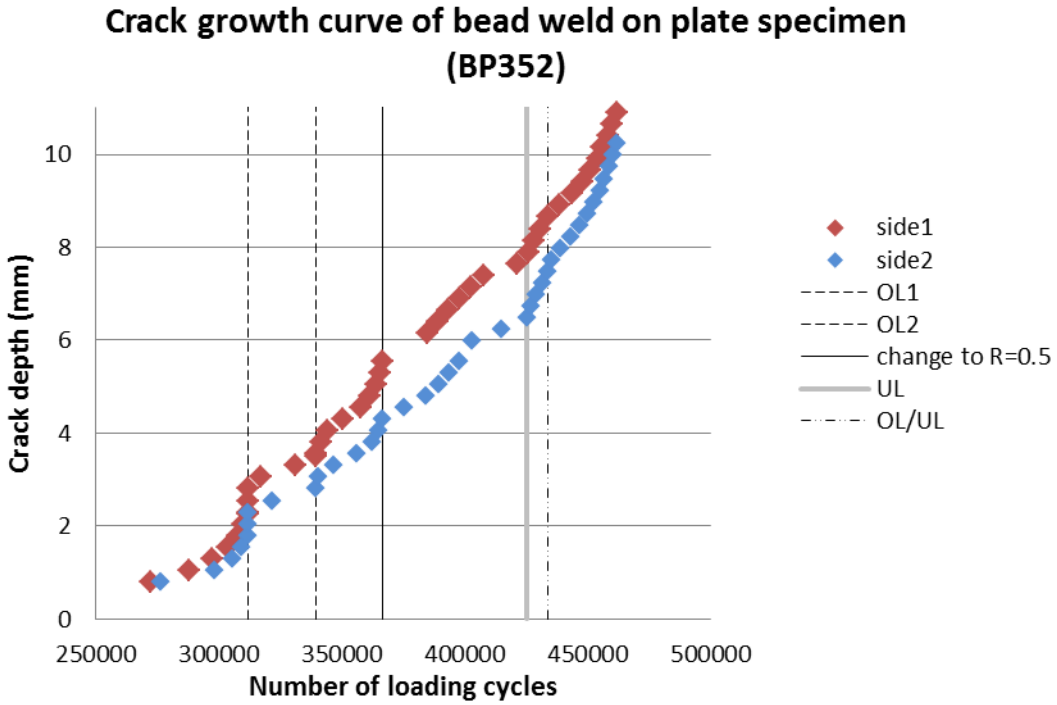


Figure 3. 28: Crack growth curve for both sides of a bead weld on plate specimen (BP352)

The crack depth difference between the sides of the welded specimen (Figure 3. 28) is larger compared to those of the base material (Figure 3. 29). This fact can be explained by the lack in homogeneity in the weld area and the heat affected zone that results in residual stresses.

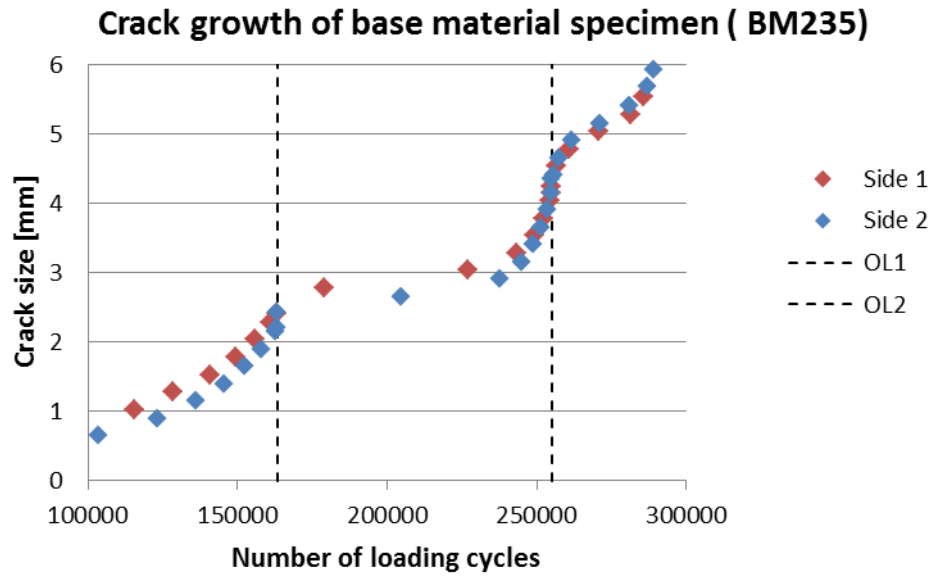


Figure 3. 29: Crack growth curve for both sides of a base material specimen (BM235)

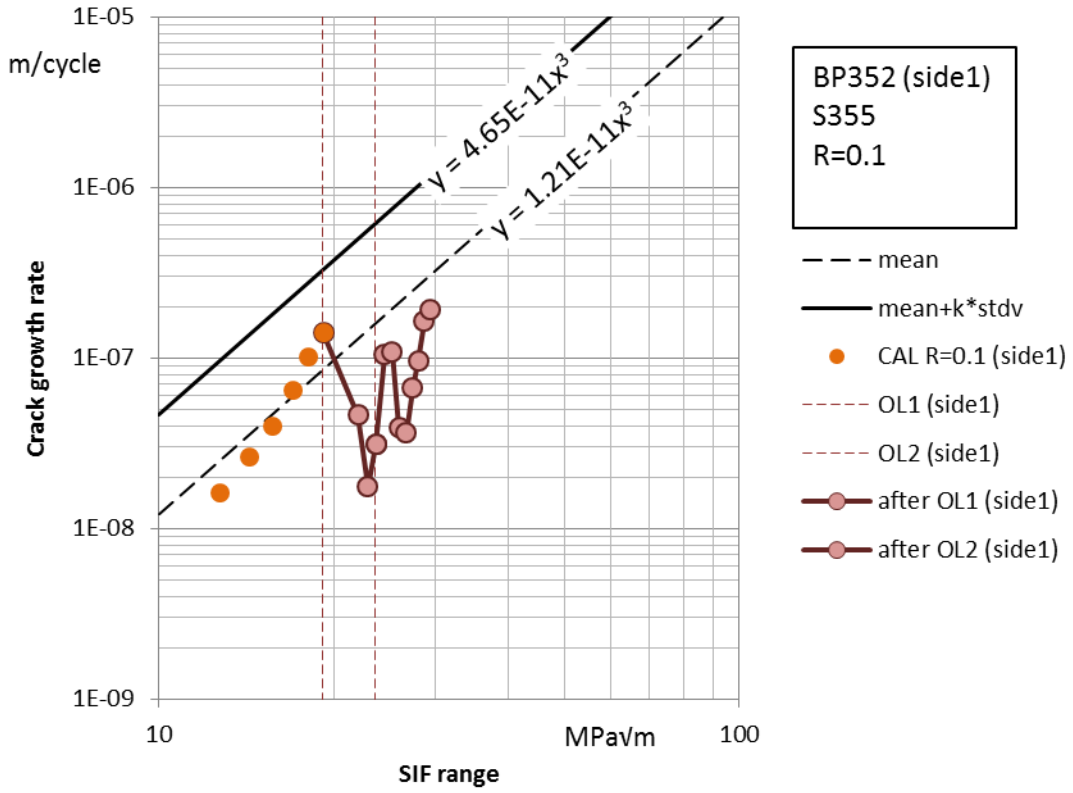


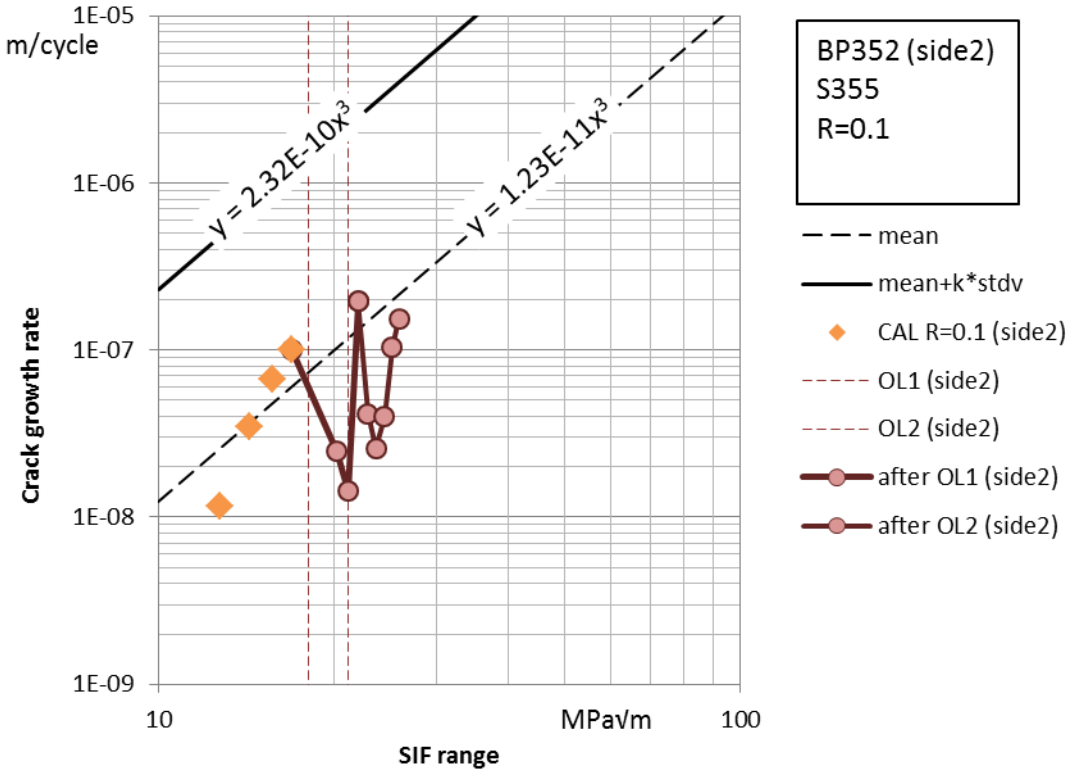


Figure 3. 30: da/dN-ΔK curve for both sides of BP352 in R=0.1

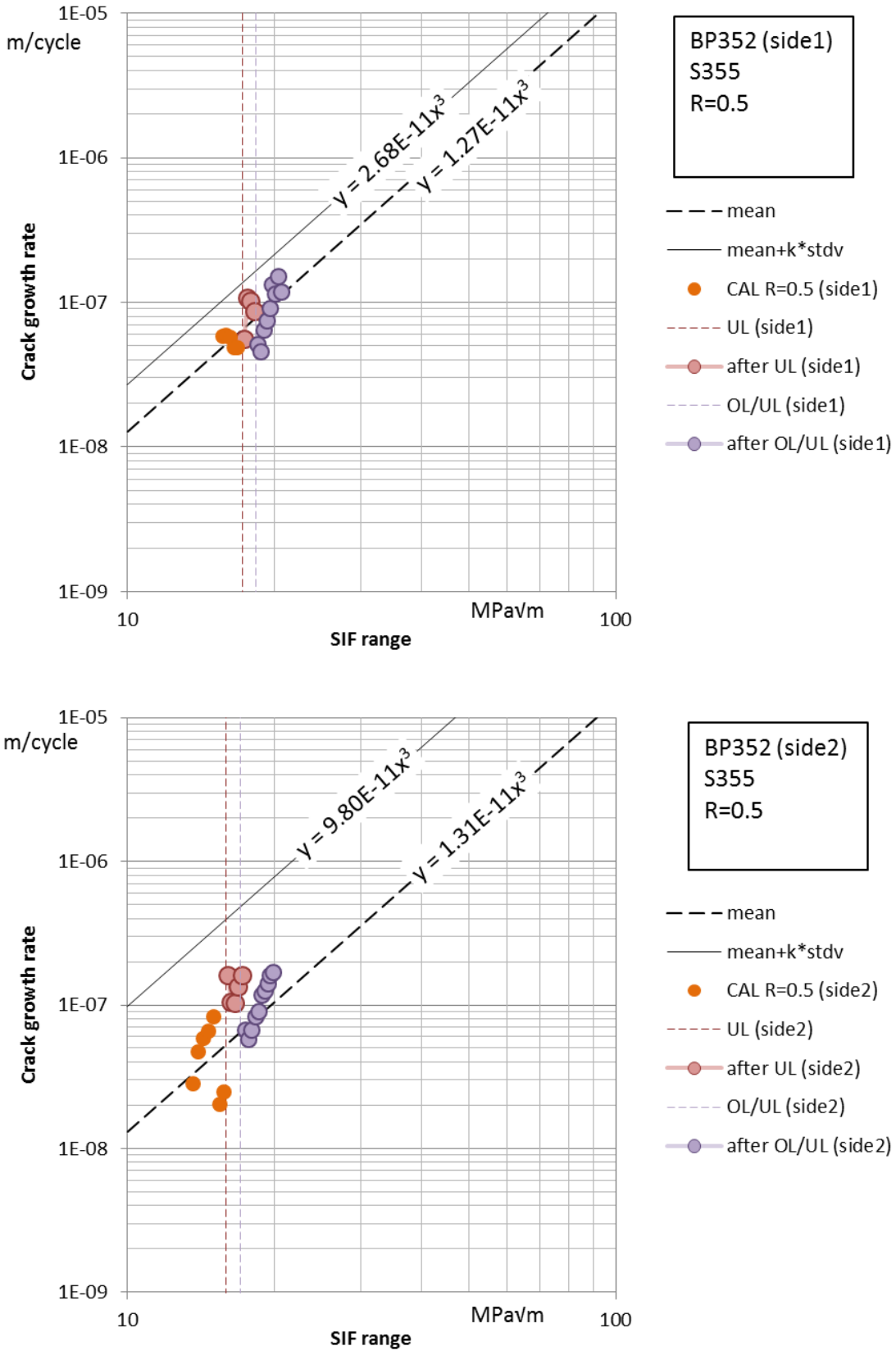


Figure 3. 31: da/dN-ΔK curve for both sides of BP352 in R=0.5

The results presented in the figures (Figure 3. 28 - Figure 3. 31) give an experimental verification of literature research regarding these load sequence effects on fatigue crack growth. Besides the OL retardation effect, the UL acceleration effect and the slight retardation effect caused by an OL followed by a consecutive UL are shown on the figures. Another worth noticing remark is the retardation effect on crack growth that is introduced by the subsequent change from R=0.1 (24MPa-240MPa) to R=0.5 (108MPa-216MPa).

To evaluate the OL retardation effects on this specimen, CAL without OL are shown in crack growth curves in order to show the additional loading cycles introduced by overloads to reach a certain crack size. As presented in Figure 3. 32 the first overload gives an effect that is still not recovered when the second overload arises.

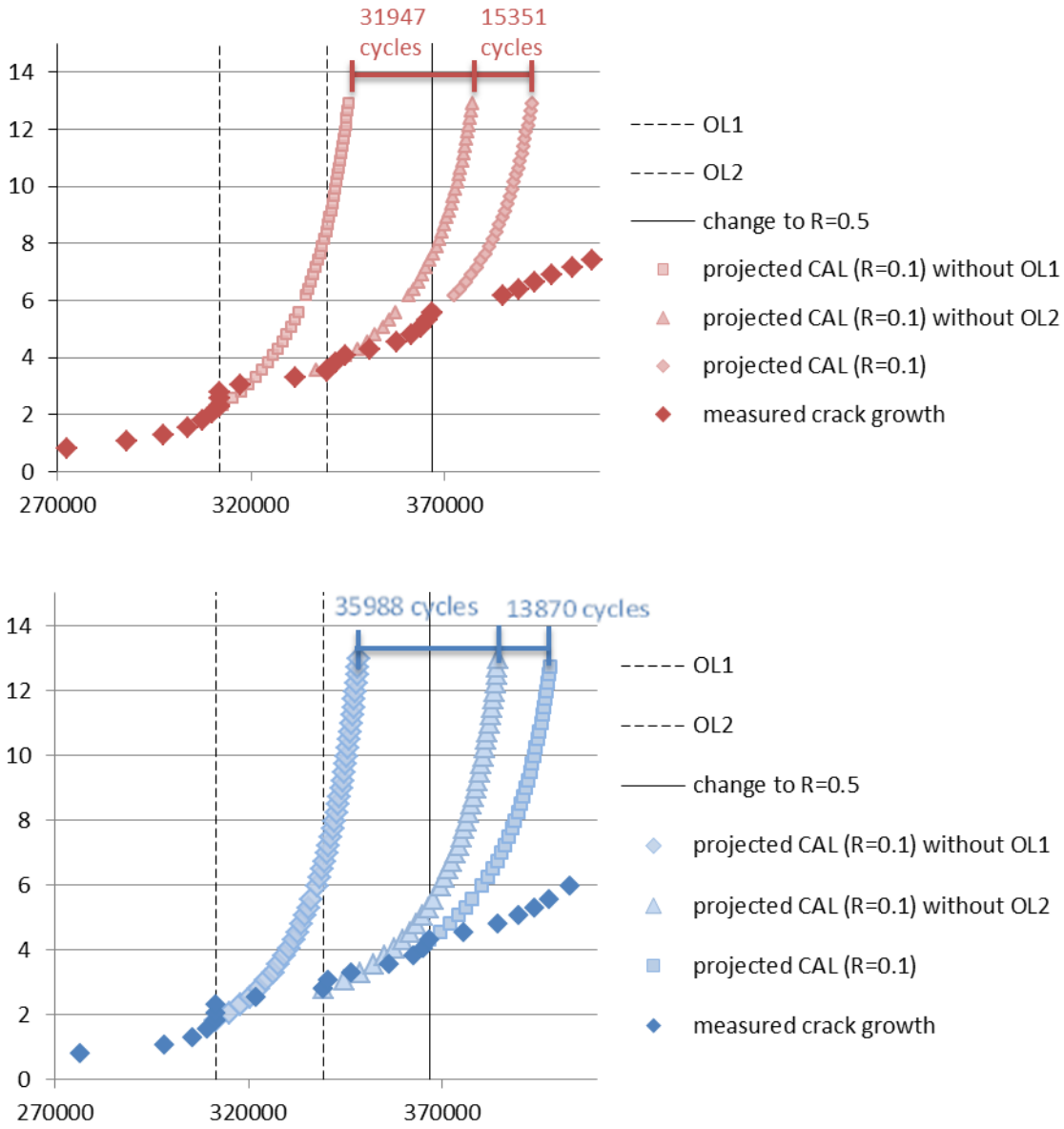


**Figure 3. 32: Crack growth and CAL projections for bead weld on plate specimen BP352 (side1 above, side2 below)**

The experimental data regarding crack growth presented in Figure 3.31 resemble the curve in Figure 2.16 where the OL's are superimposed on each other due to their short re-occurrence.

The two overloads have the same ratio (1.7) and they are applied in CAL with stress ratio equal to 0.1 (24MPa-240MPa). It can be seen clearly in the da/dN-ΔK curves (Figure 3. 32) that the second single tensile overload (OL2) is applied prior to crack growth rate recovery from the OL1 retardation effect (superimposing). This is the reason why OL2 causes an approximate retardation of 13500 to 15500 loading cycles while OL1 causes a much higher retardation of 32000 to 36000 cycles (Figure 3. 32). OL1 is applied at the same ΔK-levels as OL on specimen BP351 (ΔK=19.1 MPa√m and ΔK=18.1 MPa for side 1 and side 2 respectively). OL1 on specimen BP352 has the same OLR with OL on specimen BP351 and the results prove that they have similar retardation effect in terms of prolonging the fatigue life.

It is worth noticing that in the majority of the tested specimens crack growth acceleration is observed momentarily just after the OL and leads to a small crack size increase. A possible explanation for this instant phenomenon could be the initial crack tip opening caused by the overload plastic zone which increases the effective $\Delta K_{eff}$ and reduces crack closure.

To identify the dominant mechanism that causes the OL retardation effect some observations have to be considered. The overload delayed retardation (see the last paragraph of 2.3.3.1) that is observed in all examined 4PB specimens of this chapter excludes crack tip blunting and residual stresses ahead of the crack tip from the investigation of the most dominant mechanism due to the fact that these two mechanism result an immediate strong decrease (even a temporary crack arrest in case of crack tip blunting) in crack growth rates immediately after the OL application *[7][8]*. In addition, no crack branching occurs and the overload does not introduce significant change in the fracture surface roughness. To conclude, by excluding all the other possible mechanisms and taking into consideration that delayed retardation can be explained on the basis of plasticity induced crack closure *[9]*, it is considered that the latter one is the dominant physical concept for the examined test cases.

The delayed OL retardation effects that are noticed in the aforementioned tests indicate that plasticity induced crack closure is the dominant mechanism that contribute to crack growth retardation.

#### 3.9.2.1. Plasticity induced crack closure

Table 3. 6 provides the U-values that correspond to the OLs that applied on welded and base material specimens along with all the necessary data that affect the extent of retardation effect (OLR, $\Delta K_{baseline}$, delay cycles due to OL). Section 2.3.3.1 presents how the U-values are measured on the basis of da/dN-ΔK curve. This approach is applied for measuring the U-value per side of specimen.

Table 3. 6: Single tensile OL's data and corresponding U-values

| Applied OL ratio | specimen | ΔK baseline (MPa√m) | U - Value | Delay cycles |
|---|---|---|---|---|
| **OLR=1.7** | BP351 | 21.14 | 0.47 | 34593 |
| **OLR=1.7** | BP352 side1 | 20.82 | 0.49 | 31947 |
| **OLR=1.7** | BP352 side2 | 19.32 | 0.49 | 35988 |
| **OLR=1.7** | BM135 side1 | 22.06 | 0.49 | 69014 |
| **OLR=1.7** | BM135 side2 | 22.53 | 0.45 | 69961 |
| **OLR=1.7** | BM235 side1 | 20.82 | 0.53 | 73530 |
| **OLR=1.7** | BM235 side2 | 19.32 | 0.54 | 71092 |

*See Figure 3. 23, Figure 3. 24, Figure 3. 32, and Appendix E.

The effects of second applied tensile overloads (OL2) that are applied before crack growth rate recovery from OL1 are not included in the table above.

It is observed (Table 3. 6) that the retardation effect in terms of delay cycles is higher in base materials compared to welded ones. However, the U-values, which are considered the values that represent the amount of plasticity induced crack closure, present very slight differences between welded and base materials even the fact that it has been stated in the previous paragraph that plasticity induced crack closure is the dominant retardation mechanism in the examined specimens.

The most possible explanation could be the limited number of data regarding crack growth rates that are given from the tests which makes it difficult to detect the minimum crack growth rate value after the OL. The use of a continuous sheet instead of a pattern of resistor strands would be a more efficient way of data measuring because of the fact that it would give much more information regarding crack growth rate development.

This means that the number of delay cycles (the prolonging of fatigue life in terms of loading cycles) is the only reliable way to measure OL effect in this study.

### 3.9.3. Results from VAL tests

The load history of variable amplitude loading applied in the 4PB specimen BP353 specimen has been taken from measurements in offshore wind turbine (OWT) structures. The load sequence depicted in Figure 3. 33 is repeated every 18000 loading cycles approximately. The total number of loading cycles applied in VAL equals to $1.5\times10^6$ cycles approximately, which means that the equivalent stress range remains the same for every crack increment.

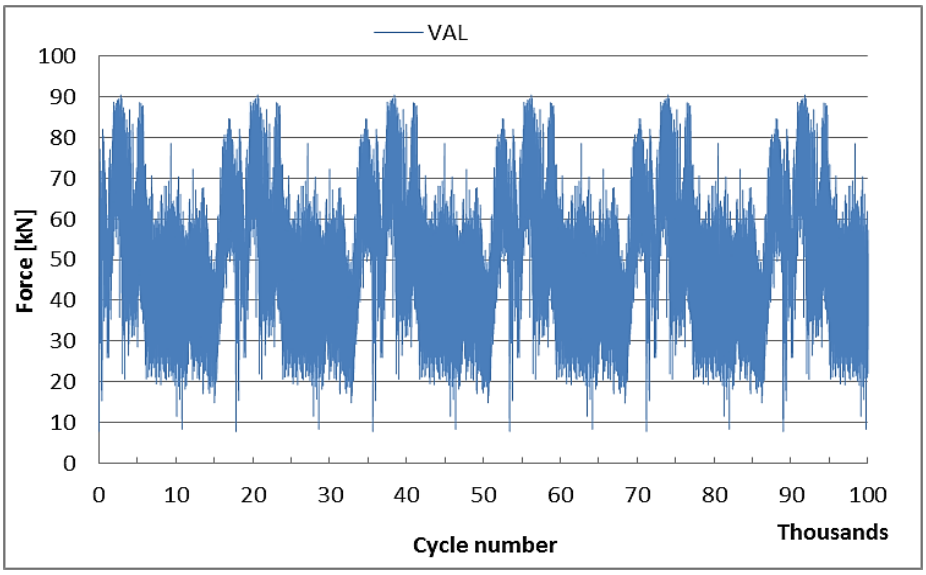


Figure 3. 33: VAL sequence

The application of rainflow counting method results in the stress range spectrum presented in Figure 3. 34 as function of the number of loading cycles and their corresponding magnitude.

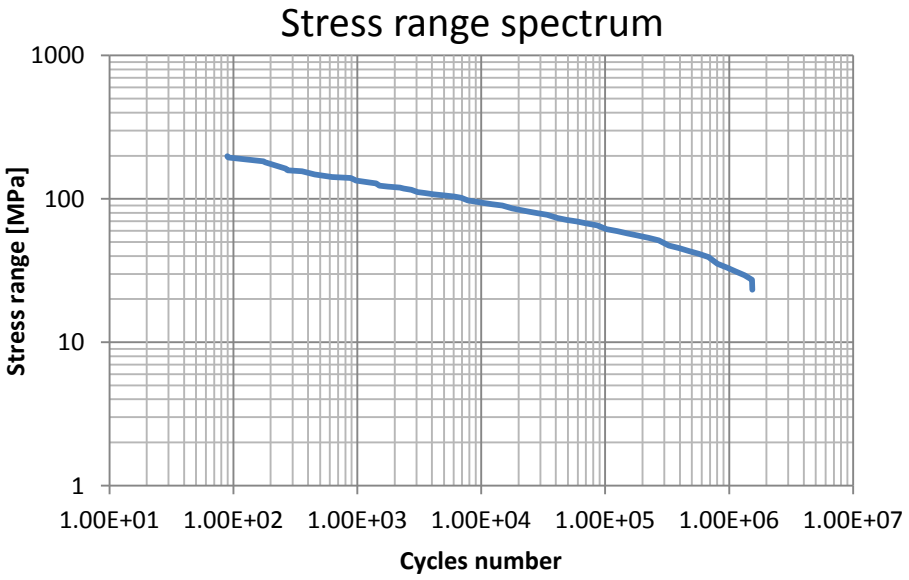


Figure 3. 34: Stress range spectrum

Crack growth rates can be derived from the crack growth curve by dividing a specific crack increment (distance between two consecutive grid lines = 0.50mm) by the number of loading cycles that have been applied during this crack increment (as described in section 3.6). Figure 3. 35 presents the fatigue crack growth curve of a bead weld plate specimen BP353 under VAL.

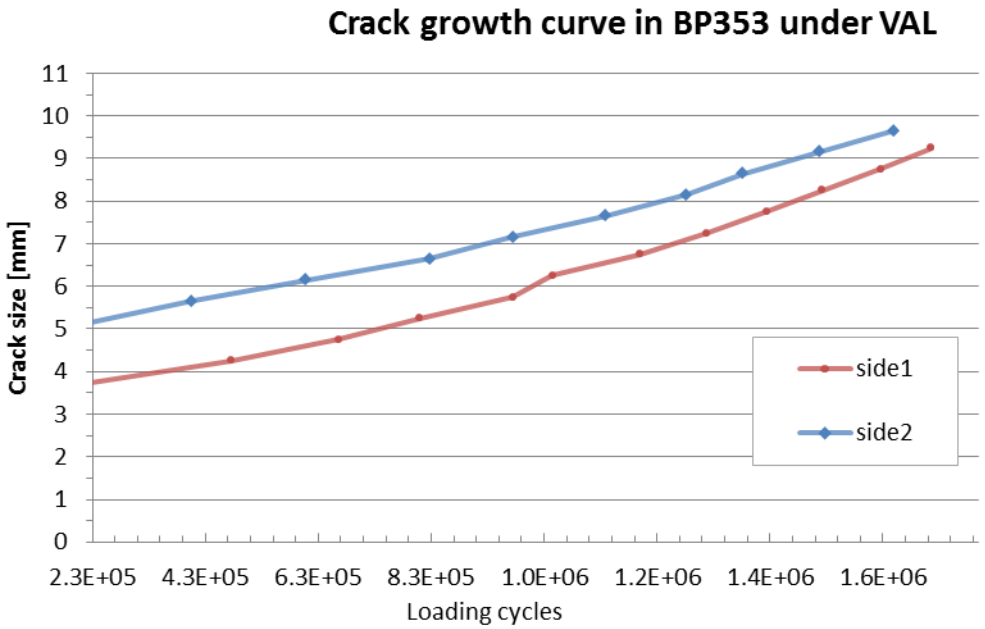


Figure 3. 35: Crack growth curve in BP353

### 3.10. Conclusions

The main conclusions from the interpretation of the test results gathered under CAL are the following:

- the fact that the crack propagation constants in welded specimens are slightly higher compared to the corresponding values of the base materials at a given stress ratio R can be explained by:
    - the material microstructure of welded specimen that permits higher crack growth rates and
    - the tensile residual stresses that exist in the heat affected zone of the weld and contribute to an increase in applied mean stress.

  It is an experimental proof that the welded material is more susceptible to fatigue damage compared to parent material.

- The test results confirm the literature finding that higher mean stress increases crack growth rate in base materials (see Figure 3. 18 and Figure 3. 19 where the da/dN-ΔK curves of base material for different stress ratios are depicted). On the other hand, the stress ratio effect cannot be proofed from the results of the welded specimens and the main reason is the fact that the measurements are taken from different crack depths where the effect of weld is not similar.

The evaluation of OL effects leads to the following remarks:

- Crack growth retardation is clearly noticed after a single tensile OL application in base material and welded specimens. The OLRs and (the ΔK when the OL is applied) are almost the same in both specimens.

- The OL retardation effect on crack growth of welded specimens is lower compared to base materials (Figure 3. 23 and Figure 3. 24) and this is attributed to:

    - the higher yield strength of the welded materials which makes the size of overload plastic zone smaller.

    - the development of additional stress in welded specimen (the tensile residual stresses) that lead to an increase in applied mean stress and as a result in a crack growth increase which makes shorter the period of recovery from OL retardation effect.

    - The weld microstructure that contribute to the crack growth rate increase and makes shorter the period of recovery from OL retardation effect.

- According to the experimental results (Table 3. 6), the OL retardation effect on base material specimens in terms of delay cycles is approximated by 2-2.5 times higher than the corresponding effect on bead weld on plate specimens for OLR = 1.7 and $\Delta K_{baseline}$ around 19-21 MPa√m.

- The delayed retardation that is observed in all the tested specimens (without any significant changes in fracture surface roughness) indicates that the dominant mechanism of the OL effect is the plasticity induced crack closure (see 2.3.3.1 and 3.9.2.1).

- The fact that there is not a full da/dN-ΔK curve in the vicinity of the threshold and an apparent effective ΔK in this region (due to limited number of data regarding da/dN after overloads) makes U-values inappropriate to measure plasticity induced crack closure.

As far as the UL and OL/UL effects on crack growth are concerned:

- The test results confirm in principle the literature research chapter (2.3.3.2) regarding the UL effect on fatigue crack growth. It is illustrated clearly in Figure 3.

23 and Figure 3. 24 that the application of a discrete OL has a crack retardation effect.

- The application of a discrete UL leads to a slight crack acceleration during the subsequent loading cycles (Figure 3. 28 and Figure 3. 31).

- The application of a discrete OL followed by a subsequent UL has as slight crack growth retardation effect as it can be seen in Figure 3. 28 and Figure 3. 31. This means that the UL immediately after the OL cancels partially its retardation effect in crack growth.

Although the number of data is not adequate in order to quantify the OL, UL and OL/UL effects on crack growth, it is observed that:

- the OL effect is more profound compared to the UL in terms of duration (how long the effect lasts till the crack growth rate returns to the same levels of CAL, see figures Figure 3. 28 - Figure 3. 31)

- the OL effect has more profound influence on crack growth rate compared to UL or OL/UL (Figure 3. 28 - Figure 3. 31).

- A change of stress ratio in this particular case (Fmax:from 100kN to 90kN, Fmin:from 10kN to 45kN see Figure 3. 36) has a slight retardation effect on crack growth which can be noticed in Figure 3. 28. This effect cannot be explained by the change of R values (from 0.1 to 0.5) but from the absolute values of Fmax and Fmin before and after the R change.

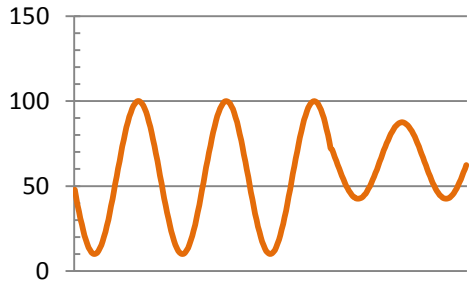


Figure 3. 36: Stress ratio change (units in kN)

## References


**[1]** ISO 12108:2012 Metallic materials - Fatigue testing - Fatigue crack growth method

**[2]** H.Tada, P.C.Paris, G.R.Irwin - The stress Analysis of Cracks Handbook - 1973

**[3]** A. Hobbacher - IIW Recommendations for Fatigue design of welded joints and components - IIW-1823-07/XII-2151r4-07/XV-1254R4-07 - December 2008

**[4]** BS 7910:2013 - Guide to methods for assessing the acceptability of flaws in metallic structures - BSI Standards Publication

**[5]** X. Shan, C.M. Davies, T. Wangsdan, N.P. O'Dowd, K.M. Nikbin - Thermo-mechanical modelling of a single-bead-on-plate weld using the finite element method - International Journal of Pressure Vessels and Piping 86 (2009) 110–121

**[6]** A.J.McEvily, S.Ishihara, Y.Mutoh – On the number of overload-induced delay cycles as a function of thickness – International Journal of Fatigue 26 (2004) 1311-1319

**[7]** J.Maljaars, R.Pijpers, H.Slot - Load sequence effects in fatigue crack growth of thick-walled welded C-Mn steel members - International Journal of Fatigue 79 (2015) pg. 10-24

**[8]** C.S.Shin, N.A.Fleck – Overload retardation in a structural steel – Fatigue Fracture Engineering Material Struct. Vol. 9, No. 5, pp. 379-393 (1987)

**[9]** K.Sadananda, A.K.Vasudevan, R.L.Holtz, E.U.Lee - Analysis of overload effects and related phenomena – International Journal of Fatigue (1999) S233-246

# 4. TUBULAR T-JOINT FATIGUE CRACK GROWTH TEST

## 4.1. Introduction

Besides small-scale specimen tests, the load sequence effects are also examined on a realistic geometry. Hence, fatigue tests on tubular T-joints have been executed in the current study. This chapter describes the procedure that was followed for the fatigue test, in which an axial load was put on the brace of the tubular T-joint (Figure 4. 1). In the evaluation of the test results, the stress distribution at the intersection of chord and brace and the fatigue crack growth behaviour of the structure are presented.

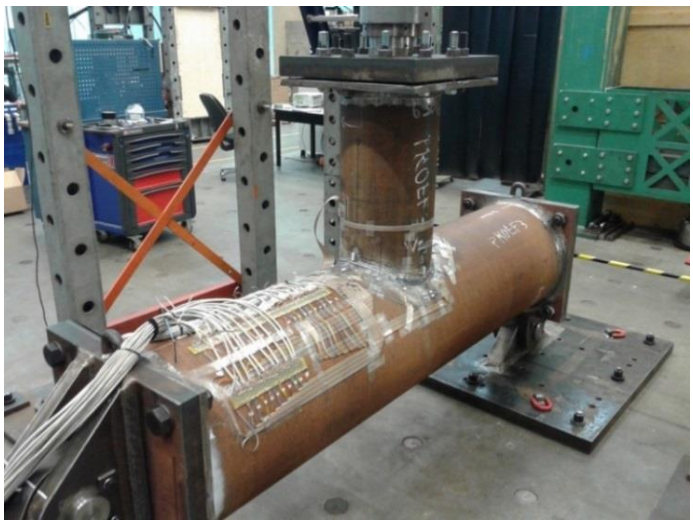

Figure 4. 1: Tubular T-joint test

The main purpose of this chapter is the evaluation of test results on the basis of structural geometry and material properties, applied fatigue loading and secondary specimen boundary conditions. The test was carried out at TNO Structural Dynamics Lab.

The fatigue loading is chosen high enough in order to initiate the crack at the weld toe of the chord at the saddle position, which is the location with the highest stress concentration factor.

## 4.2. Test matrix

Table 4. 1 presents an overview of the applied loading in relation with the number of cycles. The tested specimens are subjected to cyclic loading under ambient air conditions from laboratory at a temperature of approximately 20˚C. The brace of the T-joint is axially loaded under constant amplitude fatigue loading (CAL) in compression for the initial loading cycles and later in tension. The stress ratio under CAL is permanently equal to 0.1 (R=0.1) apart from a block of 10000 tensile cycles of R=0.9 that is applied for crack marking. During the

tensile loading cycles a discrete OL (of overload ratio 1.35) is applied at a crack depth of 8.4mm in side 1. The frequency of loading is equal to 1 Hz.

Table 4. 1: Overview of test loading conditions

| Starting cycle number | Loading type | Stress ratio/ Overload ratio | Applied loading cycles | Number of cycles | Stress [MPa] | | Stress range Δσ [MPa] |
|---|---|---|---|---|---|---|---|
| | | | | | peak | valley | |
| **0** | CAL | R=0.1 | Compressive | 421955 | -34.17 | -3.42 | 30.75 |
| **421956** | CAL | R=0.1 | Tensile | 139116 | 34.17 | 3.42 | 30.75 |
| **561072** | CAL | R=0.9 | Tensile | 10000 | 34.17 | 30.75 | 3.42 |
| **571072** | CAL | R=0.1 | Tensile | 16685 | 34.17 | 3.42 | 30.75 |
| **587757** | OL | OLR=1.35 | Tensile | 1 | 46.09 | 3.42 | 42.67 |
| **587758** | CAL | R=0.1 | Tensile | 35000 | 34.17 | 3.42 | 30.75 |

Figure 4. 2 depicts a drawing of a T-joint loaded to the brace in compression and tension.

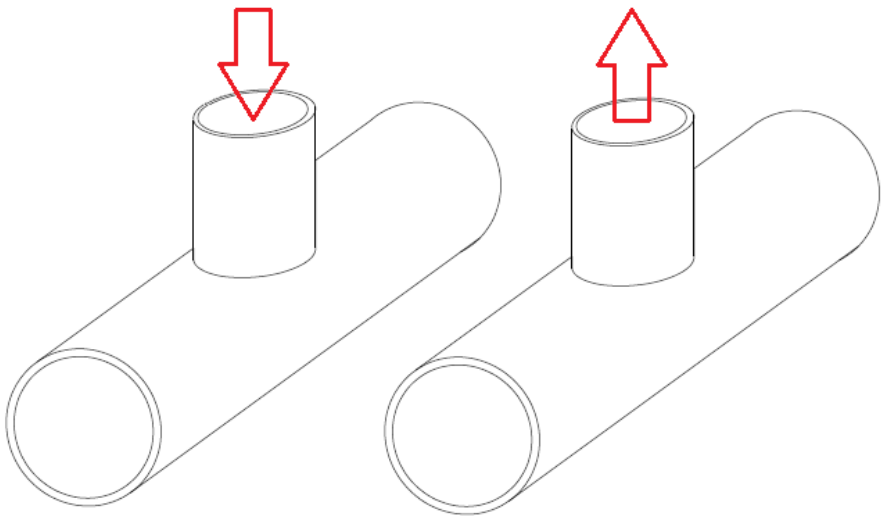

Figure 4. 2: Joint axially loaded to the brace under compression and tension

The switch from compressive to tensile loading cycles is related to practical consideration and test setup reasons which are not examined in this study.

### 4.3. Specimen

The tested specimen consists of two tubular and members provided at the ends by plates connected to each other by welding. Table 4. 2 provides the dimensions of each element and its steel grade. Hot finished structural hollow sections of fine grain steel are used for tubular elements according to EN 10210-1 and EN 10225.

Table 4. 2: Dimensions and properties of specimen components

| Element | Quantity | Length [mm] | Width/Diameter [mm] | Thickness [mm] | Grade |
|---|---|---|---|---|---|
| Steel Plate | 2 | 550 | 550 | 20 | DH36 |
| Steel Plate | 1 | 500 | 500 | 20 | DH36 |
| Steel CHS (chord) | 1 | 2000 | 508 | 25 | S355G13+N according to EN 10225 |
| Steel CHS (brace) | 1 | 650 | 323.9 | 16 | S355J2H according to EN 10210-1 |

Figure 4. 3 shows the T-joint with the dimensions.

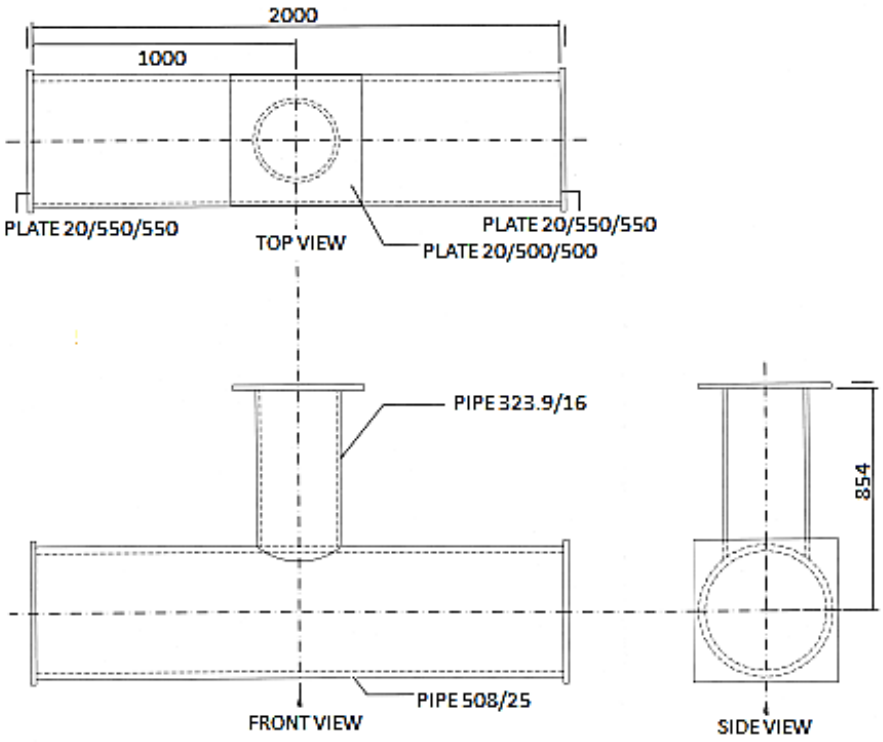


Figure 4. 3: T-Joint dimensions

Table 4. 3 and Table 4. 4 provide the chemical composition of the examined specimen for the two CHS (Circular Hollow Sections) sections.

Table 4. 3: Chemical composition for the material of the chord

| C % | Si % | Mn % | P % | S % | Al % | Cu % | Cr % |
|---|---|---|---|---|---|---|---|
| 0.14 | 0.26 | 1.44 | 0.009 | 0.002 | 0.042 | 0.02 | 0.03 |
| **Ni %** | **Mo %** | **V %** | **Ti %** | **Nb %** | **N %** | **B %** | **Ca %** |
| 0.04 | 0.04 | 0.002 | 0.015 | 0.026 | 0.003 | 0.0001 | 0.001 |

Table 4. 4: Chemical composition for the material of the brace

| C % | Si % | Mn % | P % | S % | Al % | Cu % | Cr % |
|---|---|---|---|---|---|---|---|
| 0.15 | 0.27 | 1.44 | 0.011 | 0.003 | 0.043 | 0.02 | 0.03 |
| **Ni %** | **Mo %** | **V %** | **Ti %** | **Nb %** | **N %** | **B %** | **Ca %** |
| 0.04 | 0.01 | 0.004 | 0.015 | 0.031 | 0.004 | 0.0002 | 0.001 |

Figure 4. 4: T-Joint specimen

### 4.4. Apparatus

The T-joints are tested in a built frame/rig (Figure 4. 5) with a servo-hydraulic actuator able to apply axial loading to the brace of the joint. The ends of the chord are supported by a hinge and a roll support. The total capacity of the rig is ±750kN where ''+'' is for tension and ''–'' for compression.

Figure 4. 6 presents a general layout of the experiment in relation with the test rig, servo-hydraulic actuator and boundary conditions applied in the specimen.

Figure 4. 5: The servo-hydraulic actuator and the test rig of the experiment

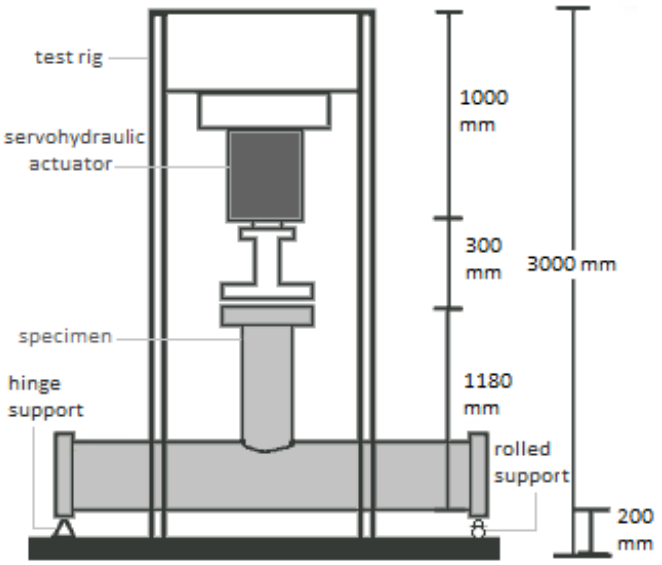


Figure 4. 6: Test apparatus adapted in the specimen

### 4.5. Data Acquisition systems

Two data acquisition systems are used in this test: the TestStar5 and the EX1629 (Figure 4. 7). TestStar5 records the number of cycles and the date and time of loading while EX1629 is a 48-channel high performance strain gauge measurement instrument which provides storage of strain measurements during loading every 0.025 sec.


Figure 4. 7: EX1629 Data Acquisition system

### 4.6. Measuring equipment

The main purposes of this test are the measurement of surface crack growth versus loading cycles and the approximation of stress field close to the joint intersection (which can be obtained by the strain gauges at these areas). Due to the surface crack assumption two crack growth rates are considered: one in width direction (along the perimeter of the intersection) and the other through the chord thickness direction. The crack growth in width direction (crack length) can be detected visually by adding petroleum in the crack and the use of a micro-camera; crack growth in depth direction is monitored by alternate current potential drop (ACPD) method combined with some supplementary validation techniques phased array and crack marking.

#### 4.6.1. Visual inspection

Pouring petroleum at the weld toe areas of the joint (where the crack is expected to initiate) combined with visual inspection through micro-camera is an effective technique for a detailed determination of crack length. Crack existence is indicated in the areas where the petroleum bubbles (Figure 4. 8) while the test runs.

Figure 4. 8: Crack length determination via microcamera

#### 4.6.2. ACPD method

When an alternating current is passed via a conductive material (such as steel) a uniform thin surface field is generated. This phenomenon, the so-called “skin effect”, is utilized in ACPD technique in order to measure the size of surface cracks in conductive materials *[1]*. A Crack MicroGauge (model U8) is the basic instrument that is used for the surface crack

measurement. The Crack MicroGauge is connected with a probe of a standard tip spacing (10mm) which takes voltage measurements in two different positions (Figure 4. 9): over the crack (crack measurement) and over an un-cracked area (reference measurement).

The value of surface voltage that is developed by applying this method depends on the following parameters:

**a.** The intensity of field current
**b.** The frequency of field current
**c.** The conductivity, permeability, shape and size of the material
**d.** The conductive metal path length between the voltage measurement positions

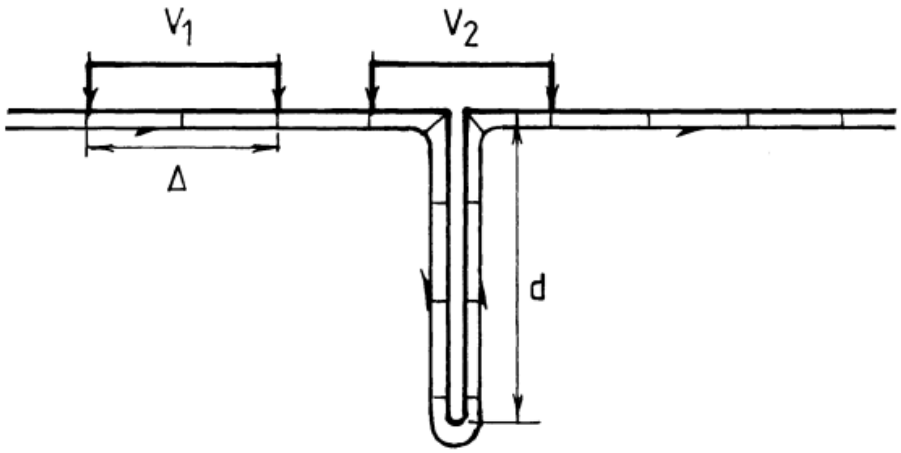


Figure 4. 9: Measurements according to ACPD method (R. Collins, 1992)[1]

In the case of a steel surface (such as on the tubular joint) where a constant field current and uniform field distribution are developed (namely the first 3 aforementioned parameters remain constant), the measured voltage becomes only proportional to the path length. Over an un-cracked area the path length is equal to the surface distance under the probe. However this is not valid for measurements over surface cracks where the double crack depth has to be taken into consideration.

A short calculation then (with the use of a micro-calculator attached to the main instrument) permits the conversion of these two voltages into the crack depth by following the formula below.

$$\boldsymbol{a = \left((V_2/V_1) - 1\right) * \Delta/2} \qquad \textit{(eq. 4.1.)}$$

where $\mathbf{V_1}$: reference voltage measurement (at the un-cracked area)

$\mathbf{V_2}$: voltage measurement over the crack

$\boldsymbol{\Delta}$: probe tip spacing (constant value equal to 10mm)


Figure 4. 10: MicroGauge device and its connected components

The instrument (Figure 4. 10) contains a current source, to generate the alternating current field, a sensitive microvoltmeter for voltage measurements and a microcalculator. In addition, the instrument is connected with a field lead which its two ends (two magnets see Figure 4. 11) contribute to uniform field distribution and a voltage probe lead (Figure 4. 12) which is used to surface voltage measuring. The magnets should be located at either side of the crack at a certain distance (80mm in our case).

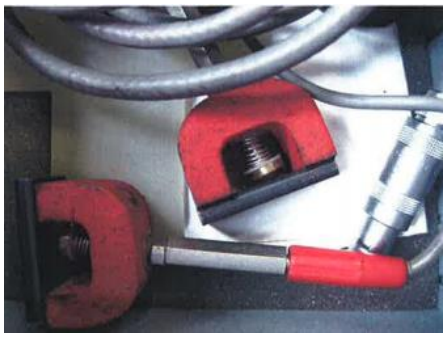

Figure 4. 11: Magnets

Figure 4. 12: Probe used for voltage measurements

The ACPD technique is a very sensitive method for measuring crack size. For this reason it is very crucial to use properly the Crack MicroGauge equipment and apply as well some additional measuring techniques to verify the ACPD results.

To ensure proper use of the ACPD equipment:

- The probe should be held firmly in contact with the structure surface
- The measured voltage values on the screen of the instrument should be stored only after being stabilized
- The exact positions where the tips are in contact with the conductive material should be marked over the specimen
- The surface voltage at a certain location in a certain stage of crack propagation should be measured many times in order to derive safe results (see Appendix)

Due to the fact that the available ACPD tool was a manual tool, the ACPD readings were not continuous, but were applied at an approximate interval of 10.000 cycles.

The additional methods that are applied to validate the ACPD results are crack front marking techniques and Phased Array inspection. Also these methods are not applied continuously during the test but only at certain stages of crack propagations to validate the ACPD method. Both are presented in the next paragraphs.

### 4.6.3. Crack front marking

Crack front marking technique was adopted in the fatigue fracture experiments, in which reducing the load amplitude by half or even more while the maximum load remains constant leads to the formation of a "beach-like pattern" on the fracture section of the specimen (Figure 4. 13). Results show that crack front marking technique can solve the problems of hard measurement of surface crack and hard observation of sectional fatigue striations for high strength steel.

Figure 4. 13: Beach-like pattern (M.Truchon)[2]

Considering the above background, a different cyclic loading compared with the others is applied at specific stages of crack propagation and has a stress ratio equal of 0.9. This loading has as an effect the formation of striations in the crack front which can be used to determine the crack depth at this particular stage. It is assumed that 10000 tensile cycles of tensile fatigue loading with a stress ratio equal to 0.9 have negligible effect on crack

extension. This can be proved by applying the Miner's rule on the S-N curves (Table 5. 5 and Table 5. 6).

The crack depth that is measured with crack marking is compared with the ACPD results when the test is completed. The main disadvantage of this method is that it cannot provide results during the test because it is a destructive method (the crack is opened completely after the specimen fails). For this reason a non-destructive method is applied as well and is presented in the following paragraph.

### 4.6.4. Phased Array

Phased Array (PA) is an advanced widely used non-destructive testing (NDT) method that applies an ultrasonic technique to detect and determine the crack size.

Phased Array ultrasonic inspection has no difference, in terms of basic principle, with the standard ultrasound. The main advantage and difference is the use of a multi-element ultrasonic probe (Figure 4. 14). In which the equipment is able to transmit audio at different angles throughout the material and to be processed by means of special software to a colored image which is evaluated by the inspector *[3]*. Further advantage can be gained through the use of electronic beam steering to direct and focus sound beams. The simultaneous use of different angles provides an extremely reliable inspection especially in case of curved geometry structures like tubulars.

Figure 4. 14: Ultrasonic probe

The PA probe consists of many small ultrasonic transducers, each of which can be pulsed separately *[4]*. The beam is swept like a search-light through the examined specimen and the data from multiple beams are put together to make a visual image showing a slice through the object (Figure 4. 15).

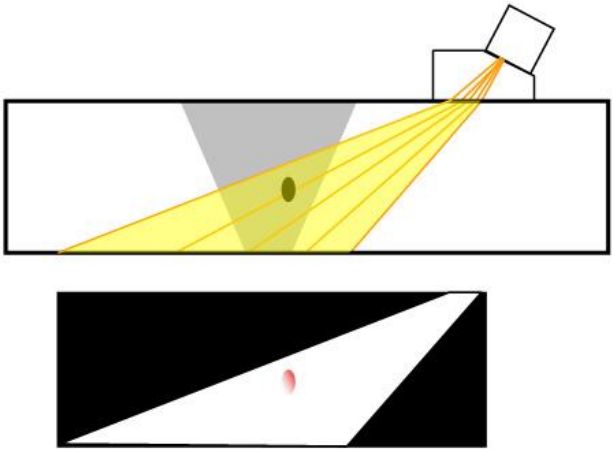

Figure 4. 15: Phased Array method

### 4.6.5. Strain gauges

Strain gauges are located around the perimeter of the joint at a distance of 5 mm from the weld toe with an interval of 30˚ degrees of angle. The gauges are connected to the data acquisition system. At the saddle points of the chord, where the highest SCF are expected, 7 strain gauges are installed at certain positions in order to determine the SCF at the weld toe by stress extrapolation (Figure 4. 16).

The stress field close to weld toe is derived under the assumption of plane strain condition due to the fact that the brace wall is considered as a restraint. On the basis of plane strain condition the conversion of strains to stresses is implemented by the following formula:

$$\Delta\sigma = \left(\frac{E}{1-\nu^2}\right)\Delta\varepsilon \qquad \textit{(eq. 4.2.)}$$

Where **Δε**: the measured strain range

$\nu$ : poisson ratio (=0.3)

**E** : modulus of elasticity for structural steel (=$210 \cdot 10^9$ N/m$^2$)

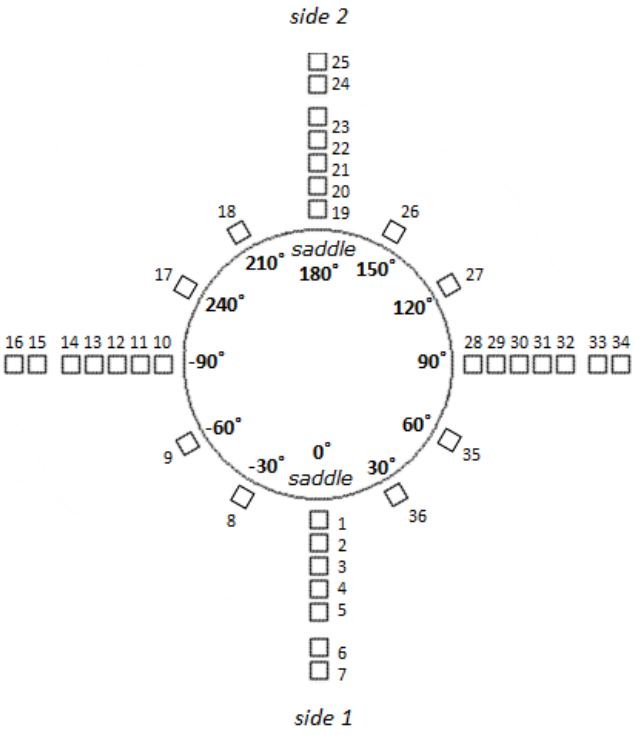


Figure 4. 16: Gauges installation close to weld toe

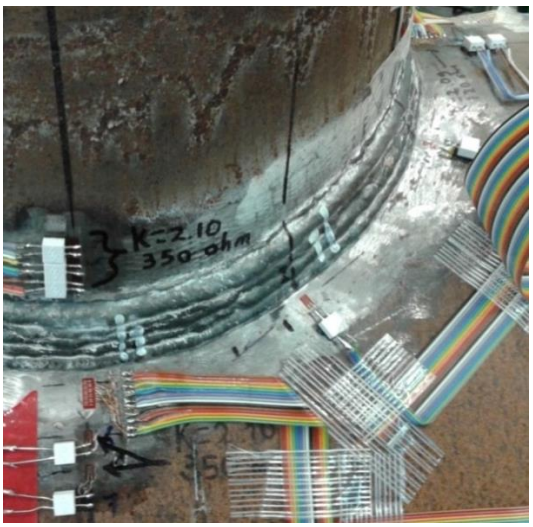


Figure 4. 17: Strain gauge positioning

## 4.7. Crack growth results

### 4.7.1. General

In this paragraph, the results of crack growth in through thickness and length direction are presented assuming that the failure criterion is a crack depth equal to half of the chord thickness (12.5 mm) at which the test has been stopped.

After 422000 compressive cycles, no crack initiation was visible. For this reason, it was decided to change the loading to a tensile range. The first crack was detected at side 1 after

474000 loading cycles where 52000 were tensile. The crack depth was first measured after 482000 cycles (422000 compressive and 60000 tensile) when the total crack length edges were at the points of 5 and 35 degrees of angle from the side 1 saddle point. The crack initiation point for side 1 is approximated at a position of 15-20˚ right from the saddle point whereas for side 2 the corresponding position is the saddle point (gauge position numbering 180˚). Compressive cycles contribute to fatigue damage but not as much as the tensile ones.

### 4.7.2. Crack depth results

Figure 4. 18 to Figure 4. 22 represent the crack depth growth curves based on ACPD measurements at (see Appendix F for further information regarding the measurements) the points of side 1 where the highest crack depth develops (close to crack initiation point of side 1). The curves depict how the crack depth at these points extends under CAL and a single tensile OL (of OLR=1.35). They show clearly an exponential increase of crack depth growth. Moreover, these figures show a decrease in the slope of crack growth line just after the OL compared with the slope before the OL application which demonstrates a slight OL retardation effect.

The 10000 loading cycles of R=0.9 that were applied for crack front marking are not taken into account assuming that their effect on crack growth is negligible (which can be proved by S-N curves see Table 5.5 and 5.6). Position numbering is based on Figure 4. 16.

Table 4. 5: Crack depth measurements at point 15˚

| Total number of loading cycles | Measured crack depth [mm] |
|---|---|
| **502000** | 2.5 |
| **512000** | 2.8 |
| **522000** | 3.2 |
| **532000** | 4.1 |
| **542000** | 5.0 |
| **552000** | 5.9 |
| **562000** | 6.7 |
| **572000** | 7.7 |
| **578000** | 8.4 |
| **578001** | Single tensile OL (OLR=1.35) |
| **588000** | 8.7 |
| **598000** | 9.7 |
| **608000** | 11.7 |
| **613000** | 12.7 |

The highest crack depth measurements are observed at the point 15˚. Table 4. 5 presents these measurements in relation with the total number of applied loading cycles and Figure 4. 18 gives the graphical representation.

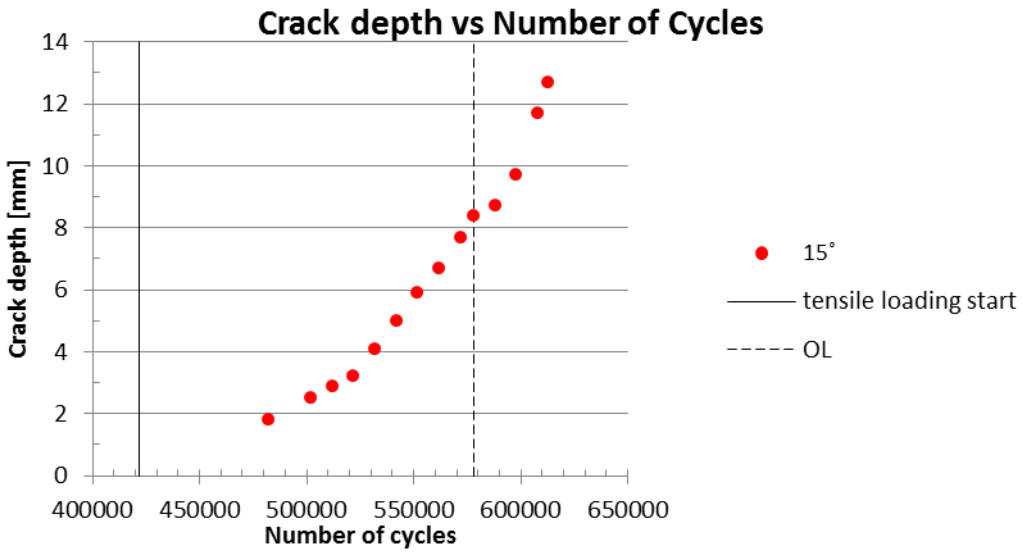


Figure 4. 18: Crack depth growth at position 15˚

A zoom-in of crack depth growth curve is presented again in Figure 4. 19 in order to show a relatively small retardation effect of the overload.

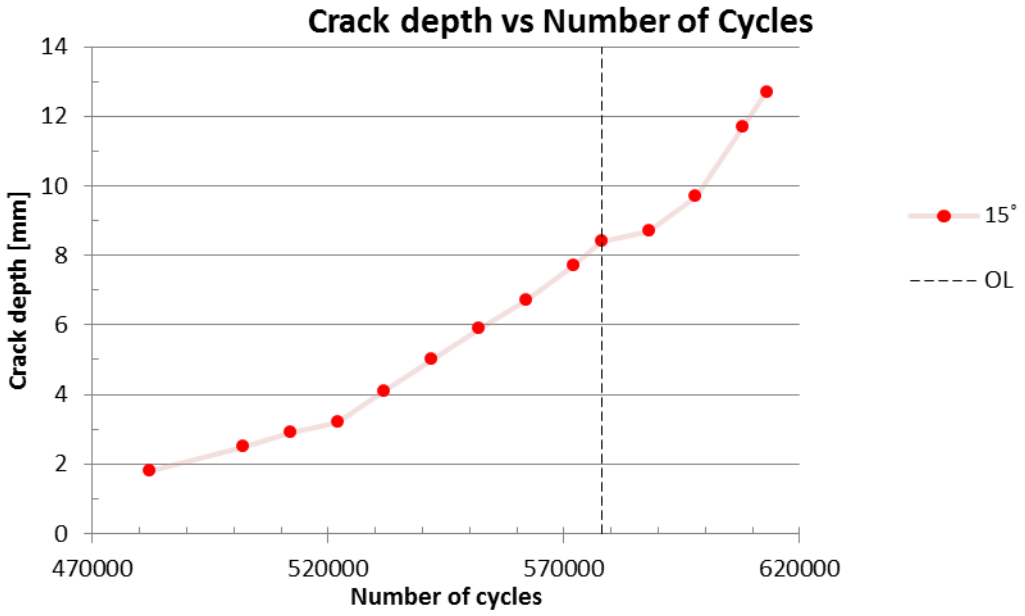


Figure 4. 19: OL effect

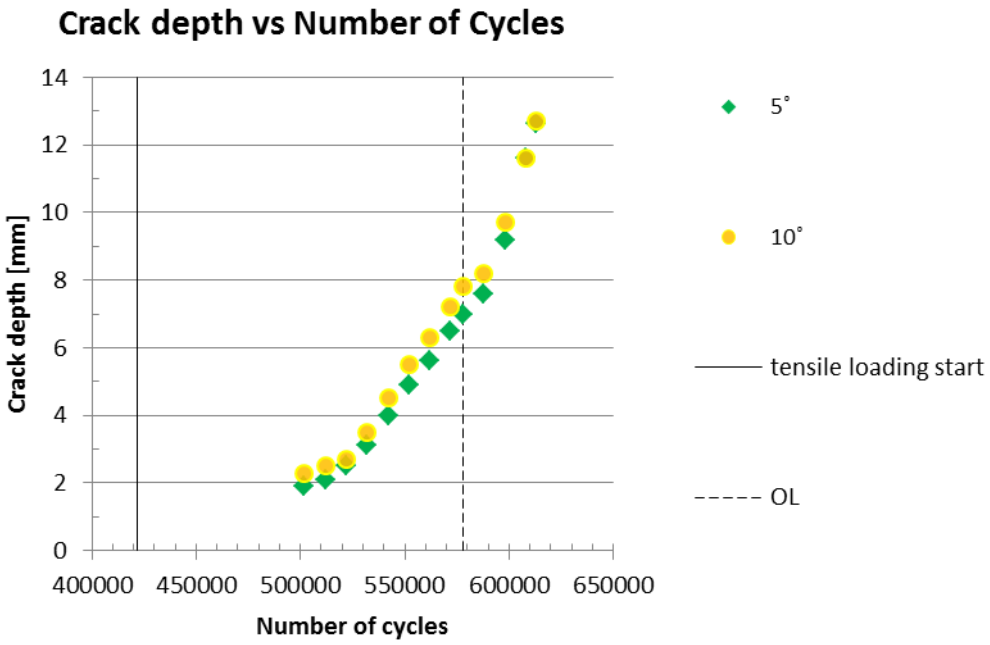


Figure 4. 20: Crack depth growth at positions 5˚ and 10˚

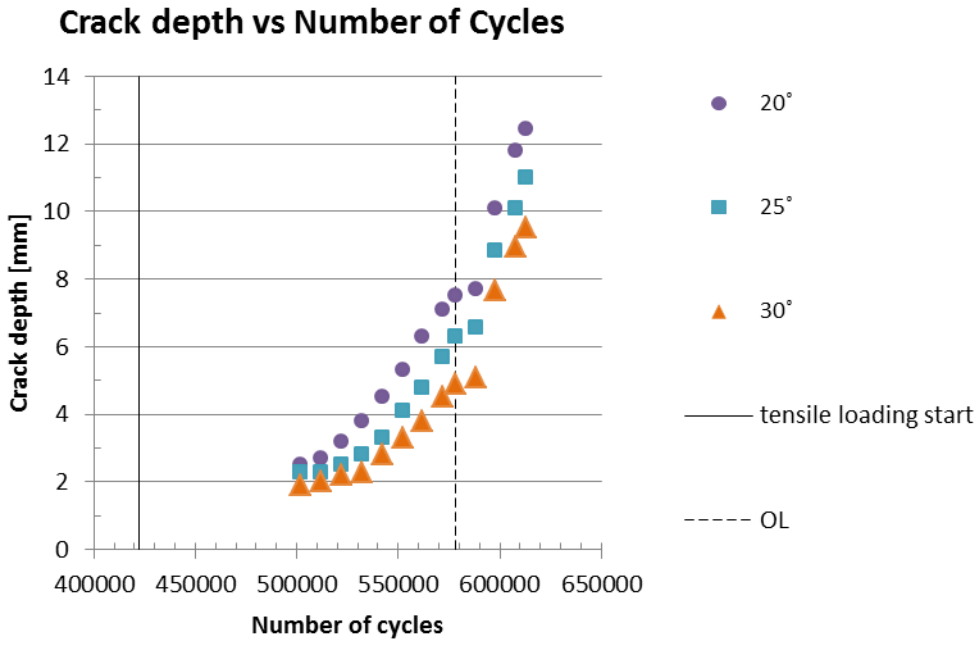


Figure 4. 21: Crack depth growth at positions 20˚, 25˚ and 30˚

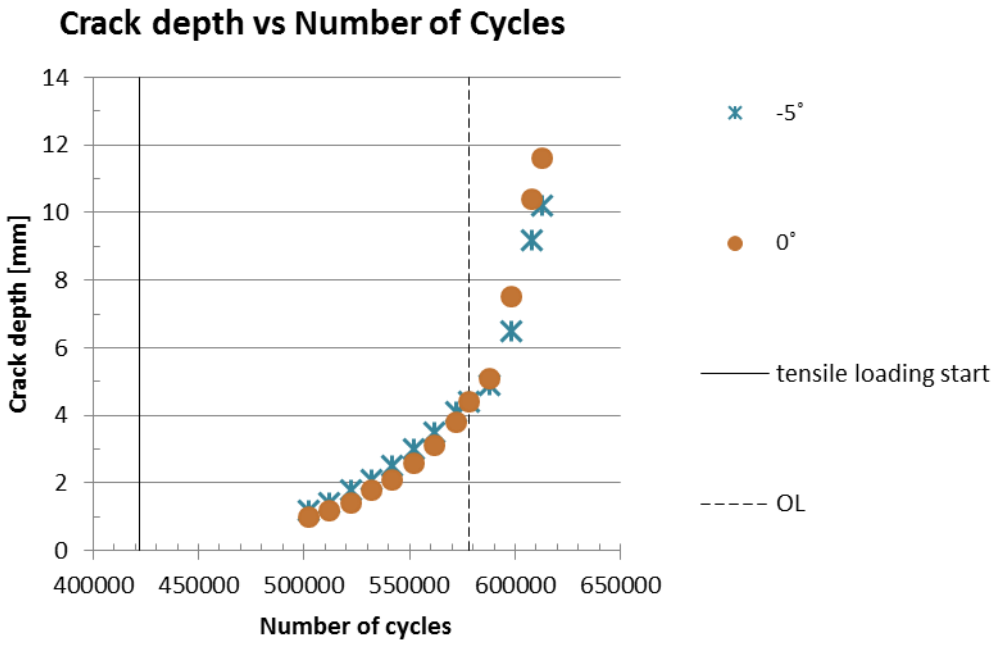


Figure 4. 22: Crack depth growth at positions -10˚, -5˚ and 0˚

Figure 4. 23 shows the crack shape against the total number of cycles at side 1 of the joint.

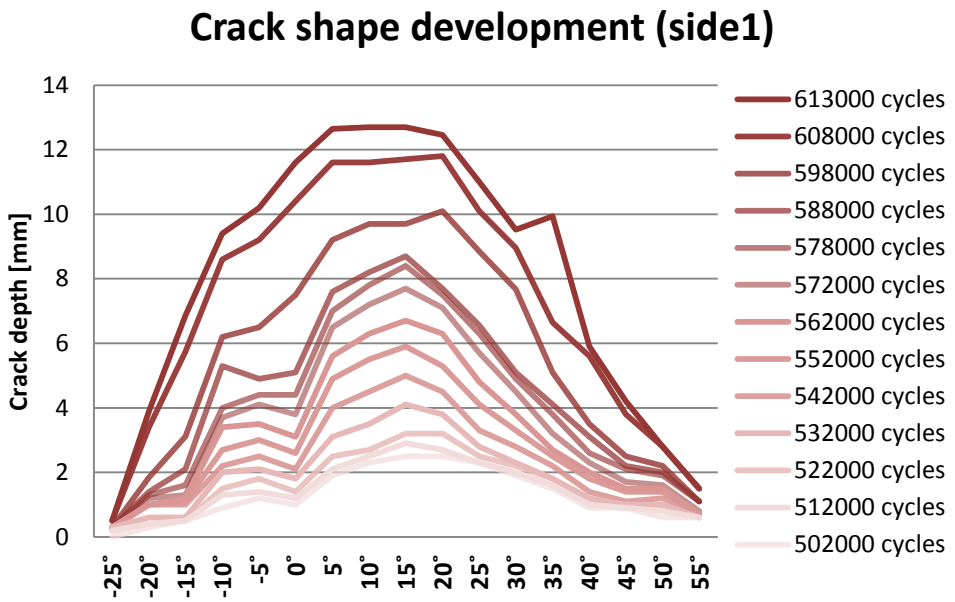


Figure 4. 23: Crack shape development for side 1

Figure 4. 24 and Figure 4. 25 depict the crack depth growth at certain positions close to the crack initiation point of side 2.

An important phenomenon that can be noticed in crack depth growth of side 2 is the crack closure effect after the discrete overload application. According to ACPD results the crack depth after the OL becomes lower which is a clear indication of crack closure effect where

residual compressive stresses bring the crack flanks in contact and a part of the crack (that was opened before the OL) remains closed.

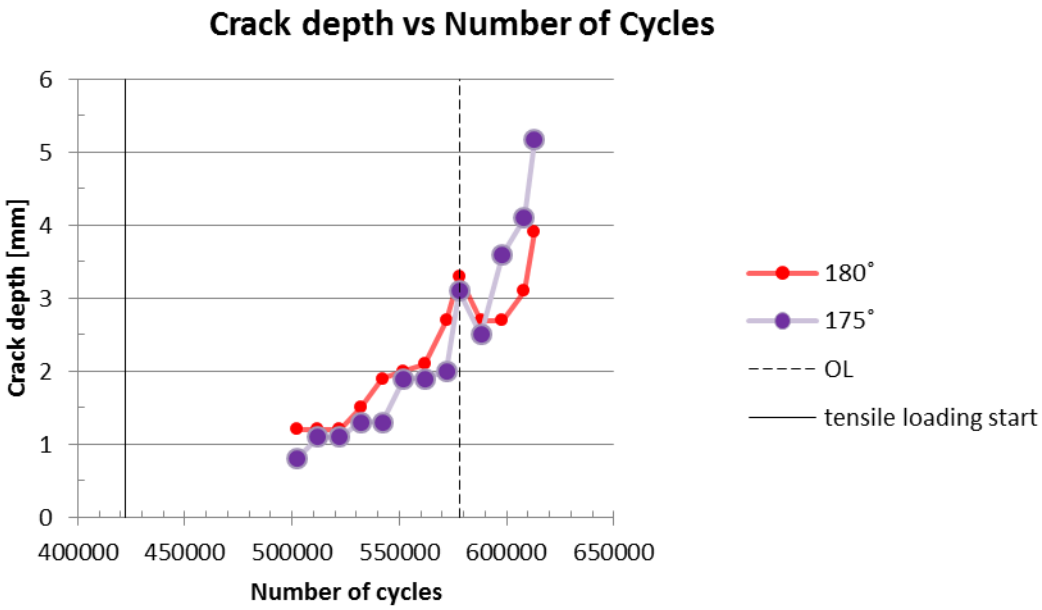


Figure 4. 24: Crack depth growth and closure effects at positions 175˚ and 180˚

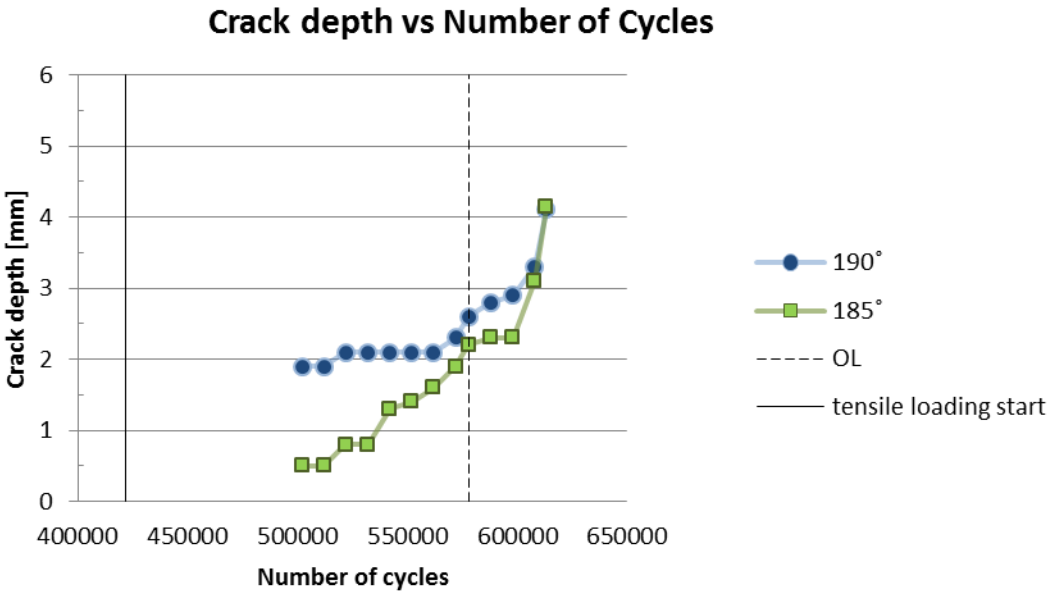


Figure 4. 25: Crack depth growth at positions 185˚ and 190˚

It is obvious from the figures that there is a difference in crack depth between the two sides. This can be explained by the fact that the weld geometry differs at side 2. Also it is a usual phenomenon that crack development does not necessarily grow identically at both sides given the scatter in fatigue crack growth. In the examined case it is possible that the crack growth at side 1 has reached  a later stage of crack propagation (where Paris law is valid, see

Figure 2. 11) while at side 2 this stage has not been reached yet and the crack growth rates are much lower. The size and position of the initial weld defects are the crucial factors for this difference.

### 4.7.3. Crack length results

Crack length extension against cyclic loading is elaborated in Figure 4. 26 and Figure 4. 27. The crack growth rate in length direction decelerates as the crack length extends, because crack edges become closer to the crown points where the SCF is relatively low. In other words, the reduction of stress concentration along the joint intersection leads to the reduction of crack growth rate in width direction as well.

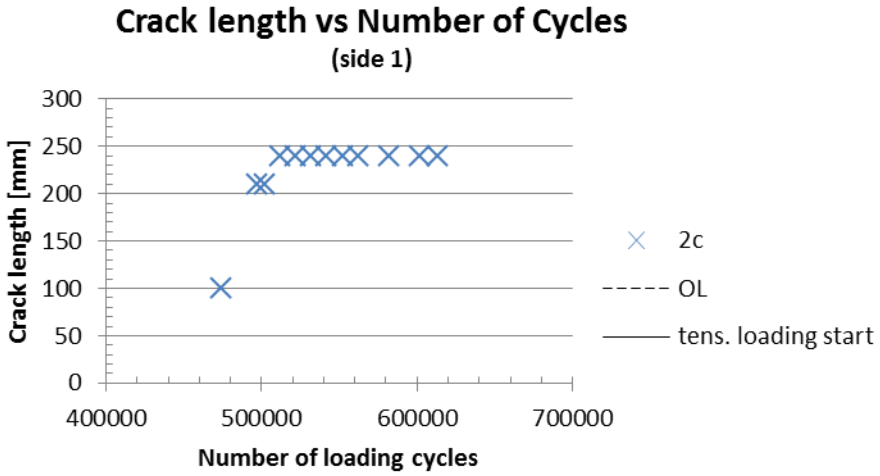


Figure 4. 26: Crack length 2c at side 1

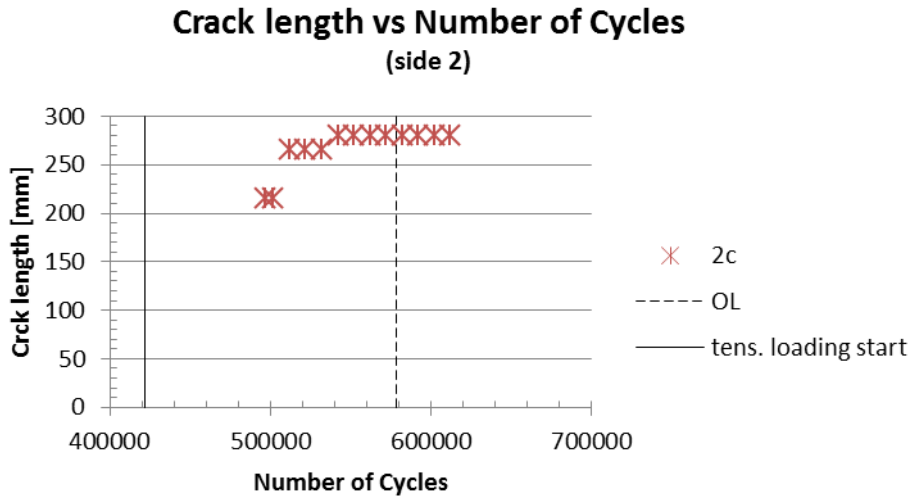


Figure 4. 27: Crack length 2c at side 2

Taking into account the crack length and crack depth curves, it can be concluded that the measured crack aspect ratio (which is equal to crack depth divided by the half of crack length) is permanently much less than 1 during crack propagation stage ($a/c < 1$).

The tubular joints include numerous initial defects at the welded connection (joint intersection) which may become crack initiation points under fatigue loading. This may result in the formation of many small non-detectable cracks at the surface of the weld during the crack coalescence stage (Figure 4. 28). These cracks contribute to the increase of crack length. The described phenomenon is observed in the examined tubular joint test and called multiple crack initiation (Figure 4. 29). Multiple crack initiation makes it difficult to measure or even to detect the crack length till the small cracks join together. Multiple crack initiation at coalescence stage is a phenomenon that can explain the fact that the first visible crack at the weld surface has a quite high length (100-200mm). Figure 4. 29 represents the fracture surface close to the edges of the crack (where crack coalescence effect is quite pronounced).

Figure 4. 23 presents the crack shape at side 1 of the joint on the basis of ACPD and visual inspection measurements. The low values of depth and the irregularities at the areas close to the surface crack edges (especially in the first measurements) indicate that crack development at these areas is still in the coalescence stage and the multiple crack initiation effect can be slightly seen.


**Figure 4. 28: Assumption of multiple crack initiation at crack coalescence stage in the surface of the weld**

**Figure 4. 29: Multiple crack initiation observed on fracture surfaces**

On the basis of previously referred crack depth and crack length measurements Figure 4. 30 presents in a 3D mode the measured surface crack developments by the number of (total) loading cycles. The surface crack is presented in 3 different stages of crack propagation.

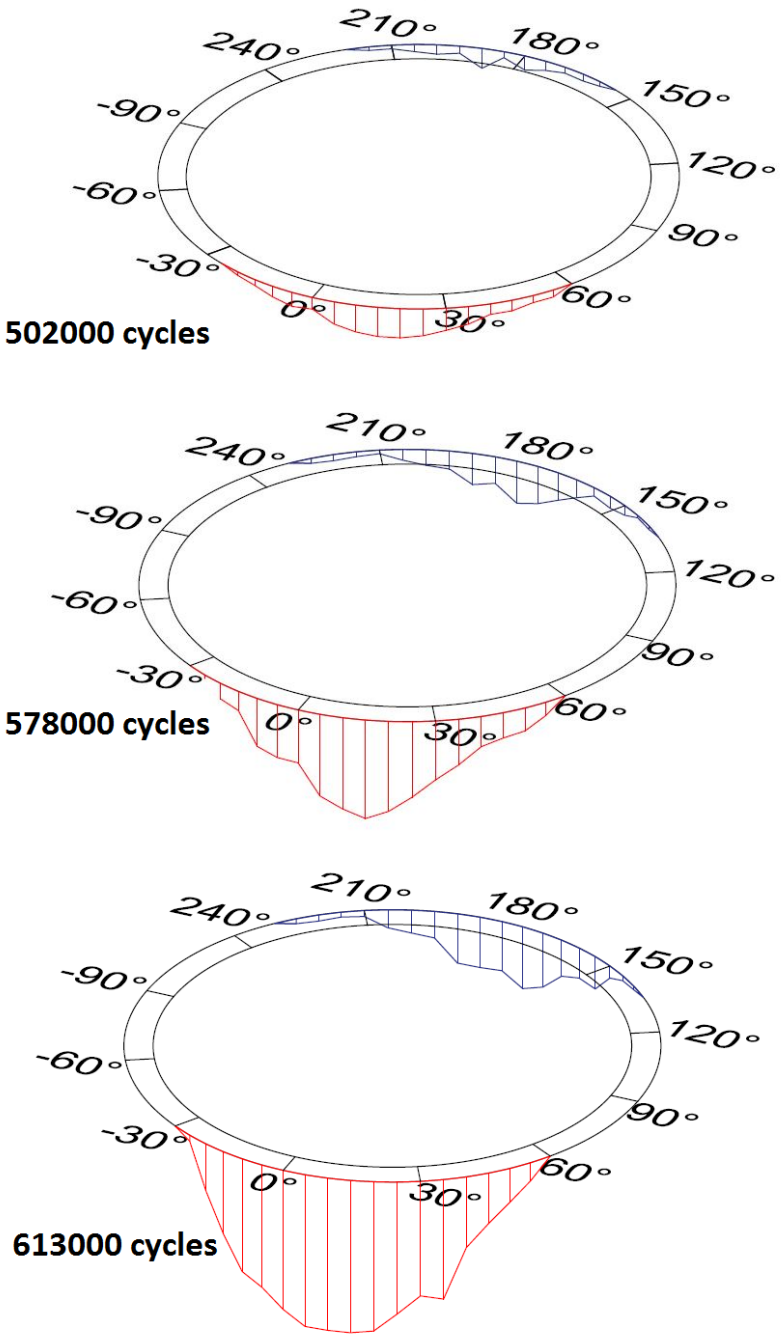


Figure 4. 30: 3D projection of surface cracks development around the joint vs. total number of loading cycles

### 4.7.4. Validation methods

Phased Array method is applied at a certain propagation stage (after 578000 loading cycles) at several points of side 1 and side 2, mainly those ones with the highest crack depth values. The ACPD measurements and Phased Array inspection results are compared in Table 4. 6.

Table 4. 6: Comparison between ACPD and PA measurements

| Side 1 (at 578000 loading cycles) | | |
|---|---|---|
| **positions** | **ACPD** | **Phased Array** |
| **-20˚** | 1.3 | 2.5 |
| **-15˚** | 1.6 | 2.5 |
| **-10˚** | 4.0 | 2.7 |
| **-5˚** | 4.4 | 2.6 |
| **0˚** | 4.4 | 3.8 |
| **5˚** | 7.0 | 6.8 |
| **10˚** | 7.8 | 7.7 |
| **15˚** | 8.4 | 8.1 |
| **20˚** | 7.5 | 7.8 |
| **25˚** | 6.3 | 5.8 |
| **30˚** | 4.9 | 5.0 |
| **35˚** | 3.8 | 3.4 |
| **40˚** | 2.6 | 2.6 |
| **45˚** | 2.1 | 2.0 |
| **50˚** | 1.9 | 1.9 |
| **55˚** | 1.1 | 1.9 |

| Side 2 (at 578000 loading cycles) | | |
|---|---|---|
| **positions** | **ACPD** | **Phased Array** |
| **170˚** | 2.3 | 1.9 |
| **175˚** | 3.1 | 3.5 |
| **180˚** | 3.3 | 3.3 |
| **185˚** | 2.2 | 3.9 |
| **190˚** | 2.6 | 4.1 |
| **195˚** | 1.5 | 3.3 |

Figure 4. 31 elaborates the projection of crack shape at side 1 according to both measurements.

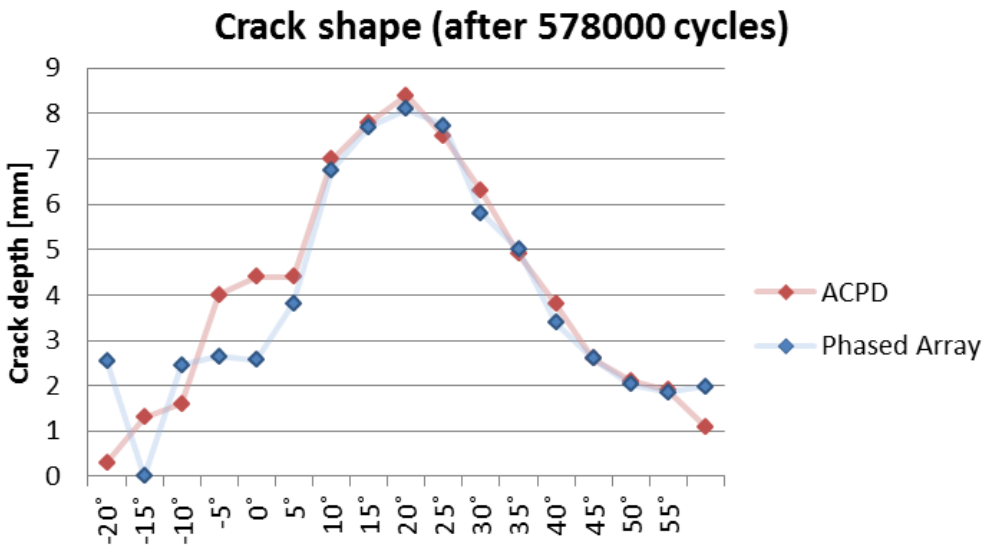


Figure 4. 31: Graphical comparison between ACPD and PA measurements

Phased array and ACPD method have ±1 mm and ±1.5 mm (see Appendix F) accuracy scatter respectively, so the measurements can be verified.

After the termination of the test, the tubular joint is cut into slices in the vertical direction (Figure 4. 32) in order to see the crack depth at the intersection of the joint and measure it with convenient means. These values are compared with the final ACPD crack depth measurements. This destructive test is an additional verification procedure for ACPD measurements.

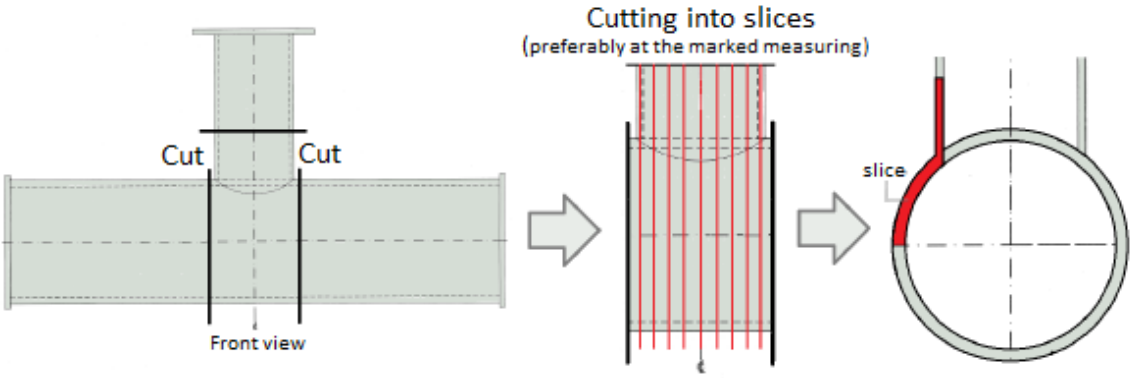


Figure 4. 32: Cutting into slices the tubular joint (destructive test)


Figure 4. 33: Measuring through thickness crack

Table 4. 7: Comparison between ACPD and real through thickness crack measurements

| Side 1 (at 613000 cycles) | | |
|---|---|---|
| **positions** | **ACPD** | **Real through thickness crack** |
| **-15˚** | 6.9 | 7.0 |
| **15˚** | 12.7 | 13.7 |
| **50˚** | 2.8 | 3.8 |
| **0˚** | 3.1 | 3.4 |

The fact that ACPD crack depth measurements are slightly lower than the through thickness cracks could be explained by the crack closure effect. ACPD method measures the path length that alternating current crosses over a cracked area. In cases of crack closure presence, where a part of the crack is closed, the path length includes only the opening part ofl crack depth. To conclude, the inability of ACPD method to take into account crack closure is the reason why the ACPD crack depth measurements are lower than the real ones.

The slice which corresponds to the saddle point of side 1 (which also includes the locations -15˚ to 15˚) is subjected in 3-point bending (Figure 4. 34) in order to open the crack (Figure 4. 35) to examine the fracture surfaces and see the results of crack front marking method (Table 4. 8).

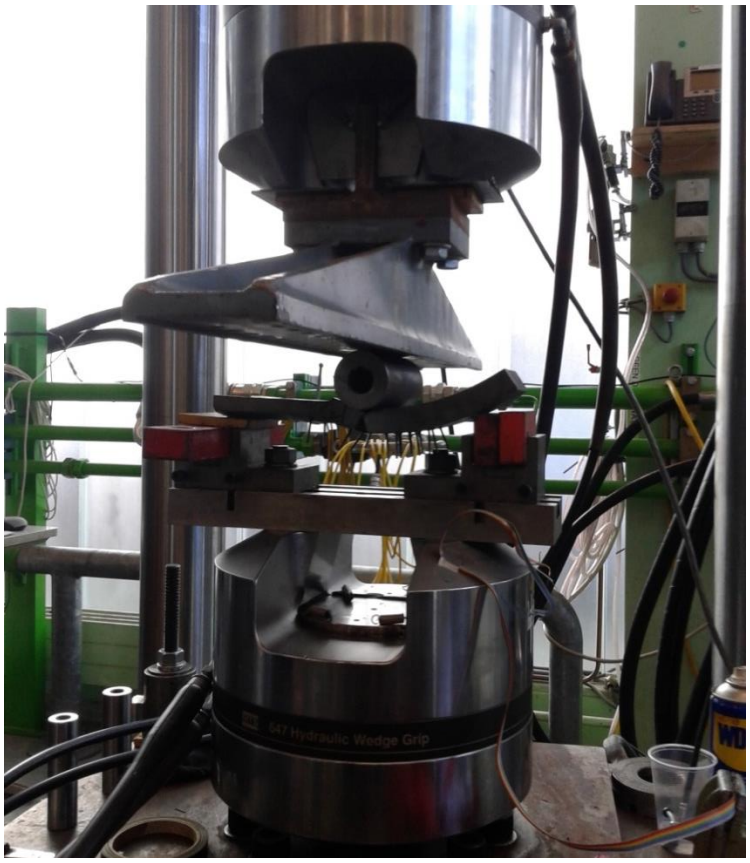

Figure 4. 34: 3-point bending test on a slice of the tubular joint

Figure 4. 35: Opened crack on a slice of tubular joint

Crack front marking technique verifies the results as well for an interval from -15˚ to 15˚ from the saddle point of side 1.

Table 4. 8: Comparison between ACPD measurements and crack front marking results

| Side 1 (at 562000 cycles) | | |
|---|---|---|
| **positions** | **ACPD** | **Crack front marking** |
| **-15˚** | 1.2 | 2.0 |
| **-10˚** | 3.4 | 4.0 |
| **-5˚** | 3.5 | 3.8 |
| **0˚** | 3.1 | 3.4 |
| **5˚** | 5.6 | 5.8 |
| **10˚** | 6.3 | 6.4 |
| **15˚** | 6.7 | 6.9 |

### 4.8. Stress field around joint intersection

Strain gauge measurements at certain locations show an important difference between the absolute values of strain ($\varepsilon_{max}$, $\varepsilon_{min}$) under compressive and tensile loading. The value of $\varepsilon_{max}$ corresponds to the force peak of cyclic loading while $\varepsilon_{min}$ to the force valley. The main explanation for these results is related to the existence of residual stresses due to shrinkage of the welded area in welded structures. However the strain range at a certain gauge position remains almost constant (negligible differences) both under compression and tension. Residual stresses contribute equally for $\varepsilon_{max}$ and $\varepsilon_{min}$ to the strain value change, so there is no change in strain range.

#### 4.8.1. Stress ranges around the joint

The strain gauges no. 1, 8, 9, 10, 17, 18, 19, 26, 27, 28, 35 and 36 are positioned around the joint at the same distance from the weld toe (5mm).

The strain gauge measurements around the joint at a distance of 5 mm from weld toe are processed and give the strain ranges at these positions. By applying equation 4.2 the strain ranges are transformed to stress ranges. The progress of these stress ranges by the fatigue loading cycles is represented in Figure 4. 36 and Figure 4. 37.

Strain gauge 9 proved to be defective and gauge 36 did not operate after 500000 loading cycles.

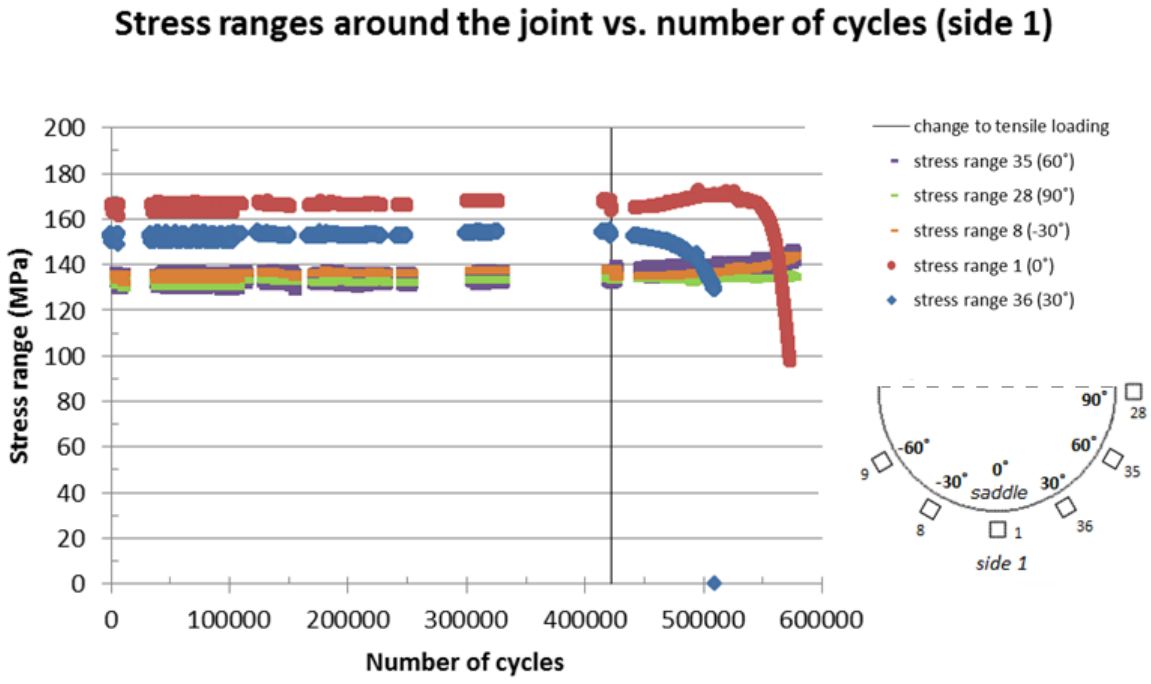


Figure 4. 36: Stress ranges around the joint vs. number of loading cycles for side 1

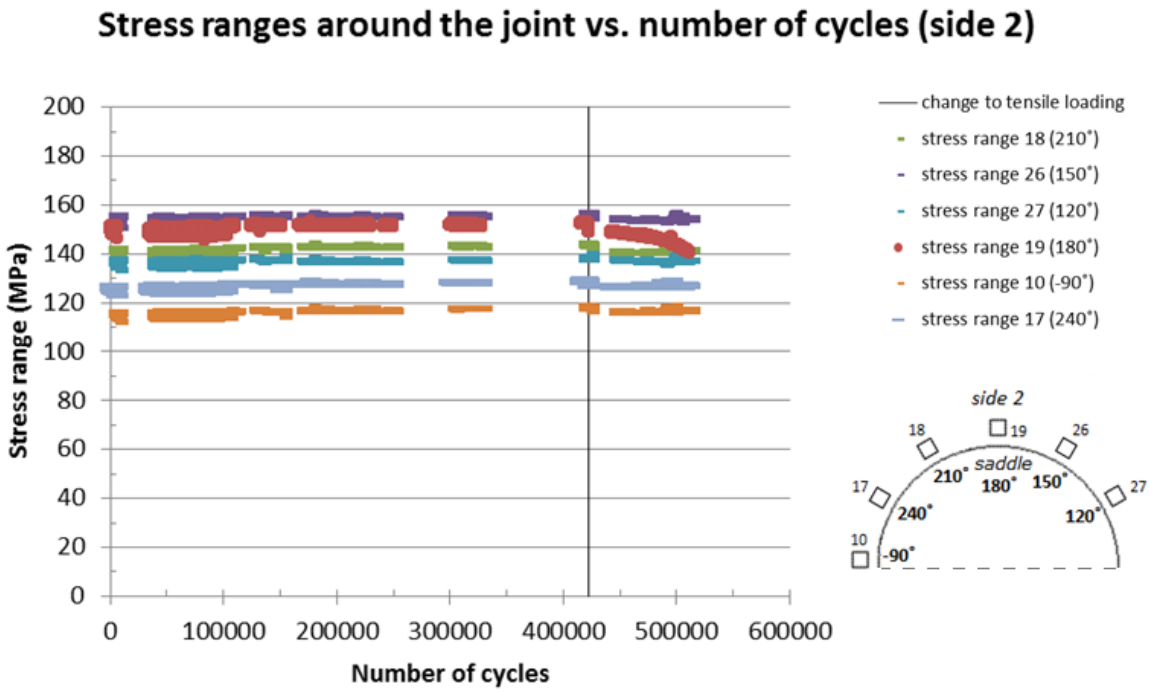


Figure 4. 37: Stress ranges around the joint vs. number of loading cycles for side 2

It is clear that the stress range falls at the positions where the crack has been developed in both dimensions and has reached a relatively high depth with non-negligible growth rates. These positions correspond to the saddle points 0˚ and 180˚ and the gauge location 36 (30˚). Figure 4. 30 indicates that the aforementioned positions are the only gauge points that are located in the middle of relatively deep cracks while they are expanded. The cracked areas cannot resist anymore the stress ranges at the surface which they could in the uncracked situation.

Hence, the stress range fall that can be noticed in Figure 4. 38 - Figure 4. 40 (with no change of the applied fatigue loading) indicates that there is crack formation at this position of the structure and the neighboring areas.

The following curves show the tensile stress ranges progress in comparison with the crack depth development at certain points where the crack is highly developed. The loading cycles only give the tensile loading.

Stress range pattern of position 36 (30˚) is different from the corresponding pattern of position 1 (0˚). This can be possibly explained by the non-simultaneous crack formation at these two locations. The first visible surface crack was extended from position of 5˚ to 35˚ degrees angle from the saddle. This length includes only gauge position 36 (30˚). When the crack reaches position 36 (30˚) the neighboring uncracked areas – such as position 1 (0˚) - are still subjected to the same levels of stress ranges or even a bit higher because of slight stress redistribution (position 1 see Figure 4. 39). As the crack continues to expand and approaches position 1 the stress range normally decreases at this point as well.

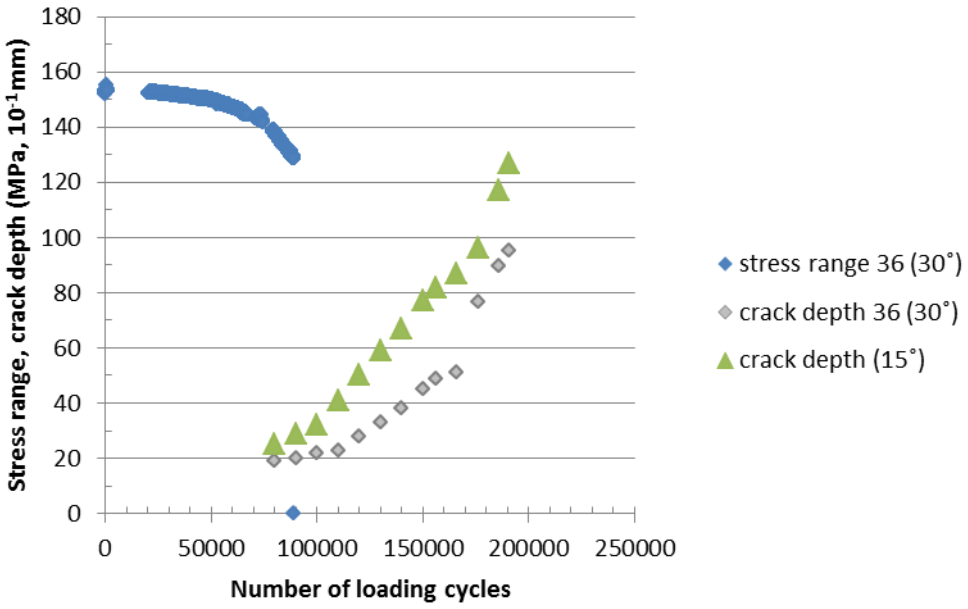


Figure 4. 38: Stress range and crack depth development at the points 15˚ and 30˚ of side 1 vs. number of tensile cycles

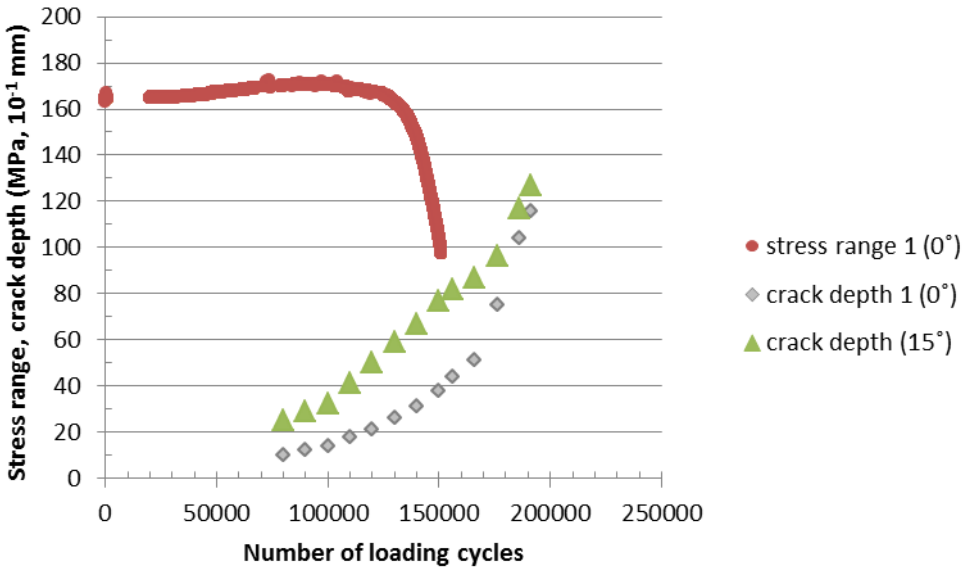


Figure 4. 39: Stress range and crack depth development at the saddle point 0˚ and the neighboring point 15˚ of side 1 vs. number of tensile cycles

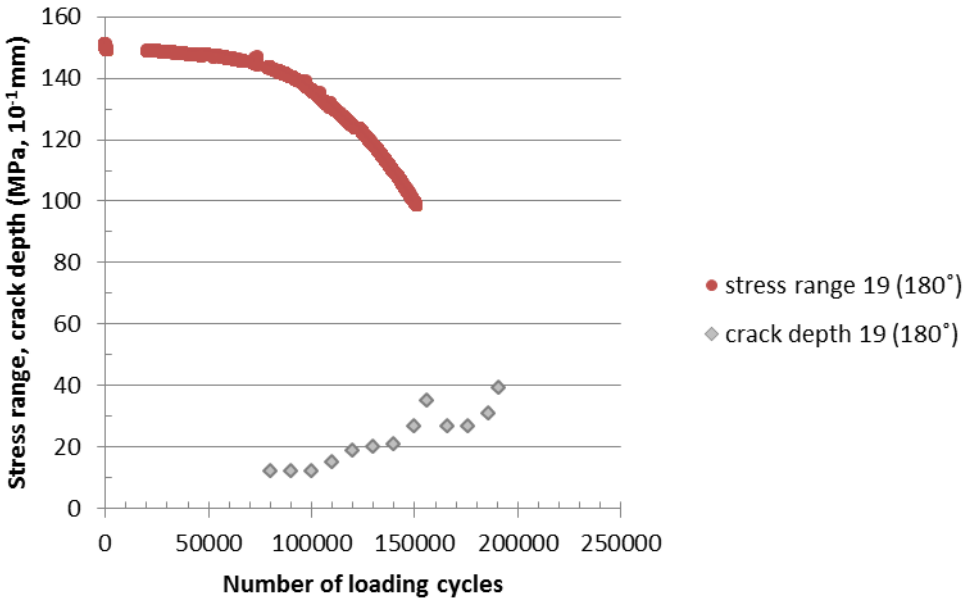


Figure 4. 40: Stress range and crack depth development at the saddle point 180˚ of side 2 vs. number of tensile cycles

Admittedly, the stress range vs. loading cycles curves at certain locations around the joint provide a useful tool for an estimation of possible crack formation at these regions.

### 4.8.2. Stress extrapolation for the determination of hot spot stress range

Strain gauges no. 1, 2, 3, 4, 5, 6, 7, 19, 20, 21, 22, 23, 24 and 25 are located at the saddle points of the joints in various distances from the weld toe as shown in Figure 4. 16. These strain gauge measurements from both sides are used in order to obtain the geometric stress range at the saddle points of the chord of the examined joint. The geometric stress range is defined as the maximum extrapolated stress range to the weld toe, taking the global geometrical effects into account.

For linear extrapolation two points are defined at the saddle points of the chord. One should be outside the nonlinear stress area *[5]*. According to DNV code *[6]* the extrapolation points should be taken at $0.5t_0$ and $1.5\ t_0$ from the weld toe, where $t_0$ is the chord thickness (Figure 4. 41).

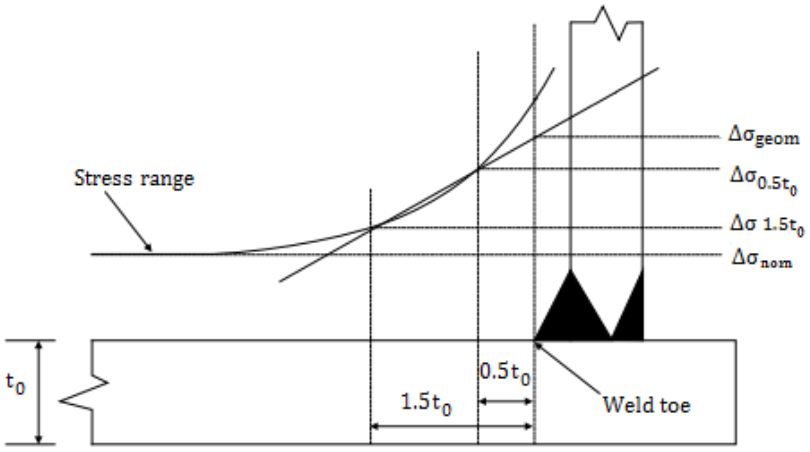


Figure 4. 41: Linear stress extrapolation according to DNV

The calculation of stress ranges at the extrapolation points is a necessary condition to apply linear stress extrapolation. These values are derived by the following procedure:

- The strain gauge measurements are taken at a certain stage of fatigue loading: after 1000 tensile loading cycles.

- The strain ranges are equal to the difference between strains corresponding to force peak and force valley.

- In the tested specimen the gauges on the saddle point are installed in the positions that are shown in Table 4. 9 and Table 4. 10 for each side where the strain ranges at these locations are presented and the corresponding stress ranges are calculated in accordance with eq. 4.2. Figure 4. 42 presents the pictures where the gauges position (and distance from weld toe) can be seen at each side.

Table 4. 9: Conversion to stress range (side 1) at first 1000 tensile cycles where there was not crack initiation yet, and therefore no fall or increase of strain ranges

| gauge number | 1 | 2 | 3 | 5 | 7 |
|---|---|---|---|---|---|
| Weld toe distance [mm] | 5 | 7 | 9 | 13 | 39 |
| Δε | 713.48 | 629.08 | 575.55 | 500.64 | 177.08 |
| Δσ [MPa] | 164.98 | 145.46 | 133.08 | 115.76 | 40.95 |

The strain gauges 4 and 6 proved to be defective

Table 4. 10: Conversion to stress ranges (side 2) at first 1000 tensile cycles

| gauge number | 19 | 20 | 21 | 22 | 23 | 24 | 25 |
|---|---|---|---|---|---|---|---|
| Weld toe distance[mm] | 5 | 7 | 9 | 11 | 13 | 23 | 37 |
| Δε | 651.67 | 585.67 | 522.93 | 505.36 | 462.32 | 300.75 | 163.79 |
| Δσ [MPa] | 150.69 | 135.42 | 120.92 | 116.85 | 106.90 | 69.54 | 37.873 |

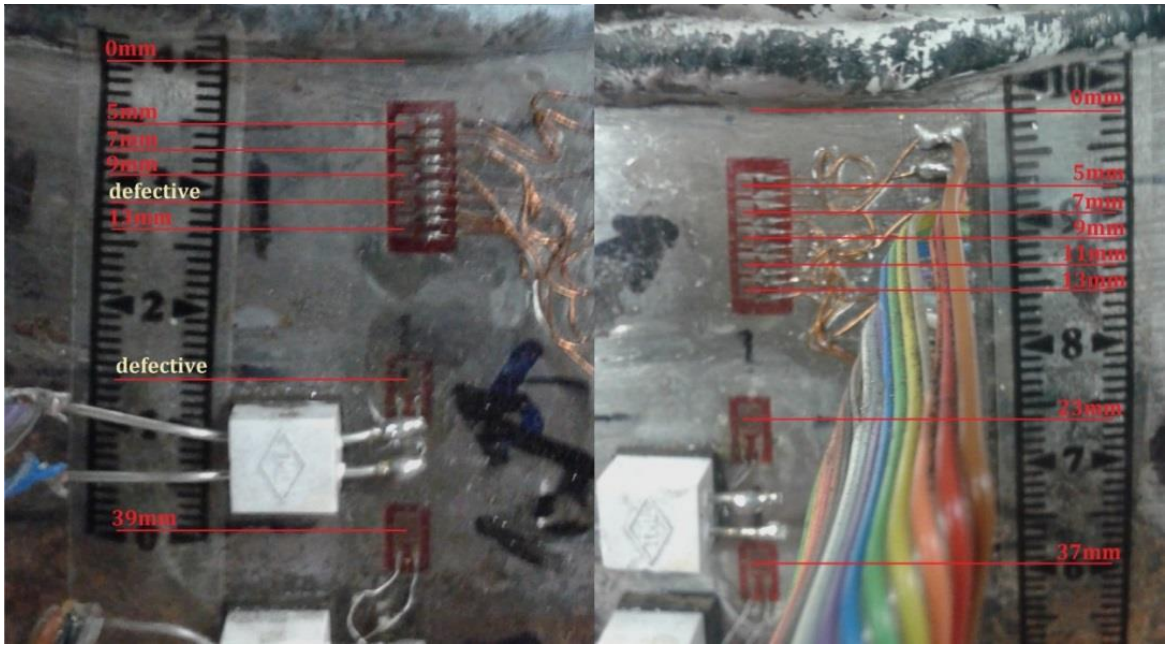


Figure 4. 42: Strain gauges positioning at the saddle points of side 1 (left) and side 2 (right)

After that, all the stress ranges values are gathered in the curve of Figure 4. 43 and an exponential trend line is designed to approximate the stress ranges at the exact positions that are required for the linear stress extrapolation ($0.5t_0$=12.5mm and $1.5t_0$=37.5mm).

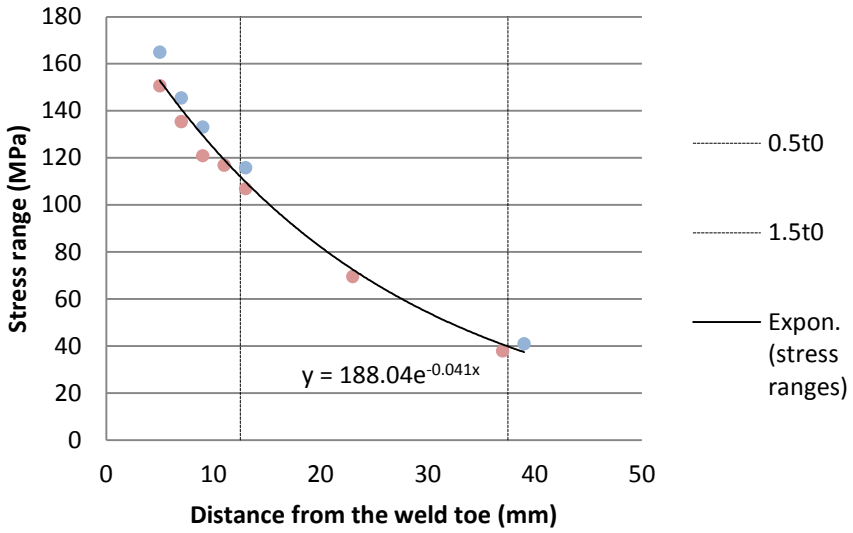


-

Figure 4. 43: Stress rages vs. distance from the weld toe and exponential trend line projection

- According to the aforementioned procedure the stress ranges are equal to 112.6 MPa and 40.4 MPa at the positions of $0.5t_0$ and $1.5t_0$ from weld toe respectively.

The next step is the linear extrapolation of the recommended points to the weld toe. The result of this procedure in accordance with DNV code is depicted in Figure 4. 44.

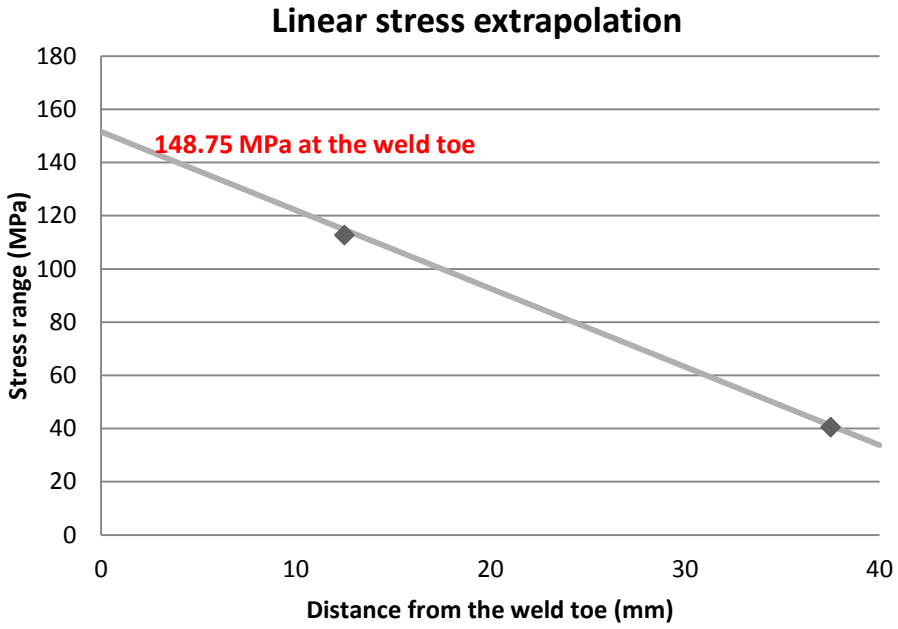


Figure 4. 44: Linear stress extrapolation

Table 4. 11 presents the geometric stress range at the weld toe and the stress concentration factors as well that are derived from the procedure described in this paragraph.

Table 4. 11: Geometric stress ranges and SCF's per side and code

| method | geometric Δσ [MPa] | SCF |
|---|---|---|
| **linear extrapolation (DNV)** | 148.75 | 4.60 |

The experimentally linearly extrapolated hot-spot stress range is used as an input in the application of S-N curves (Chapter 5) and numerical simulation of crack growth (Chapter 6).

## 4.9. Conclusions

In this last paragraph the concluding remarks and the recommendations are described below as far as the examined case is concerned:

- The impact of residual stresses cannot be neglected. Their impact on the difference between the absolute strain values under compression and tension is more than clear.

- In the examined case during crack propagation stage the crack aspect ratio (a/c) is much lower than 1.0.

- As fatigue loading continues and the surface crack propagates the crack growth in through-thickness direction accelerates while the corresponding value in

length direction decreases due to the geometry. According to this statement the failure criterion is based on the crack depth in thickness direction.

- The non-detectable initial weld defects and multiple crack initiation phenomenon in the welded area makes the estimation of crack length extension difficult especially during the early stages of crack propagation.

- The application of a single overload (even small OLR) has a retardation effect on crack depth propagation and sometimes can contribute to crack closure effect.

- The ACPD method can be considered reliable in measuring crack depth on tubular structures as long as a proper measuring procedure has been followed.

- Strain gauge measurements can give a rough estimation of cracked locations around the joint intersection and can be used as a verification method for an approximate detection crack initiation points.

**References**


**[1]** R.Collins, D.H.Michael and R.Clark – Measurements of Crack Depth in a transition weld using ACPD – Review of Progress in Quantitative Evaluation, Vol. 11, New York 1992

**[2]** M.Truchon, H.P.Lieurade – Experimental Study of Surface Crack propagation

**[3]** https://en.wikipedia.org/wiki/Phased_array_ultrasonics

**[4]** Daniel Kass and Tom Nelligan - Ultrasonic Testing of Metal Bars and Tubular Products – Quality Magazine (October 12, 2015)

**[5]** S. J. Maddox - Recommended Hot-Spot Stress Design S-N Curves for Fatigue Assessment of FPSOs - International Journal of Offshore and Polar Engineering (June 2001)

**[6]** Recommended Practice DNV-RP-C203 - Fatigue Design of Offshore Steel Structures (October 2011)

# 5. S-N CURVES COMBINED WITH HOT-SPOT STRESS METHOD

## 5.1. Introduction

In this chapter the fatigue evaluation of the tested tubular specimen presented in chapter 4 is applied with the use of S-N curves combined with the hot spot stress method. In the second chapter it is stated that the most appropriate code chosen for our study using S-N curves is the DNV code. There is a variety of adjustments that have to be done to obtain an accurate prediction of fatigue damage.

## 5.2. Stress Concentration Factors

As referred in the second chapter, the structural discontinuities of a welded tubular connection lead to stress concentrations in the vicinity of the weld. The highest stress concentration exists in the "hot-spot stress" areas and it depends on the joint configuration and loading type.

The case depicted in Figure 5. 1 is closer to any other cases provided from DNV code (in terms of boundary condition and geometry) in the examined test case. In case of an axially loaded T-joint in the brace of Figure 5. 1 the SCF variation according to *DNV-RP-C203 Fatigue Design of Offshore Steel Structures* can be used where the SCF equations are based on finite element analysis.

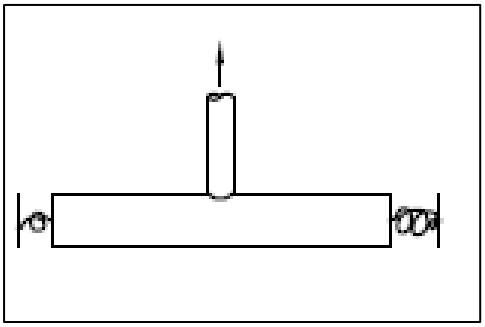

**Figure 5. 1: Tubular T-joint axially loaded in the brace under general fixity conditions**

The validity range for the equations is as follows:

$$0.2 \le \beta \le 1.0$$
$$0.2 \le \tau \le 1.0$$
$$8 \le \gamma \le 32$$
$$4 \le \alpha \le 40$$

$$\alpha = 2L/D$$

$$20^\circ \le \theta \le 90^\circ$$

The SCF equations for axially loaded T-joints are as follows:

$$SCF_{\text{chord saddle}} = \gamma\,\tau^{1.1}(1.11-3(\beta-0.52)^2)(\sin\theta)^{1.6} + C_1(0.8\alpha-6)\,\tau\,\beta^2(1-\beta^2)^{0.5}(\sin 2\theta)^2 \quad \textbf{(eq. 5.1a)}$$

$$SCF_{\text{chord crown}} = \gamma^{0.2}\,\tau\,(2.65+5(\beta-0.65)^2) + \tau\,\beta(C_2\cdot\alpha-3)\sin\theta \quad \textbf{(eq. 5.1b)}$$

$$SCF_{\text{brace saddle}} = 1.3 + \gamma\,\tau^{0.52}\,\alpha^{0.1}(0.187 - 1.25\beta^{1.1}(\beta - 0.96))\,(\sin\theta)^{(2.7-0.01\alpha)} \quad \textbf{(eq. 5.1c)}$$

$$SCF_{\text{brace crown}} = 3 + \gamma^{1.2}(0.12\exp(-4\beta) + 0.011\,\beta^2 - 0.045) + \tau\,\beta\,(C_3\cdot\alpha - 1.2) \quad \textbf{(eq. 5.1d)}$$

*C = chord end fixity parameter 0.5 ≤ C ≤ 1.0,*

*Typically: C=0.7* $C_1 = 2(C-0.5)$ $C_2 = C/2$ $C_3 = C/5$

The aforementioned parametric equations for axially loaded T-joints have been developed by Efthymiou, 1988.

In case of short chords the effect of supports should be taken into account by applying a reduction factor at the SCF calculations of the saddle points. A chord is considered short when the value of non-dimensional parameter α is less than 12. The short chord reduction factor in the examined case is calculated according to the following formula by DNV code:

$$F = 1 - (1.43\beta - 0.97\beta^2 - 0.03)\gamma^{0.04}e^{(-0.71\gamma^{-1.16}\alpha^{2.5})}$$

***(eq. 5.2)***

Applying these equations by using as an input the non-dimensional parameters of Table 5. 1 leads to the stress concentration factors for saddle and crown points of the chord and brace of the joint (Table 5. 2).

**Table 5. 1: Dimensions and non-dimensional parameters of the examined tubular joint**

| | | | |
|---|---|---|---|
| **Brace thickness (t)** | 16 mm | **α=2L/D** | 7.87 |
| **Chord thickness (T)** | 25 mm | **β=d/D** | 0.64 |
| **Brace diameter (D)** | 323.9 mm | **γ=2D/2T** | 10.16 |
| **Chord diameter (d)** | 508 mm | **τ=t/T** | 0.64 |
| **Brace angle (θ)** | 90˚ | **Chord end fixity parameter (C )** | 0.7 |

**Table 5. 2: SCF in saddle and crown points of the chord and brace according to parametric equations**

| | Chord | Brace |
|---|---|---|
| **Saddle** | **6.18** | 5.20 |
| **Crown** | 2.60 | 2.46 |

The data presented in the Table 5. 2 validate that the stress concentration in the saddle point of the chord is governing for the examined case (Figure 5. 2) and Table 5. 3 provides the geometric stress ranges at the saddle points of the chord that are derived from linear extrapolation of the experimental measurements in Chapter 4 and the Efthymiou parametric equations.

**Table 5. 3: Geometric stress ranges and SCF's at the saddle point of the chord for each method**

| method | geometric Δσ [MPa] | SCF |
|---|---|---|
| **linear extrapolation** | 148.75 | 4.60 |
| **Efthymiou equations** | 200.01 | 6.18 |

The experimental calculation of SCF for the specific specimen provides a much lower value compared to the generalized Efthymiou equations in terms of fatigue life.

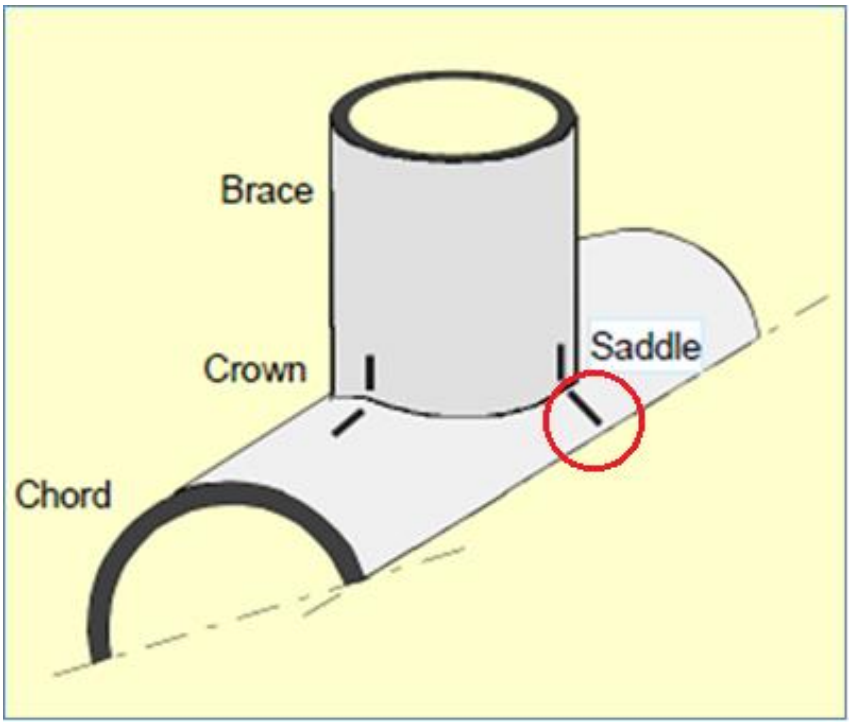


Figure 5. 2: Saddle point of the chord is the position where the highest value of SCF appears

### 5.3. Thickness effect

According to DNV code, the thickness effect is accounted for by modification of the design S-N curve for a thickness larger than the reference thickness:

$$logN = logC - m \cdot log\left(\Delta\sigma_{geom}\left(\frac{t}{t\,ref}\right)^{k}\right) \qquad \textit{(eq. 5.3)}$$

where:

$t_{ref}$ = reference thickness is 32 mm for tubular joints

t = thickness through which a crack will most likely grow (25 mm)

k = thickness exponent on fatigue strength (=0.25 according to DNV)

The thickness of the chord is 25 mm which is lower that the reference thickness (32mm). Finally, the following equation of S-N line is used:

$$logN = logC - m \cdot log\left(\Delta\sigma_{geom}\left(\frac{25}{32}\right)^{0.25}\right) = logC - m \cdot log\left(0.94\Delta\sigma_{geom}\right) \qquad \textit{(eq. 5.4)}$$

Where geometric stress $\Delta\sigma_{geom}$ =SCF·$\Delta\sigma_{nom}$ in the brace

### 5.4. Design and mean S-N curves

The design curves that used in Recommended Practice DNV-RP-C203 are based on the mean-minus-two-standard-deviation curves for relevant experimental data. The design S-N curves are thus associated with 97.7% probability of survival and rely on the equation:

$$logN = logC - m \cdot log\Delta\sigma \qquad \textit{(eq. 5.5)}$$

$\log C = \log\hat{C} - 2 \cdot s_{logN}$

where $\log\hat{C}$ = intercept of mean S-N curve with the logN axis
$s_{logN}$ = standard deviation of logN
(typical standard deviation equals to 0.2 according to DNV code)

In order to obtain the data for mean S-N curves the reverse procedure has to be followed. In other words, the double value of standard deviation of logN should be added to the intercept of log N-axis by the design S-N curves.

#### 5.4.1. S-N curves

Design and mean S-N curves for tubular joints in air environment are given in Table 5. 4. For offshore structures subjected to typical wave and wind loading the main contribution to fatigue damage is in the region $N > 10^7$ cycles and the bilinear S-N curves defined in this table should be used.

Table 5. 4: Definition of S-N curves in air

| | $N \leq 10^7$ | | $N > 10^7$ | | Fatigue limit at $10^7$ cycles | Thickness exponent *k* |
|---|---|---|---|---|---|---|
| | $m_1$ | $\log C_1$ | $m_2$ | $\log C_2$ | | |
| **Design S-N curve** | 3.0 | 12.164 | 5.0 | 15.606 | 52.63 | 0.25 for SCF ≤ 10.0 |
| **Mean S-N curve** | 3.0 | 12.564 | 5.0 | 16.006 | 71.56 | 0.25 for SCF ≤ 10.0 |

Figure 5. 3 shows the design and mean S-N curves for tubular joints in ambient air conditions.

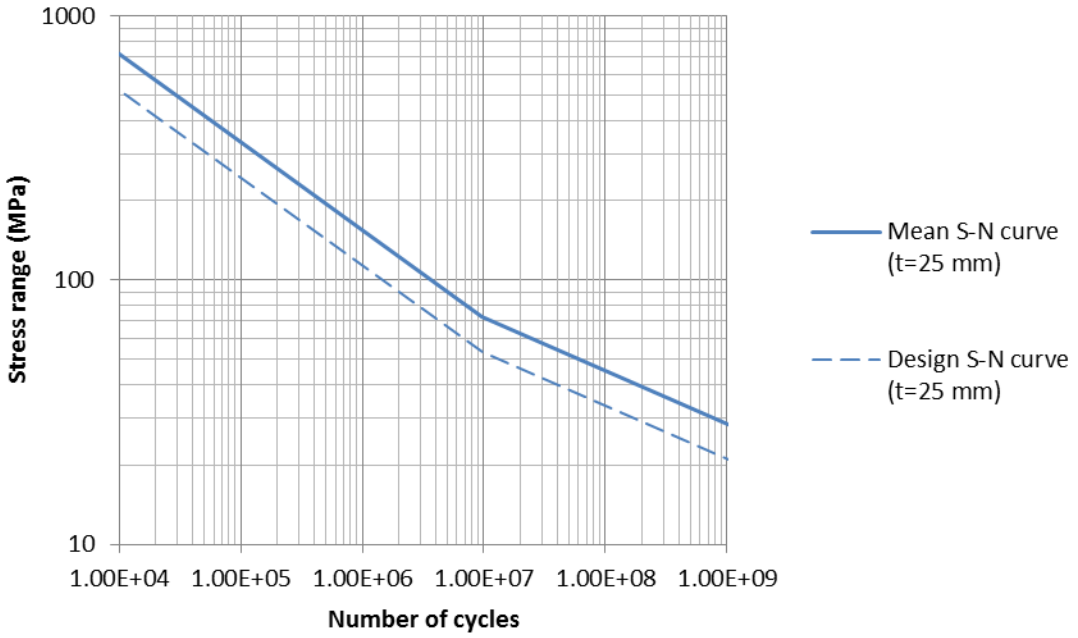


Figure 5. 3: S-N curve in ambient air conditions

In accordance with DNV code, it is assumed that CAL geometric stress ranges are lower than 52.63MPa do not contribute to fatigue damage.

A failure that occurs in less than $10^3$ loading cycles is considered either low cycle fatigue or static failure.

### 5.4.2. Miner's rule application

To calculate the fatigue damage due to applied cyclic loading the Miner's rule is applied, as it is described in chapter 2, for two different cases:

A) geometric stress range derived from experimental linear extrapolation (Table 5. 5) and

B) Efthymiou parametric equations (Table 5. 6)

In addition, in this case it is assumed that a compressive cycle contributes equally to fatigue damage as a tensile one. In S-N curves the load sequence effect is not taken into account. The failure criterion for the S-N curves presented below corresponds approximately to the thickness at the saddle point of the chord.

In Figure 5. 4 and Figure 5. 5 the projections of applied fatigue loading are depicted on mean and design S-N curves for both values of $\Delta\sigma_{geom}$.

Table 5. 5: Miner's rule application for $\Delta\sigma_{geom}$ derived from experimental linear extrapolation according to mean S-N curves (case A)

| Applied number of cycles | Stress range direction | Applied $\Delta\sigma_{nom}$ [MPa] | $\Delta\sigma_{geom}$ [MPa] | Number of cycles to failure | Fatigue damage |
|---|---|---|---|---|---|
| 191000 | tensile | 32.35 | 148.80 | 9.24E+05 | 0.207 |
| 421955 | compressive | 32.35 | 148.80 | 9.24E+05 | 0.457 |
| 1 | tensile (OL) | 48.48 | 223.03 | 2.74E+05 | 3.643E-06 |
| 10000 | tensile (crack marking) | 3.59 | 16.53 | 1.12E+10 | 8.910E-07 |
| | | | | **Total Fatigue damage** | **0.66** |

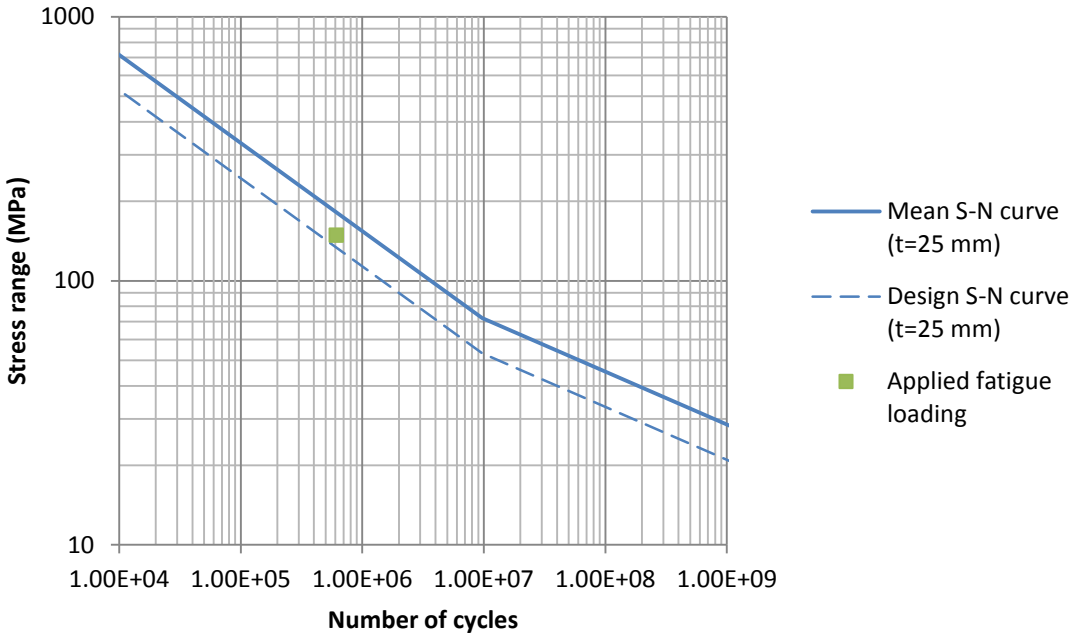


Figure 5. 4: Projection of applied fatigue loading on S-N curves

Table 5. 6: Miner's rule application for $\Delta\sigma_{geom}$ derived from Efthymiou equations according to mean S-N curves (case B)

| Applied number of cycles | Stress range direction | Applied $\Delta\sigma_{nom}$ [MPa] | $\Delta\sigma_{geom}$ [MPa] | Number of cycles to failure | Fatigue damage |
|---|---|---|---|---|---|
| 191000 | tensile | 32.35 | 200.01 | 3.81E+05 | 0.502 |
| 421955 | compressive | 32.35 | 200.01 | 3.81E+05 | 1.109 |
| 1 | tensile (OL) | 48.48 | 299.78 | 1.13E+05 | 8.847E-06 |
| 10000 | tensile (crack marking) | 3.59 | 22.22 | 2.56E+09 | 3.909E-06 |
| | | | | **Total Fatigue damage** | **1.61** |

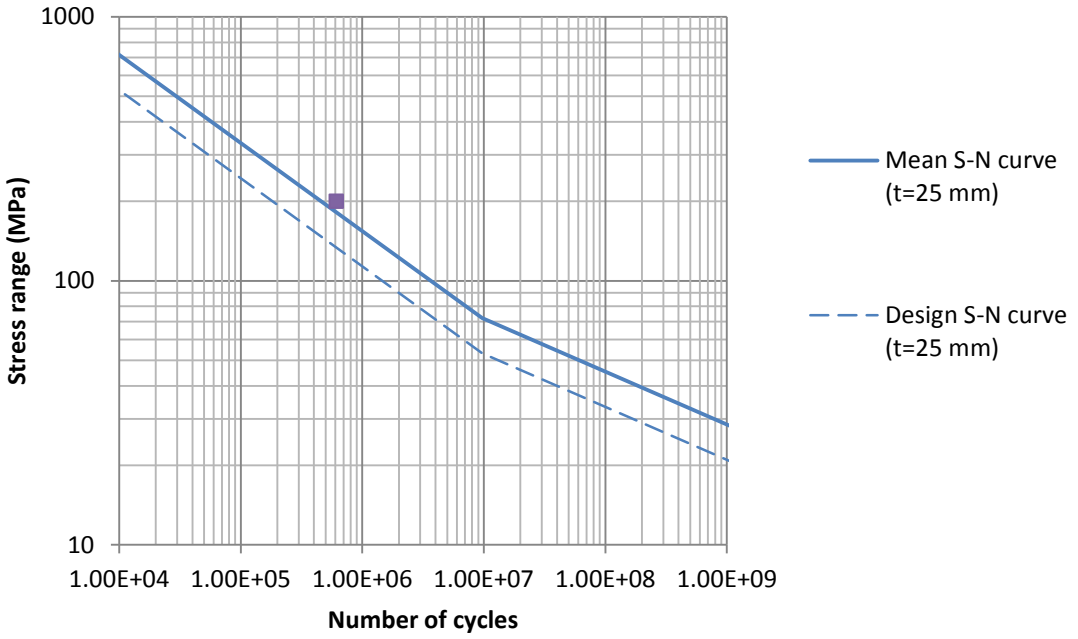


Figure 5. 5: Projection of applied fatigue loading on S-N curves

In both cases, it can be seen that the single OL effect is negligible and the crack marking tensile cycles have a stress range below the fatigue limit (52.63 MPa).

## 5.5. Conclusions

Taking into consideration the following ones:

- for the S-N curves presented in this chapter the failure criterion corresponds to full chord thickness $t_0$ while the experimental data are available only to the half chord thickness $0.5t_0$

- the crack depth growth has an increasing tendency as the crack propagation continues in constant amplitude, which means that the fatigue loading cycles that contribute to the crack extension from 0-$0.5t_0$ are more than those from $0.5t_0$-$t_0$

- there is a retardation effect (about 18 thousand cycles) introduced by OL on the tested tubular joint that is not taken into account in S-N curves

- in the S-N curves the compressive loading cycles that are applied on tested tubular joint are assumed equally fatigue damaging with the tensile ones

According to the aforementioned remarks, it can be concluded that case A gives an estimation of fatigue damage that is within the scatter band of the S-N line while case B provides a much more conservative fatigue life prediction.

## References

**[1]** Recommended Practice DNV-RP-C203 - Fatigue Design of Offshore Steel Structures (October 2011)

# 6. NUMERICAL SIMULATION OF CRACK GROWTH IN AXIALLY LOADED TUBULAR T-JOINTS

## 6.1. Introduction

A numerical calculation procedure is applied for the prediction of fatigue crack growth behavior of a tubular T-joint axially loaded on the brace. Chapter 6 describes the basic assumptions, the theoretical background, the steps and the outcome of this procedure which is carried out by the FAFRAM model.

FAFRAM (Fatigue FRActure Mechanics) is a MathCAD routine, developed by TNO which integrates numerically the crack extension in through thickness and circumferential direction of the tubular joint (width direction) in relation to the stress intensity factor range (ΔK) *[1]*.

## 6.2. Simulation of crack growth on the basis of Fracture mechanics (FM) approach

In the tubular joint, a semi-elliptical crack is assumed at the weld toe of the chord *[2], [3]* as crack growth has been monitored in the experiments (See Chapter 4). The semi-elliptical crack is an assumption of and idealized single crack initiation *[3]*. In reality, cracks initiate at multiple positions after which coalescence takes place in the growth stage of the cracks.

In case of a three dimensional structure the crack growth is examined simultaneously in through thickness and width direction (Fig. 6.1) *[1],[2]*. For the application of the numerical integration the initial and final dimensions of crack shape should be defined. The latter one corresponds to the failure criteria in depth and width direction of the structure. The crack growth simulation is based on the Paris-Erdogan formula which represents the crack propagation stage and is presented below:

$$\frac{da}{dN} = C_a \cdot \Delta K_a^{m_a} \qquad \frac{dc}{dN} = C_c \cdot \Delta K_c^{m_c} \qquad \textit{(eq. 6.1a,b)}$$

Where $\Delta K_\alpha$: Stress intensity factor range in depth direction

$\Delta K_c$: Stress intensity factor range in width direction

$C_\alpha$, $m_\alpha$: Crack propagation constants in depth direction

$C_c$, $m_c$: Crack propagation constants in width direction

These values are explained further in the following paragraphs of this chapter.

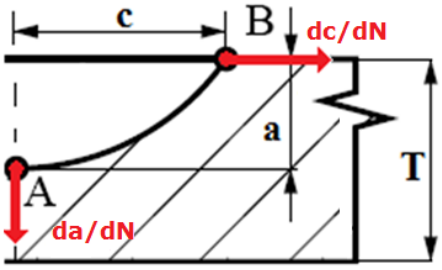


Figure 6. 1: Crack growth rates in a quarter elliptical surface crack

### 6.3. Modelling of geometry

The complicated geometry of tubular T-joints makes it rather difficult to determine the Stress Intensity factor ranges (ΔK) in those types of structures. For this reason loading cases of more simplified geometries that develop similar stress distributions at the weld toe areas are adopted for the calculation of ΔK in this study *[4]*.

According to literature, the crack growth behavior of a surface crack at the weld toe of an axially loaded tubular T-joint can be simulated by a crack growth calculation model of a semi-elliptical surface crack at the weld toe of a continuous plate to which a vertical attachment is welded *[4], [5]*.

In this model, the chord is represented by the plate and the brace by the vertical attachment which means also that the plate and attachment thickness should be equal to the chord and brace wall thickness respectively. In addition, the model includes weld geometry effects and takes into account the weld toe angle (θ), the weld width (L) and the weld toe radius (ρ).

As far as the model loading conditions are concerned, the plate is loaded by membrane and bending stresses while the attachment is unloaded so this is a non-loading carrying weld. Finite element calculations *[6]* prove that the stress field at the chord weld toe is affected to a great extent by the forces in the chord while the effect of brace forces at this position can be ignored *[4]*.

To summarize, the basic meaning of this paragraph is that the stress field at the weld toe area of an axially loaded tubular joint is represented by the stress field at the weld toe area of a T-plated structure that consists of a loaded plate and an unloaded vertical attachment (Figure 6. 2). The similarity in terms of stress field means in turn similarity in terms of crack growth behavior as well.

The weld dimensions are considered constant along joint intersection.

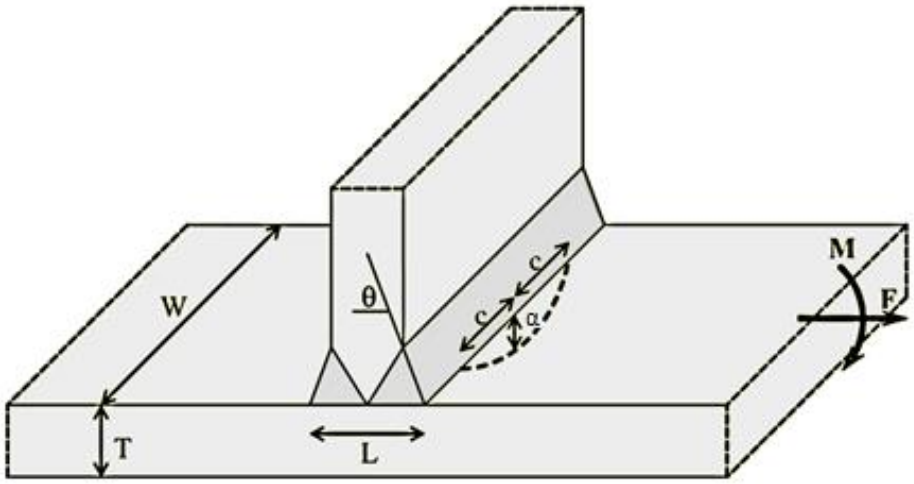


Figure 6. 2: Geometrical model

### 6.4. Stress Intensity factor range

The stress intensity factor range describes the stress field near the crack tip and is given for each direction by standard and analytical solutions for semi-elliptical cracks in plates *[5]*:

$$\Delta K_{\alpha} = \left( M_{k,m}\left(\frac{a}{T},\frac{L}{T},\theta\right)\cdot M_{m,a}(a,c)\cdot \Delta\sigma m + M_{k,b}\left(\frac{a}{T},\frac{L}{T},\theta\right)\cdot M_{b,a}(a,c)\cdot \Delta\sigma b\right)\frac{\sqrt{\pi\alpha\left(1+\frac{\Delta\alpha}{\alpha}\right)}}{\Phi(a,c)}$$

***(eq.6.2a)***

$$\Delta K_{c} = \left( M_{k,m}\left(\frac{c}{T},\frac{L}{T},\theta\right)\cdot M_{m,c}(a,c)\cdot \Delta\sigma m + M_{k,b}\left(\frac{c}{T},\frac{L}{T},\theta\right)\cdot M_{b,c}(a,c)\cdot \Delta\sigma b\right)\frac{\sqrt{\pi\alpha\left(1+\frac{\Delta\alpha}{\alpha}\right)}}{\Phi(a,c)}$$

***(eq.6.2b)***

$M_{k,m}$ $M_{k,b}$ : Stress intensity concentration factor (otherwise weld shape factors) that incorporate the effect of weld geometry such as weld shape, dimensions, angle etc. They are applied for bending or membrane part of the stress in depth or width direction.

$M_{m,a}$ $M_{b,a}$ $M_{m,c}$ $M_{b,c}$ : Stress intensity correction factors (otherwise plate depth crack shape factors) that depend on crack depth and crack length and incorporate the crack shape.

| | |
|---|---|
| $\Delta\sigma_m$ : | The membrane part of the stress range applied on the plate of the model. |
| $\Delta\sigma_b$ : | The bending part of the stress range applied on the plate of the model. |
| $\Delta\alpha = 0.01a$ | Crack increment for integration control |
| $\Phi(a,c) = \left[1 + 1.464\left(\frac{a}{c}\right)^{1.65}\right]^{0.5}$ | Elliptical integral of the second kind |
| $c$ : | half crack length (Figure 6. 2) |
| $L$ : | weld width (Figure 6. 2) |
| $T$ : | plate thickness (Figure 6. 2) |
| $\theta$ : | weld toe angle (Figure 6. 2) |

### 6.5. Stress state

The total applied stress range at the "chord" plate of the model equals to the nominal stress range on the brace multiplied by SCF(c). SCF(c) is a function of half crack length c which gives the stress concentration factor at the weld toe of the chord side around an axially loaded tubular T-joint (Appendix G). For crack length equal to zero the function becomes equal to the SCF at the saddle point of the chord (where it is the maximum for the examined case). As the crack length extends the function value tends to decrease. This function is introduced in the routine in order to incorporate the effect of descending tendency of stress concentration as the crack length extends from the saddle to the crown points. The function is based on the stress range measurements around the joint (presented in Chapter 4)

In addition, the appropriate representation of the stress field at the chord weld toe areas of the joint depends on the determination of the relative proportions of bending and membrane stresses.

According to OTC 5352 (1986) *[4]* the crack growth at a weld toe induced to a great extent by the stresses applied in the wall of the relevant member of a tubular joint. It is also known (BS7910:2013 *[7]*) that in case of an axially loaded T-joint the bending stresses are developed at the chord as a reaction to the axial stresses of the brace.

Van Delft et al. (1986) *[4]* and Van Straalen et al (1991) *[5]* recommend the use of a proportion

$$\frac{\Delta\sigma_m}{\Delta\sigma_b} = \frac{1}{3} \qquad \textit{(eq. 6.3)}$$

While in the Technical steel research report (1988) *[2]* all the stresses are assumed to be bending stresses.

Connoly et al. (1990) *[8]* present a set of parametric equations for tubular T- and Y-joints in order to determine the bending and membrane stress proportions as a function of the geometrical parameters α, β, γ, τ, θ. These equations rely on a finite element study with thin shell elements on various tubular joint geometries with different loading cases (axial loading, in-plane bending, out-of-plane bending). For a tubular T-joint (θ=π/2) under axial loading, the parametric equation to calculate the relative proportion of bending stress to the total stress at the saddle location is the following one:

$$\frac{\Delta\sigma_b}{\Delta\sigma_{tot}} = 0.7026\alpha^{0.0236} e^{\left(-0.187\beta^4+0.0097\gamma+\frac{0.0047}{\theta^3}-\frac{21.7\beta^3}{\gamma^2}+0.3038\beta\tau-\frac{0.0867\beta^2}{\theta^3}-0.001\gamma^{1.5}\theta\right)} \quad \textit{(eq. 6.4)}$$

which in the examined case equals to: $\frac{\Delta\sigma_b}{\Delta\sigma_{tot}} = 0.80$

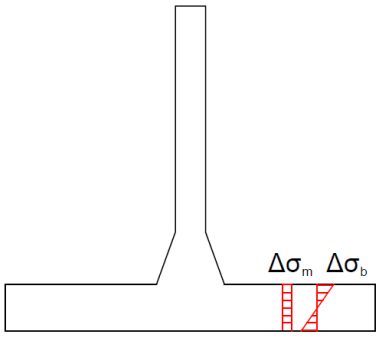


Figure 6. 3: Bending and membrane stresses applied on the plate

### 6.6. Crack propagation constants

The C and m crack propagation constants are constant values that are used in crack growth equations and they are mainly dependent on:

- the material properties of the specimen
- the environmental conditions
- the stress ratio of the applied fatigue loading

It is assumed that the examined specimen is isotropic with uniform material parameters for crack growth in all directions:

$$C_a = C_c \quad \textit{(eq.6.5a)}$$

and

$$m_a = m_c \quad \textit{(eq.6.5b)}$$

The crack propagation constants that are used in this study are either experimentally determined by the 4PB strip specimens presented in Chapter 3 (see Table 3.3 bead weld on a plate constants in R=0.1) or the recommended British Standards 7910:2013 constants for welded material (see Table 3.3 BS7910:2013 welded specimens in R=0.1)

### 6.7. Initial and final crack shape

As it is mentioned in section 6.2, it is necessary to determine the initial and the final crack shape dimensions in order to apply the numerical integration of crack growth.

The initial crack shape is set equal to the first experimental crack measurements.

The final crack shape dimensions coincide with the failure criteria in thickness and length direction which correspond to the half chord thickness and the brace external diameter respectively ($\mathrm{a} = \mathrm{T}/2$ , $c = \pi \cdot d_{brace}/4$ ) *[9]*. The numerical procedure stops in case one of these two criteria is reached.

### 6.8. FAFRAM routine

In this paragraph the main steps of the FAFRAM routine application are shown.

**1st step:** Define model dimensions (plate thickness, plate width, attachment length, weld angle), membrane and bending stress range ($\Delta\sigma_m$, $\Delta\sigma_b$) and crack propagation constants ($C_\alpha$, $C_c$, $m_\alpha$, $m_c$)

**2nd step:** Set initial crack depth $\alpha_i$ and crack length $c_i$, final crack depth $\alpha_f$ and crack length $c_f$ and initial value for cycle counting $N_i$

**3rd step:** Set integration control (crack increment): $\Delta\alpha = 0.01\alpha$ and start the iteration procedure

**4th step:** Apply crack growth rate equations (eq. 6.1.a,b) in both directions where SIF range equations (eq.6.2.a,b) are also used. The calculation of stress intensity concentration factors and stress intensity correction factors are done in subroutines where the input values are the previously referred model dimensions (plate thickness, plate width, attachment length, weld angle)

**5th step:** Assume a crack extension Δα. The corresponding number of loading cycles can be derived by the formula: $\boldsymbol{\Delta N = \frac{\Delta\alpha}{C(\Delta K_c)^{m_c}}}$

**6th step:** Increase crack shape dimensions by adding crack increment:

$$\boldsymbol{a_{i+1} = a_i + \Delta\alpha}$$

$$\boldsymbol{c_{i+1} = c_i + \Delta c}$$

**7th step:** Increase the total number of applied loading cycles

$$\boldsymbol{N_{i+1} = N_i + \Delta N}$$

**8th step:** At every crack increment all data about crack depth, crack length, total number of cycles are stored in a row in order to create a table

that shows surface crack extension in progress of the applied loading cycles

**9th step:** Iteration procedure continues with the new values of $a_{i+1}$ and $c_{i+1}$ until one of those values reach the failure criterion: $\alpha = T/2$ or $c = \pi \cdot d_{brace}/4$

### 6.9. FAFRAM Results

#### 6.9.1. General

Crack growth simulations are conducted on the basis of the mean values of crack propagation constants which are:

- Experimentally determined from 4 point bending tests (Chapter 4)
- Taken from BS7910:2013 *[7]* for welded tubular joints

Table 6.1: Crack propagation constants

| | C | | Crack propagation exponent m |
|---|---|---|---|
| | (m per cycle) /(MPa√m) | (mm per cycle) /(N/mm$^{3/2}$) | |
| **4PB tests** | $1.44 \cdot 10^{-11}$ | $4.55 \cdot 10^{-13}$ | 3.00 |
| **BS7910:2013** | $4.08 \cdot 10^{-11}$ | $1.29 \cdot 10^{-12}$ | 2.88 |

The value of C from 4-point bending test comes from the mean values of C in bead on plate welded specimens (see Chapter 3).

From BS7910:2013 the value of C is taken under the assumption of ΔK≥196 N/mm$^{3/2}$ which can be validated by the initial crack measurements. As mentioned in Chapter 4, for welded joints the constants that are used correspond to mean+2SD values and a stress ratio R≥0.5.

As far as the stress state is concerned, the model is examined for the same geometric stress range for both sides that is calculated in accordance with the DNV code *[10]* stress extrapolation procedure, as it is applied in paragraph 5.8.2, and equals to 148.75 MPa.

The input initial crack dimensions are considered equal to the initial crack depth and crack length measurement per side.

The bending and membrane stress range proportions that are used in the simulations come from the references that are presented in section 6.5 (namely: 0.75, 0.80 and 1.00).

#### 6.9.2. Crack depth

In the following figures the results of crack depth development simulations are elaborated for 2 specific positions, the crack initiation points of joint intersection:

- Crack initiation point of side 1 (15˚)
- Crack initiation point of side 2 (saddle location 180˚)

They are compared with the corresponding crack depth measurements which are used as a reference at every case. As expected, the recommended constants of BS7910 lead to models with more conservative predictions regarding fatigue life compared with the crack growth models that include the experimentally (from 4PB tests) derived constants. A comparison between Figure 6. 4 and Figure 6. 5 can prove this statement.

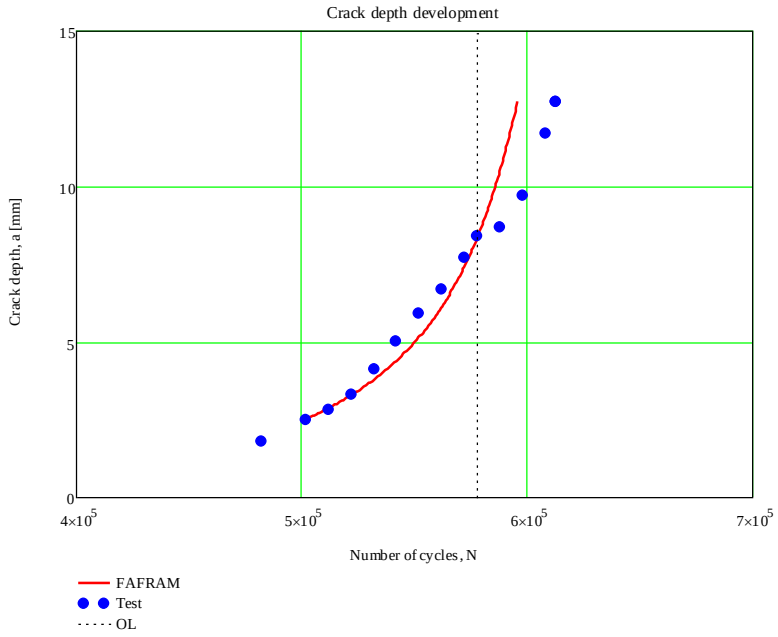


**Figure 6. 4: Crack depth growth simulation at position 15˚ on the basis of experimentally derived constants in a proportion of bending to total stress range equal to 0.75**

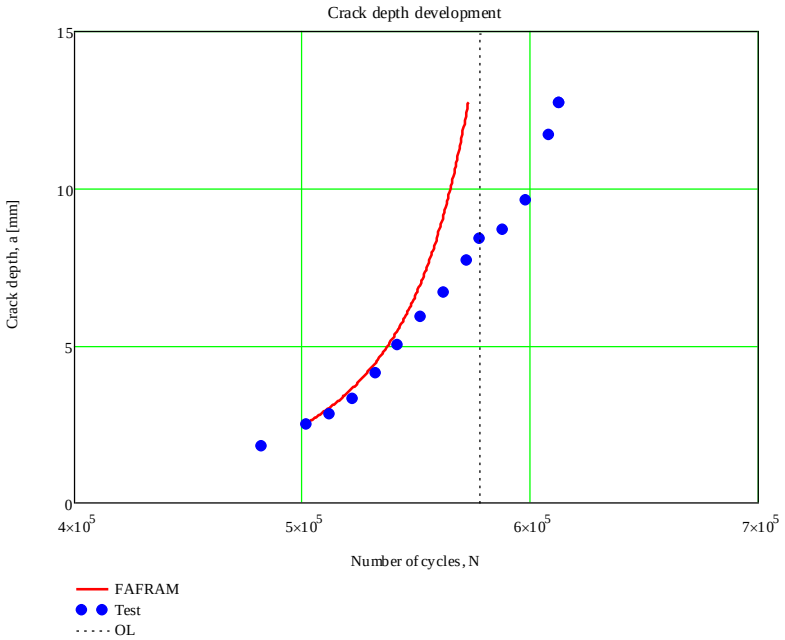


**Figure 6. 5: Crack depth growth simulation at position 15˚ on the basis of BS7910 recommended constants in a proportion of bending to total stress equal to 0.75**

Furthermore the crack depth simulation is examined in case of different bending to total stress ratio. Besides the ratio of 0.75 the simulation is executed for ratios equal to 0.80 and 1.00 according to recommendations presented in paragraph 6.5.

By making the comparison between Figure 6. 4, Figure 6. 6 and Figure 6. 7 it can be seen that a model that takes into account a bending to total stress range ratio equal to 0.75 represents the specimen crack growth behavior in depth direction better and more accurate than the other recommended values of ratio.

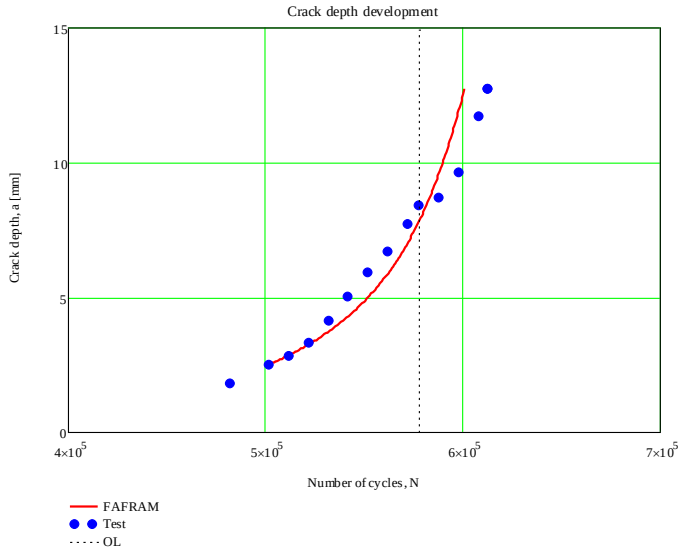


**Figure 6. 6: Crack depth growth simulation at position 15˚ on the basis of experimentally derived constants in a proportion of bending to total stress equal to 0.80**

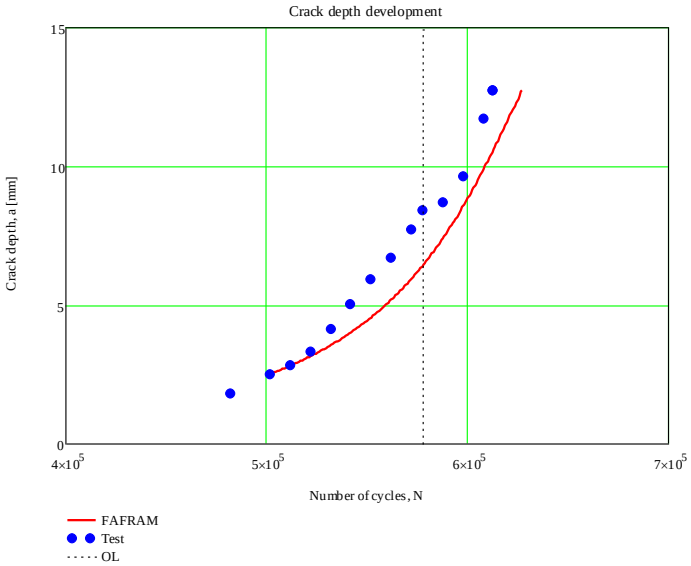


**Figure 6. 7:Crack depth growth simulation at position 15˚ on the basis of experimentally derived constants in a proportion of bending to total stress equal to 1.00**

The same comparison for bending to total stress ratio is done for the saddle point of the opposite side 2 (180˚). The model results are depicted in the graphs below.

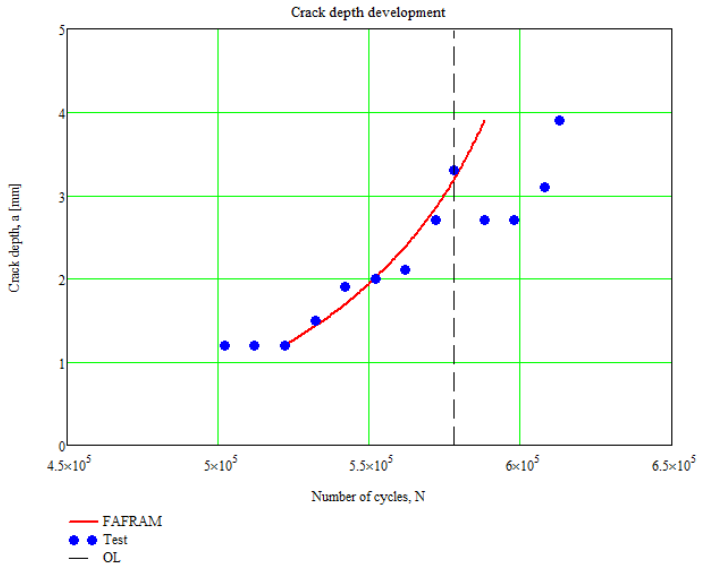


**Figure 6. 8: Crack depth growth simulation at position 180˚ on the basis of experimentally derived constants in a proportion of bending to total stress equal to 0.75**

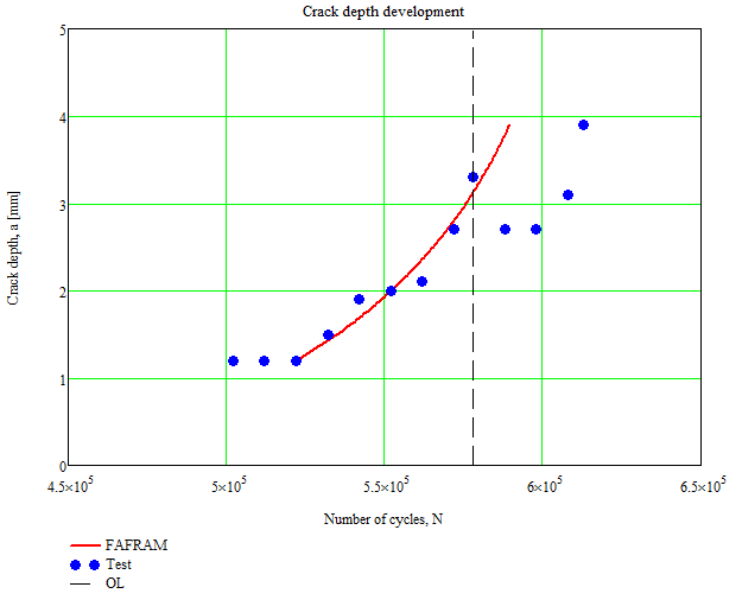


**Figure 6. 9: Crack depth growth simulation at position 180˚ on the basis of experimentally derived constants in a proportion of bending to total stress equal to 0.80**

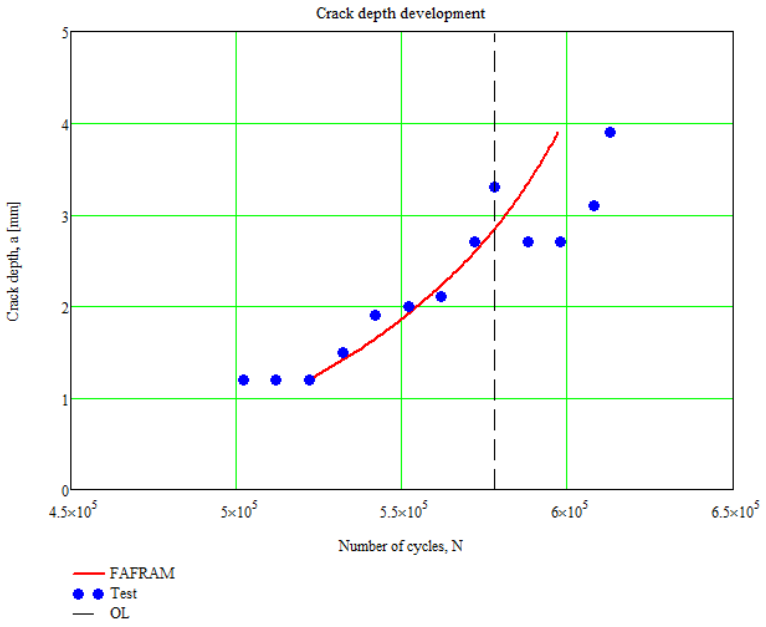


**Figure 6. 10: Crack depth growth simulation at position 180˚ on the basis of experimentally derived constants in a proportion of bending to total stress equal to 1.00**

In this particular case for the saddle position of side 2, the model which takes into consideration a bending to total stress range ratio equal to 0.75 provides the most accurate prediction of crack growth in depth direction.

### 6.9.3. OL effect on crack depth growth

Figure 6. 11 shows the projection of crack depth growth without the OL application according to FA.FRA.M routine. It is calculated that the retardation effect caused by a discrete tensile overload (OL) application in crack depth at position 15˚ in terms of prolonging fatigue life is about 18700 loading cycles. This is the approximate number of delay cycles caused by OL.

The corresponding retardation effect on crack depth growth at the saddle point of side 2 (180˚) is estimated in 26000-27000 loading cycles and it is presented in Figure 6. 12.

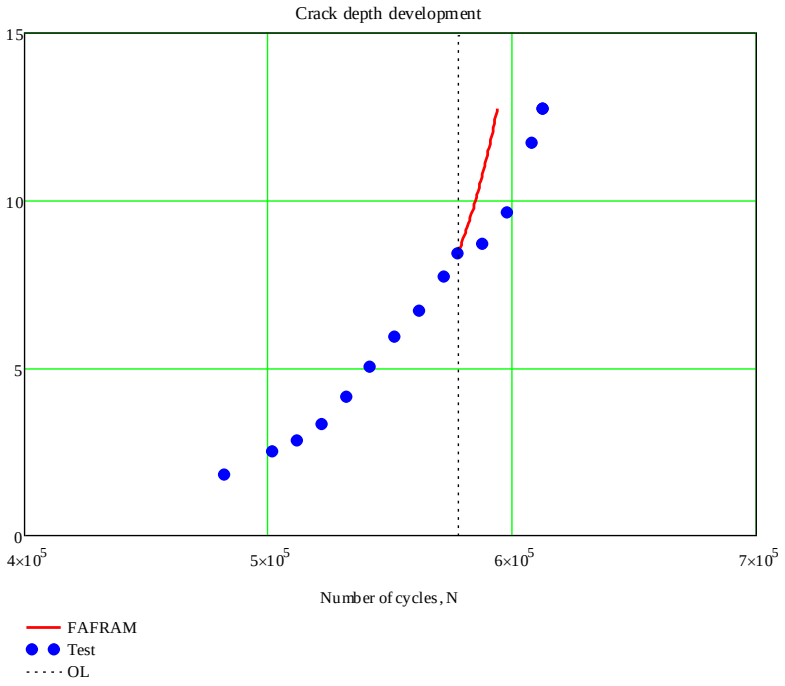


Figure 6. 11: Projection of retardation effect in terms of loading cycles at position 15˚

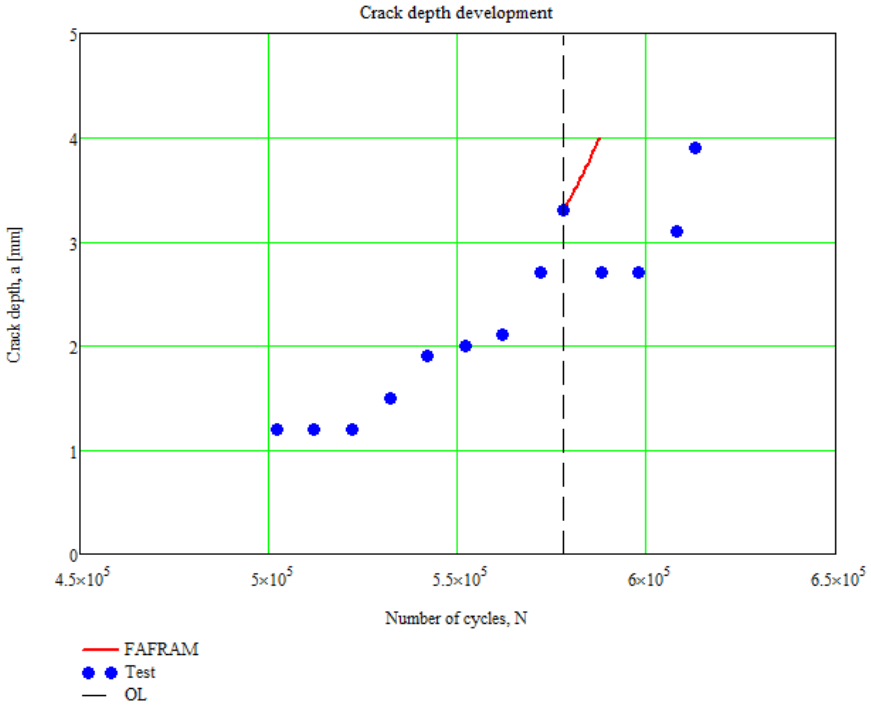


Figure 6. 12: Projection of retardation effect in terms of loading cycles at position 180˚

### 6.10. Crack propagation constant

The da/dN-ΔK curve is created and presented in Figure 6. 13 in the case of crack initiation point of side 1 (15˚) of the examined tubular joint. The crack growth rates are derived on the basis of ACPD measurements and ΔK according to the equations proposed by FA.FRA.M. The linear mean regression line is projected in order to derive the crack propagation constant.

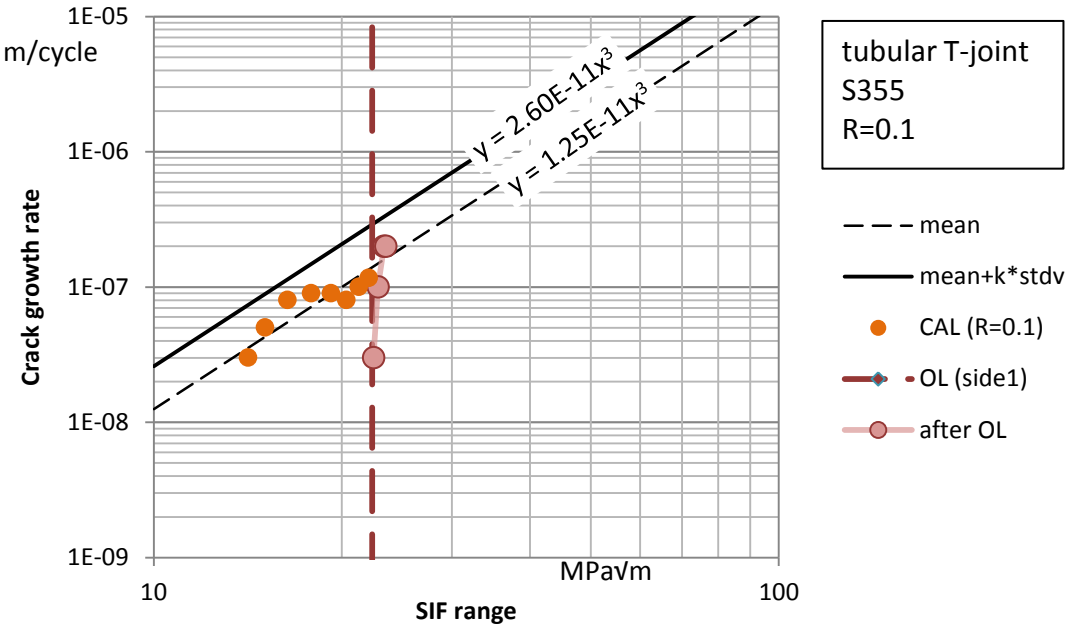


Figure 6. 13: da/dN-ΔK curve in tubular joint

The crack propagation constant is a parameter that depends on the material, environment and stress ratio. The constant that is derived for tubular joints equals to $1.25 \cdot 10^{-11}$ m/cycle/(MPa√m) while the corresponding constant derived from 4PB test (Chapter 3) equals to $1.44 \cdot 10^{-11}$ m/cycle/(MPa√m). The applied stress ratio, the environmental conditions are considered the same. Also there are no significant changes in the materials (see mechanical properties and chemical composition tables for each specimen). The negligible difference can be attributed to the measurements scatter and the different ΔK calculations procedure that have been followed (Figure 6. 14).

Table 6. 2: Crack propagation constants calculated in different ways

| Specimen | Environment | Stress ratio | Weld condition | ΔK Calculation | Measuring equipment | C [(m per cycle)-to-(MPa√m) ratio] |
|---|---|---|---|---|---|---|
| **Steel strip 4PB specimen** | Ambient air (20˚C) | 0.1 | As welded | Tada equations | Crack gauge + visual inspection | **$1.44 \cdot 10^{-11}$** |
| **Steel tubular joint** | Ambient air (20˚C) | 0.1 | As welded | FA.FRA.M. | ACPD method + visual inspection | **$1.25 \cdot 10^{-11}$** |

Figure 6. 14 depicts the mean regression lines for the examined small-scale welded steel strip specimens and tubular T-joints. The mean regression lines rely on the values of Table 6. 2 which have been calculated in a different way for every structural case. In Figure 6. 14 their scatter band of the data is taken into account on the basis of a standard deviation $s_{dtv}$=0.266 given by BS7910.

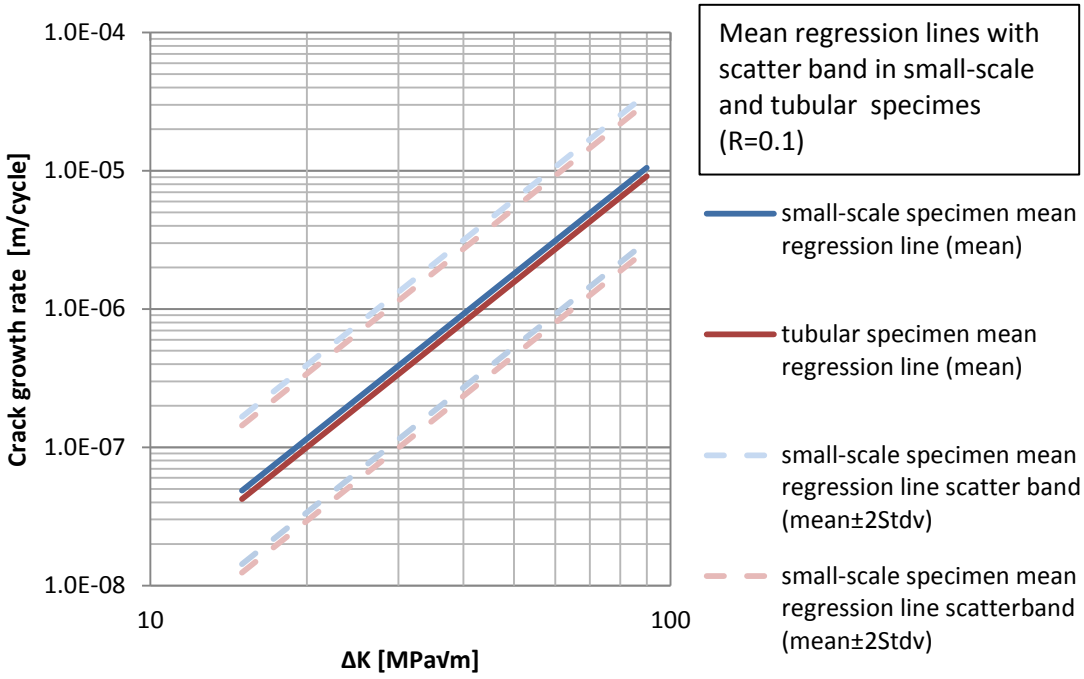


**Figure 6. 14: Mean regression lines for small-scale specimens and tubular joints under ambient conditions in R=0.1**

### 6.11. OL effect difference between tubular joint and to small-scale specimens

The parameters that affect the extent of OL effect on a structure are the followings:

- Material microstructure (represented by crack propagation constants)
- Material mechanical properties (mainly yield strength $f_y$ that defines the amount of plasticity that can be introduced from a certain load)
- $\Delta K_{baseline}$ that is ΔK value at which the OL is applied (Sadananda et al. 1999 provide a schematic illustration of $\Delta K_{baseline}$ on delay cycles)
- The development of residual stresses (which can affect the applied mean stress)
- Stress state condition at the vicinity of the crack (plane stress, plane stress or mid-thickness condition)
- Overload ratio (OLR = $K_{OL}/K_{min} = \sigma_{OL}/\sigma_{min}$), the higher the applied OLR the larger the OL plastic zone that is introduced (as long as $\sigma_{OL}>f_y$)
- Applied stress ratio R which affect the mean stress as well

- Environmental conditions

The retardation effects from the various single OL's that are applied on the examined tested specimens of this study are gathered on Table 6. 3. The same table provides the overload ratio, the ΔK baseline where the OL applied and the specific specimen.

**Table 6. 3: OL effects evaluation**

| Applied OL ratio | Specimen | Yield strength (MPa) | ΔK baseline (MPa√m) | $N_d$ | U - Value |
|---|---|---|---|---|---|
| **OLR=1.7** | BP351 | 355 | 21.14 | 34593 | 0.47 |
| **OLR=1.7** | BP352 side1 | 355 | 20.82 | 31947 | 0.49 |
| **OLR=1.7** | BP352 side2 | 355 | 19.32 | 35988 | 0.49 |
| **OLR=1.7** | BM135 side1 | 355 | 22.06 | 69014 | 0.49 |
| **OLR=1.7** | BM135 side2 | 355 | 22.53 | 69961 | 0.45 |
| **OLR=1.7** | BM235 side1 | 355 | 20.82 | 73530 | 0.53 |
| **OLR=1.7** | BM235 side2 | 355 | 19.32 | 71092 | 0.54 |
| **OLR=1.35** | Tubular T-Joint | 355 | 22.08 | 18779 | 0.60 |

***where BP:** small-scale bead weld on a plate specimens **BM:** small-scale base material specimens*

The results presented in Table 6. 3 are explained and evaluated in accordance with the aforementioned parameters influence on OL effect. Taking into account the tables 3.2, 4.1, 4.2 and 4.3 that provide information about chemical composition and mechanical properties of the specimens as well as the data presented in Figure 6. 14, it can be considered that the material of both specimens (small-scale plated specimen and tubular joint) have the same contribution (in terms of microstructure and mechanical properties) to OL effect. On the basis of similar materials and weld shape the residual stresses are assumed to be equal in both specimens as there are no measurements about their value and direction. Both tests were held under the same environmental conditions (ambient air 20˚C) and applied stress ratio (R=0.1). Also the $\Delta K_{baseline}$ are at the same levels both in tubulars and small-scale specimens as it can be seen in Table 6. 3.

By excluding all the other factors, it can be concluded that the only parameters which are not similar in both types of specimens and affect the extent of crack retardation caused by OL are the OLR and the stress condition at the crack tip.

The applied OLR on small scale specimens (both welded and base material) is higher than the applied OLR (1.7) on tubular joint (1.35) which means that the OL plastic zone that introduced is much larger (taking into consideration the similar levels of applied stresses and the same value of yield strength).

As mentioned in section 4.8 plane strain condition is considered at the vicinity of the crack of the tubular joint while small-scale specimen stress condition tend to be more close to mid

thickness conditions (between plane stress and plane strain). According to literature [6] the overload plastic zone size introduced in the case of plain strain is much smaller than plane-stress or mid thickness conditions.

It is obvious that the lower OLR and the plane strain conditions that are applied in tubular joint contribute to a smaller OL plastic zone compared to small-scale specimens case. The lower plasticity that is introduced by OL leads to a less profound retardation effect.

The differences in plasticity induced crack closure can be partially reflected on calculated U-values (see 2.3.3.1) between tubular joint and small-scale specimens.

Where: $$\boldsymbol{U = \Delta K_{eff}/\Delta K = \left(K_{max} - K_{op}\right)/(K_{max} - K_{min})} \qquad \textbf{(eq.6.6)}$$

U equals to 0.60 for tubular joint and around 0.48 in welded small-scale specimens. However, the derived U-values still cannot be used as a tool to quantify plasticity induced crack closure due to the limited data points regarding crack growth rates that have been derived (3.9.2.1). The use of a continuous sheet instead of a pattern of resistor grids would be a more efficient way of data recording in order to calculate accurately the U-values. Nonetheless, the higher U-value in T-joints indicates that opening stress after OL is lower compared to small-scale specimens. Thus the plasticity induced crack closure in tubular joint is a less pronounced phenomenon in relation to small scale specimens.

In any case, measuring retardation effect in terms of delay cycles $N_d$ remains the most reliable way for this study.

### 6.12. Crack length

The surface crack growth results in Chapter 4 show clearly that the crack growth rate in width direction (dc/dN) decelerates as the crack length increases and the crack edges approach the crown points till it finally stops. Crack length growth deceleration (and final crack arrest) occurs due to the decreasing stress concentration factor along the brace intersection (from saddle to crown points). According to this experimental observation and the theoretical explanation given, it can be stated that the critical failure criterion in tubular joints is the through thickness. This is verified by DNV code *[10]* (and various other researches) where the "failure criterion for S-N curves for tubular corresponds approximately to the thickness at the hot spot (chord or brace as relevant)".

FAFRAM routine is based on stress intensity factors for plates and the Paris-Erdogan law which is only valid for crack propagation stage. Also it is applicable under the assumption of a single initial surface crack that grows simultaneously in two directions *[9]*. The crack length is mainly dependent on the multiple narrow initial surface defects of welded structures (Figure 4.28). The multiple crack initiation phenomenon occurs before the appearance of a visible crack length (so before the crack propagation stage) and is also observed at the areas

close to surface crack edges (see Figure 4.23 and section 4.7.3) where the multiple crack initiation effect can be slightly seen.

Multiple crack initiation phenomenon at crack coalescence stage and the fact that it is not efficiently incorporated by the FAFRAM routine is the main reason why the surface crack length cannot be modelled accurately and the numerical simulation results are lower compared to the experimental (Figure 6. 15). The initial crack shape dimensions used in the figure below are derived from the crack length measurements of Chapter 4.

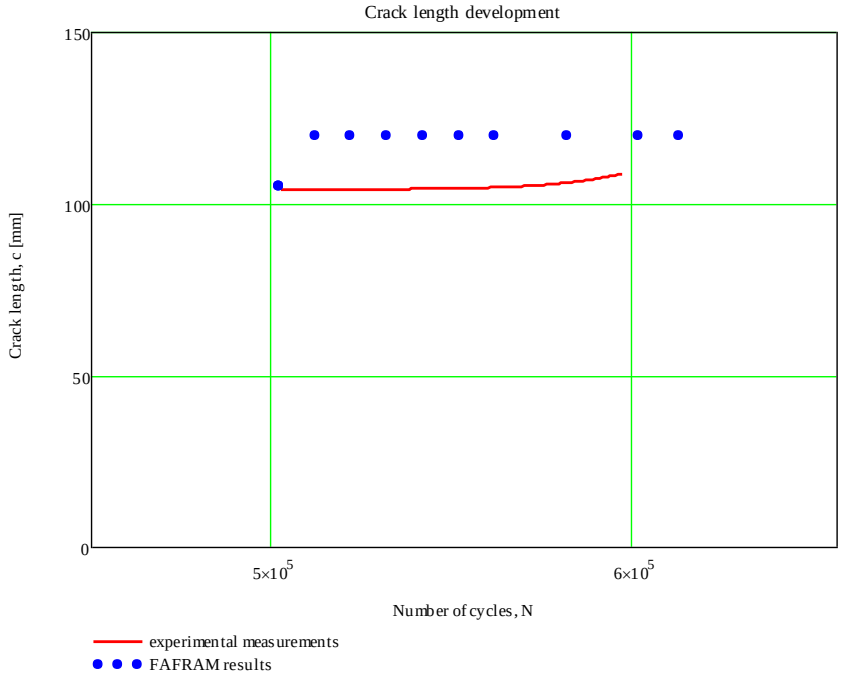


Figure 6. 15: Crack length numerical simulation results in relation with experimental measurements

## 6.13. Conclusions

- The crack growth rate parameters derived from small-scale experiments (in Chapter 3) tend to give a better match with the growth rates measured in the tubular joint than the values of the BS7910.

- Definition of bending to membrane stresses proportion is significant for the successful crack growth simulation. According to the outcomes presented in paragraph 6.9.2, crack depth growth at both sides can be simulated better by taking into consideration $\Delta\sigma_b/\Delta\sigma_{tot}$ equal to 0.75.

- The OL retardation effect has not been simulated by the existing model as it is shown in Figure 6. 4 - Figure 6. 12.

- In terms of delay cycles, the OL retardation effect on bead weld on plate specimens where OLR = 1.7 is about 1.7-2.0 times higher than the corresponding effect on tubular T-joint axially loaded on the brace (OLR=1.35) according to Table 6. 3 .

- The OL retardation effect on the tested tubular joint is more limited compared to that in the small-scale specimens (6.11) due to the lower applied OLR and different stress conditions at the vicinity of the crack (while all the other parameters that affect OL effect are considered similar).

- Measuring OL effect in delay cycles is the most reliable way for the examined case.

- The crack coalescence effect on crack length rate is not simulated in this study and this leads in differences between experimental measurements and numerical calculation results (Figure 6. 15).

## References


**[1]** R.J.M. Pijpers, M.H. Kolstein , A. Romeijn & F.S.K. Bijlaard - Fatigue strength of hybrid VHSS-Cast steel welded plates (2009) - NSCC2009

**[2]** Technical steel research – Fatigue behavior of welded joints in offshore steel structures Part 3: Fracture mechanics – Commission of the European Communities ISSN 1018-5593 (1992)

**[3]** O.D. Dijkstra, H.H. Snijder, H.J.M. van Rongen - Assessment of the remaining fatigue life of defective welded joints (1990) - IABSE report – ETH Zurich

**[4]** D.R.V. van Delft, O.D. Dijkstra and H.H. Snijder - The Calculation of Fatigue Crack Growth in Welded Tubular Joints Using Fracture Mechanics (1986) - OTC 5352

**[5]** IJ.J. van Straalen and O.D. Dijkstra – Application of the Fracture Mechanics approach to the fatigue behavior of welded tubular steel structures – 4$^{th}$ International Symposium (1991)

**[6]** D.R.V. van Delft – A Two Dimensional Analysis of the stresses at the vicinity of the weld toes of Tubular joints – TH-Stevin report 6-81-8, (1981)

**[7]** Guide to methods for assessing the acceptability of flaws in metallic structures - British Standard 7910:2013 – BSI Standards Publication

**[8]** M.P. Connolly, A.K. Hellier, W.D. Dover and J. Sutomo – A parametric study of the ratio of bending to membrane stress in tubular Y- and T-joints – International Journal of Fatigue 12 No 1 (1990) pp 3-11

**[9]** R.J.M. Pijpers - Fatigue strength of welded connections made of very high strength cast and rolled steels (2011)

**[10]** Recommended Practice DNV-RP-C203 – Fatigue Design of Offshore Steel Structures (October 2011)

**[11]** A.J.McEvily, S.Ishihara, Y.Mutoh – On the number of overload-induced delay cycles as a function of thickness – International Journal of Fatigue 26 (2004) 1311-1319

# 7. CONCLUSIONS AND RECOMMENDATIONS

## 7.1. Conclusions

The method that is developed in this study to predict the fatigue crack growth behaviour of the examined case in CAL gives quite accurate results. In general terms, the basic principles of model establishment should take into account:

- An appropriate simplified geometric model where its dimensions are correlated with the dimensions of the real structure. This makes the calculation of ΔK values possible.
- Stress state condition with the appropriate membrane – bending stress range proportion.
- Weld geometry effects should be incorporated in ΔK equations
- Crack shape idealization (assumption of semi-elliptical crack)

The experimentally derived crack propagation constants have a significant contribution to decrease conservatism on the fatigue crack growth prediction of the model. This can be proved by comparing those values with the recommended corresponding values provided by British Standard 7910 guidelines (Chapter 6). The constants that have been derived from 4PB tests and used as an input in FAFRAM routine and the constants that have been calculated on the basis of tubular joint measurements present negligible differences that can be attributed to scatter of the measurements (see 6.10).

The bead weld on small-scale plate specimens are slightly more susceptible to fatigue loading than base material specimens (see 3.9.1) due to material microstructure and tensile residual stresses that are developed in welds. The R effect on base material specimens is obvious whereas on welded specimens it is certainly less pronounced but cannot be evaluated adequately because of limited data points.

The OL retardation effect on base material specimen is more profound than on welded plate specimens (see 3.9.2) at a given OLR and same levels of $\Delta K_{baseline}$. According to the experimental results, the OL retardation effect on base material specimens in terms of delay cycles is approximated by 2-2.5 times higher than the corresponding effect on bead weld on plate specimens for OLR = 1.7 and $\Delta K_{baseline}$ around 19-21MPa√m.

The main reasons for this difference in OL effect are:

- the higher yield strength of the welded specimen at the weld toe. The higher the yield strength at the weld toe the smaller the size of plastic zone that introduced by OL which means that the corresponding retardation effect is less profound.
- The weld microstructure that permits higher crack growth rates, so shorter period of crack growth recovery from retardation effect

- The tensile residual stresses developed in welded specimens that increase mean applied tensile stress and enhance crack growth rate after OL

Furthermore, it is obvious that here the OL retardation effect in the tubular joint is much more limited (see 6.11). In terms of delay cycles, the OL retardation effect on bead weld on plate specimens where OLR = 1.7 is about 1.7-2.0 times higher than the corresponding effect on tubular T-joint axially loaded on the brace (OLR=1.35) where $\Delta K_{baseline}$-levels vary from 19 to 22 MPa√m (Table 6. 3) .This can be explained by:

- The higher applied OLR in small-scale specimens that introduce more plasticity (the yield strengths in both structures are the same and the residual stresses are assumed similar)
- The differences in stress state condition allow different amounts of plasticity (plane strain conditions are considered at the vicinity of the crack in tubular joint while mid thickness conditions in small-scale specimens)

The ACPD crack depth measurements in a T-joint can be reliable as long as a proper measuring procedure is followed (see 4.6.2).

The delayed retardation effect on small scale specimens (see 3.9.2) and at some points of the tubular joint (see Figure 4. 24) - combined with no further observations regarding crack branching and roughness at the crack faces - indicates that plasticity induced crack closure is the dominant mechanism of OL retardation effect.

The most reliable way to measure OL retardation is in terms of delay cycles, $N_d$, which is the number of cycles between the OL application and the crack growth rate re-establishment points. A more efficient data acquisition system that can provide continuous crack growth rate results is recommended in case of measuring the retardation effect in terms of U-values (see sections 3.9.2.1 and 6.11).

The S-N curves method has been applied for the examined case as well. The Miner's rule application has given two estimations regarding the way the hot-spot stress method is used:

- in case of introducing an experimentally derived extrapolated stress range (derived from Chapter 4) the given estimation is within the scatter band of S-N lines.
- in case of applying Efthymiou equations a more conservative estimation is observed.

## 7.2. Recommendations

It is recommended for the future studies (that will be related to the present thesis topic) to take into account the following aspects:

- The present study is mainly concentrated on the prediction of fatigue crack growth of a tubular T-joint under CAL and secondarily on the examination of OL effect. A much more detailed experimental investigation of OL effect on tubular joints can be done by examining and even quantifying the effects of OLR and $\Delta K_{baseline}$ on the crack growth retardation.

- An extensive experimental investigation of the other load sequence effects (e.g. UL, OL/UL etc.) on fatigue crack growth behaviour of tubular T-joint could be done. For instance it would be interesting to see whether and in what way an UL affects crack growth behaviour of tubular joints.

- In this thesis all the specimens were tested under ambient air conditions. An investigation of corrosion effect on fatigue crack propagation of steel elements would be a very significant study especially for the fatigue design of offshore structures.

- It can be seen clearly from this study that crack closure is a phenomenon that should be taken into consideration. A detailed examination of crack closure regarding its magnitude on crack growth of tubular joints could be done.

- Detailed research should be conducted regarding the residual stresses distribution at the heat affected zone of welded plated specimen.

- Further improvement of the existing crack growth model by incorporating the multiple crack initiation points phenomenon and crack coalescence effect (that are not taken into consideration in the present study) is an important step in order to figure out the fatigue crack growth behaviour of the joint at crack initiation stage.

# APPENDIX

# Appendix A

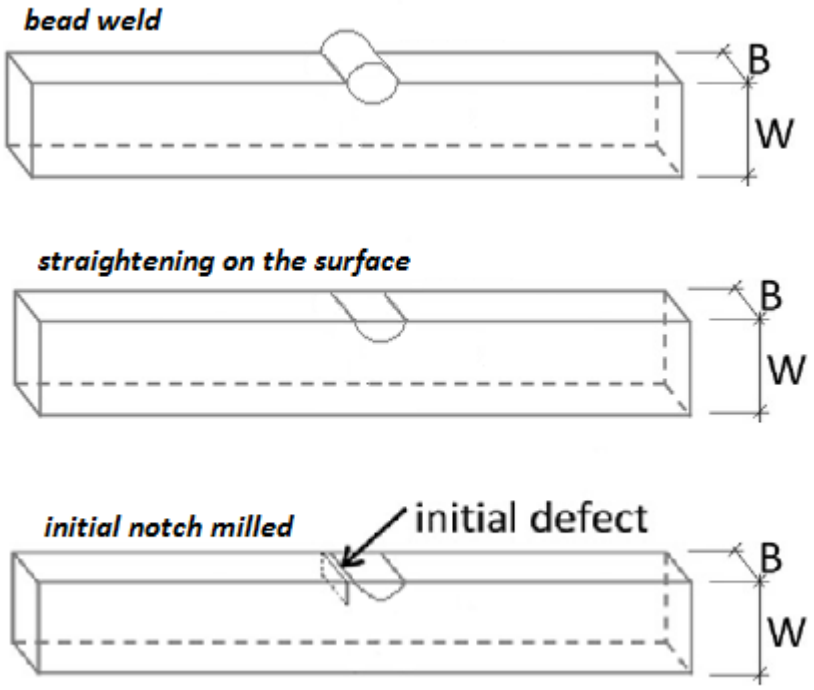


Figure A. 1: Welding, Straightening and milling initial notch

Figure A. 2: Bead weld on plate heat affected zone

## Appendix B

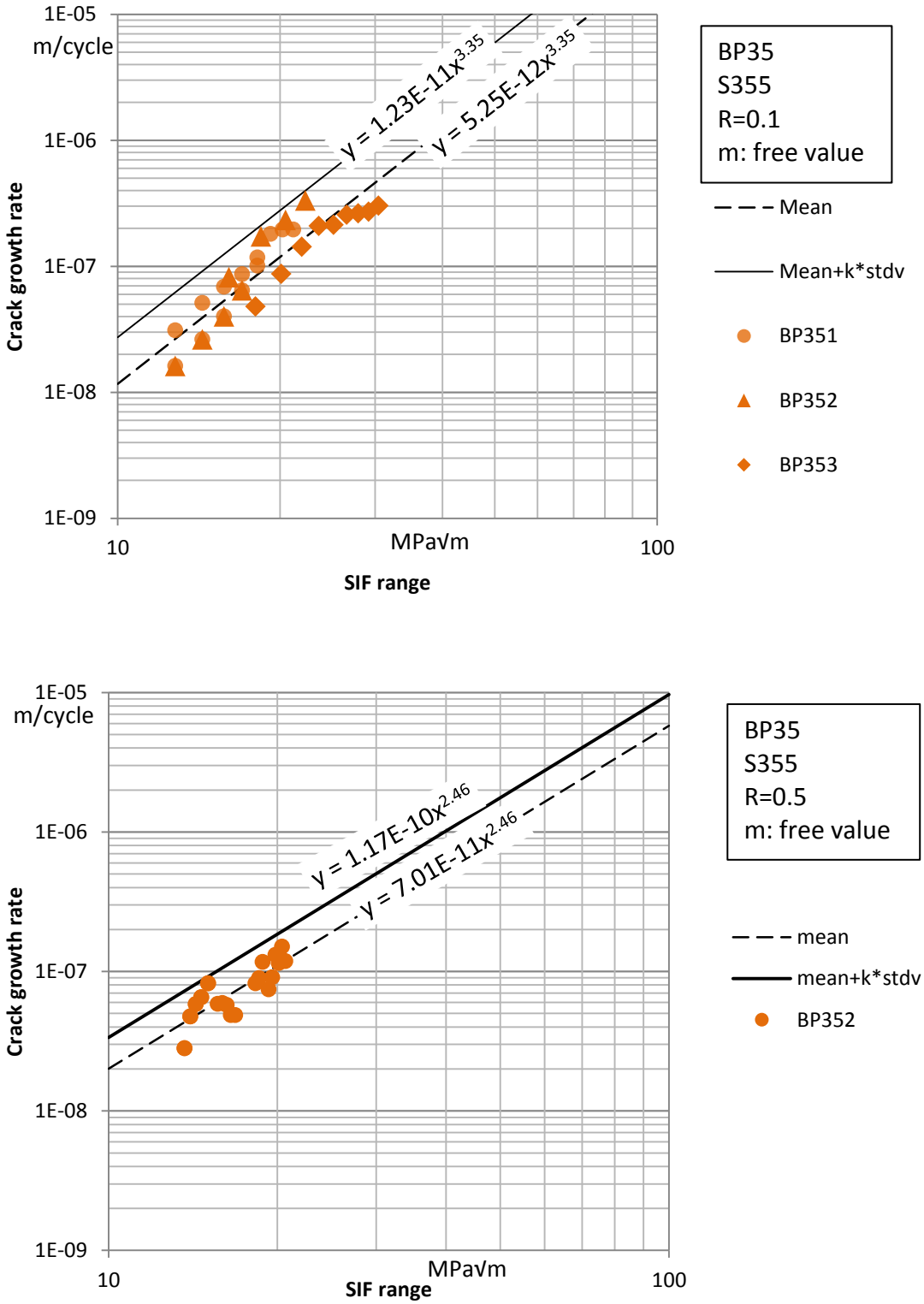


Figure A. 3: Regression lines of bead weld on plate specimens for free m-value

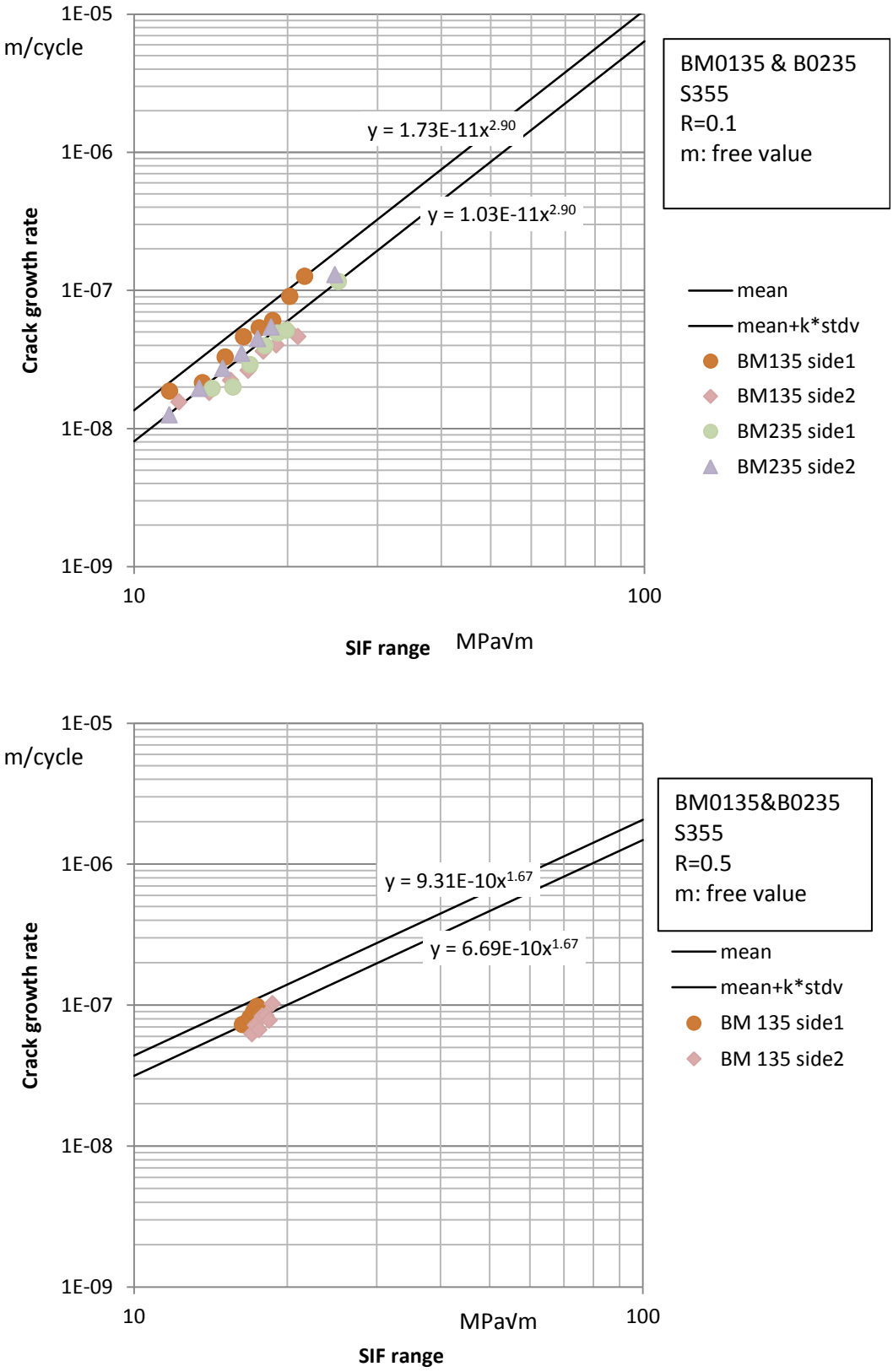


Figure A. 4: Regression lines of base material specimens for free m-value

# Appendix C

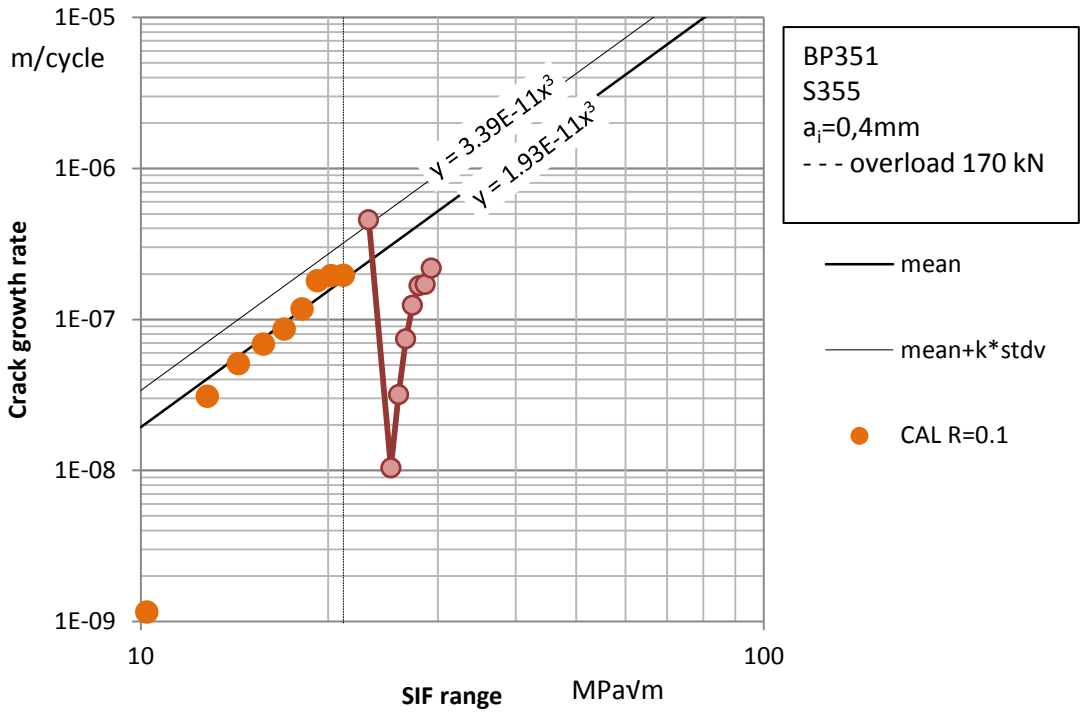


Figure A. 5: da/dn-ΔK curve for bead weld on plate specimen BP351

# Appendix D

The following figure (X. Shan et al. 2009 *[1]*) is derived from a three-dimensional thermo-mechanical finite element analysis of a single weld bead-on-plate of steel and represents the pattern of residual stresses close to the weld in both longitudinal and transversal directions of the plate.

Despite the fact that this case is not exactly similar with the examined one, it can be considered that Figure A. 6 represents approximately the residual stress distribution close to the weld for the tested welded specimens (BP351, BP352 and BP353). It is clear from the graph that close to the heat affected zone tensile residual stresses are developed in longitudinal direction.

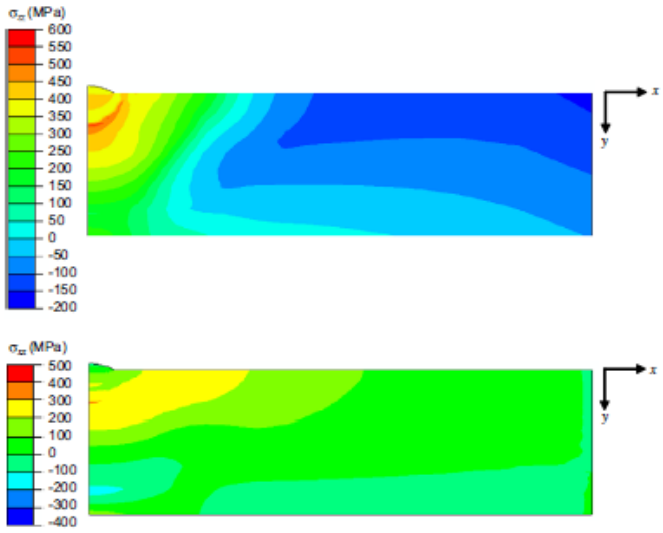


Figure A. 6: Pattern of residual stresses close to the bead weld in longitudinal and transversal direction *[1]*

## Reference


**[1]** X. Shan, C.M. Davies, T. Wangsdan, N.P. O'Dowdc, K.M. Nikbin - Thermo-mechanical modelling of a single-bead-on-plate weld using the finite element method - International Journal of Pressure Vessels and Piping 86 (2009) 110–121

# Appendix E

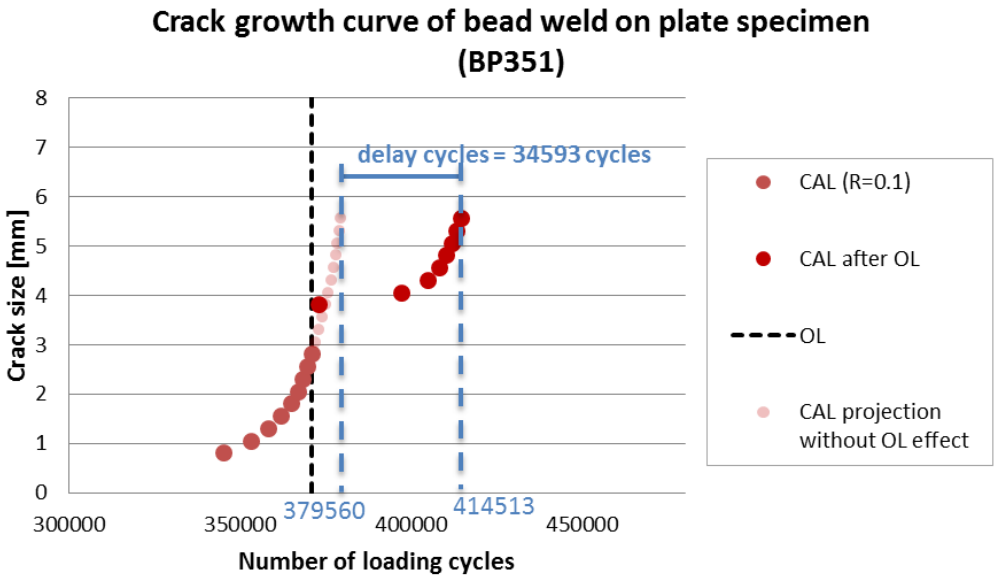


Figure A. 7: Crack growth and delay cycles in bead weld on plate specimen BP351

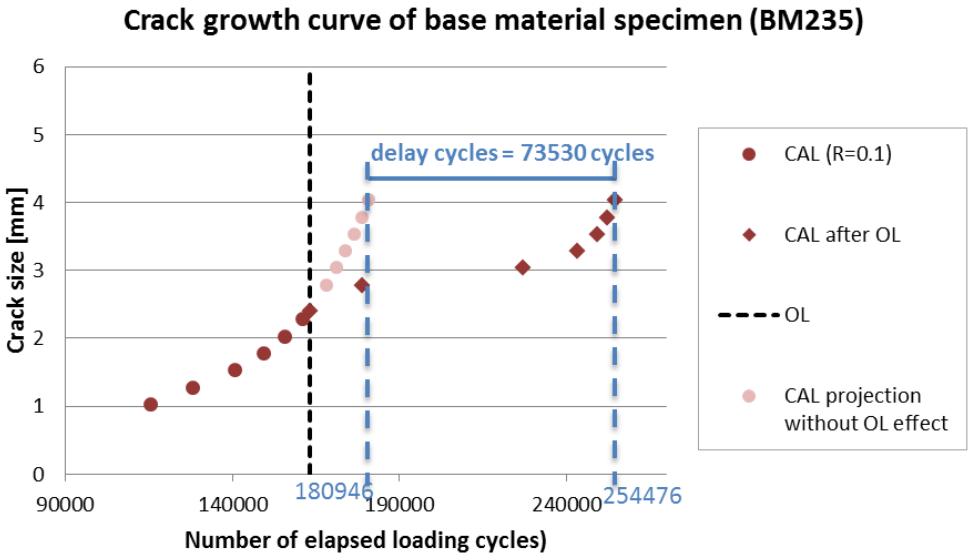


Figure A. 8: : Crack growth and delay cycles in base material specimen BM235 (side 1)

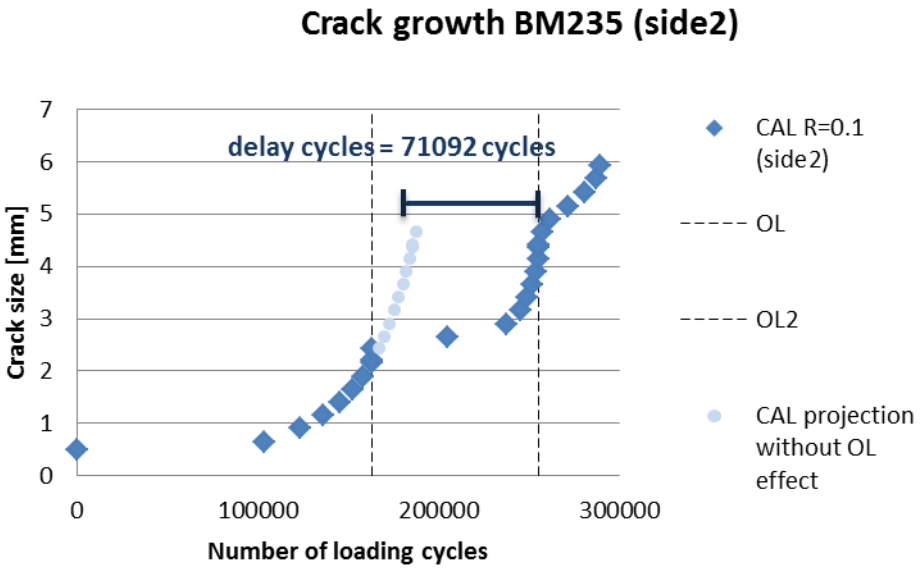


Figure A. 9: Crack growth and delay cycles in base material specimen BM235 (side 2)

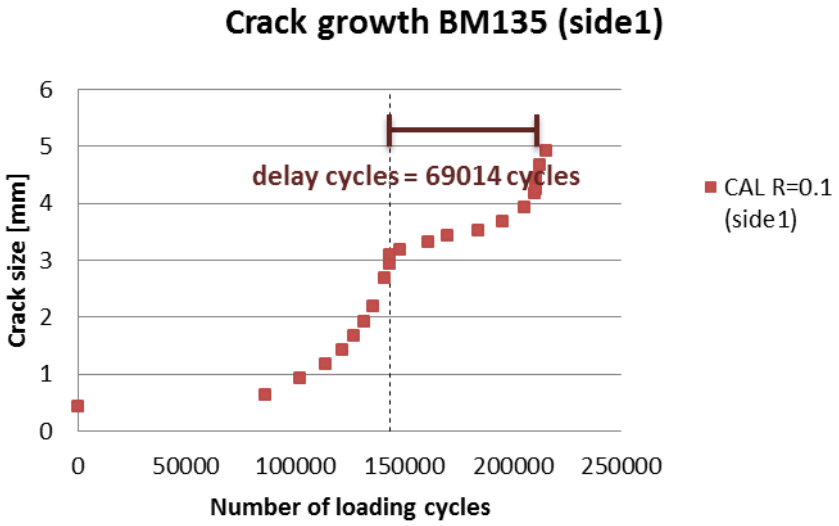


Figure A. 10: Crack growth and delay cycles in base material specimen BM135 (side 1)

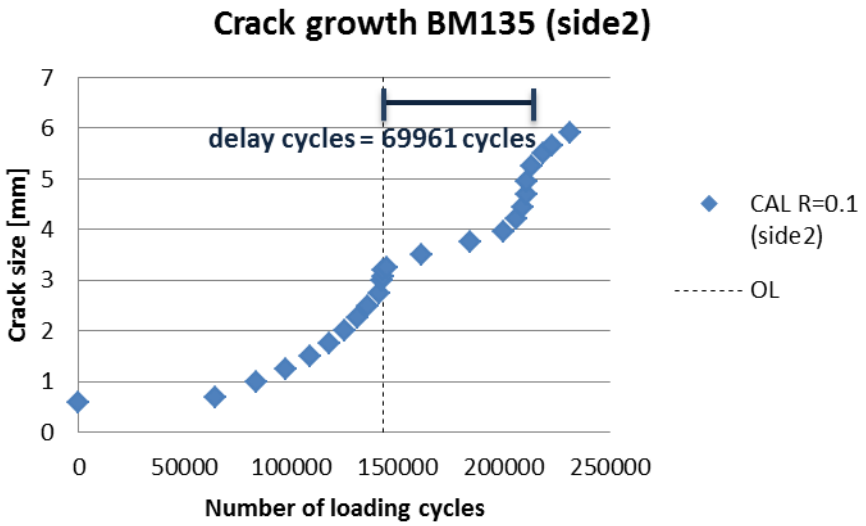


Figure A. 11: Crack growth and delay cycles in base material specimen BM135 (side 2)

## Appendix F

ACPD measurements of crack depth at certain locations around the joint vs. total number of loading cycles

Table A. 1: ACPD measurements of crack depth at certain locations around the joint vs. total number of loading cycles (T-joint side 1)

| Total number of loading cycles | -25˚ | -20˚ | -15˚ | -10˚ | -5˚ | 0˚ | 5˚ | 10˚ | 15˚ | 20˚ | 25˚ | 30˚ | 35˚ | 40˚ | 45˚ | 50˚ | 55˚ |
|---|---|---|---|---|---|---|---|---|---|---|---|---|---|---|---|---|---|
| **482000** | 0 | 0 | 0 | 0 | 0 | 0 | 1 | 1.5 | 1.8 | 2.1 | 1.3 | 1.2 | 1.5 | 0 | 0 | 0 | 0 |
| **502000** | 0 | 0.3 | 0.5 | 0.9 | 1.2 | 1 | 1.9 | 2.3 | 2.5 | 2.5 | 2.3 | 1.9 | 1.5 | 0.9 | 0.9 | 0.6 | 0.6 |
| **512000** | 0.2 | 0.4 | 0.5 | 1.3 | 1.4 | 1.2 | 2.1 | 2.5 | 2.8 | 2.7 | 2.3 | 2 | 1.6 | 1 | 0.9 | 0.8 | 0.6 |
| **522000** | 0.2 | 0.4 | 0.5 | 1.5 | 1.8 | 1.4 | 2.5 | 2.7 | 3.2 | 3.2 | 2.5 | 2.2 | 1.8 | 1.1 | 0.9 | 0.9 | 0.6 |
| **532000** | 0.3 | 0.6 | 0.6 | 2 | 2.1 | 1.8 | 3.1 | 3.5 | 4.1 | 3.8 | 2.8 | 2.3 | 1.8 | 1.2 | 1 | 1 | 0.6 |
| **542000** | 0.3 | 1 | 1 | 2.2 | 2.5 | 2.1 | 4 | 4.5 | 5 | 4.5 | 3.3 | 2.8 | 2.2 | 1.4 | 1.1 | 1.2 | 0.7 |
| **552000** | 0.3 | 1 | 1.1 | 2.7 | 3 | 2.6 | 4.9 | 5.5 | 5.9 | 5.3 | 4.1 | 3.3 | 2.5 | 1.8 | 1.4 | 1.4 | 0.7 |
| **562000** | 0.3 | 1 | 1.2 | 3.4 | 3.5 | 3.1 | 5.6 | 6.3 | 6.7 | 6.3 | 4.8 | 3.8 | 2.7 | 2 | 1.5 | 1.5 | 0.7 |
| **572000** | 0.3 | 1.2 | 1.3 | 3.7 | 4.1 | 3.8 | 6.5 | 7.2 | 7.7 | 7.1 | 5.7 | 4.5 | 3.2 | 2.3 | 1.7 | 1.6 | 0.8 |
| **578000** | 0.3 | 1.3 | 1.6 | 4 | 4.4 | 4.4 | 7 | 7.8 | 8.4 | 7.5 | 6.3 | 4.9 | 3.8 | 2.6 | 2.1 | 1.9 | 1.1 |
| **588000** | 0.3 | 1.4 | 2.1 | 5.3 | 4.9 | 5.1 | 7.6 | 8.2 | 8.7 | 7.7 | 6.6 | 5.1 | 4.1 | 3.1 | 2.2 | 2.0 | 1.1 |
| **598000** | 0.3 | 1.9 | 3.1 | 6.2 | 6.5 | 7.5 | 9.2 | 9.7 | 9.7 | 10.1 | 8.9 | 7.7 | 5.1 | 3.5 | 2.5 | 2.2 | 1.1 |
| **608000** | 0.5 | 3.4 | 5.7 | 8.6 | 9.2 | 10.4 | 11.6 | 11.6 | 11.7 | 11.8 | 10.1 | 9.0 | 6.6 | 5.6 | 3.8 | 2.8 | 1.5 |
| **613000** | 0.5 | 3.9 | 6.9 | 9.4 | 10.2 | 11.6 | 12.7 | 12.7 | 12.7 | 12.5 | 11.0 | 9.5 | 7.9 | 5.9 | 4.2 | 2.8 | 1.5 |

*At 482000 cycles the ACPD measurements were taken once for each location and the voltage measurements were not recorded.

Table A. 2: ACPD measurements of crack depth at certain locations around the joint vs. total number of loading cycles (T-joint side 2)

| | 195˚ | 190˚ | 185˚ | 180˚ | 175˚ | 170˚ |
|---|---|---|---|---|---|---|
| **502000** | 0.6 | 1.9 | 0.5 | 1.2 | 0.8 | 0.5 |
| **512000** | 0.6 | 1.9 | 0.5 | 1.2 | 1.1 | 0.7 |
| **522000** | 1.1 | 2.1 | 0.8 | 1.2 | 1.1 | 0.8 |
| **532000** | 1.1 | 2.1 | 0.8 | 1.5 | 1.3 | 0.8 |
| **542000** | 1.1 | 2.1 | 1.3 | 1.9 | 1.3 | 0.8 |
| **552000** | 1.4 | 2.1 | 1.4 | 2 | 1.9 | 1.2 |
| **562000** | 1.4 | 2.1 | 1.6 | 2.1 | 1.9 | 1.4 |
| **572000** | 1.5 | 2.3 | 1.9 | 2.7 | 2 | 1.5 |
| **578000** | 1.5 | 2.6 | 2.2 | 3.3 | 3.1 | 2.3 |
| **588000** | | 2.8 | 2.3 | 2.7 | 2.5 | |
| **598000** | 1.7 | 2.9 | 2.3 | 2.7 | 3.6 | 3 |
| **608000** | 2.1 | 3.3 | 3.1 | 3.1 | 4.1 | 3.1 |
| **613000** | 2.2 | 4.1 | 4.1 | 3.9 | 5.2 | 4.1 |

Table A. 3: Voltage measurements and conversion to crack size (502000 cycles)

| -25 | | | -20 | | | -15 | | | -10 | | | -5 | | | 0 | | |
|---|---|---|---|---|---|---|---|---|---|---|---|---|---|---|---|---|---|
| over crack | reference | crack size | over crack | reference | crack size | over crack | reference | crack size | over crack | reference | crack size | over crack | reference | crack size | over crack | reference | crack size |
| 557 | 562 | 0.0 | 557 | 533 | 0.2 | 571 | 494 | 0.8 | 534 | 455 | 0.9 | 546 | 438 | 1.2 | 520 | 440 | 0.9 |
| 552 | 552 | 0.0 | 552 | 518 | 0.3 | 528 | 480 | 0.5 | 545 | 469 | 0.8 | 543 | 437 | 1.2 | 558 | 444 | 1.3 |
| 554 | 559 | 0.0 | 554 | 526 | 0.3 | 542 | 498 | 0.4 | 550 | 454 | 1.1 | 535 | 424 | 1.3 | 522 | 449 | 0.8 |
| | | | | | | 532 | 496 | 0.4 | 550 | 463 | 0.9 | | | | 530 | 451 | 0.9 |
| | | | | | | | | | 550 | 458 | 1.0 | | | | 545 | 453 | 1.0 |
| | | | | | | | | | | | | | | | 544 | 451 | 1.0 |
| | | | | | | | | | | | | | | | 567 | 448 | 1.3 |
| | | | | | | | | | | | | | | | 532 | 452 | 0.9 |
| | | | | | | | | | | | | | | | 541 | 456 | 0.9 |
| | | **0.0** | | | **0.3** | | | **0.5** | | | **0.9** | | | **1.2** | | | **1.0** |

| 5 | | | 10 | | | 15 | | | 20 | | | 25 | | | 30 | | |
|---|---|---|---|---|---|---|---|---|---|---|---|---|---|---|---|---|---|
| over crack | reference | crack size | over crack | reference | crack size | over crack | reference | crack size | over crack | reference | crack size | over crack | reference | crack size | over crack | reference | crack size |
| 643 | 442 | 2.3 | 606 | 423 | 2.2 | 661 | 423 | 2.8 | 663 | 435 | 2.6 | 607 | 434 | 2.0 | 613 | 443 | 1.9 |
| 602 | 441 | 1.8 | 622 | 418 | 2.4 | 621 | 420 | 2.4 | 665 | 433 | 2.7 | 603 | 418 | 2.2 | 631 | 423 | 2.5 |
| 610 | 447 | 1.8 | 618 | 422 | 2.3 | 618 | 411 | 2.5 | 644 | 432 | 2.5 | 604 | 407 | 2.4 | 645 | 447 | 2.2 |
| 610 | 439 | 1.9 | 625 | 432 | 2.2 | 609 | 418 | 2.3 | 672 | 436 | 2.7 | 603 | 408 | 2.4 | 611 | 457 | 1.7 |
| 603 | 446 | 1.8 | 616 | 417 | 2.4 | 629 | 427 | 2.4 | 665 | 437 | 2.6 | 607 | 414 | 2.3 | 633 | 459 | 1.9 |
| | | | 630 | 425 | 2.4 | | | | 632 | 424 | 2.5 | | | | 618 | 451 | 1.9 |
| | | | | | | | | | 675 | 446 | 2.6 | | | | 641 | 457 | 2.0 |
| | | | | | | | | | 632 | 428 | 2.4 | | | | 623 | 465 | 1.7 |
| | | | | | | | | | 636 | 428 | 2.4 | | | | 624 | 461 | 1.8 |
| | | **1.9** | | | **2.3** | | | **2.5** | | | **2.5** | | | **2.3** | | | **1.9** |

| 35 | | | 40 | | | 45 | | | 50 | | | 55 | | |
|---|---|---|---|---|---|---|---|---|---|---|---|---|---|---|
| over crack | reference | crack size | over crack | reference | crack size | over crack | reference | crack size | over crack | reference | crack size | over crack | reference | crack size |
| 590 | 450 | 1.6 | 586 | 494 | 0.9 | 575 | 482 | 1.0 | 572 | 515 | 0.6 | 542 | 481 | 0.6 |
| 582 | 451 | 1.5 | 579 | 489 | 0.9 | 578 | 488 | 0.9 | 573 | 492 | 0.8 | 529 | 459 | 0.8 |
| 570 | 453 | 1.3 | 585 | 493 | 0.9 | 568 | 482 | 0.9 | 543 | 500 | 0.4 | 504 | 477 | 0.3 |
| 576 | 432 | 1.7 | | | | | | | 544 | 478 | 0.7 | 544 | 484 | 0.6 |
| | | | | | | | | | | | | 534 | 476 | 0.6 |
| | | | | | | | | | | | | | | |
| | | | | | | | | | | | | | | |
| | | | | | | | | | | | | | | |
| | | | | | | | | | | | | | | |
| | | **1.5** | | | **0.9** | | | **0.9** | | | **0.6** | | | **0.6** |

Table A. 4: Voltage measurements and conversion to crack size (512000 cycles)

| -25 | | | -20 | | | -15 | | | -10 | | | -5 | | | 0 | | |
|---|---|---|---|---|---|---|---|---|---|---|---|---|---|---|---|---|---|
| over crack | reference | crack size | over crack | reference | crack size | over crack | reference | crack size | over crack | reference | crack size | over crack | reference | crack size | over crack | reference | crack size |
| 580 | 549 | 0.2 | 571 | 537 | 0.3 | 439 | 398 | 0.5 | 494 | 373 | 1.6 | 493 | 369 | 1.6 | 479 | 401 | 1.0 |
| 626 | 597 | 0.2 | 554 | 510 | 0.4 | 450 | 413 | 0.4 | 454 | 356 | 1.3 | 631 | 511 | 1.1 | 494 | 386 | 1.4 |
| | | | 639 | 590 | 0.4 | 452 | 409 | 0.5 | 596 | 493 | 1.2 | 664 | 528 | 1.2 | 491 | 396 | 1.2 |
| | | | | | | 431 | 398 | 0.4 | 599 | 497 | 1 | 571 | 418 | 1.8 | 499 | 405 | 1.2 |
| | | | | | | | | | 613 | 498 | 1.1 | 576 | 448 | 1.4 | 512 | 394 | 1.5 |
| | | | | | | | | | 491 | 377 | 1.5 | 581 | 468 | 1.2 | 504 | 399 | 1.3 |
| | | | | | | | | | 626 | 490 | 1.3 | | | | 531 | 409 | 1.5 |
| | | | | | | | | | | | | | | | 473 | 403 | 0.9 |
| | | | | | | | | | | | | | | | 506 | 404 | 1.3 |
| | | | | | | | | | | | | | | | | | |
| | | 0.2 | | | 0.4 | | | 0.5 | | | 1.3 | | | 1.4 | | | 1.2 |

| 5 | | | 10 | | | 15 | | | 20 | | | 25 | | | 30 | | |
|---|---|---|---|---|---|---|---|---|---|---|---|---|---|---|---|---|---|
| over crack | reference | crack size | over crack | reference | crack size | over crack | reference | crack size | over crack | reference | crack size | over crack | reference | crack size | over crack | reference | crack size |
| 558 | 399 | 1.9 | 591 | 395 | 2.4 | 603 | 395 | 2.6 | 689 | 444 | 2.8 | 606 | 423 | 2.2 | 612 | 436 | 2.0 |
| 578 | 409 | 2 | 598 | 398 | 2.5 | 632 | 394 | 3.0 | 681 | 439 | 2.8 | 667 | 467 | 2.1 | 608 | 439 | 1.9 |
| 574 | 400 | 2.1 | 582 | 395 | 2.3 | 616 | 388 | 2.9 | 684 | 442 | 2.7 | 677 | 464 | 2.3 | 623 | 452 | 1.9 |
| 564 | 389 | 2.2 | 601 | 400 | 2.5 | 630 | 398 | 2.9 | 679 | 444 | 2.6 | 663 | 463 | 2.2 | 632 | 453 | 2.0 |
| 577 | 393 | 2.3 | 604 | 399 | 2.5 | 624 | 397 | 2.9 | 683 | 442 | 2.7 | 673 | 473 | 2.1 | 614 | 447 | 1.9 |
| 562 | 388 | 2.2 | 599 | 403 | 2.4 | 632 | 400 | 2.9 | 682 | 440 | 2.8 | 671 | 460 | 2.3 | 627 | 446 | 2.0 |
| 559 | 390 | 2.1 | 610 | 401 | 2.6 | 626 | 399 | 2.8 | 678 | 437 | 2.8 | 669 | 469 | 2.1 | 625 | 436 | 2.2 |
| 554 | 387 | 2.1 | 593 | 400 | 2.4 | 604 | 396 | 2.6 | 691 | 447 | 2.7 | 665 | 464 | 2.2 | 617 | 441 | 2.0 |
| | | | | | | | | | 685 | 446 | 2.7 | 661 | 442 | 2.5 | 618 | 453 | 1.8 |
| | | | | | | | | | 681 | 444 | 2.7 | 674 | 444 | 2.6 | 624 | 447 | 2.0 |
| | | 2.1 | | | 2.5 | | | 2.8 | | | 2.7 | | | 2.3 | | | 2.0 |

| 35 | | | 40 | | | 45 | | | 50 | | | 55 | | |
|---|---|---|---|---|---|---|---|---|---|---|---|---|---|---|
| over crack | reference | crack size | over crack | reference | crack size | over crack | reference | crack size | over crack | reference | crack size | over crack | reference | crack size |
| 637 | 480 | 1.6 | 590 | 500 | 0.9 | 601 | 501 | 1.0 | 524 | 472 | 0.6 | 541 | 481 | 0.6 |
| 635 | 477 | 1.7 | 587 | 498 | 0.9 | 602 | 503 | 1.0 | 564 | 474 | 0.9 | 542 | 457 | 0.9 |
| 641 | 478 | 1.7 | 588 | 489 | 1.0 | 604 | 511 | 0.9 | 549 | 472 | 0.8 | 495 | 479 | 0.2 |
| 637 | 480 | 1.6 | 596 | 490 | 1.1 | 606 | 511 | 0.9 | 595 | 507 | 0.8 | 533 | 462 | 0.8 |
| 638 | 475 | 1.7 | 593 | 490 | 1.1 | 598 | 506 | 0.9 | | | | 534 | 476 | 0.6 |
| 630 | 480 | 1.6 | | | | | | | | | | 533 | 481 | 0.5 |
| 637 | 481 | 1.6 | | | | | | | | | | | | |
| | | | | | | | | | | | | | | |
| | | | | | | | | | | | | | | |
| | | | | | | | | | | | | | | |
| | | 1.6 | | | 1.0 | | | 0.9 | | | 0.8 | | | 0.6 |

Table A. 5: Voltage measurements and conversion to crack size (522000 cycles)

| -25 | | | -20 | | | -15 | | | -10 | | | -5 | | | 0 | | |
|---|---|---|---|---|---|---|---|---|---|---|---|---|---|---|---|---|---|
| over crack | reference | crack size | over crack | reference | crack size | over crack | reference | crack size | over crack | reference | crack size | over crack | reference | crack size | over crack | reference | crack size |
| 575 | 551 | 0.2 | 535 | 492 | 0.4 | 505 | 457 | 0.5 | 548 | 413 | 1.6 | 542 | 399 | 1.8 | 540 | 400 | 1.8 |
| 581 | 553 | 0.2 | 517 | 476 | 0.4 | 497 | 454 | 0.5 | 552 | 422 | 1.5 | 543 | 377 | 2.2 | 513 | 395 | 1.5 |
| 578 | 548 | 0.3 | 520 | 479 | 0.4 | 500 | 454 | 0.5 | 537 | 416 | 1.5 | 528 | 388 | 1.8 | 501 | 393 | 1.4 |
| 577 | 555 | 0.2 | 518 | 485 | 0.4 | 500 | 457 | 0.5 | 542 | 423 | 1.4 | 530 | 386 | 1.9 | 513 | 398 | 1.4 |
| 574 | 554 | 0.2 | 514 | 486 | 0.4 | | | | 550 | 411 | 1.7 | 533 | 397 | 1.7 | 524 | 411 | 1.4 |
| | | | | | | | | | | | | 529 | 395 | 1.7 | 504 | 395 | 1.4 |
| | | | | | | | | | | | | 537 | 396 | 1.8 | 511 | 416 | 1.1 |
| | | | | | | | | | | | | | | | 507 | 399 | 1.4 |
| | | | | | | | | | | | | | | | 513 | 393 | 1.5 |
| | | | | | | | | | | | | | | | 521 | 402 | 1.5 |
| | | | | | | | | | | | | | | | | | |
| | | 0.2 | | | 0.4 | | | 0.5 | | | 1.5 | | | 1.8 | | | 1.4 |

| 5 | | | 10 | | | 15 | | | 20 | | | 25 | | | 30 | | |
|---|---|---|---|---|---|---|---|---|---|---|---|---|---|---|---|---|---|
| over crack | reference | crack size | over crack | reference | crack size | over crack | reference | crack size | over crack | reference | crack size | over crack | reference | crack size | over crack | reference | crack size |
| 566 | 374 | 2.6 | 680 | 442 | 2.6 | 717 | 439 | 3.1 | 727 | 424 | 3.6 | 687 | 460 | 2.4 | 654 | 463 | 2.1 |
| 585 | 379 | 2.7 | 673 | 427 | 2.8 | 701 | 426 | 3.2 | 724 | 444 | 3.2 | 692 | 459 | 2.5 | 652 | 458 | 2.1 |
| 605 | 405 | 2.5 | 681 | 424 | 3 | 702 | 422 | 3.3 | 721 | 449 | 3.0 | 701 | 464 | 2.5 | 642 | 445 | 2.2 |
| 595 | 403 | 2.4 | 674 | 443 | 2.6 | 715 | 436 | 3.1 | 722 | 446 | 3.1 | 709 | 471 | 2.5 | 661 | 444 | 2.4 |
| 614 | 401 | 2.7 | 673 | 430 | 2.8 | 708 | 430 | 3.2 | 751 | 422 | 3.9 | 695 | 465 | 2.5 | 634 | 461 | 1.9 |
| 600 | 382 | 2.9 | 676 | 448 | 2.5 | 712 | 438 | 3.1 | 721 | 436 | 3.3 | 707 | 460 | 2.7 | 653 | 451 | 2.2 |
| 582 | 378 | 2.7 | 692 | 452 | 2.6 | 718 | 420 | 3.5 | 717 | 429 | 3.4 | 689 | 470 | 2.3 | | | |
| 571 | 405 | 2.0 | 673 | 441 | 2.6 | 699 | 438 | 3.0 | 723 | 445 | 3.1 | | | | | | |
| 609 | 404 | 2.5 | 677 | 432 | 2.8 | 707 | 430 | 3.2 | 711 | 449 | 2.9 | | | | | | |
| | | | | | | | | | 721 | 447 | 3.1 | | | | | | |
| | | | | | | | | | | | | | | | | | |
| | | 2.5 | | | 2.7 | | | 3.2 | | | 3.2 | | | 2.5 | | | 2.2 |

| 35 | | | 40 | | | 45 | | | 50 | | | 55 | | |
|---|---|---|---|---|---|---|---|---|---|---|---|---|---|---|
| over crack | reference | crack size | over crack | reference | crack size | over crack | reference | crack size | over crack | reference | crack size | over crack | reference | crack size |
| 629 | 455 | 1.9 | 578 | 486 | 0.9 | 600 | 470 | 1.4 | 600 | 506 | 0.9 | 602 | 533 | 0.6 |
| 628 | 447 | 2 | 582 | 474 | 1.1 | 599 | 498 | 1.0 | 598 | 510 | 0.9 | | | |
| 627 | 456 | 1.8 | 637 | 511 | 1.2 | 593 | 508 | 0.8 | | | | | | |
| 615 | 459 | 1.6 | 610 | 496 | 1.1 | 583 | 517 | 0.6 | | | | | | |
| 640 | 482 | 1.6 | 615 | 509 | 1 | 614 | 519 | 0.9 | | | | | | |
| 626 | 462 | 1.7 | | | | 610 | 523 | 0.8 | | | | | | |
| | | | | | | | | | | | | | | |
| | | | | | | | | | | | | | | |
| | | | | | | | | | | | | | | |
| | | | | | | | | | | | | | | |
| | | | | | | | | | | | | | | |
| | | 1.8 | | | 1.1 | | | 0.936485 | | | 0.9 | | | 0.6 |

Table A. 6: Voltage measurements and conversion to crack size (532000 cycles)

| -25 | | | -20 | | | -15 | | | -10 | | | -5 | | | 0 | | |
|---|---|---|---|---|---|---|---|---|---|---|---|---|---|---|---|---|---|
| over crack | reference | crack size | over crack | reference | crack size | over crack | reference | crack size | over crack | reference | crack size | over crack | reference | crack size | over crack | reference | crack size |
| 562 | 521 | 0.3 | 558 | 493 | 0.7 | 550 | 482 | 0.7 | 622 | 443 | 2 | 627 | 439 | 2.1 | 620 | 442 | 2.0 |
| 555 | 523 | 0.3 | 541 | 512 | 0.3 | 546 | 494 | 0.5 | 627 | 446 | 2 | 629 | 440 | 2.1 | 616 | 456 | 1.8 |
| | | | 553 | 482 | 0.7 | 542 | 499 | 0.4 | | | | 630 | 444 | 2.1 | 611 | 441 | 1.9 |
| | | | | | | | | | | | | 629 | 443 | 2.1 | 605 | 438 | 1.9 |
| | | | | | | | | | | | | | | | 615 | 445 | 1.9 |
| | | | | | | | | | | | | | | | 601 | 449 | 1.7 |
| | | | | | | | | | | | | | | | 605 | 453 | 1.7 |
| | | | | | | | | | | | | | | | | | |
| | | | | | | | | | | | | | | | | | |
| | | | | | | | | | | | | | | | | | |
| | | | | | | | | | | | | | | | | | |
| | | 0.302964 | | | 0.6 | | | 0.6 | | | 2 | | | 2.120719 | | | 1.8 |

| 5 | | | 10 | | | 15 | | | 20 | | | 25 | | | 30 | | |
|---|---|---|---|---|---|---|---|---|---|---|---|---|---|---|---|---|---|
| over crack | reference | crack size | over crack | reference | crack size | over crack | reference | crack size | over crack | reference | crack size | over crack | reference | crack size | over crack | reference | crack size |
| 676 | 416 | 3.1 | 670 | 392 | 3.5 | 746 | 409 | 4.1 | 739 | 416 | 3.8 | 715 | 455 | 2.8 | 671 | 447 | 2.5 |
| 681 | 417 | 3.1 | 680 | 397 | 3.6 | 743 | 405 | 4.1 | 745 | 420 | 3.8 | 709 | 454 | 2.8 | 663 | 449 | 2.4 |
| 675 | 419 | 3.1 | 691 | 395 | 3.7 | 741 | 410 | 4.0 | 732 | 422 | 3.7 | 708 | 459 | 2.7 | 671 | 453 | 2.4 |
| 674 | 411 | 3.2 | 681 | 401 | 3.5 | 743 | 408 | 4.1 | 741 | 423 | 3.8 | 711 | 453 | 2.8 | 652 | 453 | 2.2 |
| 679 | 421 | 3.1 | 670 | 400 | 3.4 | 742 | 412 | 4.0 | 740 | 417 | 3.9 | 704 | 459 | 2.7 | 671 | 456 | 2.4 |
| | | | | | | 739 | 406 | 4.1 | 741 | 425 | 3.7 | | | | 651 | 457 | 2.1 |
| | | | | | | | | | | | | | | | 655 | 459 | 2.1 |
| | | | | | | | | | | | | | | | 653 | 455 | 2.2 |
| | | | | | | | | | | | | | | | 664 | 451 | 2.4 |
| | | | | | | | | | | | | | | | | | |
| | | | | | | | | | | | | | | | | | |
| | | 3.1 | | | 3.5 | | | 4.1 | | | 3.8 | | | 2.8 | | | 2.3 |

| 35 | | | 40 | | | 45 | | | 50 | | | 55 | | |
|---|---|---|---|---|---|---|---|---|---|---|---|---|---|---|
| over crack | reference | crack size | over crack | reference | crack size | over crack | reference | crack size | over crack | reference | crack size | over crack | reference | crack size |
| 611 | 445 | 1.8 | 564 | 454 | 1.2 | 543 | 470 | 0.7 | 556 | 462 | 1 | 532 | 481 | 0.5 |
| 624 | 456 | 1.9 | 560 | 458 | 1.1 | 534 | 449 | 0.9 | 555 | 464 | 0.9 | 534 | 479 | 0.6 |
| 615 | 451 | 1.8 | 559 | 452 | 1.2 | 564 | 458 | 1.1 | 558 | 473 | 0.9 | | | |
| | | | | | | 568 | 463 | 1.1 | 549 | 460 | 1.0 | | | |
| | | | | | | | | | 547 | 463 | 0.9 | | | |
| | | | | | | | | | 543 | 458 | 1 | | | |
| | | | | | | | | | 551 | 445 | 1.1 | | | |
| | | | | | | | | | | | | | | |
| | | | | | | | | | | | | | | |
| | | | | | | | | | | | | | | |
| | | | | | | | | | | | | | | |
| | | 1.833333 | | | 1.2 | | | 0.95 | | | 1.0 | | | 0.6 |

Table A. 7: Voltage measurements and conversion to crack size (542000 cycles)

| -25 | | | -20 | | | -15 | | | -10 | | | -5 | | | 0 | | |
|---|---|---|---|---|---|---|---|---|---|---|---|---|---|---|---|---|---|
| over crack | reference | crack size | over crack | reference | crack size | over crack | reference | crack size | over crack | reference | crack size | over crack | reference | crack size | over crack | reference | crack size |
| 544 | 508 | 0.3 | 562 | 470 | 0.9 | 620 | 515 | 1 | 693 | 473 | 2.3 | 720 | 478 | 2.5 | 722 | 477 | 2.6 |
| 540 | 511 | 0.3 | 546 | 447 | 1.1 | 595 | 517 | 0.8 | 687 | 482 | 2.1 | 714 | 472 | 2.5 | 684 | 493 | 1.9 |
| | | | | | | 620 | 492 | 1.3 | 690 | 476 | 2.2 | 723 | 470 | 2.7 | 699 | 488 | 2.2 |
| | | | | | | 614 | 531 | 0.8 | 686 | 485 | 2.1 | 712 | 481 | 2.4 | 682 | 487 | 2.0 |
| | | | | | | | | | 696 | 470 | 2.4 | 716 | 475 | 2.5 | 673 | 483 | 2.0 |
| | | | | | | | | | | | | 717 | 480 | 2.5 | 688 | 487 | 2.1 |
| | | | | | | | | | | | | | | | 701 | 483 | 2.3 |
| | | | | | | | | | | | | | | | | | |
| | | | | | | | | | | | | | | | | | |
| | | | | | | | | | | | | | | | | | |
| | | | | | | | | | | | | | | | | | |
| | | 0.291879 | | | 1 | | | 1.0 | | | 2.2 | | | 2.5 | | | 2.1 |

| 5 | | | 10 | | | 15 | | | 20 | | | 25 | | | 30 | | |
|---|---|---|---|---|---|---|---|---|---|---|---|---|---|---|---|---|---|
| over crack | reference | crack size | over crack | reference | crack size | over crack | reference | crack size | over crack | reference | crack size | over crack | reference | crack size | over crack | reference | crack size |
| 726 | 403 | 4 | 776 | 394 | 4.8 | 805 | 422 | 4.5 | 839 | 441 | 4.5 | 771 | 462 | 3.3 | 743 | 457 | 3.1 |
| 749 | 405 | 4.2 | 787 | 416 | 4.4 | 806 | 387 | 5.4 | 840 | 442 | 4.5 | 769 | 463 | 3.3 | 723 | 462 | 2.8 |
| 750 | 408 | 4.2 | 791 | 415 | 4.5 | 820 | 385 | 5.6 | 838 | 441 | 4.5 | 772 | 460 | 3.4 | 717 | 463 | 2.7 |
| 723 | 404 | 3.9 | 789 | 413 | 4.5 | 816 | 384 | 5.6 | 839 | 440 | 4.5 | 771 | 461 | 3.4 | 711 | 459 | 2.7 |
| 725 | 401 | 4.0 | 771 | 411 | 4.5 | 827 | 421 | 4.8 | 839 | 445 | 4.4 | 770 | 464 | 3.3 | 723 | 457 | 2.9 |
| 733 | 407 | 4.0 | 777 | 421 | 4.5 | 831 | 413 | 5.1 | 842 | 442 | 4.5 | | | | 720 | 459 | 2.8 |
| 728 | 408 | 3.9 | 784 | 403 | 4.5 | 829 | 420 | 4.9 | | | | | | | 712 | 467 | 2.6 |
| | | | | | | 806 | 423 | 4.5 | | | | | | | | | |
| | | | | | | 811 | 408 | 4.9 | | | | | | | | | |
| | | | | | | 813 | 409 | 4.9 | | | | | | | | | |
| | | | | | | 819 | 411 | 5.0 | | | | | | | | | |
| | | | | | | | | | | | | | | | | | |
| | | 4.044915 | | | 4.528571 | | | 5.0 | | | 4.497846 | | | 3.3 | | | 2.8 |

| 35 | | | 40 | | | 45 | | | 50 | | | 55 | | |
|---|---|---|---|---|---|---|---|---|---|---|---|---|---|---|
| over crack | reference | crack size | over crack | reference | crack size | over crack | reference | crack size | over crack | reference | crack size | over crack | reference | crack size |
| 684 | 464 | 2.4 | 676 | 479 | 2.1 | 603 | 491 | 1.1 | 605 | 487 | 1.2 | 583 | 504 | 0.8 |
| 697 | 482 | 2.2 | 642 | 496 | 1.5 | 606 | 492 | 1.2 | 605 | 488 | 1.2 | 588 | 506 | 0.8 |
| 680 | 491 | 1.9 | 640 | 499 | 1.4 | 600 | 492 | 1.1 | 607 | 487 | 1.2 | 581 | 513 | 0.7 |
| 702 | 487 | 2.2 | 642 | 506 | 1.3 | | | | | | | 580 | 510 | 0.7 |
| 677 | 478 | 2.1 | 643 | 500 | 1.4 | | | | | | | | | |
| | | | 638 | 502 | 1.4 | | | | | | | | | |
| | | | 632 | 500 | 1.3 | | | | | | | | | |
| | | | 641 | 503 | 1.4 | | | | | | | | | |
| | | | 629 | 503 | 1.3 | | | | | | | | | |
| | | | | | | | | | | | | | | |
| | | | | | | | | | | | | | | |
| | | | | | | | | | | | | | | |
| | | 2.2 | | | 1.4 | | | 1.1 | | | 1.2 | | | 0.7 |

Table A. 8: Voltage measurements and conversion to crack size (552000 cycles)

| -25 | | | -20 | | | -15 | | | -10 | | | -5 | | | 0 | | |
|---|---|---|---|---|---|---|---|---|---|---|---|---|---|---|---|---|---|
| over crack | reference | crack size | over crack | reference | crack size | over crack | reference | crack size | over crack | reference | crack size | over crack | reference | crack size | over crack | reference | crack size |
| 544 | 508 | 0.4 | 560 | 470 | 0.9 | 613 | 500 | 1.1 | 721 | 462 | 2.8 | 778 | 480 | 3.1 | 732 | 488 | 2.5 |
| 541 | 511 | 0.3 | 559 | 457 | 1.1 | 618 | 505 | 1.1 | 727 | 471 | 2.7 | 785 | 483 | 3.1 | 728 | 478 | 2.6 |
| 540 | 511 | 0.3 | 559 | 473 | 0.9 | | | | 737 | 488 | 2.6 | 775 | 473 | 3.1 | 721 | 482 | 2.5 |
| | | | | | | | | | 735 | 473 | 2.8 | 767 | 478 | 3 | 738 | 482 | 2.7 |
| | | | | | | | | | 721 | 474 | 2.6 | 770 | 492 | 2.8 | 731 | 485 | 2.5 |
| | | | | | | | | | | | | 777 | 483 | 3 | | | |
| | | | | | | | | | | | | 679 | 410 | 3.2 | | | |
| | | | | | | | | | | | | | | | | | |
| | | | | | | | | | | | | | | | | | |
| | | | | | | | | | | | | | | | | | |
| | | | | | | | | | | | | | | | | | |
| | | | | | | | | | | | | | | | | | |
| | | 0.310543 | | | 0.969697 | | | 1.1 | | | 2.7 | | | 3.0 | | | 2.6 |

| 5 | | | 10 | | | 15 | | | 20 | | | 25 | | | 30 | | |
|---|---|---|---|---|---|---|---|---|---|---|---|---|---|---|---|---|---|
| over crack | reference | crack size | over crack | reference | crack size | over crack | reference | crack size | over crack | reference | crack size | over crack | reference | crack size | over crack | reference | crack size |
| 911 | 458 | 4.9 | 870 | 402 | 5.8 | 891 | 412 | 5.8 | 924 | 504 | 4.2 | 806 | 406 | 4.9 | 833 | 500 | 3.3 |
| 912 | 449 | 5.2 | 869 | 402 | 5.8 | 893 | 411 | 5.9 | 891 | 481 | 4.3 | 803 | 463 | 3.7 | 834 | 487 | 3.6 |
| 881 | 447 | 4.9 | 878 | 414 | 5.6 | 901 | 410 | 6.0 | 928 | 451 | 5.3 | 869 | 468 | 4.3 | 832 | 512 | 3.1 |
| 872 | 447 | 4.8 | 881 | 418 | 5.5 | 903 | 397 | 6.4 | 949 | 462 | 5.3 | 858 | 464 | 4.2 | 834 | 516 | 3.1 |
| 890 | 440 | 5.1 | 848 | 425 | 5.0 | 872 | 399 | 5.9 | 989 | 461 | 5.7 | 886 | 484 | 4.2 | 822 | 511 | 3.0 |
| 868 | 449 | 4.7 | 867 | 408 | 5.6 | 870 | 368 | 6.8 | 1017 | 495 | 5.3 | 883 | 496 | 3.9 | 852 | 499 | 3.5 |
| 893 | 442 | 5.1 | 850 | 402 | 5.6 | 939 | 444 | 5.6 | 1027 | 476 | 5.8 | 873 | 488 | 3.9 | 820 | 496 | 3.3 |
| | | | 873 | 410 | 5.6 | 995 | 456 | 5.9 | 956 | 440 | 5.9 | 890 | 492 | 4.0 | 804 | 482 | 3.3 |
| | | | 882 | 415 | 5.6 | 957 | 460 | 5.4 | 987 | 493 | 5.0 | 872 | 490 | 3.9 | 821 | 509 | 3.1 |
| | | | 814 | 411 | 4.9 | 912 | 431 | 5.580046 | 990 | 467 | 5.6 | 872 | 466 | 4.4 | 824 | 498 | 3.3 |
| | | | 876 | 411 | 5.7 | | | | 941 | 445 | 5.6 | 862 | 468 | 4.2 | | | |
| | | | 870 | 408 | 5.7 | | | | | | | | | | | | |
| | | 4.9 | | | 5.5 | | | 5.9 | | | 5.3 | | | 4.148615 | | | 3.3 |

| 35 | | | 40 | | | 45 | | | 50 | | | 55 | | |
|---|---|---|---|---|---|---|---|---|---|---|---|---|---|---|
| over crack | reference | crack size | over crack | reference | crack size | over crack | reference | crack size | over crack | reference | crack size | over crack | reference | crack size |
| 757 | 511 | 2.4 | 667 | 475 | 2 | 652 | 512 | 1.3 | 656 | 510 | 1.4 | 588 | 511 | 0.7 |
| 764 | 506 | 2.5 | 681 | 505 | 1.7 | 642 | 494 | 1.4 | 650 | 509 | 1.4 | 580 | 508 | 0.7 |
| 771 | 522 | 2.3 | 673 | 505 | 1.6 | 642 | 499 | 1.4 | 654 | 500 | 1.5 | | | |
| 756 | 508 | 2.4 | 671 | 490 | 1.9 | 645 | 498 | 1.5 | 651 | 503 | 1.5 | | | |
| 771 | 510 | 2.5 | 675 | 490 | 1.8 | 654 | 509 | 1.4 | 652 | 511 | 1.4 | | | |
| 761 | 506 | 2.5 | 668 | 492 | 1.7 | | | | | | | | | |
| 764 | 503 | 2.5 | 673 | 488 | 1.8 | | | | | | | | | |
| 759 | 498 | 2.6 | 679 | 490 | 1.9 | | | | | | | | | |
| | | | | | | | | | | | | | | |
| | | | | | | | | | | | | | | |
| | | | | | | | | | | | | | | |
| | | | | | | | | | | | | | | |
| | | 2.5 | | | 1.8 | | | 1.4 | | | 1.4 | | | 0.7 |

Table A. 9: Voltage measurements and conversion to crack size (562000 cycles)

| -25 | | | -20 | | | -15 | | | -10 | | | -5 | | | 0 | | |
|---|---|---|---|---|---|---|---|---|---|---|---|---|---|---|---|---|---|
| over crack | reference | crack size | over crack | reference | crack size | over crack | reference | crack size | over crack | reference | crack size | over crack | reference | crack size | over crack | reference | crack size |
| 540 | 510 | 0.3 | 571 | 499 | 0.7 | 587 | 470 | 1.2 | 639 | 402 | 3.3 | 699 | 413 | 3.4 | 780 | 450 | 3.7 |
| 540 | 505 | 0.3 | 558 | 478 | 0.8 | 596 | 479 | 1.2 | 639 | 379 | 3.4 | 708 | 415 | 3.5 | 712 | 430 | 3.3 |
| 542 | 509 | 0.3 | 573 | 489 | 0.9 | 584 | 469 | 1.2 | 680 | 410 | 3.2 | 714 | 415 | 3.6 | 718 | 451 | 3.0 |
| | | | 574 | 459 | 1.3 | | | | 664 | 388 | 3.5 | 714 | 416 | 3.5 | 712 | 450 | 2.9 |
| | | | 569 | 451 | 1.3 | | | | 688 | 392 | 3.7 | 715 | 417 | 3.5 | 709 | 444 | 3.0 |
| | | | 560 | 448 | 1.3 | | | | 684 | 404 | 3.4 | | | | 723 | 456 | 2.9 |
| | | | | | | | | | 683 | 408 | 3.3 | | | | | | |
| | | | | | | | | | | | | | | | | | |
| | | | | | | | | | | | | | | | | | |
| | | | | | | | | | | | | | | | | | |
| | | | | | | | | | | | | | | | | | |
| | | | | | | | | | | | | | | | | | |
| | | | | | | | | | | | | | | | | | |
| | | 0.3 | | | 1.0 | | | 1.2 | | | 3.4 | | | 3.5 | | | 3.1 |

| 5 | | | 10 | | | 15 | | | 20 | | | 25 | | | 30 | | |
|---|---|---|---|---|---|---|---|---|---|---|---|---|---|---|---|---|---|
| over crack | reference | crack size | over crack | reference | crack size | over crack | reference | crack size | over crack | reference | crack size | over crack | reference | crack size | over crack | reference | crack size |
| 899 | 421 | 5.6 | 971 | 428 | 6.3 | 1012 | 427 | 6.8 | 1028 | 458 | 6.3 | 970 | 491 | 4.8 | 834 | 479 | 3.7 |
| 897 | 422 | 5.6 | 969 | 428 | 6.3 | 1016 | 433 | 6.7 | 1028 | 464 | 6.1 | 974 | 494 | 4.8 | 843 | 459 | 4.2 |
| 897 | 420 | 5.6 | 979 | 437 | 6.2 | 1012 | 431 | 6.7 | 1030 | 452 | 6.3 | 972 | 489 | 4.9 | 822 | 511 | 3.0 |
| 905 | 420 | 5.7 | 983 | 431 | 6.4 | 1015 | 434 | 6.6 | 1031 | 455 | 6.3 | 961 | 488 | 4.8 | 852 | 476 | 3.9 |
| 907 | 425 | 5.7 | 982 | 435 | 6.2 | 1016 | 429 | 6.8 | 1062 | 452 | 6.7 | 963 | 489 | 4.8 | 887 | 496 | 3.9 |
| 888 | 422 | 5.5 | | | | 1018 | 428 | 6.8 | 1038 | 460 | 6.3 | | | | 824 | 479 | 3.6 |
| 891 | 422 | 5.6 | | | | 1015 | 431 | 6.7 | | | | | | | 862 | 478 | 4.0 |
| | | | | | | 1011 | 435 | 6.6 | | | | | | | 831 | 475 | 3.7 |
| | | | | | | 1010 | 438 | 6.5 | | | | | | | 823 | 487 | 3.4 |
| | | | | | | | | | | | | | | | 872 | 483 | 4.0 |
| | | | | | | | | | | | | | | | | | |
| | | | | | | | | | | | | | | | | | |
| | | 5.6 | | | 6.3 | | | 6.7 | | | 6.3 | | | 4.8 | | | 3.8 |

| 35 | | | 40 | | | 45 | | | 50 | | | 55 | | |
|---|---|---|---|---|---|---|---|---|---|---|---|---|---|---|
| over crack | reference | crack size | over crack | reference | crack size | over crack | reference | crack size | over crack | reference | crack size | over crack | reference | crack size |
| 752 | 484 | 2.7 | 672 | 491 | 1.8 | 679 | 516 | 1.5 | 648 | 498 | 1.5 | 595 | 519 | 0.7 |
| 764 | 483 | 2.9 | 674 | 485 | 1.9 | 676 | 520 | 1.5 | 634 | 482 | 1.5 | 595 | 517 | 0.8 |
| 753 | 499 | 2.5 | 682 | 485 | 2 | 677 | 518 | 1.5 | 637 | 489 | 1.5 | 593 | 518 | 0.7 |
| 775 | 504 | 2.7 | 693 | 484 | 2.1 | | | | | | | | | |
| 775 | 500 | 2.8 | 689 | 483 | 2.1 | | | | | | | | | |
| 778 | 496 | 2.8 | 679 | 488 | 1.9 | | | | | | | | | |
| 767 | 505 | 2.5 | | | | | | | | | | | | |
| 774 | 497 | 2.7 | | | | | | | | | | | | |
| | | | | | | | | | | | | | | |
| | | | | | | | | | | | | | | |
| | | | | | | | | | | | | | | |
| | | | | | | | | | | | | | | |
| | | | | | | | | | | | | | | |
| | | 2.7 | | | 2.0 | | | 1.5 | | | 1.5 | | | 0.7 |

Table A. 10: Voltage measurements and conversion to crack size (572000 cycles)

| -25 | | | -20 | | | -15 | | | -10 | | | -5 | | | 0 | | |
|---|---|---|---|---|---|---|---|---|---|---|---|---|---|---|---|---|---|
| over crack | reference | crack size | over crack | reference | crack size | over crack | reference | crack size | over crack | reference | crack size | over crack | reference | crack size | over crack | reference | crack size |
| 519 | 489 | 0.3 | 563 | 483 | 0.8 | 612 | 479 | 1.3 | 755 | 429 | 3.7 | 823 | 457 | 4.0 | 810 | 450 | 4.0 |
| 520 | 489 | 0.3 | 579 | 450 | 1.4 | 613 | 479 | 1.4 | 761 | 434 | 3.7 | 845 | 452 | 4.3 | 801 | 460 | 3.7 |
| 520 | 486 | 0.3 | 534 | 413 | 1.5 | 576 | 452 | 1.4 | 758 | 431 | 3.7 | 849 | 467 | 4.1 | 798 | 467 | 3.5 |
| | | | 577 | 466 | 1.2 | 587 | 470 | 1.2 | 757 | 435 | 3.7 | 834 | 461 | 4.0 | 807 | 463 | 3.7 |
| | | | 576 | 479 | 1.0 | 620 | 489 | 1.3 | 753 | 439 | 3.6 | 860 | 459 | 4.4 | 813 | 453 | 4.0 |
| | | | 587 | 459 | 1.4 | | | | | | | 833 | 462 | 4.0 | | | |
| | | | 577 | 467 | 1.2 | | | | | | | 876 | 478 | 4.2 | | | |
| | | | 579 | 459 | 1.3 | | | | | | | 852 | 472 | 4.0 | | | |
| | | | 577 | 468 | 1.2 | | | | | | | 860 | 471 | 4.1 | | | |
| | | | 578 | 468 | 1.2 | | | | | | | | | | | | |
| | | | | | | | | | | | | | | | | | |
| | | | | | | | | | | | | | | | | | |
| | | | | | | | | | | | | | | | | | |
| | | 0.3 | | | 1.2 | | | 1.3 | | | 3.7 | | | 4.1 | | | 3.8 |

| 5 | | | 10 | | | 15 | | | 20 | | | 25 | | | 30 | | |
|---|---|---|---|---|---|---|---|---|---|---|---|---|---|---|---|---|---|
| over crack | reference | crack size | over crack | reference | crack size | over crack | reference | crack size | over crack | reference | crack size | over crack | reference | crack size | over crack | reference | crack size |
| 1077 | 473 | 6.3 | 1116 | 461 | 7.1 | 1130 | 457 | 7.8 | 1146 | 470 | 7.1 | 1113 | 518 | 5.8 | 954 | 487 | 4.8 |
| 1052 | 450 | 6.6 | 1120 | 453 | 7.3 | 1162 | 448 | 7.9 | 1163 | 479 | 7.2 | 1113 | 520 | 5.7 | 936 | 496 | 4.4 |
| 1044 | 453 | 6.5 | 1132 | 454 | 7.4 | 1163 | 459 | 7.6 | 1162 | 479 | 7.1 | 1106 | 516 | 5.7 | 923 | 513 | 4.0 |
| 1069 | 489 | 6.6 | 1124 | 456 | 7.3 | 1143 | 458 | 7.6 | 1178 | 487 | 7 | 1116 | 525 | 5.6 | 942 | 501 | 4.4 |
| 1064 | 462 | 6.5 | 1133 | 462 | 7.2 | 1168 | 457 | 7.7 | 1169 | 481 | 7.1 | 1110 | 519 | 5.6 | 972 | 538 | 4.0 |
| 1072 | 463 | 6.5 | 1131 | 462 | 7.2 | 1167 | 457 | 7.7 | 1173 | 482 | 7.1 | | | | 923 | 469 | 4.8 |
| 1073 | 469 | 6.4 | 1134 | 462 | 7.2 | 1166 | 452 | 7.9 | | | | | | | 925 | 478 | 4.7 |
| 1068 | 463 | 6.5 | 1137 | 468 | 7.1 | 1170 | 460 | 7.7 | | | | | | | | | |
| 1063 | 464 | 6.4 | 1123 | 467 | 7 | 1153 | 449 | 7.8 | | | | | | | | | |
| 1092 | 461 | 6.8 | 1128 | 463 | 7.1 | 1156 | 452 | 7.7 | | | | | | | | | |
| | | | | | | | | | | | | | | | | | |
| | | | | | | | | | | | | | | | | | |
| | | | | | | | | | | | | | | | | | |
| | | 6.5 | | | 7.2 | | | 7.7 | | | 7.1 | | | 5.7 | | | 4.5 |

| 35 | | | 40 | | | 45 | | | 50 | | | 55 | | |
|---|---|---|---|---|---|---|---|---|---|---|---|---|---|---|
| over crack | reference | crack size | over crack | reference | crack size | over crack | reference | crack size | over crack | reference | crack size | over crack | reference | crack size |
| 842 | 509 | 3.2 | 783 | 543 | 2.2 | 721 | 521 | 1.9 | 779 | 568 | 1.6 | 643 | 550 | 0.8 |
| 836 | 505 | 3.2 | 780 | 536 | 2.2 | 722 | 579 | 1.5 | 776 | 556 | 1.6 | 641 | 539 | 0.9 |
| 810 | 500 | 3.1 | 783 | 534 | 2.3 | 746 | 561 | 1.6 | | | | 626 | 557 | 0.8 |
| 823 | 497 | 3.2 | 782 | 527 | 2.4 | 760 | 553 | 1.8 | | | | | | |
| 824 | 502 | 3.2 | 782 | 527 | 2.4 | 763 | 555 | 1.8 | | | | | | |
| | | | | | | 754 | 555 | 1.7 | | | | | | |
| | | | | | | | | | | | | | | |
| | | | | | | | | | | | | | | |
| | | | | | | | | | | | | | | |
| | | | | | | | | | | | | | | |
| | | | | | | | | | | | | | | |
| | | | | | | | | | | | | | | |
| | | | | | | | | | | | | | | |
| | | 3.2 | | | 2.3 | | | 1.7 | | | 1.6 | | | 0.8 |

Table A. 11: Voltage measurements and conversion to crack size (578000 cycles just before OL)

| -25 | | | -20 | | | -15 | | | -10 | | | -5 | | | 0 | | |
|---|---|---|---|---|---|---|---|---|---|---|---|---|---|---|---|---|---|
| over crack | reference | crack size | over crack | reference | crack size | over crack | reference | crack size | over crack | reference | crack size | over crack | reference | crack size | over crack | reference | crack size |
| 492 | 467 | 0.3 | 633 | 486 | 1.5 | 662 | 519 | 1.4 | 786 | 475 | 3.3 | 840 | 446 | 4.4 | 857 | 457 | 4.4 |
| 496 | 466 | 0.3 | 631 | 489 | 1.5 | 689 | 524 | 1.6 | 778 | 466 | 3.3 | 855 | 454 | 4.4 | 876 | 460 | 4.5 |
| 495 | 466 | 0.3 | 613 | 482 | 1.4 | 686 | 526 | 1.5 | 895 | 427 | 5.5 | 848 | 449 | 4.4 | 855 | 464 | 4.2 |
| | | | 611 | 467 | 1.5 | 683 | 519 | 1.6 | 841 | 434 | 4.7 | 847 | 445 | 4.5 | 856 | 466 | 4.2 |
| | | | 577 | 491 | 0.9 | 676 | 517 | 1.5 | 850 | 458 | 4.3 | 897 | 445 | 5 | 856 | 457 | 4.3 |
| | | | 593 | 468 | 1.3 | 610 | 462 | 1.6 | 791 | 487 | 3.1 | 893 | 445 | 5 | 828 | 448 | 4.2 |
| | | | 548 | 484 | 0.7 | 664 | 503 | 1.6 | 828 | 459 | 4.0 | 850 | 449 | 4.4 | 864 | 449 | 4.6 |
| | | | 586 | 457 | 1.4 | 673 | 511 | 1.6 | 834 | 445 | 4.4 | 857 | 446 | 4.6 | 856 | 460 | 4.3 |
| | | | 593 | 452 | 1.6 | 664 | 510 | 1.5 | 814 | 456 | 3.9 | 843 | 442 | 4.5 | 886 | 456 | 4.7 |
| | | | 585 | 449 | 1.5 | 678 | 509 | 1.7 | 818 | 465 | 3.8 | 844 | 440 | 4.5 | 860 | 461 | 4.3 |
| | | | 574 | 428 | 1.7 | | | | | | | 860 | 441 | 4.7 | 855 | 467 | 4.2 |
| | | | 529 | 447 | 0.9 | | | | | | | 851 | 441 | 4.6 | | | |
| | | | 586 | 439 | 1.7 | | | | | | | 768 | 525 | 2.3 | | | |
| | | | | | | | | | | | | 870 | 470 | 4.2 | | | |
| | | | | | | | | | | | | | | | | | |
| | | 0.3 | | | 1.3 | | | 1.6 | | | 4.0 | | | 4.4 | | | 4.4 |

| 5 | | | 10 | | | 15 | | | 20 | | | 25 | | | 30 | | |
|---|---|---|---|---|---|---|---|---|---|---|---|---|---|---|---|---|---|
| over crack | reference | crack size | over crack | reference | crack size | over crack | reference | crack size | over crack | reference | crack size | over crack | reference | crack size | over crack | reference | crack size |
| 1133 | 474 | 7.0 | 1107 | 443 | 7.494357 | 1135 | 411 | 8.8 | 1120 | 464 | 7.6 | 1069 | 474 | 6.3 | 970 | 485 | 5 |
| 1162 | 471 | 7.3 | 1148 | 443 | 7.957111 | 1127 | 415 | 8.6 | 1136 | 449 | 7.6 | 1063 | 475 | 6.2 | 944 | 483 | 4.7 |
| 1154 | 475 | 7.1 | 1147 | 432 | 8.275463 | 1125 | 417 | 8.5 | 1140 | 449 | 7.6 | 1074 | 482 | 6.1 | 956 | 480 | 5.0 |
| 1111 | 485 | 6.5 | 1147 | 449 | 7.772829 | 1110 | 408 | 8.6 | 1137 | 451 | 7.6 | 1073 | 479 | 6.2 | 960 | 482 | 5.0 |
| 1179 | 488 | 7.1 | 1148 | 464 | 7.37069 | 1052 | 403 | 8.1 | 1147 | 467 | 7.2 | 1084 | 479 | 6.3 | 963 | 479 | 5.1 |
| 1173 | 462 | 7.7 | 1137 | 439 | 7.949886 | 1152 | 414 | 8.9 | 1137 | 449 | 7.6 | 1077 | 473 | 6.4 | | | |
| 1143 | 484 | 6.8 | 1128 | 451 | 7.505543 | 1062 | 404 | 8.1 | 1141 | 451 | 7.6 | | | | | | |
| 1194 | 498 | 7.0 | 1124 | 451 | 7.461197 | 1098 | 404 | 8.6 | 1129 | 452 | 7.4 | | | | | | |
| 1131 | 514 | 6.0 | 1145 | 435 | 8.16092 | 1103 | 433 | 7.7 | 1141 | 457 | 7.4 | | | | | | |
| 1163 | 476 | 7.2 | 1136 | 452 | 7.566372 | 1096 | 436 | 7.6 | 1138 | 451 | 7.6 | | | | | | |
| | | | | | | 1103 | 409 | 8.5 | | | | | | | | | |
| | | | | | | 1095 | 413 | 8.3 | | | | | | | | | |
| | | | | | | 1102 | 432 | 7.8 | | | | | | | | | |
| | | | | | | 1123 | 402 | 9.0 | | | | | | | | | |
| | | | | | | | | | | | | | | | | | |
| | | 7.0 | | | 7.8 | | | 8.4 | | | 7.5 | | | 6.3 | | | 4.9 |

| 35 | | | 40 | | | 45 | | | 50 | | | 55 | | |
|---|---|---|---|---|---|---|---|---|---|---|---|---|---|---|
| over crack | reference | crack size | over crack | reference | crack size | over crack | reference | crack size | over crack | reference | crack size | over crack | reference | crack size |
| 857 | 481 | 3.9 | 756 | 503 | 2.3 | 705 | 493 | 2.2 | 688 | 503 | 1.8 | 634 | 496 | 1.4 |
| 861 | 495 | 3.7 | 750 | 502 | 2.4 | 715 | 495 | 2.2 | 695 | 485 | 2.1 | 594 | 484 | 1.1 |
| 852 | 483 | 3.8 | 755 | 495 | 2.6 | 709 | 496 | 2.1 | 699 | 492 | 2.1 | 604 | 508 | 1 |
| 870 | 487 | 3.9 | 753 | 496 | 2.5 | 711 | 497 | 2.2 | 688 | 509 | 1.7 | 612 | 513 | 0.9 |
| 866 | 495 | 3.7 | 758 | 494 | 2.6 | 700 | 496 | 2.1 | 671 | 490 | 1.8 | 615 | 518 | 0.9 |
| | | | | | | | | | | | | | | |
| | | | | | | | | | | | | | | |
| | | | | | | | | | | | | | | |
| | | | | | | | | | | | | | | |
| | | | | | | | | | | | | | | |
| | | | | | | | | | | | | | | |
| | | | | | | | | | | | | | | |
| | | | | | | | | | | | | | | |
| | | | | | | | | | | | | | | |
| | | 3.8 | | | 2.5 | | | 2.1 | | | 1.9 | | | 1.1 |

Table A. 12: Voltage measurements and conversion to crack size (588000 cycles after OL)

| -25 | | | -20 | | | -15 | | | -10 | | | -5 | | | 0 | | |
|---|---|---|---|---|---|---|---|---|---|---|---|---|---|---|---|---|---|
| over crack | reference | crack size | over crack | reference | crack size | over crack | reference | crack size | over crack | reference | crack size | over crack | reference | crack size | over crack | reference | crack size |
| 523 | 591 | 0.3 | 625 | 542 | 0.7 | 749 | 491 | 2.6 | 902 | 441 | 5.2 | 947 | 493 | 4.6 | 1007 | 468 | 5.7 |
| | | | 645 | 526 | 1.1 | 767 | 504 | 2.6 | 918 | 450 | 5.2 | 1023 | 476 | 5.7 | 999 | 450 | 6.1 |
| | | | 758 | 521 | 2.2 | 733 | 494 | 2.4 | 924 | 433 | 5.6 | 1038 | 502 | 5.3 | 965 | 444 | 5.8 |
| | | | 713 | 560 | 1.3 | 748 | 506 | 2.4 | 933 | 426 | 5.9 | 1025 | 510 | 5.0 | 973 | 439 | 6 |
| | | | 648 | 525 | 1.1 | 726 | 537 | 1.8 | 915 | 440 | 5.3 | 980 | 497 | 4.9 | 979 | 443 | 6 |
| | | | 687 | 491 | 1.9 | 746 | 510 | 2.3 | 932 | 463 | 5 | 1009 | 489 | 5.3 | 967 | 507 | 4.5 |
| | | | | | | 739 | 567 | 1.5 | 928 | 425 | 5.9 | 999 | 512 | 4.8 | 979 | 461 | 4.6 |
| | | | | | | 751 | 541 | 1.9 | 925 | 458 | 5 | 974 | 481 | 5.1 | 969 | 445 | 5.8 |
| | | | | | | 762 | 568 | 1.7 | 890 | 465 | 4.5 | 978 | 454 | 5.8 | 998 | 465 | 5.7 |
| | | | | | | 727 | 534 | 1.8 | 929 | 448 | 5.3 | 972 | 534 | 4.1 | 1015 | 474 | 5.7 |
| | | | | | | 757 | 497 | 2.6 | 934 | 440 | 5.6 | 978 | 497 | 4.8 | 1003 | 460 | 5.9 |
| | | | | | | 766 | 519 | 2.4 | 954 | 466 | 5.2 | 971 | 494 | 4.8 | 1001 | 499 | 5 |
| | | | | | | 760 | 568 | 1.7 | 915 | 443 | 5.3 | 979 | 509 | 4.6 | 995 | 517 | 4.6 |
| | | | | | | | | | | | | 997 | 519 | 4.6 | 976 | 488 | 5 |
| | | | | | | | | | | | | 988 | 530 | 4.3 | 1004 | 548 | 4.1 |
| | | | | | | | | | | | | 1015 | 515 | 4.9 | 939 | 575 | 3.1 |
| | | | | | | | | | | | | | | | 1011 | 527 | 4.5 |
| | | | | | | | | | | | | | | | 1004 | 540 | 4.2 |
| | | | | | | | | | | | | | | | 959 | 483 | 4.9 |
| | | | | | | | | | | | | | | | 1016 | 468 | 5.8 |
| | | | | | | | | | | | | | | | 1056 | 508 | 5.3 |
| | | | | | | | | | | | | | | | 1004 | 515 | 4.1 |
| | | | | | | | | | | | | | | | 961 | 492 | 4.7 |
| | | | | | | | | | | | | | | | 979 | 502 | 4.7 |
| | | | | | | | | | | | | | | | | | |
| | | 0.3 | | | 1.4 | | | 2.1 | | | 5.3 | | | 4.9 | | | 5.1 |

| 5 | | | 10 | | | 15 | | | 20 | | | 25 | | | 30 | | |
|---|---|---|---|---|---|---|---|---|---|---|---|---|---|---|---|---|---|
| over crack | reference | crack size | over crack | reference | crack size | over crack | reference | crack size | over crack | reference | crack size | over crack | reference | crack size | over crack | reference | crack size |
| 1102 | 453 | 7.2 | 1083 | 400 | 8.5 | 1224 | 447 | 7.7 | 1107 | 430 | 7.8 | 1123 | 467 | 7 | 1056 | 566 | 4.3 |
| 1087 | 416 | 8.1 | 1103 | 410 | 8.5 | 1066 | 375 | 9.2 | 1116 | 513 | 5.8 | 1080 | 469 | 6.5 | 898 | 461 | 4.7 |
| 1121 | 435 | 7.9 | 1158 | 438 | 8.2 | 1068 | 393 | 8.5 | 1112 | 429 | 7.9 | 1178 | 528 | 6.1 | 989 | 479 | 5.3 |
| 1095 | 415 | 8.2 | 1192 | 491 | 7.1 | 1072 | 344 | 10.5 | 1184 | 509 | 6.6 | 1106 | 471 | 6.7 | 956 | 450 | 5.6 |
| 1123 | 422 | 8.3 | 1196 | 493 | 7.1 | 1068 | 343 | 10.5 | 1204 | 520 | 6.5 | 1137 | 451 | 7.6 | 948 | 452 | 5.5 |
| 1113 | 456 | 7.2 | 1152 | 439 | 8.1 | 1236 | 422 | 9.6 | 1219 | 492 | 7.3 | 1111 | 470 | 6.8 | 1023 | 517 | 4.9 |
| 1106 | 470 | 6.8 | 1140 | 420 | 8.6 | 1135 | 416 | 8.6 | 1173 | 493 | 6.8 | 1111 | 486 | 6.4 | 933 | 484 | 4.6 |
| 1068 | 418 | 7.8 | 1123 | 402 | 9.0 | 1056 | 336 | 10.7 | 1240 | 415 | 9.9 | 1100 | 499 | 6 | 982 | 530 | 4.3 |
| 1146 | 479 | 7.0 | 1132 | 419 | 8.5 | 1175 | 442 | 8.2 | 1257 | 437 | 9.3 | 1108 | 489 | 6.3 | 1023 | 462 | 6.1 |
| 1097 | 457 | 7.0 | 1135 | 425 | 8.4 | 1175 | 461 | 7.7 | 1180 | 481 | 7.2 | 1105 | 494 | 6.1 | 1029 | 496 | 5.4 |
| 1103 | 423 | 8.0 | 1126 | 421 | 8.4 | 1070 | 365 | 9.6 | 1277 | 533 | 6.9 | | | | 993 | 497 | 5.0 |
| 1107 | 436 | 7.7 | 1139 | 426 | 8.4 | 1249 | 464 | 8.4 | 1334 | 540 | 7.3 | | | | | | |
| 1196 | 474 | 7.6 | 1125 | 441 | 7.8 | 1131 | 409 | 8.8 | 1222 | 439 | 8.9 | | | | | | |
| 1181 | 468 | 7.6 | | | | 1210 | 434 | 8.9 | 1197 | 442 | 8.5 | | | | | | |
| | | | | | | 1212 | 427 | 9.1 | 1325 | 495 | 8.3 | | | | | | |
| | | | | | | 1215 | 450 | 8.5 | | | | | | | | | |
| | | | | | | 1078 | 382 | 9.1 | | | | | | | | | |
| | | | | | | 1195 | 458 | 8 | | | | | | | | | |
| | | | | | | 1237 | 442 | 8.9 | | | | | | | | | |
| | | | | | | 1126 | 399 | 9.1 | | | | | | | | | |
| | | | | | | 1230 | 435 | 9.1 | | | | | | | | | |
| | | | | | | 1218 | 481 | 7.6 | | | | | | | | | |
| | | | | | | 1229 | 488 | 7.5 | | | | | | | | | |
| | | | | | | 1250 | 450 | 8.8 | | | | | | | | | |
| | | | | | | 1218 | 448 | 8.5 | | | | | | | | | |
| | | | | | | 1164 | 462 | 7.5 | | | | | | | | | |
| | | | | | | 1291 | 473 | 8.6 | | | | | | | | | |
| | | | | | | 1265 | 488 | 7.9 | | | | | | | | | |
| | | | | | | 1207 | 483 | 7.7 | | | | | | | | | |
| | | | | | | | | | | | | | | | | | |
| | | 7.6 | | | 8.2 | | | 8.7 | | | 7.7 | | | 6.6 | | | 5.1 |

| 35 | | | 40 | | | 45 | | | 50 | | | 55 | | |
|---|---|---|---|---|---|---|---|---|---|---|---|---|---|---|
| over crack | reference | crack size | over crack | reference | crack size | over crack | reference | crack size | over crack | reference | crack size | over crack | reference | crack size |
| 920 | 505 | 4.1 | 868 | 532 | 3.2 | 706 | 468 | 2.5 | 687 | 485 | 2 | 652 | 529 | 1.2 |
| 950 | 493 | 4.6 | 787 | 483 | 3.1 | 711 | 508 | 2.0 | 721 | 527 | 1.8 | 681 | 560 | 1 |
| 910 | 526 | 3.7 | 803 | 512 | 2.8 | 761 | 534 | 2.1 | 625 | 499 | 1.9 | | | |
| 903 | 496 | 4.1 | 792 | 494 | 3.0 | 762 | 533 | 2.1 | 705 | 503 | 2 | | | |
| 910 | 491 | 4.3 | 813 | 518 | 2.8 | 772 | 534 | 2.2 | 669 | 469 | 2.1 | | | |
| 900 | 491 | 4.2 | 761 | 454 | 3.4 | | | | | | | | | |
| 886 | 483 | 4.2 | | | | | | | | | | | | |
| 896 | 473 | 4.5 | | | | | | | | | | | | |
| 880 | 483 | 4.1 | | | | | | | | | | | | |
| 893 | 492 | 4.1 | | | | | | | | | | | | |
| 937 | 528 | 3.9 | | | | | | | | | | | | |
| | | | | | | | | | | | | | | |
| | | 4.1 | | | 3.1 | | | 2.2 | | | 2.0 | | | 1.1 |

Table A. 13: Voltage measurements and conversion to crack size (598000 cycles)

| -25 | | | -20 | | | -15 | | | -10 | | | -5 | | | 0 | | |
|---|---|---|---|---|---|---|---|---|---|---|---|---|---|---|---|---|---|
| over crack | reference | crack size | over crack | reference | crack size | over crack | reference | crack size | over crack | reference | crack size | over crack | reference | crack size | over crack | reference | crack size |
| 437 | 405 | 0.3 | 616 | 459 | 2.1 | 854 | 542 | 2.8 | 1013 | 461 | 6.0 | 1061 | 480 | 6.1 | 1118 | 442 | 7.6 |
| 427 | 398 | 0.3 | 615 | 452 | 1.8 | 848 | 522 | 3.1 | 1018 | 466 | 5.9 | 1113 | 487 | 6.4 | 1130 | 440 | 7.8 |
| 449 | 418 | 0.3 | 608 | 424 | 2.1 | 840 | 510 | 3.2 | 1024 | 455 | 6.3 | 1113 | 477 | 6.6 | 1101 | 442 | 7.4 |
| | | | 623 | 448 | 1.9 | 832 | 502 | 3.2 | 1002 | 468 | 5.7 | 1105 | 483 | 6.4 | 1153 | 457 | 7.6 |
| | | | 677 | 499 | 1.7 | 832 | 503 | 3.2 | 1028 | 453 | 6.3 | 1087 | 467 | 6.6 | 1119 | 425 | 8.1 |
| | | | 648 | 502 | 1.4 | 840 | 517 | 3.1 | 1011 | 446 | 6.3 | 1205 | 520 | 6.5 | 1240 | 499 | 7.4 |
| | | | 700 | 501 | 1.9 | 853 | 516 | 3.2 | 1131 | 495 | 6.4 | 1201 | 513 | 6.7 | 1236 | 502 | 7.3 |
| | | | 727 | 517 | 2 | | | | 1127 | 494 | 6.4 | 1184 | 515 | 6.4 | 1237 | 499 | 7.3 |
| | | | 737 | 529 | 1.9 | | | | 1136 | 501 | 6.3 | 1195 | 518 | 6.5 | 1238 | 499 | 7.4 |
| | | | | | | | | | 1136 | 499 | 6.4 | 1212 | 514 | 6.7 | 1235 | 502 | 7.3 |
| | | | | | | | | | | | | | | | | | |
| | | 0.3 | | | 1.9 | | | 3.1 | | | 6.2 | | | 6.5 | | | 7.5 |

| 5 | | | 10 | | | 15 | | | 20 | | | 25 | | | 30 | | |
|---|---|---|---|---|---|---|---|---|---|---|---|---|---|---|---|---|---|
| over crack | reference | crack size | over crack | reference | crack size | over crack | reference | crack size | over crack | reference | crack size | over crack | reference | crack size | over crack | reference | crack size |
| 1339 | 463 | 9.5 | 1374 | 475 | 9.5 | 1365 | 454 | 10.0 | 1309 | 416 | 10.7 | 1383 | 476 | 9.5 | 1205 | 473 | 7.7 |
| 1340 | 470 | 9.3 | 1360 | 453 | 10.0 | 1349 | 444 | 10.2 | 1312 | 422 | 10.5 | 1345 | 476 | 9.1 | 1199 | 457 | 8.1 |
| 1313 | 461 | 9.2 | 1360 | 462 | 9.7 | 1345 | 451 | 9.9 | 1295 | 406 | 10.9 | 1363 | 496 | 8.7 | 1189 | 463 | 7.8 |
| 1320 | 459 | 9.4 | 1342 | 443 | 10.1 | 1339 | 441 | 10.2 | 1322 | 428 | 10.4 | 1374 | 508 | 8.5 | 1187 | 466 | 7.7 |
| 1322 | 467 | 9.2 | 1341 | 444 | 10.1 | 1323 | 446 | 9.8 | 1325 | 432 | 10.3 | 1371 | 507 | 8.5 | 1196 | 466 | 7.8 |
| 1386 | 491 | 9.1 | 1356 | 448 | 10.1 | 1418 | 504 | 9.1 | 1332 | 429 | 10.5 | 1370 | 506 | 8.5 | 1199 | 464 | 7.9 |
| 1389 | 486 | 9.3 | 1345 | 477 | 9.1 | 1414 | 482 | 9.7 | 1356 | 449 | 10.1 | 1354 | 486 | 8.9 | 1192 | 483 | 7.3 |
| 1384 | 485 | 9.3 | 1434 | 494 | 9.5 | 1418 | 504 | 9.1 | 1359 | 461 | 9.7 | 1343 | 492 | 8.6 | 1222 | 488 | 7.5 |
| 1385 | 491 | 9.1 | 1428 | 493 | 9.5 | 1406 | 494 | 9.2 | 1382 | 475 | 9.5 | 1349 | 481 | 9.0 | 1224 | 481 | 7.7 |
| 1396 | 496 | 9.1 | 1438 | 489 | 9.7 | 1413 | 493 | 9.3 | 1383 | 476 | 9.5 | 1325 | 466 | 9.2 | 1252 | 508 | 7.3 |
| | | | 1428 | 491 | 9.5 | | | | 1402 | 489 | 9.3 | | | | | | |
| | | | | | | | | | 1401 | 482 | 9.5 | | | | | | |
| | | | | | | | | | | | | | | | | | |
| | | 9.2 | | | 9.7 | | | 9.7 | | | 10.1 | | | 8.9 | | | 7.7 |

| 35 | | | 40 | | | 45 | | | 50 | | | 55 | | |
|---|---|---|---|---|---|---|---|---|---|---|---|---|---|---|
| over crack | reference | crack size | over crack | reference | crack size | over crack | reference | crack size | over crack | reference | crack size | over crack | reference | crack size |
| 1081 | 544 | 4.9 | 928 | 556 | 3.3 | 801 | 532 | 2.5 | 755 | 515 | 2.3 | 712 | 583 | 1.1 |
| 1080 | 522 | 5.3 | 984 | 570 | 3.6 | 799 | 531 | 2.5 | 755 | 536 | 2.0 | 701 | 570 | 1.1 |
| 1077 | 528 | 5.2 | 916 | 536 | 3.5 | 800 | 537 | 2.4 | | | | | | |
| 1080 | 538 | 5.0 | | | | | | | | | | | | |
| 1083 | 544 | 5.0 | | | | | | | | | | | | |
| | | | | | | | | | | | | | | |
| | | 5.1 | | | 3.5 | | | 2.5 | | | 2.2 | | | 1.1 |

Table A. 14: Voltage measurements and conversion to crack size (608000 cycles)

| -25 | | | -20 | | | -15 | | | -10 | | | -5 | | | 0 | | |
|---|---|---|---|---|---|---|---|---|---|---|---|---|---|---|---|---|---|
| over crack | reference | crack size | over crack | reference | crack size | over crack | reference | crack size | over crack | reference | crack size | over crack | reference | crack size | over crack | reference | crack size |
| 544 | 494 | 0.5 | 778 | 463 | 3.4 | 975 | 443 | 6.0 | 1181 | 427 | 8.8 | 1246 | 438 | 9.2 | 1313 | 431 | 10.2 |
| 541 | 490 | 0.5 | 763 | 453 | 3.4 | 991 | 454 | 5.9 | 1174 | 424 | 8.8 | 1240 | 434 | 9.3 | 1310 | 424 | 10.4 |
| 551 | 497 | 0.5 | 755 | 453 | 3.3 | 999 | 478 | 5.4 | 1165 | 430 | 8.5 | 1242 | 440 | 9.1 | 1305 | 426 | 10.3 |
| | | | | | | 1004 | 463 | 5.8 | 1170 | 433 | 8.5 | 1248 | 436 | 9.3 | 1306 | 423 | 10.4 |
| | | | | | | 997 | 469 | 5.6 | 1161 | 430 | 8.5 | | | | 1306 | 420 | 10.5 |
| | | | | | | | | | | | | | | | | | |
| | | 0.5 | | | 3.4 | | | 5.8 | | | 8.6 | | | 9.2 | | | 10.4 |

| 5 | | | 10 | | | 15 | | | 20 | | | 25 | | | 30 | | |
|---|---|---|---|---|---|---|---|---|---|---|---|---|---|---|---|---|---|
| over crack | reference | crack size | over crack | reference | crack size | over crack | reference | crack size | over crack | reference | crack size | over crack | reference | crack size | over crack | reference | crack size |
| 1414 | 421 | 11.8 | 1437 | 437 | 11.4 | 1432 | 438 | 11.3 | 1424 | 421 | 11.9 | 1375 | 454 | 10.1 | 1236 | 441 | 9.0 |
| 1413 | 425 | 11.6 | 1443 | 436 | 11.5 | 1420 | 420 | 11.9 | 1411 | 410 | 12.2 | 1368 | 447 | 10.3 | 1229 | 445 | 8.8 |
| 1414 | 425 | 11.6 | 1439 | 433 | 11.6 | 1427 | 432 | 11.5 | 1413 | 415 | 12.0 | 1377 | 455 | 10.1 | 1228 | 438 | 9.0 |
| 1396 | 427 | 11.3 | 1446 | 432 | 11.7 | 1442 | 423 | 12.0 | 1408 | 418 | 11.8 | 1379 | 456 | 10.1 | 1215 | 442 | 8.7 |
| 1397 | 423 | 11.5 | 1441 | 431 | 11.7 | 1450 | 436 | 11.6 | 1408 | 416 | 11.9 | 1375 | 457 | 10.0 | 1227 | 429 | 9.3 |
| | | | 1440 | 433 | 11.6 | 1453 | 429 | 11.9 | 1402 | 419 | 11.7 | | | | | | |
| | | | 1443 | 429 | 11.8 | 1458 | 426 | 12.1 | 1400 | 419 | 11.7 | | | | | | |
| | | | | | | 1434 | 437 | 11.4 | 1408 | 418 | 11.8 | | | | | | |
| | | | | | | 1466 | 441 | 11.6 | 1403 | 425 | 11.5 | | | | | | |
| | | | | | | | | | 1394 | 417 | 11.7 | | | | | | |
| | | | | | | | | | | | | | | | | | |
| | | 11.6 | | | 11.6 | | | 11.7 | | | 11.8 | | | 10.1 | | | 9.0 |

| 35 | | | 40 | | | 45 | | | 50 | | | 55 | | |
|---|---|---|---|---|---|---|---|---|---|---|---|---|---|---|
| over crack | reference | crack size | over crack | reference | crack size | over crack | reference | crack size | over crack | reference | crack size | over crack | reference | crack size |
| 1090 | 473 | 6.5 | 1007 | 478 | 5.5 | 869 | 491 | 3.8 | 763 | 495 | 2.7 | 672 | 511 | 1.6 |
| 1134 | 443 | 7.8 | 995 | 487 | 5.2 | 895 | 490 | 4.1 | 782 | 492 | 2.9 | 670 | 517 | 1.5 |
| 1183 | 508 | 6.6 | 1061 | 476 | 6.1 | 876 | 513 | 3.5 | | | | | | |
| 1096 | 502 | 5.9 | | | | | | | | | | | | |
| 1050 | 469 | 6.2 | | | | | | | | | | | | |
| | | | | | | | | | | | | | | |
| | | 6.6 | | | 5.6 | | | 3.8 | | | 2.8 | | | 1.5 |

Table A. 15: Voltage measurements and conversion to crack size (613000 cycles)

| -25 | | | -20 | | | -15 | | | -10 | | | -5 | | | 0 | | |
|---|---|---|---|---|---|---|---|---|---|---|---|---|---|---|---|---|---|
| over crack | reference | crack size | over crack | reference | crack size | over crack | reference | crack size | over crack | reference | crack size | over crack | reference | crack size | over crack | reference | crack size |
| 580 | 523 | 0.5 | 787 | 445 | 3.8 | 1048 | 440 | 6.9 | 1235 | 431 | 9.3 | 1298 | 427 | 10.2 | 1346 | 392 | 12.2 |
| | | | 779 | 439 | 3.9 | 1056 | 435 | 7.1 | 1238 | 430 | 9.4 | 1299 | 424 | 10.3 | 1379 | 415 | 11.6 |
| | | | 785 | 435 | 4.0 | 1045 | 457 | 6.4 | 1230 | 421 | 9.6 | 1300 | 428 | 10.2 | 1361 | 417 | 11.3 |
| | | | | | | 1047 | 442 | 6.8 | 1232 | 427 | 9.4 | 1303 | 431 | 10.1 | 1396 | 420 | 11.6 |
| | | | | | | 1049 | 433 | 7.1 | 1229 | 432 | 9.2 | 1301 | 430 | 10.1 | 1365 | 419 | 11.3 |
| | | | | | | | | | | | | | | | | | |
| | | 0.5 | | | 3.9 | | | 6.9 | | | 9.4 | | | 10.2 | | | 11.6 |

| 5 | | | 10 | | | 15 | | | 20 | | | 25 | | | 30 | | |
|---|---|---|---|---|---|---|---|---|---|---|---|---|---|---|---|---|---|
| over crack | reference | crack size | over crack | reference | crack size | over crack | reference | crack size | over crack | reference | crack size | over crack | reference | crack size | over crack | reference | crack size |
| 1424 | 394 | 13.1 | 1458 | 402 | 13.1 | 1454 | 406 | 12.9 | 1447 | 418 | 12.3 | 1384 | 421 | 11.4 | 1259 | 414 | 10.2 |
| 1403 | 403 | 12.4 | 1452 | 401 | 13.1 | 1448 | 378 | 14.2 | 1434 | 399 | 13.0 | 1407 | 440 | 11.0 | 1305 | 449 | 9.5 |
| 1435 | 395 | 13.2 | 1496 | 438 | 12.1 | 1411 | 394 | 12.9 | 1426 | 398 | 12.9 | 1386 | 430 | 11.1 | 1306 | 459 | 9.2 |
| 1453 | 417 | 12.4 | 1501 | 432 | 12.4 | 1437 | 416 | 12.3 | 1416 | 400 | 12.7 | 1437 | 461 | 10.6 | 1320 | 464 | 9.2 |
| 1459 | 422 | 12.3 | 1593 | 455 | 12.5 | 1463 | 411 | 12.8 | 1440 | 419 | 12.2 | 1443 | 453 | 10.9 | | | |
| | | | 1586 | 448 | 12.7 | 1489 | 431 | 12.3 | 1486 | 436 | 12.0 | | | | | | |
| | | | 1589 | 451 | 12.6 | 1496 | 432 | 12.3 | 1478 | 432 | 12.1 | | | | | | |
| | | | 1594 | 450 | 12.7 | 1501 | 428 | 12.5 | | | | | | | | | |
| | | | | | | 1501 | 434 | 12.3 | | | | | | | | | |
| | | | | | | 1497 | 433 | 12.3 | | | | | | | | | |
| | | | | | | | | | | | | | | | | | |
| | | 12.7 | | | 12.7 | | | 12.7 | | | 12.5 | | | 11.0 | | | 9.5 |

| 35 | | | 40 | | | 45 | | | 50 | | | 55 | | |
|---|---|---|---|---|---|---|---|---|---|---|---|---|---|---|
| over crack | reference | crack size | over crack | reference | crack size | over crack | reference | crack size | over crack | reference | crack size | over crack | reference | crack size |
| 1142 | 439 | 8.0 | 1049 | 480 | 5.9 | 897 | 484 | 4.3 | 779 | 498 | 2.8 | 638 | 488 | 1.5 |
| 1167 | 457 | 7.8 | 1046 | 479 | 5.9 | 899 | 486 | 4.2 | | | | | | |
| 1189 | 456 | 8.0 | 1052 | 485 | 5.8 | 884 | 485 | 4.1 | | | | | | |
| | | | | | | | | | | | | | | |
| | | 7.9 | | | 5.9 | | | 4.2 | | | 2.8 | | | 1.5 |

# Appendix G

$SCF(c)=z \cdot SCF_{saddle,chord}$